ВЕСТНИК ТРАНСПЛАНТОЛОГИИ И ИСКУССТВЕННЫХ ОРГАНОВ

VESTNIK TRANSPLANTOLOGII I ISKUSSTVENNYKH ORGANOV

RUSSIAN JOURNAL OF TRANSPLANTOLOGY AND ARTIFICIAL ORGANS

УЧРЕДИТЕЛИ: ОБЩЕРОССИЙСКАЯ ОБЩЕСТВЕННАЯ ОРГАНИЗАЦИЯ ТРАНСПЛАНТОЛОГОВ «РОССИЙСКОЕ ТРАНСПЛАНТОЛОГИЧЕСКОЕ ОБЩЕСТВО»
ФГБУ «НМИЦ ТИО ИМЕНИ АКАДЕМИКА В.И. ШУМАКОВА» МИНЗДРАВА РОССИИ
ФГАОУ ВО ПЕРВЫЙ МГМУ ИМЕНИ И.М. СЕЧЕНОВА МИНЗДРАВА РОССИИ (СЕЧЕНОВСКИЙ УНИВЕРСИТЕТ)

THE OFFICIAL JOURNAL OF ALL-RUSSIAN PUBLIC ORGANIZATION OF TRANSPLANTOLOGISTS "RUSSIAN TRANSPLANT SOCIETY"
SHUMAKOV NATIONAL MEDICAL RESEARCH CENTER OF TRANSPLANTOLOGY AND ARTIFICIAL ORGANS
I.M. SECHENOV FIRST MOSCOW STATE MEDICAL UNIVERSITY (SECHENOV UNIVERSITY)

2023. Том XXV. № 2

2023. Vol. XXV. № 2

Научно-практический журнал основан в 1999 г.
Регистр. № 018616

Scientific and Practical Journal was founded in 1999
Reg. № 018616

Журнал «Вестник трансплантологии и искусственных органов» включен ВАК РФ в перечень российских рецензируемых научных изданий, в которых должны быть опубликованы результаты диссертационных работ

Журнал «Вестник трансплантологии и искусственных органов» включен ФГБУ «НМИЦ ТИО им. ак. В.И. Шумакова» Минздрава России в перечень российских рецензируемых научных изданий, в которых должны быть опубликованы основные результаты исследований в рамках диссертаций, представляемых к защите в диссертационный совет ФГБУ «НМИЦ ТИО им. ак. В.И. Шумакова» Минздрава России

Журнал «Вестник трансплантологии и искусственных органов» индексируется в Scopus и размещен на платформе Web of Science Core Collection: Emerging Science Citation Index

"Russian Journal of Transplantology and Artificial Organs" is included in the list of leading peer-reviewed scientific publication editions, produced in the Russian Federation and is recommended for publication of primary results of dissertation research

"Russian Journal of transplantology and artificial organs" is included by the Federal State Budgetary Institution "Shumakov National Medical Research Center of Transplantology and Artificial Organs" of the Ministry of Health of Russia in the list of Russian peer-reviewed scientific publications in which the main results of research should be published within the framework of dissertations submitted for defense to the dissertation council of Shumakov National Medical Research Center of Transplantology and Artificial Organs

"Russian Journal of Transplantology and Artificial Organs" is indexed in Scopus and in the Emerging Science Citation Index of the Web of Science Core Collection

ISSN 1995-1191

Адрес для корреспонденции:

Россия, 123182, Москва, ул. Щукинская, 1
Тел./факс +7 (499) 193 87 62
E-mail: vestniktranspl@gmail.com
Интернет-сайт журнала: http://journal.transpl.ru
Научная электронная библиотека: http://elibrary.ru

Address for correspondence:

1, Shchukinskaya st., Moscow 123182, Russia
Tel./Fax +7 (499) 193 87 62
E-mail: vestniktranspl@gmail.com
Journal's web site: http://journal.transpl.ru
Scientific eLibrary: http://elibrary.ru

Подписной индекс в каталоге почты России – ПН380

СОДЕРЖАНИЕ

CONTENTS

ИННОВАЦИОННЫЕ РАЗРАБОТКИ ФГБУ «НМИЦ ТИО ИМ. АК. В.И. ШУМАКОВА» МИНЗДРАВА РОССИИ ОТМЕЧЕНЫ СРЕДИ ВАЖНЕЙШИХ ДОСТИЖЕНИЙ РОССИЙСКОЙ НАУКИ В 2022 ГОДУ

Глубокоуважаемые коллеги!

23 мая 2023 года в Москве в докладе президента Российской академии наук Г.Я. Красникова Общему собранию академии были представлены наиболее значимые научные достижения российских ученых как важнейший стратегический и интеллектуальный ресурс для решения приоритетных государственных задач. Речь идет об инновационных разработках, базирующихся на достижениях фундаментальной науки и направленных на обеспечение технологического суверенитета России.

Среди достижений в области медицины были отмечены разработанные в ФГБУ «НМИЦ трансплантологии и искусственных органов им. ак. В.И. Шумакова» Минздрава России методы и технологии для трансплантации жизненно важных органов у детей и взрослых, в частности технология изолированной перфузии донорских легких, позволяющая не только сохранять, но и реабилитировать донорский орган для трансплантации.

Созданы отечественные системы вспомогательного кровообращения для двухэтапной трансплантации сердца. Разработки

INNOVATIONS AT SHUMAKOV CENTER COUNTED AMONG THE MOST IMPORTANT ACHIEVEMENTS IN RUSSIAN SCIENCE IN 2022

Dear esteemed colleagues,

On May 23, 2023, the President of the Russian Academy of Sciences, Prof. Gennady Krasnikov, presented a report before the General Assembly, the Academy's supreme organ. Important strategic and intellectual resource for solving Russia's priority challenges were recognized as the most significant scientific achievements by Russian scientists. These are innovative developments based on breakthroughs in fundamental science and aimed at ensuring Russia's technological sovereignty.

Among the achievements recognized in the field of medicine were inventions developed at Shumakov National Medical Research Center of Transplantology and Artificial Organs. These were techniques and technologies for transplantation of vital organs in children and adults. Prominent among them is isolated lung perfusion, which has shown to be highly effective in preserving and rehabilitating donor organs for transplantation.

Included in the list of achievements are Russian-made circulatory support systems designed to facilitate two-stage heart transplant surgeries. The inventions are currently being mass

доведены до стадии серийного производства, имеется успешный опыт их клинического применения. Оригинальные конструкции отечественных систем вспомогательного кровообращения зарегистрированы в форме двух международных заявок на патенты. Завершены доклинические исследования первого в мире искусственного желудочка сердца для педиатрических пациентов.

Разработанные технологии обеспечивают увеличение доступности и числа трансплантаций сердца, легких для детей и взрослых, улучшение клинических результатов трансплантации, позволяют отказаться от зарубежных аналогов.

Представленные научные достижения НМИЦ ТИО им. ак. В.И. Шумакова в области трансплантологии и искусственных органов убедительно демонстрируют возможность успешного развития научных разработок российских ученых от идеи и фундаментальных исследований до серийного производства продукта и его клинического применения. Именно такой подход отвечает вызовам сегодняшнего дня.

С уважением,
главный редактор
академик РАН С.В. Готье

produced and have been successfully applied in clinical practice. Two international patents have been filed to protect the original designs of these circulatory assist systems. Preclinical studies of the world's first artificial heart ventricle for pediatric patients have been completed.

All these inventions have increased the availability and number of heart-lung transplants for children and adults, improved clinical transplant outcomes, and eliminated the need for foreign systems.

The presented scientific achievements by Shumakov National Medical Research Center of Transplantology and Artificial Organs demonstrate convincingly that scientific inventions of Russian scientists can be successfully developed from the idea and fundamental research to mass production of the product and clinical application. It is this approach that meets today's challenges.

Sincerely,

Sergey Gautier,
Editor-in-chief, Russian Journal of Transplantology and Artificial Organs.
Member, Russian Academy of Sciences

DOI: 10.15825/1995-1191-2023-2-8-14

INTEGRATED STRATEGY FOR PREVENTING DELAYED RENAL GRAFT FUNCTION

A.V. Shabunin[1, 2], O.B. Loran[1, 2], D.Yu. Pushkar[1], E.I. Veliev[1], M.G. Minina[1], P.A. Drozdov[1, 2], I.V. Nesterenko[1], D.A. Makeev[1], V.M. Sevostiyanov[1], O.S. Zhuravel[1], S.A. Astapovich[1], L.R. Karapetyan[1]

[1] Botkin Hospital, Moscow, Russian Federation
[2] Russian Medical Academy of Continuous Professional Education, Moscow, Russian Federation

Objective: to determine the efficacy and safety of an integrated strategy aimed at preventing delayed renal graft function (DGF). **Materials and methods.** From June 2018 to December 2022, 478 deceased-donor kidney transplants were performed at Botkin Hospital, Moscow. The patients were divided into two groups: Group I consisted of 128 patients who did not use the integrated strategy; Group II included 67 patients in whom the DGF prevention strategy was used at the perioperative stage. The integrated strategy involved the use of hypothermic oxygenated machine perfusion (HOPE) using expanded criteria donors, the use of a second warm ischemia (SWI) elimination device, personalized initial calcineurin inhibitor (CI) dosing, and use of alprostadil for high vascular resistance in renal graft arteries. **Results.** DGF occurred in 5 of 44 patients (11.4%) that used the integrated strategy, and in 13 of 44 patients (29.5%) in the control group. The differences were statistically significant ($p = 0.034$), there was a medium strength relationship between the traits ($V = 0.225$). The use of the integrated DGF prevention approach reduced the chances of developing DGF by a factor of 0.3 (95% CI: 0.1–0.95). The risk of DGF in the integrated strategy group was 61.3% of the risk of DGF in the non-strategy group, thus the relative risk (RR) is 1.63 (95% CI: 1.1–2.4). Median duration of graft function normalization was statistically significantly lower in group II: 5 (IQR: 3–9) versus 15 (IQR: 7–19) days ($p = 0.012$). Mean length of hospital stay was 19.1 ± 4.2 (95% CI: 14.5–26.1) bed-days in group I and 13.9 ± 3.4 (95% CI: 9.3–17.2) bed-days in group II. Differences in this indicator were also statistically significant ($p = 0.043$). **Conclusion.** The set of DGF prevention measures, developed at Botkin Hospital, evidence-based and implemented in clinical practice, can reduce the burden of modifiable risk factors of this complication significantly, thereby improving treatment outcomes for kidney transplant recipients considerably.

Keywords: kidney transplantation, delayed renal graft function, risk factors.

INTRODUCTION

According to 2021 annual data report from the United States Renal Data System (USRDS), the 5-year graft survival rate for recipients of kidney from a deceased donor was 77.6%, compared to 46.5% and 41.7% for patients on peritoneal dialysis and hemodialysis, respectively. Improvement in surgical technique, achievements in transplantation immunobiology, increased availability of kidney transplantation (KTx) as a result of better organ donation coordination [1–4], have made KTx the gold standard for treatment of patients with end-stage chronic kidney disease (CKD) without absolute contraindications [5, 6].

Organ shortage is a global problem in clinical transplantology. One of the justified steps to reduce its burden is the expansion of the donor pool through suboptimal donors (expanded criteria donors) [7]. The donation criteria expansion strategy, on one hand, allows increasing the availability of transplant care. On the other hand, however, the use of transplants obtained from suboptimal donors is associated with increased incidence of postoperative complications and shorter duration of graft functioning, which has been reported by many authors. One of such complications is DGF, which is associated both with a higher number of early postoperative complications and with worse long-term renal graft survival outcomes [8].

Previously, we have identified potentially modifiable risk factors for DGF [8] and preventive measures were developed for each of them to reduce their impact on renal graft [9–13].

The next stage of our work was to evaluate the effectiveness of the integrated strategy, which consisted of the combined use of HOPE, use of an SWI elimination device, personalized initial CI dosing, and use of alprostadil for high vascular resistance.

Corresponding author: Pavel Drozdov. Address: 15/8, Brusilov str., Moscow, 117148, Russian Federation. Phone: (962) 985-04-41. E-mail: dc.drozdov@gmail.com

MATERIALS AND METHODS

From June 2018 to December 2022, 478 deceased-donor kidney transplants were performed at Botkin Hospital, Moscow.

Patients were divided into two groups: Group I consisted of 128 patients in whom the integrated DGF prevention strategy was not applied; Group II included 67 patients who used the strategy. Patient mean age was 46.91 ± 9.9 (20–70) years. There were 49 women, mean age was 46.26 ± 9.4 (20–71) years. Men were 79, mean age was 47.14 ± 10.1 (20–71) years. All patients were diagnosed with stage 5 CKD. CKD developed in 72 patients (56.3%) against chronic glomerulonephritis, in 9 patients (7%) as a result of autosomal dominant polycystic kidney disease (ADPKD), in 8 patients (6.3%) as a result of diabetic nephropathy, in 7 patients (5.5%) as a result of chronic pyelonephritis, in 7 patients (5 in 6 (4.7%) against urogenital anomaly, in 5 patients (3.9%) against nephroangiosclerosis, in 5 patients (3.9%) against urolithiasis, in 5 patients (3.9%) against hemorrhagic vasculitis, and in 4 patients (3.0%) against focal segmental glomerulosclerosis. There were 99 patients (77.3%) on hemodialysis, 23 patients (17.9%) on peritoneal dialysis, and 6 patients (4.8%) on predialysis. Preoperative diuresis was present in 81 patients (63.2%) and absent in 47 (36.8%). This was the first KTx for 107 patients (83.6%), the second for 20 (15.6%) patients, and the third for 1 (0.8%) patient. Median recipient BMI was 25.08 (IQR: 21–33) kg/m^2. Increased levels of preexisting class I antibodies were observed in 6 patients (4.7%), and class II in 8 patients (6.3%).

In all cases, KTx was performed from a deceased donor. The kidney donor was recognized as a standard donor in 86 cases (67.2%), as an expanded criteria donor in 40 cases (31.3%) and as a donor after cardiac death in 2 cases (1.5%). Median donor age was 47 (IQR: 41–55) years and BMI was 26.2 (IQR: 24.0–31.1) kg/m^2. Median creatinine levels and ICU length of stay were 87.37 (IQR: 70–93) μmol/L and 43 (IQR: 32.3–78.1) hours, respectively. Vasopressor support was used in 101 donors (78.9%), among whom 4/101 (3.9%) had a norepinephrine dose >1000 ng/kg/min or a second vasopressor was connected.

Median cold storage time was 10.1 (IQR: 8.2–12.5) hours. Median SWI time (vascular anastomosis formation) was 41 (IQR: 31–51) minutes. Mean operative time and intraoperative blood loss were 221.3 ± 44.5 (95% CI: 226.5–244.2) minutes and 115.3 ± 75.2 (95% CI: 113.4–134.2) mL, respectively. In all cases, intraoperative Doppler ultrasound of the renal graft was performed with determination of arterial resistivity index (RI), the median of which was 0.7 (IQR: 0.63–0.85). A standard technique was used to reduce the effect of SWI. A triple-therapy regimen consisting of prolonged-release tacrolimus, mycophenolic acid derivatives and methylprednisolone was used in all cases as immunosuppressive therapy in the early postoperative period. Basiliximab was used intraoperatively in all cases for induction and on day 4. Similarly, 500 mg of methylprednisolone was administered intraoperatively on days 3 and 5. The target tacrolimus trough level in the early postoperative period was 10–12 ng/mL.

Group II included 67 patients in whom the integrated strategy to the prevention of DGF was used at the perioperative stage. Mean patient age was 45.53 ± 10.7 (20–71) years. There were 22 women, the mean age was 45.43 ± 10.6 (21–72) years. Men were 45, mean age was 45.67 ± 10.1 (20–72) years. All patients were diagnosed with stage 5 CKD. In 35 patients (52.3%) CKD developed against chronic glomerulonephritis, in 8 patients (11.9%) against ADPKD, in 8 patients (11.9%) against diabetic nephropathy, in 6 patients (9%) against chronic pyelonephritis, in 6 patients (9%) against chronic tubulointerstitial nephritis, and in 4 patients (5.9%) against urogenital anomaly. There were 59 patients (88%) on hemodialysis, 6 patients (9%) on peritoneal dialysis, and 2 patients (3%) on predialysis. Preoperative diuresis was present in 52 patients (77.6%) and absent in 15 (22.4%). This was the first KTx for 64 patients (95.5%) and the second for 3 (4.5%) patients. Median recipient BMI was 25.66 (IQR: 21–32) kg/m^2. Increased levels of preexisting class I antibodies were found in 4 patients (5.9%), and class II in 7 patients (10.4%).

In all cases, KTx was performed from a deceased donor. The kidney donor was recognized as a standard donor in 35 cases (52.2%), as an expanded criteria donor in 26 cases (38.8%) and as a donor after cardiac death in 6 cases (9%). Median donor age was 49.6 (IQR: 45–56) years and BMI was 26.9 (IQR: 24.6–31.3) kg/m^2. Median creatinine levels and ICU length of stay were 89.9 (IQR: 74–98) μmol/L and 45 (IQR: 32.3–78.1) hours, respectively. Vasopressor support was used in 56 donors (83.5%), among whom 4/56 (7.1%) had a norepinephrine dose >1000 ng/kg/min or a second vasopressor was connected.

The average perfusion time was 211.35 ± 42.67 (180–320) minutes. When perfusion was performed, median static hypothermic preservation time was 278.35 ± 94.26 (250–450) minutes. Median SWI time (vascular anastomosis formation) was 40 (IQR: 31–52) minutes. A device developed at the clinic was used to reduce the effect of SWI. Mean operative time and intraoperative blood loss were 219.3 ± 45.3 (95% CI: 214.7–249.5) minutes and 117.9 ± 74.1 (95% CI: 115.3–140.9) mL, respectively. In all cases, intraoperative Doppler ultrasound of the renal graft was performed with determination of RI, the median being 0.76 (IQR: 0.6–1). To correct RI, patients in this group received continuous infusion of alprostadil at a dose of 120 μg per day. A triple-therapy regimen consisting of prolonged-release tacrolimus, mycophenolic acid derivatives and methylprednisolone was used

in all cases as immunosuppressive therapy in the early postoperative period. Basiliximab was used for induction in all cases intraoperatively and on day 4. Basiliximab was used intraoperatively in all cases for induction and on day 4. Similarly, 500 mg of methylprednisolone was administered intraoperatively on days 3 and 5. The starting tacrolimus dose taken by the patient before surgery was determined individually based on the patient's age and weight. Target tacrolimus trough level in the early postoperative period was 10–12 ng/mL.

Methods and statistical analysis

The exclusion criteria for both groups were the following: primary nonfunction, postoperative complica-

Table 1

Comparative characteristics of perioperative factors in groups I and II

Indicator	Group I (n = 128)	Group II (n = 67)	p
Sex: *Male* *Female*	 80 48	 44 22	0.871
Average age (years)	44.34 ± 13.47	45.53 ± 10.7	0.981
Diagnosis: *Chronic glomerulonephritis* *Polycystic kidney disease* *Diabetic nephropathy* *Chronic pyelonephritis* *Chronic tubulointerstitial nephritis* *Urolithiasis* *Developmental anomaly* *Hemorrhagic vasculitis* *Hypertensive nephroangiosclerosis*	 75 12 11 8 7 3 7 2 2 1	 35 8 8 6 6 0 4 0 0 0	0.645
Diuresis: *Adequate* *Oligoanuria*	 83 45	 52 15	0.798
Dialysis: *Hemodialysis* *Peritoneal dialysis* *Pre-dialysis patient*	 98 22 8	 59 8 2	0.674
Transplant history: *First transplantation* *Second transplantation* *Third transplantation*	 109 19 0	 64 3 0	0.791
Increased pre-existing antibodies: *Class I* *Class II*	 8 9	 4 7	0.77
Recipient median body mass index (kg/m^2)	24.26	25.66	0.453
Donor type: *Standard DBD donor* *Expanded criteria DBD donor* *DCD donor*	 83 44 1	 35 26 6	 0.56 ***0.007**
Donor median age (years)	42.3	49.6	***0.042**
Donor median body mass index (kg/m^2)	24.7	26.9	0.85
Donor median creatinine level (μmol/L)	88.2	89.9	0.873
Donor median length of hospital stay (hours)	47	45	0.76
Donor vasopressor support: *No* *Yes*	 19 109	 11 56	0.59
Mean total hypothermic preservation time (static + oxygenated perfusion) (minutes)	661.45 ± 159.4	649 ± 123.8	0.341
Average hypothermic oxygenated machine perfusion (minutes)	0	214.7 ± 49.1	***<0.001**
Median second warm ischemia time (minutes)	43	40	0.74
Mean surgical time (minutes)	239.2 ± 51.4	219.3 ± 45.3	0.125
Median blood loss volume (mL)	134.3 ± 82.9	117.9 ± 74.1	0.229
Median intraoperative resistive index	0.72	0.73	0.94

tions requiring emergency graftectomy in the first week after transplantation, and recipient death in the first 7 days. The groups were comparable in terms of basic recipient characteristics, perioperative parameters, and a number of donor characteristics except for age ($p = 0.042$) and proportion of asystolic donors ($p = 0.007$). Detailed comparative characteristics are presented in Table 1.

Due to significant differences in two important risk factors for DGF – donor age and frequency of donors after cardiac death (DCD) ($p = 0.047$ and $p < 0.001$, respectively) – we performed pseudorandomization of the compared groups by PSM (0.1 compliance (or matching or conformity) tolerance). The resulting pseudorandomization groups had 44 patients each and were comparable for donor age ($p = 0.732$) and proportion of DCD donors ($p = 0.612$).

RESULTS

Analysis of the immediate results in the two study groups after pseudorandomization showed that DGF developed in 5 of 44 patients (11.4%) in the integrated strategy group, and in 13 of 44 patients (29.5%) in the control group. The differences were statistically significant ($p = 0.034$) and there was a medium strength relationship between the traits ($V = 0.225$). The use of the integrated preventive strategy reduced the chances of developing DGF by a factor of 0.3 (95% CI: 0.1–0.95). The risk of DGF in the integrated strategy group was 61.3% of the risk of DGF in the group that did not use the strategy, thus RR = 1.63 (95% CI: 1.1–2.4). Median duration of graft function normalization was statistically significantly lower in group V: 5 (IQR: 3–9) versus 15 (IQR: 7–19) days ($p = 0.012$). Mean length of hospital stay was 19.1 ± 4.2 (95% CI: 14.5–26.1) bed-days in group I and 13.9 ± 3.4 (95% CI: 9.3–17.2) bed-days in group V. Differences in this indicator were also statistically significant ($p = 0.043$).

Clinical outcomes of treatment of kidney recipients in groups I and II before and after pseudorandomization are presented in Table 2.

DISCUSSION

DGF is a multifactorial problem that has a significant negative impact on both immediate and long-term outcomes of KTx. This complication is enhanced significantly by donor characteristics that transplant physicians cannot correct. At the same time, there are a number of factors that can have an additional damaging effect on the renal graft at the stage of preservation (static hypothermic preservation time), surgery (SWI time) and in the early postoperative period (nephrotoxicity of CIs, increased vascular resistance). The more donor-associated risk factors for DGF, the more attention should be paid to the correction of perioperative risk factors.

In our opinion, correction of potentially modifiable risk factors should be carried out at all the above stages – preservation, surgery and in the early postoperative period – since mitochondrial damage in kidney graft cells can be prevented using HOPE, but severe ischemia-reperfusion injury can be caused due to prolonged SWI with development of high vascular resistance with impaired perfusion of the renal graft cortex. On the other hand, a short SWI time and a perfectly selected initial CI dose are not able to prevent severe ischemia-reperfusion injury during prolonged static hypothermic preservation with cell organelle death.

Clinical data obtained demonstrate the benefits of our integrated DGF prevention strategy, which consists of the use of HOPE for expanded criteria donors, the use of an SWI elimination device, personalized initial CI dosing, and the use of alprostadil for high vascular resistance in renal graft arteries. There was a significant decrease in DGF incidence ($p = 0.034$) and median duration of DGF ($p = 0.012$) compared with the control group. This led to shorter average length of hospital stay ($p = 0.043$).

CONCLUSION

The set of DGF prevention measures, which were developed at Botkin Hospital, evidence-based and implemented in clinical practice, can reduce the burden of modifiable risk factors of this complication significantly,

Table 2

Comparative analysis of treatment outcomes in groups I and II before and after pseudorandomization

Indicator	Pre-pseudorandomization			Post-pseudorandomization		
	Group I (n = 128)	Group VI (n = 67)	p	Group I (n = 44)	Group VI (n = 44)	p
Donor median age (years)	42.3	49.6	***0.042**	46.7	47.1	0.732
Proportion of asystolic donors	1/128 (0.8%)	6/67 (9%)	***<0.001**	1/44 (2%)	3/44 (7%)	0.612
Frequency of DGF	37/128 (28.9%)	15/67 (22.4%)	0.609	13/44 (29.5%)	5/44 (11.4%)	***0.034**
Median DGF duration (days)	13	6	***0.029**	15	5	***0.012**
Average length of hospital stay (bed-days)	16.21 ± 8.4	15.37 ± 4.2	0.312	19.1 ± 4.2	13.9 ± 3.4	***0.043**
Incidence of all complications	22/128 (22%)	6/67 (8.9%)	0.134	12/44 (27.3%)	3/44 (6.8%)	0.27
Incidence of acute graft rejection	0	1/67 (1.4%)	0.89	0	0	1
In-hospital mortality	0	0	1	0	0	1

thereby improving treatment outcomes for kidney transplant recipients considerably.

The authors declare no conflict of interest.

REFERENCES

1. *Johansen KL, Chertow GM, Foley RN, Gilbertson DT, Herzog CA, Ishani A*. US Renal Data System 2020 Annual Data Report: Epidemiology of Kidney Disease in the United States. Am J Kidney Dis. 2021; 77 (4): A7–A8. PMID: 33752804. https://doi.org/10.1053/j.ajkd.2021.01.002.
2. *Minina MG, Ignatov NA, Trukhmanov RB*. Mathematical analysis of the need and availability of donor kidneys for transplantation. *Russian Journal of Transplantology and Artificial Organs*. 2018; 19 (4): 27–33.
3. *Pinchuk AV, Vinogradov VL, Minina MG*. Ethical aspects of the concept of brain death. *Transplantologiya. The Russian Journal of Transplantation*. 2013; 2: 28–33.
4. *Minina MG*. Reasons for the ineffective development of organ donation. *Transplantologiya. The Russian Journal of Transplantation*. 2011; 1: 71–75. https://doi.org/10.23873/2074-0506-2011-0-1-71-74.
5. *Gautier SV, Khomyakov SM*. Organ donation and transplantation in the Russian Federation in 2019. 12th report from the Registry of the Russian Transplant Society. *Russian Journal of Transplantology and Artificial Organs*. 2020; 22 (2): 8–34. https://doi.org/10.15825/1995-1191-2020-2-8-34.
6. *Andrusev AM, Tomilina NA, Peregudova NG*. Kidney replacement therapy for end stage kidney disease in russian federation, 2015–2019. Russian national kidney replacement therapy registry report of russian public organization of nephrologists Russian Dialysis Society. *Nephrology and dialysis*. 2021; 23 (3): 255–329.
7. *Nesterenko IM, Vatazin AV, Filiptsev PYa et al*. Morphological evaluation of renal transplants obtained from marginal donors. *Russian Journal of Transplantology and Artificial Organs*. 2008; 1: 65–68.
8. *Shabunin AV, Drozdov PA, Nesterenko IV, Makeev DA, Zhuravel OS, Astapovich SA*. Risk factors for delayed kidney graft function from a deseased donor. *Transplantologiya. The Russian Journal of Transplantation*. 2022; 14 (3): 265–277. https://doi.org/10.23873/2074-0506-2022-14-3-265-277.
9. *Shabunin AV, Minina MG, Drozdov PV, Nesterenko IV, Makeev DA, Zhuravel OS et al*. Early experiments with hypothermic oxygenated machine perfusion of kidney grafts from extended criteria donors. *Russian Journal of Transplantology and Artificial Organs*. 2022; 24 (1): 143–150. https://doi.org/10.15825/1995-1191-2022-1-143-150.
10. *Drozdov PA, Shabunin AV*. Sposob gipotermicheskoy oksigenirovannoy perfuzii v transplantatsii pecheni i pochki. Patent na izobretenie № 2773291.
11. *Shabunin AV, Drozdov PA, Nesterenko IV, Makeev DA, Astapovich SA*. Ustroystvo dlya eliminatsii vtorichnoy teplovoy ishemii pri transplantatsii pochki. Patent na izobretenie № 2783671.
12. *Drozdov PA, Nesterenko IV, Makeev DA, Zhuravel OS, Astapovich SA, Solomatin DA, Lidzhieva EA*. Influence of alprostadil on the dynamics of blood flow resistance index and renal graft function in the early postoperative period. *Transplantologiya. The Russian Journal of Transplantation*. 2022; 14 (4): 452–461. https://doi.org/10.23873/2074-0506-2022-14-4-452-461.
13. *Shabunin AV, Drozdov PA, Makeev DA, Nesterenko IV, Zhuravel OS, Karapetyan LR et al*. Personalized dosing protocol for extended-release tacrolimus in kidney transplant recipients in the early postoperative period. *Russian Journal of Transplantology and Artificial Organs*. 2023; 25 (1): 52–61. (In Russ.). https://doi.org/10.15825/1995-1191-2023-1-52-61.

The article was submitted to the journal on 13.04.2023

DOI: 10.15825/1995-1191-2023-2-15-25

CHOICE OF TREATMENT METHOD FOR SYMPTOMATIC BLADDER OUTLET OBSTRUCTION IN PATIENTS WITH BENIGN PROSTATIC HYPERPLASIA AFTER KIDNEY TRANSPLANTATION

S.V. Popov[1], R.G. Huseynov[1, 3], D.A. Saydulaev[2], S.V. Sadovnikov[2], Yu.V. Kisil[1], K.V. Sivak[1], N.S. Bunenkov[1, 4, 5], V.V. Perepelitsa[1], A.S. Ulitina[1, 4], T.A. Lelyavina[5]

[1] St. Luke's Clinical Hospital, St. Petersburg, Russian Federation
[2] Shumakov National Medical Research Center of Transplantology and Artificial Organs, Moscow, Russian Federation
[3] St. Petersburg State University, St. Petersburg, Russian Federation
[4] Pavlov University, St. Petersburg, Russian Federation
[5] Almazov National Medical Research Centre, St. Petersburg, Russian Federation

The paper presents a comparative assessment of different methods of treating symptomatic bladder outlet obstruction (BOO) in patients with benign prostatic hyperplasia (BPH) who underwent kidney transplantation (KT).

Keywords: bladder outlet obstruction, benign prostatic hyperplasia, kidney transplantation.

INTRODUCTION

Ninety-one years ago, on April 3, 1932, Soviet surgeon, Yury Voronoy, performed the first kidney transplantation (KT) in the world. Since then, there have been major breakthroughs in the field of KT in Russia and around the world [1–3]. KT is championed as the gold standard treatment for patients with end-stage kidney failure [3].

In 2018, over 95,000 KTs were performed worldwide [1]. In the Russian Federation, the number of kidney transplant surgeries increases every year [2].

In the early and late post-KT period, there is a high likelihood of various complications [4–8]. Urological complications in KT recipients, whose incidence is 3–14%, causes longer hospital stay, graft dysfunction and increased mortality [5–10]. One of the complications is bladder outlet obstruction (BOO) in the background of benign prostatic hyperplasia (BPH) [5, 6, 8, 11].

At the same time, the incidence of BPH-associated BOO in the postoperative period increases every year, as the age of recipients increases [4–8, 11, 12]. Urological problems in transplanted kidney recipients are associated with decreased graft survival and lead to higher morbidity and mortality [13–17].

The age of kidney transplant recipients increases every year and, on average, exceeds 55 years [14]. However, it should be taken into account that 50–70% of men over 50 years of age present with lower urinary tract symptoms (LUTS) associated with BPH; LUTS prevalence reaches 80% in men aged 80 [17].

In the pre-transplant period, against oliguria accompanying chronic kidney disease, symptoms of chronic urinary fade into the background and do not bother the patient. The patient may have no characteristic complaints. Whereas after successful KT, manifestations of BOO on the background of BPH increase and significantly worsen the quality of life (QoL) of patients.

In recent years, there have been significant advances in the treatment of urological complications, largely due to advances in therapy [6–16, 18–21]. A comparative analysis of the availability and efficacy of different methods of treatment of BOO against BPH in kidney transplant recipients is presented in this review.

METHODS OF TREATING SYMPTOMATIC BOO IN BPH PATIENTS WHO UNDERWENT KIDNEY TRANSPLANTATION

Treatment of BOO in KT recipients can be therapeutic, surgical, or combined [18, 19].

It is necessary that the above approaches be personalized after analyzing the comorbidities, age of the patient, size of the prostate gland, etc. [20–27]. After careful examination, the patient's management tactics are determined: dynamic monitoring, drug therapy or surgical treatment [20–26]. Surgical treatment is indicated if conservative approaches to BOO therapy fail [20–27].

Drug therapy for BOO in BPH patients who underwent kidney transplantation

Given the progressive nature of the disease, BPH medication therapy is carried out for a long time, in some patients – for theшк entire life. In BPH treatment in all patients, several kinds of medicines are used. However, the basic therapy consists of three groups of drugs: alpha-1 blockers (A1Bs, adrenergic alpha-1 receptor ant-

Corresponding author: Tatiana Lelyavina. Address: 2, Akkuratova str., St. Petersburg, 197341, Russian Federation. Phone: (981) 908-90-18. E-mail: tatianalelyavina@mail.ru

agonists), 5-alpha-reductase inhibitors (5-ARIs), phosphodiesterase type 5 (PDE5) inhibitors [20–26, 28–31].

In the general population, drug treatment of BPH-associated LUTS in kidney transplant recipients initially includes alpha blockers and finasteride in most cases [31]. Medication therapy with A1Bs can be used as the first stage of treatment. Adrenergic alpha-1 receptor antagonists are first-line drugs and are used for moderate to severe lower urinary tract syndromes. The action of these drugs begins 48 hours after intake [28, 30].

Currently, five drugs of this group are used in clinical practice: alfuzosin, doxazosin, silodosin, tamsulosin, terazosin [28, 30, 32–34]. The differences between the listed drugs lie in their tolerability, which is due to their pharmacodynamics and pharmacokinetics. A1Bs are effective in correcting LUTS symptoms, but do not reduce prostate size or protect against the development of acute urinary retention in the long term. Tamsulosin is the most commonly used A1Bs in the world [28, 33].

Several randomized, placebo-controlled clinical trials (RPCCTs): three phase III RPCCTs and two phase IV RPCCTs have been performed to investigate the effectiveness of A1Bs in a subgroup of patients with severe BOO [28, 30, 32, 33].

Disease severity was assessed by two or more of the following criteria: International Prostate Symptom Score (IPSS), QoL score, maximum urinary output (Q_{max}) <5 mL/s or residual bladder volume ≥100 mL, prostate volume ≥50 mL [30]. The main endpoint of the study was the change in IPSS score relative to baseline.

Comparison of silodosin and placebo among patients with severe LUTS revealed statistically significant differences in favor of the active treatment group compared to the placebo group in terms of improvements in QoL, IPSS, its subscores, and Q_{max}. 53% of patients with severe LUTS and a baseline total IPSS score ≥20 included in a phase III placebo-controlled RPCCT showed an 8–19 improvement in IPSS scores after treatment, 10.2% improved their IPSS score by 0–7 points, and 36.8% showed no significant improvement from baseline. The corresponding figures for patients receiving placebo were 36.6%, 4.8%, and 58.6%. The proportion of patients receiving silodosin who reported improvement (5–6 to 0–4), no effect, and worsening (0–4 to 5–6) of QoL scores was 44.2%, 54.7%, and 1.1%, respectively, and the same rates among patients receiving placebo were 26.4%, 70.6%, and 3.0% ($p = 0.0009$) [30].

Thus, silodosin monotherapy provides statistically significant clinical improvement in the group of patients with severe BOO. These results correlate with the data obtained in the study of patients receiving tamsulosin or alfuzosin, and confirm the favorable pharmacodynamic effect of this class of drugs [30, 32]. It was noted that IPSS scores in patients with severe LUTS against the background of tamsulosin therapy at a dose of 0.4 mg/day improved by an average of 5.8–14.3 points [30].

AB are more effective in severe than in minor manifestations of LUTS [31]. Debruyne et al. [30] found mean improvements in IPSS scores assessing bladder filling and emptying by 1.9 and 3.9 points, respectively, among patients with severe BOO who received tamsulosin at a dose of 0.4 mg/day. These results support the assumption that the effect of AB is mainly to reduce obstruction. Also Debruyne et al. [30] showed an improvement in QoL after 12 months of treatment with tamsulosin 0.4 mg/day. Improvement in Q_{max} was clinically insignificant. This conclusion is consistent with previously published data demonstrating non-significant correlations between improvements in IPSS parameters and changes in Q_{max} results against the background of AB therapy [32].

Incomplete reported data on prostate volume, residual urine volume, adverse events (AEs), and isolated outcomes and consequences constitutes a limitation of the aforementioned RPCCTs [28, 30, 32, 33]. As a consequence, results must be interpreted with caution, since severe BOO symptoms may be associated with late stages of bladder wall remodeling [34].

Nevertheless, it can be concluded that daily AB administration significantly improves QoL against the background of reduced severity of BOO, especially in patients with severe LUTS [23, 33]. In this group, drugs provide a 30–40% reduction in the IPSS score and remain effective for several years [35, 36]. Adverse events associated with the use of alpha-blockers include abnormal ejaculation due to decreased or absent seminal fluid, dizziness, and postural hypotension [35, 36].

In moderate to severe LUTS, prostate volume exceeding 40 cm^3, 5-alpha-reductase inhibitors, dutasteride and finasteride, are prescribed and are associated with a reduced risk of BPH progression against a reduced incidence of acute urinary retention [36–39].

5-alpha-reductase inhibitors help to reduce IPSS by 15–30%, reduce prostate volume threefold from the initial volume, increase in Q_{max} by 1.5–2 ml/s, reduce the risk of acute urinary retention, and reduce the frequency of surgical interventions in a long-term (more than 1 year) run. The effect of this group of drugs comes slower than that of 5-ARIs, and is more noticeable with large prostate volumes. Adverse events observed in patients receiving 5-ARIs, include erectile dysfunction, decreased libido and less often ejaculatory dysfunction, retrograde ejaculation and gynecomastia [23].

Muscarinic receptor antagonists can be used against a background of moderate to severe LUTS, although this group of drugs is associated with increased incidence of acute urinary retention [20, 22–24].

With BPH progression and with large prostate gland volume, large residual urine volume, low Q_{max}, and age >62 years, surgical treatment should be considered [40].

Non-drug methods of treatment of symptomatic BOO in BPH patients who have undergone kidney transplantation

Until the 1970s, the only available treatment and relief for LUTS was open adenomectomy (for very large prostate) or endoscopic surgery in the form of transurethral resection to remove or resect prostatic tissue [41].

In the general population, surgical procedures performed for infravesical obstruction in patients with BPH who have undergone renal transplantation include minimally invasive surgical treatments, such as laser techniques, vaporization techniques, mono- and bipolar resections, open, laparoscopic and robotic adenomectomy, etc. [18, 19, 21, 42, 43].

Transurethral resection of the prostate (TURP) is one of the methods of surgical treatment of BOO against BPH in kidney transplant recipients [44–47]. Against the background of the high efficiency of TURP in controlling LUTS, long-term adverse effects or adverse events, such as erectile and ejaculatory dysfunction, risk of urinary incontinence, and other complications, have been noted [44–48].

Minimally invasive surgical treatments have emerged as an alternative to TURP, successfully reducing BOO symptoms, while minimizing side effects and complications, and reducing the length of hospital stay [43]. These include transurethral electrovaporization (Rezūm technique), transurethral enucleation, laser enucleation, urolifting, and temporary implantable nitinol device [43].

Electrovaporization involves vaporization of the prostate using high-frequency and high-power currents with coagulation of the underlying layers, without capillary bleeding and without coagulation of large vessels and venous sinuses [49, 50]. *Bipolar vaporization* involves simultaneous bipolar resection and vaporization [49, 50].

Rezūm water vapor thermal therapy (Rezūm System, Boston Scientific, Marlborough, Massachusetts) is an innovative minimally invasive surgical treatment approved by the US Food and Drug Administration (FDA) in 2015 to reduce prostate tissue volume associated with BPH, including central zone and/or middle lobe hyperplasia [49–50]. The accumulated thermal energy (540 calories/ml H_2O) is transferred as vapor to the prostate tissue. Thermal effects do not occur beyond the target treatment area [49, 50], thus eliminating the limitations of conductive heat transfer seen in transurethral needle ablation of the prostate (TUNA) and transurethral microwave thermotherapy (TUMT) [51–54].

The most unique feature of this technique is the possibility to influence the lateral and central zones of the prostate gland. Complex anatomical variants, such as intravesical prostatic protrusion, can be treated without affecting sexual function [53]. This technique has been used throughout the United States and Europe for 5 years since FDA approval [49–58]. According to the multicenter, prospective, blinded, controlled trial of water vapor heat therapy (Rezūm II Study, NCT01912339), the wide use of this technique is attributed to sustained relief of LUTS, improved QoL, and long-term response to treatment [49–58]. An RPCCT (Rezūm II Study, NCT01912339) showed that BPH heat therapy has clinically significant results and a proven long-term effect [49, 51–53]. Five years after the procedure, a 30% improvement in IPSS and no recurrence of BPH were found [49–57]. Despite the fact that the majority of patients had pronounced manifestations of LUTS at inclusion in the study (72.5% with IPSS 19–35), these parameters improved in comparison with the initial ones 3 months after a single water vapor heat therapy procedure, without a negative effect on erectile function [49–58].

Other minimal surgical techniques, such as prostatic urethral lift (PUL) or other implantable devices, provide symptomatic relief without tissue removal [59–61]. However, repeated interventions are required to achieve a permanent reduction in LUTS severity with urethral lift surgery [60, 61].

Patients in the general population who may be candidates for water vapor thermal therapy are often referred for more invasive surgical techniques such as TURP, holmium laser enucleation of the prostate, or other treatments that have a high risk of bleeding, longer recovery time, reduced erectile function, and other undesirable side effects [62–65].

In 2018, a study was performed on the long-term outcomes of treatment of lower urinary tract symptoms caused by BPH using a single Rezūm® System water vapor thermotherapy treatment with daily drug therapy: doxazosin and/or finasteride [63]. Thermal therapy resulted in a 50% improvement in IPSS scores at 36 months ($p < 0.0001$). The improvement in symptoms was more pronounced than with one of the drugs, but similar to that with the combined drugs ($p \leq 0.02$ and 0.73, respectively). Q_{max} improved by 4–5 mL per second after thermal therapy and doxazosin, while thermal therapy was superior to finasteride and combination drugs at 24 and 12 months.

Thus, a single session of water vapor thermal therapy provided effective and sustained improvement in symptom scores with a lower observed rate of clinical progression compared with daily long-term use of pharmaceuticals [63].

High-tech methods of LUTS treatment, such as transurethral enucleation of the prostate with a holmium or thulium laser, are now widely used [66–69].

Laser enucleation involves excising the prostate gland up to its surgical capsule, and the enucleated tissue is then moved into the bladder and removed [66–69]. *Holmium laser enucleation of the prostate (HoLEP)* is used for moderate to severe LUTS against a prostate volume exceeding 80 cm^3 [67, 68], and the risk of bleeding against anticoagulant therapy is reduced.

In 2020, data from a multicenter, retrospective pilot comparative study of the efficacy, safety and complications, registered within 1 year, after the following interventions were published: holmium laser enucleation of the prostate, greenlight photoselective vaporization of the prostate (GL-PVP) and TURP performed after KT [70].

From January 2013 to April 2018, 60 BPH endoscopic surgical procedures in KT recipients were performed: 17 patients in the HoLEP group, 9 in the GL-PVP group, and 34 in the TURP group. Age, body mass index, preoperative serum creatinine, preoperative IPSS score, preoperative Q_{max}, preoperative prostate-specific antigen, medical history of acute urinary retention, urinary tract infection and indwelling urethral catheter were similar in all study groups. Mean preoperative prostate volume was higher in the HoLEP group. The rate of overall postoperative complications was statistically higher in the HoLEP group (11/17 [64.7%] vs 1/9 [11.1%] vs 12/34 [35.3%] in HoLEP group, GL PVP group, and TURP group, respectively, p = 0.02). After interventions, Q_{max} were comparably improved in both groups [70].

Considering the above data, it can be concluded that the rate of postoperative complications is higher with HoLEP procedure, in comparison with GL-PVP, for the treatment of BPH after KT [70]. One-year efficacy is similar in HoLEP, GL PVP, and TURP groups [70].

One year later, data from a study was published to compare the efficacy and safety of water vapor thermal therapy using the Rezūm™ system and PUL using the Urolift™ system in men with lower urinary tract symptoms due to BPH [71].

From December 2017 to November 2019, consecutive patients who underwent Rezūm™ and Urolift™ procedures in two urology centers were retrospectively considered. Only patients with a prostate size less than 80 mL were included.

A total of 61 (52.1%) and 56 (47.9%) patients underwent Rezum™ and Urolift™ procedures, respectively. At 12 months, higher IPSS improvement was observed in the Rezum™ group (median:4 [IQR 3–5]) than in the Urolift™ group (median:8 [IQR 7–12]), without statistical difference (p = 0.08). Improvement in QoL at 12 months was similar in the two groups (p = 0.43). Reintervention rates were 25% (Urolift™) and 8.3% (Rezum™), p = 0.24. Erection and ejaculatory function scores did not change significantly in either treatment group.

Results have shown that both Rezum™ and Urolift™ provide clinically significant improvements in symptoms and QoL, although the Rezum™ procedure appeared to be more effective in the immediate and long-term postoperative period [71].

TURP is the gold standard treatment for BPH in 30–80 cm^3 prostate volumes with moderate to severe LUTS [18–21]. *Monopolar TURP* is a well-established option for surgical treatment of BOO due to benign prostatic enlargement. However, this intervention continues to be associated with a significant risk of postoperative complications [72]. In the light of this, new techniques have been developed to reduce the risk of complications. Unlike monopolar TURP, *bipolar TURP* uses energy confined between the active electrode (resection loop) and the return electrode located on the resectoscope tip or sheath, and lower voltage, theoretically eliminating the risk of TURP syndrome and reducing thermal damage to surrounding tissue [72].

Despite existing studies on the efficacy and safety of monopolar and bipolar TURP over the past decade, there remains uncertainty about the differences between these two surgical techniques. Systematic reviews published prior to 2020 that compared these surgical techniques [73–78] did not include a significant number of recently published randomized controlled trials and did not always adhere to strict methodological standards.

A comprehensive systematic electronic literature search was carried out up to 19 March 2019 via CENTRAL, MEDLINE, Embase, ClinicalTrials.gov, PubMed, and WHO ICTRP. Handsearching of abstract proceedings of major urological conferences and of reference lists of included trials, systematic reviews, and health technology assessment reports was undertaken to identify other potentially eligible studies. No language restrictions were applied. Randomized controlled trials, comparing monopolar and bipolar TURP in men (>18 years) for the treatment of LUTS secondary to BPH, were selected.

A total of 59 RPCCTs with 8924 participants were included. The mean age of the included participants was 67 years; mean prostate volume was 39–83 cm^3.

Based on the results of this review, it was shown that bipolar TURP and monopolar TURP relieve LUTS both to a similar degree. Bipolar TURP probably reduces the severity of clinical manifestations of TURP syndrome and postoperative blood transfusion compared to monopolar TURP. The impact of both procedures on erectile function is probably similar. The moderate certainty of evidence available for the primary outcomes of this review suggests that there is no need for further RPCCTs comparing bipolar TURP and monopolar TURP [70]. The most severe complication after prostate gland TURP, with an incidence >7%, is bleeding requiring blood transfusion [70].

In patients in the general population with prostate gland volume <30 cm^3, *transurethral incision* of the prostate (TUIP) [79], in which electrosurgical dissection of the prostate gland tissue is performed using a resectoscope loop, is indicated [79].

According to a small study [80] of the early and long-term outcomes of TURP and TUIP procedures performed in the first month following KT, at a median of 19 days

(range 8–30 days), due to BOO against BPH, no AEs were found.

In the early postoperative period, 5 patients (13.1%) developed urinary tract infection. The mean Q_{max} (22.4 ± 11.1 mL/sec) increased significantly ($p < 0.001$). At the end of follow-up, the groups did not differ in Q_{max} and IPSS scores (P = .89, P = .27, P = .08, and P = .27). Among postoperative complications, the incidence of urinary tract infections and retrograde ejaculation was higher in the TURP than in the TUIP group (12.7% versus 6.2% and 68.1% versus 25%, respectively), whereas urethral strictures were more common in the TUIP group (12.5% versus 6.3%).

Thus, TURP and TUIP techniques have been shown to be equally safe and effective in the surgical treatment of BPH-induced urinary retention in KT recipients with a prostate volume <30 cm^3 [80, 81].

As shown above, prostate volume is the main criterion for choosing the method of surgical treatment of BPH [49–82].

Open adenomectomy is the most effective and unfortunately, the most invasive method of surgical treatment of BPH in patients with a prostate volume >80 cm^3. After this intervention, the effect is most durable [19–21].

Laparoscopic adenomectomy is a minimally invasive surgical procedure that is an alternative to open adenomectomy in patients with a prostate volume ≥90–100 cm^3 [19–21].

TUNA is less effective than TURP among patients in the general population; it is reserved for patients with severe comorbidities, as this procedure does not require hospitalization of the patient and general anesthesia [84].

In *prostate artery embolization*, blood arteries of the prostate gland are occluded by introducing emboli [85, 86]. With this intervention, acute urinary retention episodes are more frequent in the postoperative period [87].

Prostatic stent is used in patients with contraindications to surgical intervention. This procedure is accompanied by a temporary reduction in LUTS and frequent AEs, so its use is limited.

Robotic surgery has shown high efficiency on the background of significant correction of LUTS, exclusion of postoperative complications and fast recovery after surgery [83].

CONCLUSION

The kidney is the most transplantable organ in the world. In the early post-KT period, urinary retention caused by BOO can directly affect the success of transplantation. Accurate assessment and optimal treatment of LUTS in renal transplant candidates and recipients is crucial for improving the QoL and preserving allograft function [88–98].

LUTS should be carefully evaluated before KT. Postoperative symptoms of moderate to severe LUTS should be carefully investigated so that early intervention can prevent graft compromise and associated complications. If indicated, BOO surgery can be performed early after renal transplantation [99–101].

Evidence suggests that many of the proposed treatments for BPH-associated BOO developing after KT can offer effective relief of LUTS. Nevertheless, a number of factors may influence the personalized choice of a particular intervention for each patient. This decision depends on patient characteristics like age, comorbidities, severity of LUTS, concomitant treatment such as ongoing anticoagulant therapy and unpredictable drug interactions. It is necessary to balance the desired results with possible risks. Possible effects on sexual function, frequency of reoperation, and the cost of treatment must be considered.

Despite all the advantages of minimally invasive obstruction therapies, several obstacles limit their wider adoption, the first of which are equipment limitations. For example, urolifting requires a special elongated lens, and Rezūm requires a special computerized radiofrequency steam generator [102].

The second limitation in the new technology is the cost, which is well over €1,000 just for the equipment, in addition to the requirement to perform the procedures in specially designated operating conditions [102]. As cost-benefit analysis has shown, the cheaper minimally invasive methods were €900 more expensive than drug therapy for 2 years [102].

Based on a review of disparate literature data, there is insufficient evidence to offer a reliable recommendation for a specific treatment technique for BOO in all BPH kidney recipients. Further clinical trials with longer follow-up comparing different interventions with routine and evidence-based methods are required.

The authors declare no conflict of interest.

REFERENCES

1. Godovoy otchet o transplantologii v Evrope za 2019 god. https://www.eurotransplant.org/wp-content/uploads/2020/06/AnnualReport-2019.pdf.
2. *Gautier SV, Khomyakov SM.* Donorstvo i transplantatsiya organov v Rossiyskoy Federatsii v 2018 godu. XII soobshchenie Rossiyskogo transplantologicheskogo obshchestva. *Vestnik transplantologii i iskusstvennykh organov*. 2019; 21 (3): 7–32. https://doi.org/10.15825/1995-1191-2019.
3. *Kabanova SA, Bogopol'skiy PM.* Peresadka pochki: istoriya, itogi i perspektivy. *Transplantologiya*. 2015; (2): 49–58.
4. *Sultanov PK, Khadzhibaev FA, Ergashev DN, Ismatov AA*. Analiz oslozhneniy posle transplantatsii pochki. *Vestnik ekstrennoy meditsiny*. 2021; 14 (1): 55–63.
5. *Dos Santos Mantovani M, Coelho de Carvalho N, Archangelo TE, Modelli de Andrade LG, Pires Ferreira Filho S, de Souza Cavalcante R et al*. Frailty predicts surgical complications after kidney transplantation.

A propensity score matched study. *PLoS One*. 2020 Feb 26; 15 (2): e0229531.
6. *Bessede T, Hammoudi Y, Bedretdinova D, Parier B, Francois H, Durrbach A, Benoit G.* Preoperative Risk Factors Associated With Urinary Complications After Kidney Transplantation. *Transplant Proc*. 2017 Nov; 49 (9): 2018–2024.
7. *Hickman LA, Sawinski D, Guzzo T, Locke JE.* Urologic malignancies in kidney transplantation. *Am J Transplant*. 2018 Jan; 18 (1): 13–22.
8. *Shimizu T, Sugihara T, Kamei J, Takeshima S, Kinoshita Y, Kubo T et al*. Predictive factors and management of urinary tract infections after kidney transplantation: a retrospective cohort study. *Clin Exp Nephrol*. 2021 Feb; 25 (2): 200–206.
9. *Thuret R, Timsit MO, Kleinclauss F.* Chronic kidney disease and kidney transplantation. *Prog Urol*. 2016 Nov; 26 (15): 882–908.
10. *Billis A, Freitas LLL, Costa LBE, Barreto IS, Botega AAR, Pereira TA, D'Ancona CA*. Lower Urinary Tract Symptoms Due to Xanthoma of the Prostate After Kidney Transplantation: A Case Report. *Transplant Proc*. 2020 Nov; 52 (9): 2736–2738.
11. *Frascà GM, Brigante F, Volpe A, Cosmai L, Gallieni M, Porta C.* Kidney transplantation in patients with previous renal cancer: a critical appraisal of current evidence and guidelines. *J Nephrol*. 2019 Feb; 32 (1): 57–64.
12. *Tan JHS, Bhatia K, Sharma V, Swamy M, van Dellen D, Dhanda R, Khambalia H.* Enhanced recovery after surgery recommendations for renal transplantation: guidelines. *Br J Surg*. 2022 Dec 13; 110 (1): 57–59.
13. *Thuret R, Kleinclauss F, Terrier N, Karam G, Timsit MO.* Challenges in renal transplantation. *Prog Urol*. 2016 Nov; 26 (15): 1001–1044.
14. *Maggiore U, Abramowicz D, Budde K.* Renal transplantation in the elderly. *Transplant Rev (Orlando)*. 2015 Oct; 29 (4): 191–192.
15. *Rodríguez Faba O, Boissier R, Budde K, Figueiredo A, Taylor CF, Hevia V et al*. European Association of Urology Guidelines on Renal Transplantation: Update 2018. *Eur Urol Focus*. 2018 Mar; 4 (2): 208–215.
16. *Cheung CY, Tang SCW.* An update on cancer after kidney transplantation. *Nephrol Dial Transplant*. 2019 Jun 1; 34 (6): 914–920.
17. *Egan KB.* The epidemiology of benign prostatic hyperplasia associated with lower urinary tractsymptoms: prevalence and incident rates. *Urol Clin North Am*. 2016; 43: 289.
18. *De Oliveira Marinho AC, Tavares-da-Silva E, Bastos CA, Roseiro A, Parada B, Retroz E et al*. Acute Urinary Retention After Kidney Transplant: Effect on Graft Function, Predictive Factors, and Treatment. *Transplant Proc*. 2021 Jul-Aug; 53 (6): 1933–1938.
19. *Sarier M, Yayar O, Yavuz A, Turgut H, Kukul E.* Update on the Management of Urological Problems Following Kidney Transplantation. *Urol Int*. 2021; 105 (7–8): 541–547.
20. *Lerner LB, McVary KT, Barry MJ, Bixler BR, Dahm P, Das AK et al*. Management of Lower Urinary Tract Symptoms Attributed to Benign Prostatic Hyperplasia: AUA GUIDELINE PART I – Initial Work-up and Medical Management. *J Urol*. 2021 Oct; 206 (4): 806–817.
21. *Lerner LB, McVary KT, Barry MJ, Bixler BR, Dahm P, Das AK et al*. Management of Lower Urinary Tract Symptoms Attributed to Benign Prostatic Hyperplasia: AUA GUIDELINE PART II – Surgical Evaluation and Treatment. *J Urol*. 2021 Oct; 206 (4): 818–826.
22. *Kasyan GR, Khodyreva LA, Dudareva AA i dr.* Kombinirovannoe lechenie simptomov nizhnikh mochevykh putey u muzhchin. *Meditsinskiy sovet*. 2016; 5: 84–90.
23. *Seo JH, Han JS, Lee Y, Myong JP, Ha US.* Fall risk related to subtype-specific alpha-antagonists for benign prostatic hyperplasia: a nationwide Korean population-based cohort study. *World J Urol*. 2022 Dec; 40 (12): 3043–3048.
24. *Pushkar' DYu, Rasner PI, Kharchilava RR.* Rossiyskie klinicheskie rekomendatsii s sovremennymi dannymi vedushchikh rossiyskikh spetsialistov. Simptomy nizhnikh mochevyvodyashchikh putey i dobrokachestvennaya giperplaziya predstatel'noy zhelezy. *Urologiya*. 2016; (2, prilozh.): 4–19.
25. *Rasner PI, Gazimiev MA, Gadzhieva ZK i dr.* Rasstroystva mocheispuskaniya u muzhchin: metodicheskie rekomendatsii, № 6. M.: ABV-press, 2017; 35.
26. *Pavlov VN, Galimzyanov VZ, Kazikhinurov AA, Pushkarev AM, Zagitov AR, Kazikhinurova AA, Sharipov IR.* Simptomy nizhnikh mochevyvodyashchikh putey i dobrokachestvennaya giperplaziya predstatel'noy zhelezy: uchebnoe posobie. Ufa: BGMU, 2018; 86.
27. *Foster HE, Dahm P, Kohler TS et al.* Surgical management of lower urinary tract symptom sattributed to benign prostatic hyperplasia: AUA Guideline amendment 2019. *J Urol*. 2019; 202: 592.
28. *Marks LS, Gittelman MC, Hill LA, Volinn W, Hoel G*. Rapid efficacy of the highly selective α1A-adrenoceptor antagonist silodosin in men with signs and symptoms of benign prostatic hyperplasia: pooled results of 2 phase 3 studies. *J Urol*. 2013; 189 (1 Suppl): S122–S128.
29. *Homma Y, Kawabe K, Tsukamoto T et al*. Estimate criteria for diagnosis and severity in benign prostatic hyperplasia. *Int J Urol*. 1996; 3: 261–266.
30. *Debruyne F, Boyle P, Calais Da Silva F et al*. Evaluation of the clinical benefit of permixon and tamsulosin in severe BPH patients – PERMAL study subset analysis. *Eur Urol*. 2004; 45: 773–779.
31. *Razek M, Abolyosr A, Mhammed O, Fathi A, Talaat M, Hassan A.* Prospective comparison of tadalafil 5 mg alone, silodosin 8 mg alone, and the combination of both in treatment of lower urinary tract symptoms related to benign prostatic hyperplasia. *World J Urol*. 2022. Aug; 40 (8): 2063–2070.
32. *Lukacs B, Grange JC, Comet D*. One-year follow-up of 2829 patients with moderate to severe lower urinary tract symptoms treated with alfuzosin in general practice according to IPSS and a health-related quality-of-life questionnaire. *BPM Group in General Practice Urology*. 2000; 55: 540–546.
33. *Barendrecht MM, Abrams P, Schumacher H, de a Rosette JJ, Michel MC*. Do α1-adrenoceptor antagonists improve lower urinary tract symptoms by reducing

bladder outlet resistance? *Neurourol Urodyn*. 2008; 27: 226–230.
34. *Fusco F, Creta M, De Nunzio C et al*. Progressive bladder remodeling due to bladder outlet obstruction: a systematic review of morphological and molecular evidences in humans. *BMC Urol*. 2018; 18: 15.
35. *Gul ZG, Kaplan SA*. BPH: why do patients fail medical therapy? *Curr Urol Rep*. 2019; 20: 40.
36. *La Vignera S, Aversa A, Cannarella R, Condorelli RA, Duca Y, Russo GI, Calogero AE.* Pharmacological treatment of lower urinary tract symptoms in benign prostatic hyperplasia: consequences on sexual function and possible endocrine effects. *Expert Opin Pharmacother*. 2021 Feb; 22 (2): 179–189.
37. *Alcaraz A, Castro-Díaz D, Gacci M, Salonia A, Ficarra V, Carballido-Rodríguez J et al.* Efficacy and Tolerability of 6-Month Treatment with Tamsulosin Plus the Hexanic Extract of Serenoa repens versus Tamsulosin Plus 5-Alpha-Reductase Inhibitors for Moderate-to-Severe LUTS-BPH Patients: Results of a Paired Matched Clinical Study. On Behalf Of The Qualiprost Study Group. *J Clin Med*. 2022 Jun 22; 11 (13): 3615.
38. *Bauer SR, Walter LC, Ensrud KE, Suskind AM, Newman JC, Ricke WA et al*. Assessment of Frailty and Association With Progression of Benign Prostatic Hyperplasia Symptoms and Serious Adverse Events Among Men Using Drug Therapy. *JAMA Netw Open*. 2021 Nov 1; 4 (11): e2134427.
39. *Kuzmenko AV, Kuzmenko VV, Gyaurgiev TA*. Comparative analysis of the effectiveness of early and delayed initiation of combined DRUG therapy for bph. *Urologiia*. 2021 May; (2): 27–30.
40. *Gravas S, Cornu JN, Gacci M et al.* EAU guidelines on management of non-neurogenic male LUTS. Presented at 2020 EAU Annual Congress, Amsterdam, Arnhem, The Netherlands. Available at http://uroweb.org/guidelines/compilations-of-all-guidelines/.
41. *Anderson BB, Pariser JJ, Helfand BT.* Comparison of Patients Undergoing PVP Versus TURP for LUTS/BPH. *Curr Urol Rep*. 2015 Aug; 16 (8): 55.
42. *Drouin S, Defortescu G, Prudhomme T, Culty T, Verhoest G, Doerfler A et al*. Lower urinary tract symptoms and urinary incontinence in renal transplant recipients and candidates: The French guidelines from CTAFU. *Prog Urol*. 2021 Jan; 31 (1): 45–49.
43. *Checcucci E, Veccia A, De Cillis S, Piramide F, Volpi G, Amparore D et al*. New Ultra-minimally Invasive Surgical Treatment for Benign Prostatic Hyperplasia: A Systematic Review and Analysis of Comparative Outcomes. Uro-technology and SoMe Working Group of the Young Academic Urologists Working Party of the European Association of Urology and of the Lower Tract and Research Group of the European Section of Uro-technology. *Eur Urol Open Sci*. 2021 Sep 22; 33: 28–41.
44. *Righetto M, Mancini M, Modonutti D, Calpista A, Beltrami P, Dal Moro F.* Patients with renal transplant and moderate-to-severe LUTS benefit from urodynamic evaluation and early transurethral resection of the prostate. *World J Urol*. 2021 Dec; 39 (12): 4397–4404.
45. *Sarier M, Tekin S, Duman İ, Yuksel Y, Demir M, Alptekinkaya F et al*. Results of transurethral resection of the prostate in renal transplant recipients: a single center experience. *World J Urol*. 2018 Jan; 36 (1): 99–103.
46. *Rassweiler J, Teber D, Kuntz R et al.* Complications of transurethral resection of the prostate (TURP) dincidence, management, and prevention. *Eur Urol*. 2006; 50: 969.
47. *Liu Z, Li YW, Wu WR et al.* Long-term clinicale fficacy and safety profile of transurethral resection of prostate versus plasma kinetic resection of the prostate for benign prostatic hyperplasia. *Urology*. 2017; 103: 198.
48. *Friedl A, Schneeweiss J, Stangl K et al.* The adjustable transobturator male system in stress urinary incontinence after transurethral resection of the prostate. *Urology*. 2017; 109: 184.
49. Boston Scientific Corporation: Intended use. *Rezum Instruction for Use*, 10-2019; 5.
50. *Dixon CM, Rijo Cedano E, Mynderse LA et al.* Transurethral convective water vapor as atreatment for lower urinary tract symptom-atology due to benign prostatic hyperplasiausing the Rezum(R) system: evaluation of acuteablative capabilities in the human prostate. *Res Rep Urol*. 2015; 7: 13.
51. *Bouza C, Lopez T, Magro A et al.* Systematic review and meta-analysis of transurethral needle ablation in symptomatic benign prostatic hyperplasia. *BMC Urol*. 2006; 6: 14.
52. *McVary KT, Rogers T, Mahon J et al.* Is sexual function better preserved after water vapor thermal therapy or medical therapy for lower urinary tract symptoms due to benign prostatic hyperplasia? *J Sex Med*. 2018; 15: 1728.
53. National Institute for Health and Care Excellence: Rezum for treating lower urinary tractsymptoms secondary to benign prostatic hyperplasia (24 June 2020). NICE Guideline No. MTG49.
54. *Mynderse LA, Roehrborn CG, Partin AW et al.* Results of a 5-year multicenter trial of a new generation cooled high energy transurethral microwave thermal therapy catheter for benign prostatic hyperplasia. *J Urol*. 2011; 185: 1804.
55. *Gravas S, Cornu JN, Gacci M et al.* EAU Guidelines on the Assessment of Non-neurogenic Male Lower Urinary Tract Symptoms including Benign Prostatic Obstruction. Arnhem, The Netherlands: EAU Guidelines Office. 2020.
56. *McVary KT, Rogers T, Roehrborn CG.* Rezum water vapor thermal therapy for lower urinarytract symptoms associated with benign prostatichyperplasia: 4-year results from randomized controlled study. *Urology.* 2019; 126: 171.
57. *McVary KT, Roehrborn CG.* Three-year out-comes of the prospective, randomized controlled Rezum System Study: convective radio frequency thermal therapy for treatment of lower urinarytract symptoms due to benign prostatic hyperplasia. *Urology*. 2018; 111: 1.
58. U.S. Food and Drug Administration: Select Up-dates for Guidance for the Non-Clinical and Clinical Investigation of Devices Used for the Treatment of Benign Prosta-

tic Hyperplasia (BPH): Draft Guidance for Industry and Food and Drug Administration Staff (July 14, 2020).
59. *Roehrborn CG, Wilson TH, Black LK.* Quantifying the contribution of symptom improvement to satisfaction of men with moderate to severe benign prostatic hyperplasia: 4-year data from the CombAT trial. *J Urol*. 2012; 187: 1732.
60. *Miller LE, Chughtai B, Dornbier RA et al.* Surgical reintervention rate after prostatic urethral lift: systematic review and meta-analysis involving over 2,000 patients. *J Urol*. 2020; 204: 1019.
61. *Roehrborn CG, Barkin J, Gange SN et al.* Five year results of the prospective randomized controlled prostatic urethral L.I.F.T. study. *Can J Urol*. 2017; 24: 8802.
62. *Zlotta AR, Giannakopoulos X, Maehlum O et al.* Long-term evaluation of transurethral needle ablation of the prostate (TUNA) for treatment of symptomatic benign prostatic hyperplasia: clinical outcome up to five years from three centers. *Eur Urol*. 2003; 44: 89.
63. *Rosario DJ, Phillips JT, Chapple CR.* Durability and cost-effectiveness of transurethral needle ablation of the prostate as an alternative to transurethral resection of the prostate when alpha-adrenergic antagonist therapy fails. *J Urol*. 2007; 177: 1047.
64. *Hill B, Belville W, Bruskewitz R et al.* Transurethral needle ablation versus transurethral resection of the prostate for the treatment of symptomatic benign prostatic hyperplasia: 5-year results of a prospective, randomized, multicenter clinical trial. *J Urol*. 2004; 171: 2336.
65. *Gupta N, Rogers T, Holland B et al.* Three-year treatment outcomes of water vapor thermal therapy compared to doxazosin, finasteride and combination drug therapy in men with benign prostatic hyperplasia: cohort data from the MTOPS trial. *J Urol*. 200; 405: 2018.
66. *Malde S, Rajagopalan A, Patel N et al.* Potassium-titanyl-phosphate laser photoselective vaporization for benign prostatic hyperplasia: 5-year follow-up from a district general hospital. *J Endourol*. 2012; 26: 878.
67. *Lee HE, Kim B, Yoon HS, Suh J, Oh SJ.* Outcome of Patients With Elevated Prostate-Specific Antigen and Lower Urinary Tract Symptoms Receiving Holmium Laser Enucleation of the Prostate. *Int Neurourol J*. 2022 Sep; 26 (3): 248–257.
68. *Takeuchi Y, Sawada Y, Watanabe S, Ni-Itsu Y, Sekido N.* Age-specific effect of transurethral holmium laser enucleation of the prostate on overactive bladder in men with benign prostatic hyperplasia: An investigation using an overactive bladder symptom score. *Low Urin Tract Symptoms*. 2022 Dec 11.
69. *Nohara T, Matsuyama S, Shima T, Kawaguchi S, Seto C.* Holmium Laser Enucleation of the Prostate With Percutaneous Nephrostomy Into the Transplanted Kidney in Patient With Severe Benign Prostatic Hyperplasia With Vesicoureteral Reflux – A Case Report. *Urol Case Rep*. 2015 Dec 10; 4: 33–35.
70. *Prudhomme T, Marquette T, Péré M.* Benign Prostatic Hyperplasia Endoscopic Surgical Procedures in Kidney Transplant Recipients: A Comparison Between Holmium Laser Enucleation of the Prostate, GreenLight Photoselective Vaporization of the Prostate, and Transurethral Resection of the Prostate. *J Endourol*. 2020 Feb; 34 (2): 184–191.
71. *Baboudjian M, Fourmarier M, Gondran-Tellier B, Pradere B, Userovici M, Alegorides C, Barry Delongchamps N.* Head-to-head comparison of prostatic urethral lift and water vapor thermal therapy for the treatment of symptomatic benign prostatic hyperplasia: a real-life study. *Int Urol Nephrol*. 2021 Sep; 53 (9): 1757–1763.
72. *Alexander CE, Scullion MM, Omar MI, Yuan Y, Mamoulakis C, N'Dow JM et al*. Bipolar versus monopolar transurethral resection of the prostate for lower urinary tract symptoms secondary to benign prostatic obstruction. *Cochrane Database Syst Rev*. 2019 Dec 3; 12 (12): CD009629.
73. *Mamoulakis C, Ubbink DT, de la Rosette JJ.* Bipolar versus monopolar transurethral resection of the prostate: A systematic review and meta-analysis of randomized controlled trials. *Eur Urol*. 2009; 56: 798–809. doi: 10.1016/j.eururo.2009.06.037.
74. *Ahyai SA, Gilling P, Kaplan SA et al.* Meta-analysis of functional outcomes and complications following transurethral procedures for lower urinary tract symptoms resulting from benign prostatic enlargement. *Eur Urol*. 2010; 58: 384–397.
75. *Burke N, Whelan JP, Goeree L et al.* Systematic review and meta-analysis of transurethral resection of the prostate vs. minimally invasive procedures for the treatment of benign prostatic obstruction. *Urology*. 2010; 75: 1015–1022.
76. *Omar MI, Lam TBL, Cameron A et al.* Systematic review and meta-analysis of the clinical effectiveness of bipolar compared to monopolar transurethral resection of the prostate. *BJU Int*. 2014; 113: 24–35.
77. *Cornu JN, Ahyai S, Bachmann A et al.* A systematic review and meta-analysis of functional outcomes and complications following transurethral procedures for lower urinary tract symptoms resulting from benign prostatic obstruction: An update. *Eur Urol*. 2015; 67: 1066–1096.
78. *Mamoulakis C, Sofras F, de la Rosette J et al.* Bipolar vs. monopolar transurethral resection of the prostate for lower urinary tract symptoms secondary to benign prostatic obstruction. *Cochrane Database Syst Rev*. 2014; 1: CD009629.
79. *Taylor BL, Jaffe WI.* Electrosurgical transurethral resection of the prostate and transurethral incision of the prostate (monopolar techniques). *Can J Urol*. 2015 Oct; 22 Suppl 1: 24–29.
80. *Sarıer M, Duman İ, Demir M, Yüksel Y, Emek M, Kukul E.* The outcomes of transurethral incision/resection of the prostate (TUIP/TURP) performed early after renal transplantation. *Turk J Urol*. 2018 Mar; 44 (2): 172–177.
81. *Sarier M, Duman I, Kilic S, Yuksel Y, Demir M, Aslan M et al*. Comparative Results of Transurethral Incision with Transurethral Resection of The Prostate in Renal Transplant Recipients with Benign Prostate Hyperplasia. *Urol J*. 2018 Jul 10; 15 (4): 209–213.

82. *Duty BD, Conlin MJ, Fuchs EF, Barry JM.* The current role of endourologic management of renal transplantation complications. *Adv Urol*. 2013; 2013: 246520.
83. *Cardi A, Palleschi G, Patruno G, Tuffu G, D'Amico FE, De Vico A et al.* Robot-assisted simple prostatectomy for treatment of large prostatic adenomas: surgical technique and outcomes from a high-volume robotic centre. *World J Urol*. 2022 Dec 25.
84. *Law YXT, Chen WJK, Shen L, Chua WJ.* Is transurethral needle ablation of prostate out of fashion? Outcomes of single session office-based transurethral needle ablation of prostate in patients with symptomatic benign prostatic hyperplasia. *Investig Clin Urol*. 2019 Sep; 60 (5): 351–358.
85. *Powell T, Rahman S, Staib L, Bhatia S, Ayyagari R.* Operator Learning Curve for Prostatic Artery Embolization and Its Impact on Outcomes in 296 Patients. *Cardiovasc Intervent Radiol*. 2022 Dec 1.
86. *Goyal P, Salem R, Mouli SK*. Controversies in Prostate Artery Embolization: Future Best Practice. *Semin Intervent Radiol*. 2022 Dec 20; 39 (6): 562–570.
87. *Gondran-Tellier B, McManus R, Sichez PC, Akiki A, Gaillet S, Toledano H et al*. Efficacy and Safety of Surgery for Benign Prostatic Obstruction in Patients with Preoperative Urinary Catheter. *J Endourol*. 2021 Jan; 35 (1): 102–108.
88. *Yaremin BI, Kharitonov BI, Mironov AA, Maslikova UV, Aleksandrova VE.* Transplantatsiya pochki – poisk optimal'noy khirurgicheskoy tekhniki. *Vestnik meditsinskogo instituta "REAVIZ"*. 2017; (5): 94–104.
89. *Chadban SJ, Ahn C, Axelrod DA, Foster BJ, Kasiske BL, Kher V et al*. KDIGO Clinical Practice Guideline on the Evaluation and Management of Candidates for Kidney Transplantation. *Transplantation*. 2020 Apr; 104 (4S1 Suppl 1): S11–S103.
90. *Choudhury S, Haldar B, Pal DK.* Spectrum of lower urinary tract symptoms after renal transplant among adult non-urologic anuric patients and their management in a tertiary care center. *Urologia*. 2022 Feb 3: 3915603211048150. doi: 10.1177/03915603211048150.
91. Klinicheskie rekomendatsii Evropeyskoy assotsiatsii urologov [Elektronnyy resurs]. M.: Medkongress, 2019; 1368.
92. Integrativnaya urologiya. Rukovodstvo dlya vrachey / Pod red. P.V. Glybochko, Yu.G. Alyaeva. M.: Medforum, 2014: 128–239, 314–326.
93. *Sánchez-Puy A, Bravo-Balado A, Diana P, Baboudjian M, Piana A, Girón I et al*. New Generation Pulse Modulation in Holmium:YAG Lasers: A Systematic Review of the Literature and Meta-Analysis. *J Clin Med*. 2022 Jun 4; 11 (11): 3208.
94. *Perri A, Izzo G, Lofaro D, La Vignera S, Brunetti A, Calogero AE, Aversa A.* Erectile Dysfunction after Kidney Transplantation. *J Clin Med*. 2020 Jun 25; 9 (6): 1991.
95. *Kleinclauss F, Thuret R, Murez T, Timsit MO.* Urologic malignancies in renal transplant candidates and recipients. *Prog Urol*. 2016 Nov; 26 (15): 1094–1113.
96. *Danovich MG.* Transplantatsiya pochki. Per. s angl. pod red. Ya.G. Moysyuka. M.: GEOTAR Media, 2014; 848.
97. *Latchamsetty KC, Mital D, Jensik S.* Use of collagen injections for vesicoureteral reflux in transplanted kidney. *Transplant Proc*. 2003; 35: 1378.
98. *Li Marzi V, Filocamo MT, Dattolo E*. The treatment of fistulae and ureteral stenosis after kidney transplantation. *Transplant Proc*. 2005; 37: 2516.
99. *Mokos I, Kastelan Z, Basić-Jukić N, Kes P, Pasini J.* Transurethral incision/resection of the prostate (TUIP/TURP) in operative treatment of repeated bladder outlet obstruction early after kidney transplantation. *Acta Clin Croat*. 2011 Sep; 50 (3): 381–384.
100. *Védrine N, Nsabimbona B, Soares P, Deteix P, Boiteux JP, Guy L.* Transurethral resection or incision of the prostate in the immediate postoperative follow-up of renal transplantation. *Prog Urol*. 2009 Dec; 19 (11): 845–849.
101. *Gratzke C, Pahde A, Dickmann M, Reich O, Seitz M, Jauch K et al*. Predictive factors for urinary retention following kidney transplantation in male patients. *Scand J Urol Nephrol*. 2012 Feb; 46 (1): 44–47.
102. *Gill BC, Ulchaker JC.* Costs of managing benign prostatic hyperplasia in the office and operating room. *Curr Urol Rep.* 2018; 19: 72.

The article was submitted to the journal on 07.02.2023

DOI: 10.15825/1995-1191-2023-2-26-37

EFFECT OF SECOND WARM ISCHEMIA ELIMINATION ON KIDNEY GRAFT FUNCTION: AN EXPERIMENT AND CLINICAL STUDY

A.V. Shabunin[1, 2], P.A. Drozdov[1], D.A. Makeev[1], I.V. Nesterenko[1], O.S. Zhuravel[1, 2], S.A. Astapovich[1], E.A. Lidjieva[3]

[1] Botkin Moscow City Clinical Hospital, Moscow, Russian Federation
[2] Russian Medical Academy of Continuous Professional Education, Moscow, Russian Federation
[3] Sechenov University, Moscow, Russian Federation

Objective: to evaluate the effectiveness of a new device for second warm ischemia (SWI) elimination in kidney transplantation (KT). **Materials and methods.** The study included clinical and experimental stages. The clinical stage included 63 patients out of 219 who underwent KT at Botkin Moscow City Clinical Hospital between July 2018 and August 2022. The inclusion criteria were kidneys from donation after brain death (DBD) donors with expanded criteria or kidneys from donation after circulatory death (DCD) donors, and an SWI time greater than 45 minutes. The first group consisted of 24 recipients operated on using the new SWI elimination device. The second retrospective control group consisted of 39 patients where sterile ice bags were used at the implantation stage. The groups had no statistically significant differences in the main recipient and donor characteristics, as well as in perioperative parameters. Also, from November 2021 to April 2022, 23 kidney autotransplantation experiments in female Landrace pigs were performed. The animals were cared for in accordance with the European Convention for the Protection of Vertebrate Animals used for Experimental and other Scientific Purposes (Strasbourg, 18 March 1986). Efficiency of different SWI elimination techniques was compared on two experimental models: standard donor (group 1, n = 12) and asystolic donor (group 2, n = 11). **Results.** In the clinical trial group, mean graft temperature (t_m) before reperfusion was statistically significantly lower in group 1 using the special SWI elimination device: 6.4 ± 1.7 °C (95% CI 3.2–8.5) versus 22.1 ± 2.3 °C (18.1–24.6), $p < 0.001$. The risk of delayed graft function (DGF) was 3.86 times higher (95% CI 1.11–13.43) with the standard SWI elimination technique. In the experimental group, in the subgroups using the new device (n = 12), graft t_m before reperfusion was 5.1 ± 0.4 °C (95% CI 4.5–5.8), whereas in the ice bag subgroups (n = 11), t_m was 29.3 ± 1.3 °C (95% CI 27.7–30.8), which was significantly higher ($p < 0.001$). The overall 1-week survival of the experimental animals was significantly higher in the SWI elimination device subgroup (logrank p = 0.036). **Conclusion.** The developed device is effective in eliminating SWI of renal graft.

Keywords: kidney transplantation, second warm ischemia, delayed graft function, DGF, SWI.

INTRODUCTION

Kidney transplantation (KT) is the gold standard therapy for end-stage kidney disease in patients without absolute contraindications for KT [1]. Delayed graft function (DGF) is one of the most frequent postoperative complications. According to various reports, DGF occurs in more than 20% of cases on average [2, 3]. It should be noted that DGF is associated with many long-term adverse effects of LT, including increased incidence of postoperative complications and decreased graft survival [3–8].

Prolonged secondary warm ischemia time (>45 minutes) is one of the significant risk factors for DGF [9]. It has been found that with every minute of formation of vascular anastomoses, graft temperature increases on average by 10 °C [10], which can aggravate its ischemic preservative injury. To prevent graft heating during vascular anastomosis formation, various methods of graft surface cooling have been suggested. The classic technique for elimination of second warm ischemia (SWI) is to wrap the kidney in a sterile ice bag [11]. It is universally used but comes with a number of disadvantages. For example, during implantation, ice may melt or spill into the wound, resulting in not achieving optimal graft cooling. This probably gave rise to the development of other methods of SWI elimination by means of "packages" made of silicone, polyurethane, polyethylene and other materials [9, 12–14]. Many of these devices are complex and expensive.

In our previous work, prolonged SWI was strongly associated with DGF [15]. This was the reason for developing a new SWI elimination device, whose efficiency we evaluated in experimental and clinical conditions.

Corresponding author: Elza Lidjieva. Address: 2, building 4, B. Pirogovskaya str., Moscow, 119435, Russian Federation. Phone: (963) 648-16-59. E-mail: lidjieva99@mail.ru

MATERIAL AND METHODS

From July 2018 to November 2021, 219 isolated LTs from deceased donors were performed at the transplant ward of Botkin Hospital. In order to eliminate SWI of the graft, standard packaging in an ice bag was used in all cases. During retrospective analysis of treatment outcomes, it was found that there was prolonged SWI time (>45 minutes) in 61 cases (27.9%). These patients were 1.98 (95% CI: 1.04 to 3.77) times more likely to develop DGF, which was statistically significant ($p = 0.035$). In order to prevent ischemic injury to the graft during implantation, our center developed a special SWI elimination device.

Description of the special SWI elimination device

The device is a gauze/fabric pack for a renal graft and an ice slush. It has three spaces isolated from each other. The middle space has two openings through which it communicates with the external environment. The renal vascular pedicle and the ureter is placed into these openings. Ice chips are placed in the two outer spaces that do not communicate with the environment (Fig. 1).

All three spaces are closed from above by tightening a purse-string suture. During formation of vascular anastomoses, the purse-string suture can be loosened, and ice chips can be added to the outer spaces as needed (Fig. 2). Upon completion of formation of vascular anastomoses, the device is dissected along the anterior wall and disposed of.

The safety and efficacy of the developed device in comparison with the standard SWI elimination technique based on the standard ice bag were studied in an experiment and then, in clinical conditions.

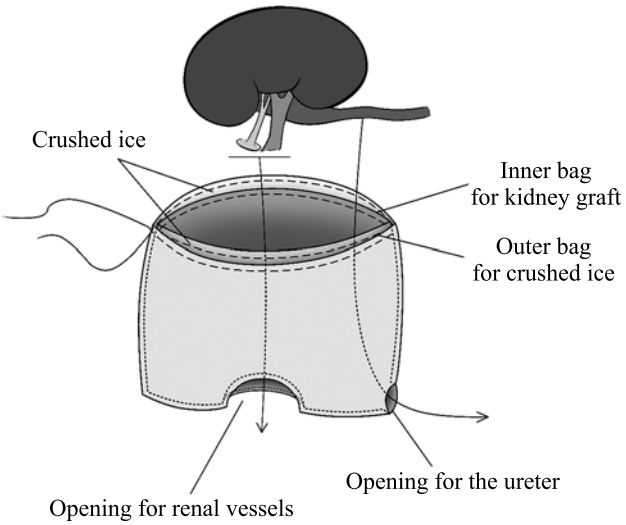

Fig. 1. SWI elimination device. Placing the kidney

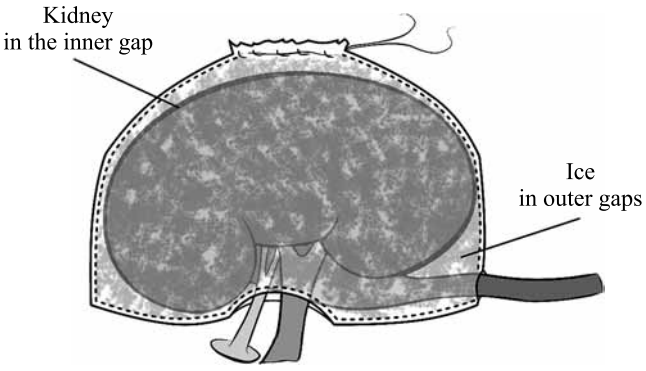

Fig. 2. SWI elimination device. Tightening the purse-string suture

Experimental stage

From November 2021 till April 2022, we carried out 23 experiments on kidney autotransplantation in female Landrace pigs with the average weight of 31 ± 1.4 (from 29 to 34) kg. Preoperative preparation, anesthetic support, care of the animal in the postoperative period, and withdrawal from the experiment were all performed in accordance with the European Convention for the Protection of Vertebrate Animals used for Experimental and other Scientific Purposes (Strasbourg, 18 March 1986). A comparative study of the efficacy of different SWI elimination methods was performed in the experimental models of the standard donor (n = 12) and asystolic donor (n = 11). The study design is shown in Fig. 3.

Kidney autotransplantation was performed according to the following protocol:

1. Midline total laparotomy, kidney mobilization from the retroperitoneal space. At this stage, the anatomical features of each of the renal pedicles were evaluated and a decision was made as to which kidney would be subsequently transplanted (Fig. 4, a, b).
   a) when performing KT in the standard donor model, immediate cold preservation was performed after the future graft has been removed;
   b) when performing KT in the asystolic donor model, before removal and preservation of the future graft, its vessels were clamped with atraumatic clamps for 30 minutes (Fig. 4, c).
2. Removal of the contralateral kidney for the most accurate assessment of graft function after surgery.
3. Custodiol HTK solution was used in all cases for static cold preservation. After perfusion, the graft vessels were treated on a back-table. The median cold ischemia time of the renal graft was 180 minutes (IQR: 175–190).
4. Before implantation, the aorta and inferior vena cava were mobilized in the lower half of the abdominal cavity.
5. The kidney was implanted by means of arterial and venous anastomoses with the main vessels in an end-to-side manner. Experimental conditions made it pos-

sible to create identical prolonged implantation times in each operation. Thus, the median second warm ischemia time was 70 minutes (IQR: 70–75). We used the SWI elimination device (Fig. 5, b) and the standard ice bag technique (Fig. 5, a) in 12 experiments and 11 experiments, respectively).

6. Upon completion of vascular anastomosis formation, we performed graft reperfusion, formed ureteroneocystostomy anastomosis, performed revision and layer-by-layer suturing of the wound.

At the stages of graft immersion into the wound and immediately before reperfusion, its surface temperature was recorded using a remote thermometer at a distance of 2–3 cm (Fig. 6).

Laboratory monitoring of graft function was performed for 7 days after surgery: creatinine, urea, blood gases and electrolytes were determined once every 2 days. Daily diuresis was also monitored during the first 3–4 days, then the urethral catheter was removed for humanitarian reasons. Euthanasia under anesthesia was used to withdraw the animals from the experiment. After the animal's death, an autopsy was performed followed by morphological study of the renal autograft.

The presence of oliguria (<500 ml/day) at postoperative day 3–4 and/or hyperkalemia (>6.0 mmol/l) within a week after surgery were considered as criteria for DGF. If DGF developed, the animal was withdrawn from the experiment ahead of time. We assessed and compared the dynamics of creatinine and potassium levels, daily diuresis rates and frequency of DGF between the subgroups.

Clinical stage

The study included 63 patients operated at Botkin Hospital from July 2018 to August 2022. The inclusion

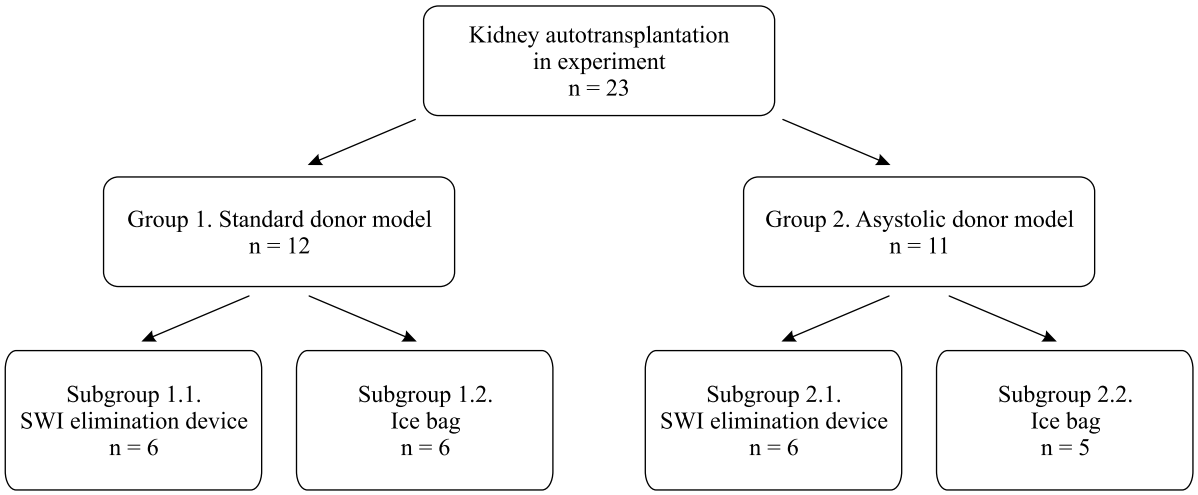

Fig. 3. Experimental stage of the comparative study of SWI elimination techniques

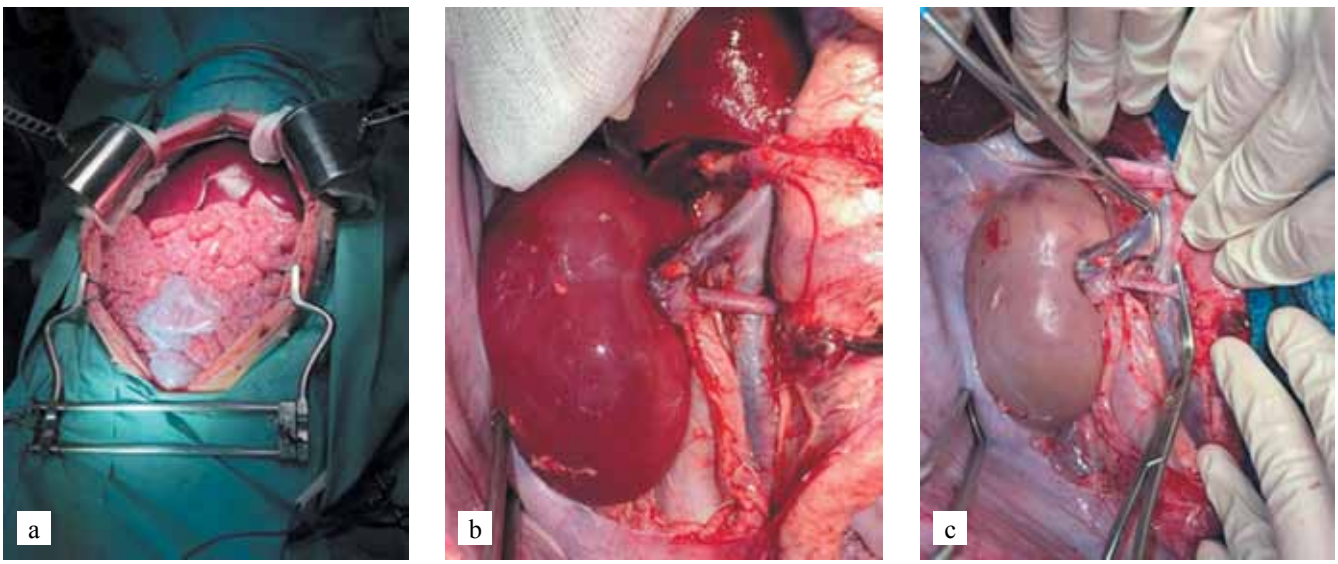

Fig. 4. Experimental kidney autotransplantation in a pig model: nephrectomy stage (intraoperative photo): a, midline total laparotomy, installing the retractors; b, isolation of the right kidney from retroperitoneal space, vascular stem dissection; c, placing clamps on renal vessels

criteria were: use of a renal graft obtained from a DBD donor with expanded criteria or DCD donor, and prolonged SWI time (>45 minutes). A patient was excluded from the study if they developed primary nonfunction, died or underwent emergency graftectomy within 7 days after surgery, and if hypothermic oxygenated machine perfusion was used during organ preservation. Preoperative examination, KT and postoperative management of the recipients were performed in accordance with national clinical guidelines. A prolonged-release tacrolimus-based triple-drug immunosuppression regimen was used as a supportive immunosuppressive therapy. The starting dose of the drug was administered at 0.2 mg per kg of the recipient's weight and was taken before surgery. The target tacrolimus level was considered to be 10–12 ng/ml. Delayed graft function was defined as the need for hemodialysis within week 1 after surgery.

The first group consisted of 24 kidney transplant recipients who used the developed special SWI elimination device during the operation. Among them were 14 men (58.3%) and 10 women (41.7%). Median recipient age was 48 (IQR: 39–55) years, median BMI was 27.5 (IQR: 23.0–31.0) kg/m^2. The main causes of end-stage renal disease were chronic glomerulonephritis (16/24, 66.7%),

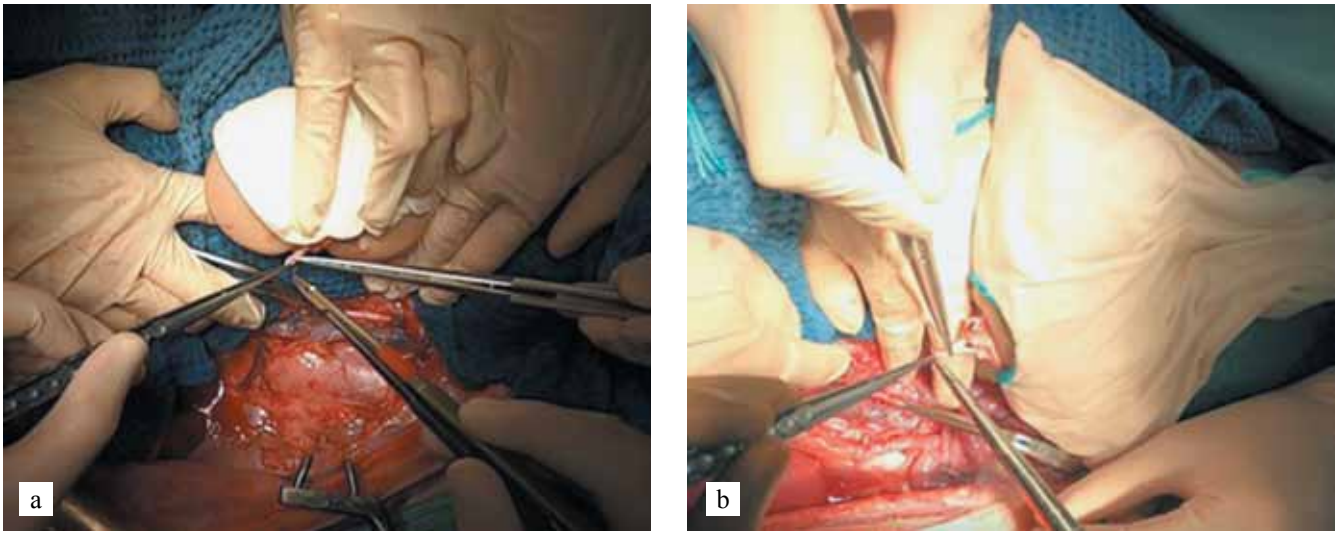

Fig. 5. Experimental kidney autotransplantation in a pig model: implantation stage (intraoperative photo): a, implantation using an ice bag; b, implantation using the special SWI elimination device

Fig. 6. Measuring the graft surface temperature with a remote thermometer

diabetes (3/24, 12.5%), and others (5/24, 20.8%). Median residual daily urine output before transplantation was 300 (IQR: 100–600) ml. In all cases, the kidney graft was obtained from an expanded criteria brain-dead donor. Median donor age was 65 (IQR: 54–68) years, the median BMI was 34.0 (IQR: 27.2 to 36.0).

Retrospective control group 2 consisted of 39 patients who had used an ice bag for SWI elimination during surgery. Among them were 28 men (71.8%) and 11 women (28.2%). Median recipient age was 51 (IQR: 39–54) years, median BMI was 26.0 (IQR: 24.0–28.3) kg/m^2. The main causes of end-stage renal disease were chronic glomerulonephritis (21/39, 53.8%), diabetes (4/39, 10.2%), chronic tubulointerstitial nephritis (3/39, 7.7%), and others (11/39, 28.2%). Median residual daily urine output before transplantation was 300 (IQR: 0–700) ml. In 37 cases (94.9%), the kidney graft was obtained from an expanded criteria brain-dead donor; in 2 cases, the graft was procured from a donor with irreversible effective circulatory arrest (5.1%). Median donor age was 62 (IQR: 53–67) years, median BMI was 32.5 (IQR: 25.3–34.5).

The groups had no statistically significant differences in the main recipient and donor characteristics, as well as a number of perioperative parameters. Detailed comparative characteristics are presented in Table 1.

Statistical analysis

Statistical processing and data analysis were performed using IBM SPSS Statistics 26 version for Microsoft Windows (USA). Mann–Whitney U test was used to compare two groups of quantitative indicators, given the small sample size, regardless of the distribution type. Qualitative data were compared using Pearson's chi-squared test or Fisher's exact test to determine the OR and 95% CI, as well as the closeness of association of the studied characteristics according to Cramer's V. Survival analysis was performed using Kaplan–Meier estimate with determination of statistically significant differences using Mantel–Cox long-rank test. Differences were considered statistically significant at $p < 0.05$.

RESULTS

Experimental stage

In all 23 experimental operations, mean graft temperature before immersion into the wound was 4.8 ± 1.1 (95% CI: 4.2–5.9) °C and did not differ between subgroups ($p > 0.05$). In subgroups 1.1 and 2.1, where SWI elimination was performed with the developed device (n = 12), mean graft temperature at the completion of vascular anastomoses was 5.1 ± 0.4 (95% CI: 4.5–5.8) °C, whereas in subgroups 1.2 and 2.2 featuring ice bags (n = 11) it was 29.3 ± 1.3 (95% CI: 27.7–30.8) °C, which was statistically significantly higher ($p < 0.001$).

Life-threatening surgical complications developed in the first 3/23 (13.04%) experiments: renal autograft artery thrombosis (n = 2) and massive lymphorrhea in the abdominal cavity (n = 1). These animals were withdrawn from the experiment early.

In group 1 (experimental model of KT from a standard donor), we found statistically significant differences in creatinine levels on day 1, 3 and 5, and diuresis rates on postoperative day 1 between the subgroups. In subgroup 1.1, the differences were statistically significantly higher ($p < 0.05$). In contrast, the studied subgroups had no significant differences in potassium levels ($p > 0.05$), and in no case was there DGF. The results of the comparative study in group 1 are presented in Table 2.

Morphological study showed that in group 1 (experimental kidney autotransplantation in the standard donor model), renal grafts implanted using the standard SWI elimination technique, had slightly more pronounced microscopic signs of renal tubular injury (Fig. 7).

In the experimental kidney autotransplantation group in the asystolic donor model, there were no surgical complications and associated mortality. In subgroup 2.1 featuring the special SWI elimination device, a condition meeting the DGF criteria accepted for experimental animals developed in one case (1/6, 16.7%). As a result, the animal was withdrawn from the experiment on postoperative day 4. In subgroup 2.2, in turn, DGF developed in 4 out of 5 cases (80%), and therefore the animals were withdrawn from the experiment on postoperative day 2, 4, and 5. Thus, the survival rate of experimental animals in postoperative week 1 was statistically significantly higher in the "special SWI elimination device" subgroup (log-rank $p = 0.036$). Plots of survival of experimental animals with immediate renal graft function depending on the SWI elimination method used are shown in Fig. 8.

Morphological study revealed that in group 2 (experimental kidney autotransplantation in the asystolic donor model), grafts implanted using the ice bag SWI elimination technique, had significantly more pronounced signs of renal tubular necrosis and injury (Fig. 9).

Clinical stage

Of the 63 cases selected in the clinical phase of the study, there were no hospital mortality or severe surgical complications of KT (Clavien–Dindo >II) in the early postoperative period. mean graft temperature before reperfusion was statistically significantly lower in group 1 that used the developed special SWI elimination de-

Table 1

Comparative characteristics of the groups based on the SWI elimination method

Parameter	Group 1 SWI elimination device n = 24		Group 2 Ice bag n = 39		p-value
	M	IQR	M	IQR	
Recipient age (years)	48	39–55	51	39–54	0.657
Recipient's BMI (kg/m^2)	27.5	23.0–31.0	26.0	24.0–27.3	0.725
Residual diuresis (ml)	300	100–600	300	0–700	0.756
Donor age (years)	65	54–68	62	53–67	0.645
Donor's BMI (kg/m^2)	34.0	27.2–36.0	32.5	25.3–35.0	0.238
Cold preservation time (min)	725	550–820	775	640–790	0.343
Second warm ischemia time (min)	58	50–65	62	55–75	0.411
Highest tacrolimus C_0 in the first week (ng/ml)	19.2	17.0–25.1	22.4	18.6–28.3	0.19

vice: 6.4 ± 1.7 (95% CI: 3.2–8.5) °C versus 22.1 ± 2.3 (18.1–24.6) °C ($p < 0.001$).

In the retrospective group, DGF developed in 17 of 39 recipients (43.6%), which was statistically significantly lower than in group 1: 4/24 (16.7%) ($p = 0.032$). The odds of developing DGF for the standard SWI elimination technique were 3.86 times higher (95% CI: 1.11–13.43) and there was a moderate association between the traits ($V = 0.277$). The average length of stay in the hospital in group 1 was 14.5 ± 4.4 (12 to 18) bed days, which was also statistically significantly lower ($p = 0.024$) than in the retrospective control group – 18.3 ± 3.2 (16 to 25) bed days. The results of the clinical phase of the study of the safety and efficacy of the developed SWI elimination device in comparison with the standard method are presented in Table 3.

DISCUSSION

DGF, according to Russian and foreign authors, is a common early post-transplant complication in recipients. Undoubtedly, its increased frequency is mainly associated with the inevitable – expansion of the deceased donor selection criteria, in view of the enormous demand for KT. At the same time, understanding the extreme urgency

Table 2

Dynamics of laboratory and clinical indicators of graft function after kidney autotransplantation in the standard donor model

Parameter	Subgroup 1.1 SWI elimination device n = 5		Subgroup 1.2 Ice bag n = 4		p-value
	M	IQR	M	IQR	
Creatinine (before surgery)	53.4	52.0–54.2	53.0	52.2–54.0	0.758
Creatinine (day 0), μmol/l	159.2	156.4–163.0	173.2	158.1–175.1	0.152
Creatinine (day 1), μmol/l	252.0	235.3–282.1	324.8	301.4–356.5	**0.031**
Creatinine (day 3), μmol/l	221.4	213.3–253.6	345.0	322.4–398.3	**0.008**
Creatinine (day 5), μmol/l	168.9	142.2–211.5	234.4	201.6–269.5	**0.043**
Potassium (before surgery), mmol/l	4.3	4.3–4.5	4.2	4.1–4.5	0.823
Potassium (day 0), mmol/l	4.7	4.4–5.0	4.9	4.5–5.0	0.743
Potassium (day 1), mmol/l	4.0	3.8–4.3	4.5	3.9–4.7	0.521
Potassium (day 3), mmol/l	4.4	4.3–5.4	5.3	4.2–5.3	0.213
Potassium (day 5), mmol/l	4.7	4.3–4.8	4.6	4.3–4.9	0.642
Diuresis (day 1), ml	1200	1000–1200	600	600–700	**0.025**
Diuresis (day 2), ml	1500	1300–1600	1300	1200–1500	0.342
Diuresis (day 3), ml	1300	1000–1500	1400	1100–1400	0.412

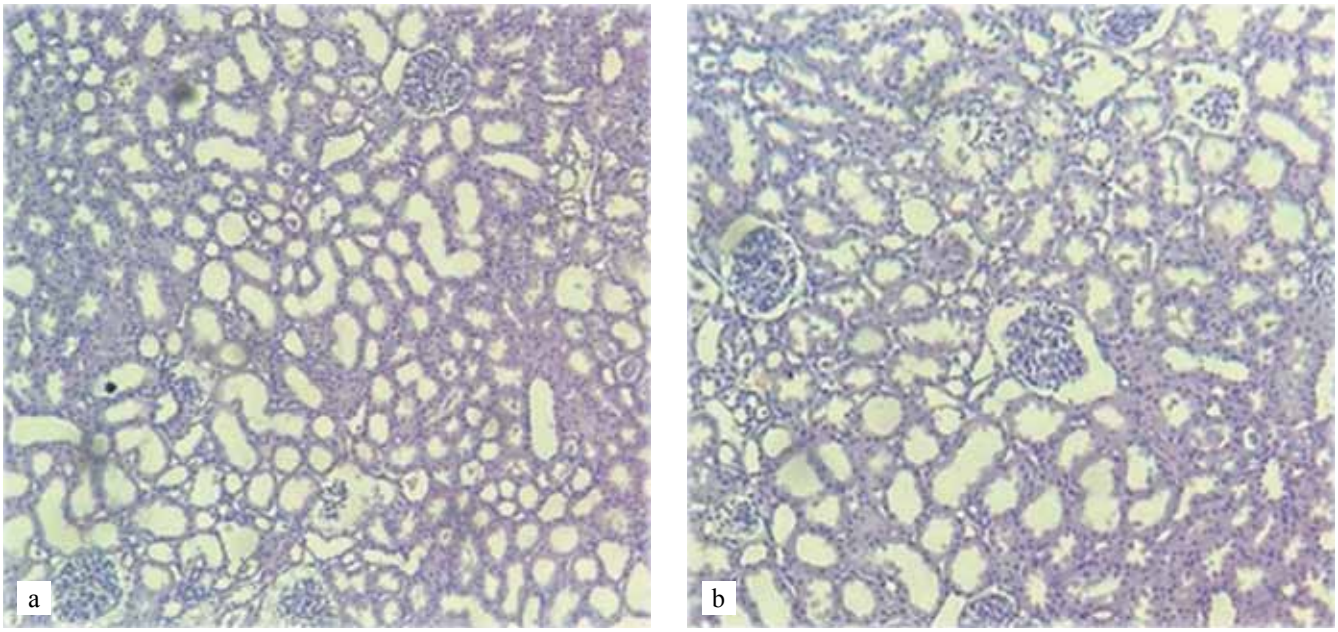

Fig. 7. Microscopic examination of kidney grafts after kidney autotransplantation in the standard donor model: a, after using the special SWI elimination device; b, after using the standard SWI elimination technique

of this problem, taking into account the increased risk of complications and decreased long-term graft survival, it is necessary to strive to influence every modifiable factor that increases the risk of DGF.

Table 3

Outcomes of treatment of renal transplant recipients in the early postoperative period depending on the SWI elimination technique used during surgery

Parameter	Group 1 SWI elimination device (n = 24)	Group 2 Ice bag (n = 39)	p-value
Mean graft temperature before reperfusion	6.4 ± 1.7 (3.2–9.5) °C	17.1 ± 2.3 (13.1–24.6) °C	**0.013**
DGF frequency	4/24 (16.7%)	17/39 (43.6%)	**0.032**
Length of hospital stay	14.5 ± 4.4 (12–18)	18.3 ± 3.2 (16–25)	**0.024**
Hospital mortality	0	0	1
Complications (Clavien–Dindo >II)	0	0	1

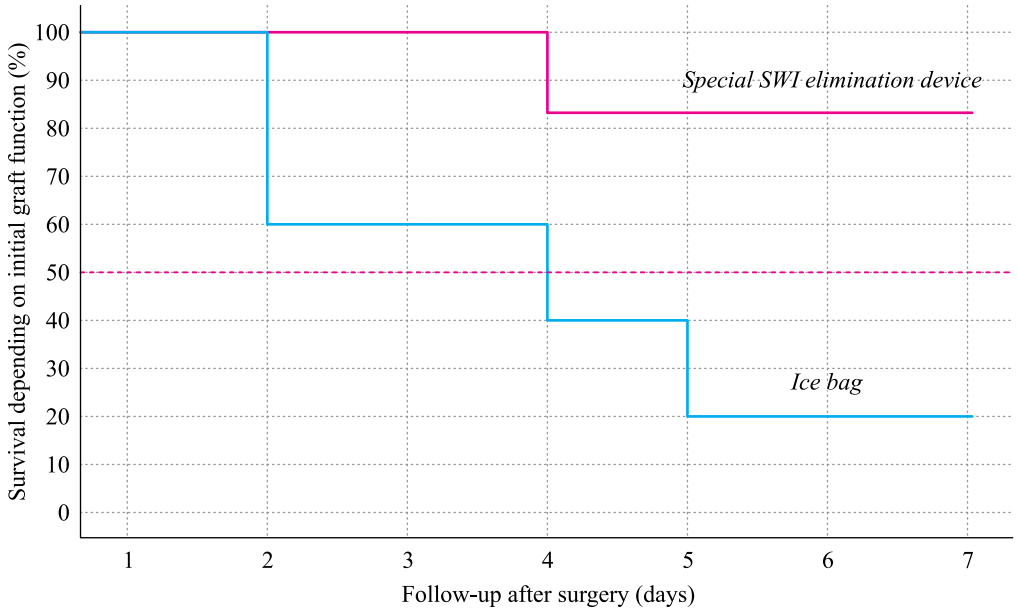

Fig. 8. Survival with immediate renal graft function in the early postoperative period depending on the SWI elimination technique used during kidney autotransplantation in the asystolic donor model

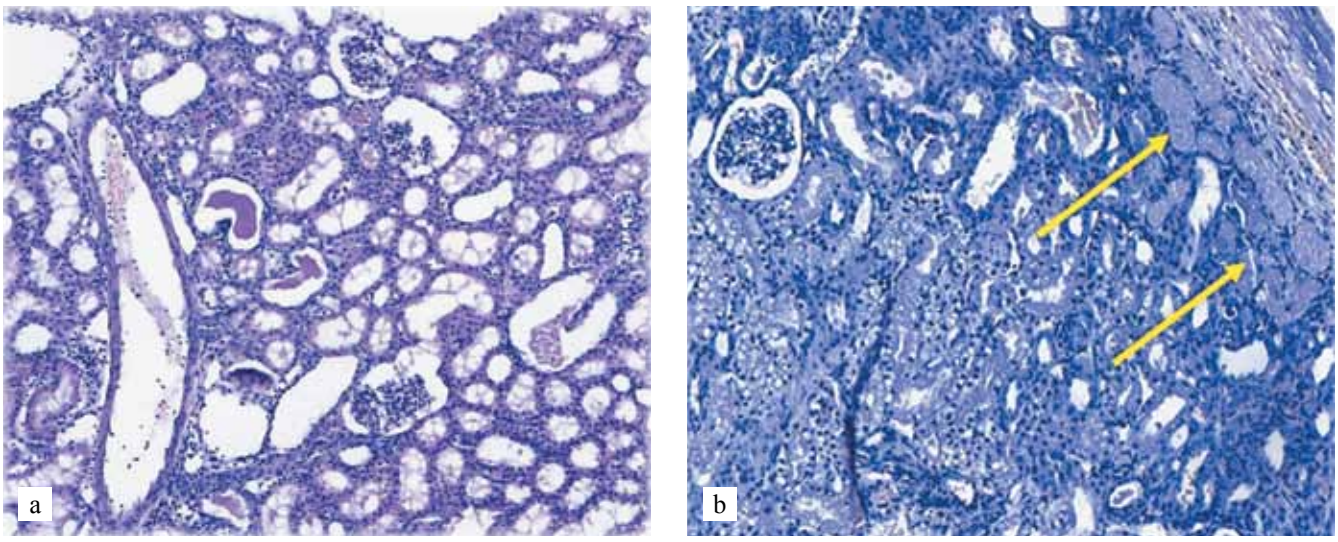

Fig. 9. Microscopic examination of kidney grafts after kidney autotransplantation in the asystolic donor model: a, after using a special SWI elimination device; b, after using the standard SWI elimination technique (yellow arrows indicate foci of acute tubular necrosis)

Both in many works and in our study, prolonged SWI time was a statistically significant and modifiable risk factor for DGF ($p = 0.035$). Nevertheless, the need for SWI elimination to date, is not clear. According to a retrospective study by Karipineni et al. (2014), SWI elimination did not improve graft function after surgery and did not influence long-term outcomes [12]. This was probably due to the fact that DGF has many risk factors on both the donor and recipient side, which was not taken into account by the authors when forming comparison groups. In contrast, Kamińska et al. (2016) investigated the effect of SWI elimination on paired kidneys and, by virtually eliminating the effect of donor-side DGF risk factors, the authors obtained the expected result: SWI was an independent predictor of DGF and acute renal graft rejection in both single- and multivariate analyses, confirming the need to eliminate it [14]. The authors also noted that grafts obtained from donors with expanded criteria are probably more sensitive to SWI.

We took this assumption as the basis, and it was reflected in two stages of the study. The first experimental stage was performed on large pigs, a generally recognized optimal model for preclinical studies in nephrotransplantology. The use of experimental model of kidney autotransplantation made it possible at the planning stage of the study to exclude potential risk factors of DGF besides the one under study at the planning stage of the study: all experimental operations were performed in pigs of the same breed, age and body weight, and use of kidney autograft made it possible to exclude immunological conflict. Also, experimental conditions made it possible to create identical cold preservation time and SWI time in the groups. In KT from a standard donor, DGF did not develop in any of the cases in our study. Probably, the contribution of SWI time factor alone is not enough for the development of severe ischemic injury and poor initial graft function. However, when combined with other risk factors, prolonged vascular anastomosis formation can lead to DGF. Thus, in the model of kidney transplantation from an asystolic donor, DGF incidence in the subgroup using the standard SWI elimination method was 4.8-fold higher than that using the developed SWI elimination device, which was statistically significant ($p = 0.036$).

Thus, we have proved that the developed device allows for more effective cooling of the renal graft during formation of vascular anastomoses, even under prolonged implantation periods ($p < 0.001$). The use of this device in KT from a standard donor can slightly improve graft function, but without affecting the DGF incidence. Its use in KT from an asystolic donor significantly reduces the severity of graft ischemic injury and DGF incidence ($p = 0.036$).

Indeed, prolonged SWI is often an unpredictable risk factor for DGF. Patients with end-stage renal disease, being on hemodialysis for a long time, almost always have atherosclerotic lesion and/or calcinosis of iliac arteries. When transplanting a kidney from suboptimal age donors, the aortic area and the renal artery wall may also be affected by atherosclerotic process. So, even with an experienced surgeon, vascular reconstruction may require more time, during which graft heating is inevitable. Our SWI elimination device allows to maintain an optimally low graft temperature for long during implantation, in contrast to the classical ice bag technique ($p < 0.001$), which we demonstrated both in an experiment and in a clinical study. "Effective" SWI elimination with the developed new device was associated with statistically significantly lower incidence of DGF ($p = 0.032$) and length of hospital stay ($p = 0.024$) in patient groups comparable in terms of the main risk factors of DGF.

Thus, the use of our developed special SWI elimination device significantly reduced the burden of DGF and, thus, improved treatment outcomes in recipients of a kidney obtained from a suboptimal donor.

CONCLUSIONS

1. Prolonged SWI time (>45 minutes) is a statistically significant risk factor for DGF ($p = 0.035$).
2. The most sensitive to SWI are grafts obtained from expanded criteria donors. We provided evidence to this in an experimental model of kidney autotransplantation from an asystolic donor. The incidence of DGF in "ineffective" SWI elimination can reach 80%.
3. Our developed special SWI elimination device allows to optimally cool a graft during the entire implantation procedure, even if the surgery is prolonged. This is in contrast to the classical ice bag technique ($p < 0.001$).
4. The use of the developed special SWI elimination device in clinical practice reduces DGF incidence safely and effectively ($p = 0.032$) for grafts obtained from expanded criteria donors and with prolonged implantation time.

The authors declare no conflict of interest.

REFERENCES

1. *Chadban SJ, Ahn C, Axelrod DA, Foster BJ, Kasiske BL, Kher V et al.* KDIGO clinical practice guideline on the evaluation and management of candidates for kidney transplantation. *Transplantation*. 2020; 104 (4S1): S11–S103. PMID: 32301874. https://doi.org/10.1097/TP.0000000000003136.
2. *Chen R, Wang H, Song L, Hou J, Peng J, Dai H et al.* Predictors and one-year outcomes of patients with delayed graft function after deceased donor kidney transplantation. *BMC Nephrology.* 2020; 21 (1): 1–10. PMID: 33276737. https://doi.org/10.1186/s12882-020-02181-1.
3. *Siedlecki A, Irish W, Brennan DC.* Delayed graft function in the kidney transplant. *American Journal of Transplantation*. 2011; 11 (11): 2279–2296. PMID: 21929642. https://doi.org/10.1111/j.1600-6143.2011.03754.x.

4. *Narayanan R, Cardella CJ, Cattran DC, Cole HC, Tinckam KJ, Schiff J et al.* Delayed graft function and the risk of death with graft function in living donor kidney transplant recipients. *Am J Kidney Dis*. 2010; 56 (5): 961–970. PMID: 20870331. https://doi.org/10.1053/j.ajkd.2010.06.024.
5. *Tapiawala SN, Tinckam KJ, Cardella CJ, Schiff J, Cattranet DC, Cole EH et al.* Delayed graft function and the risk for death with a functioning graft. *J Am Soc Nephrol.* 2010; 21 (1): 153–161. PMID: 19875806. https://doi.org/10.1681/ASN.2009040412.
6. *Nagaraja P, Roberts GW, Stephens M, Horvath S, Fialovaet J, Chavez R et al.* Influence of delayed graft function and acute rejection on outcomes after kidney transplantation from donors after cardiac death. *Transplantation.* 2012; 94 (12): 1218–1223. PMID: 23154212. https://doi.org/10.1097/TP.0b013e3182708e30.
7. *Kayler LK, Magliocca J, Zendejas I, Srinivas TR, SholdImpact JD.* Impact of cold ischemia time on graft survival among ECD transplant recipients: a paired kidney analysis. *American Journal of Transplantation.* 2011; 11 (12): 2647–2656. PMID: 21906257. https://doi.org/10.1111/j.1600-6143.2011.03741.x.
8. *Wu WK, Famure O, Li Y, Kim SJ*. Delayed graft function and the risk of acute rejection in the modern era of kidney transplantation. *Kidney International*. 2015; 88 (4): 851–858. PMID: 26108067. https://doi.org/10.1038/ki.2015.190.
9. *Hameed AM, Yuen L, Pang T, Rogers N, Hawthorne WJ, Pleass HC.* Techniques to Ameliorate the Impact of Second Warm Ischemic Time on Kidney Transplantation Outcomes. *Transplantation Proceedings.* 2018; 50 (10): 3144–3151. PMID: 30577180. https://doi.org/10.1016/j.transproceed.2018.09.003.
10. *Dienst SG, Ansari MR.* Use of a Cooling Jacket During Kidney Transplantation. *Henry Ford Hospital Medical Journal*. 1971; 19 (3): 127–134.
11. *Danovitch GM* (Ed.). Handbook of kidney transplantation. Lippincott Williams & Wilkins. 2009.
12. *Karipineni F, Campos S, Parsikia A, Durinka JB, Chang PN, Khanmoradi K et al.* Elimination of warm ischemia using the Ice Bag Technique does not decrease delayed graft function. *International Journal of Surgery.* 2014; 12 (6): 551–556. PMID: 24735894. https://doi.org/10.1016/j.ijsu.2014.04.002.
13. *Khan T, Kwarcinski J, Pang T, Hameed A, Boughton P, O'Grady G et al.* Protection From the Second Warm Ischemic Injury in Kidney Transplantation Using an *Ex Vivo* Porcine Model and Thermally Insulating Jackets. *Transplantation Proceedings*. 2021; 53 (2): 750–754. PMID: 33581848. https://doi.org/10.1016/j.transproceed.2021.01.037.
14. *Kamińska D, Kościelska-Kasprzak K, Chudoba P, Hałoń A, Mazanowska O, Gomółkiewicz A et al.* The influence of warm ischemia elimination on kidney injury during transplantation – clinical and molecular study. *Scientific Reports*. 2016; 6 (1): 1–10. PMID: 27808277. https://doi.org/10.1038/srep36118.
15. *Shabunin AV, Drozdov PA, Nesterenko IV, Makeev DA, Zhuravel OS, Astapovich SA*. Risk factors for delayed kidney graft function from a deseased donor. *Transplantologiya. The Russian Journal of Transplantation*. 2022; 14 (3): 265–277. https://doi.org/10.23873/2074-0506-2022-14-3-265-277.

The article was submitted to the journal on 15.02.2023

DOI: 10.15825/1995-1191-2023-2-38-48

PERCUTANEOUS LEFT VENTRICULAR ASSIST DEVICE AS A SHORT-TERM MECHANICAL CIRCULATORY SUPPORT BEFORE HEART TRANSPLANTATION IN PATIENTS WITH HIGH PRE-TRANSPLANT PULMONARY HYPERTENSION (SERIES OF CLINICAL CASES)

V.N. Poptsov, V.V. Slobodyanik, E.A. Spirina, N.V. Petukhov, A.K. Solodovnikova, V.Yu. Voronkov, A.A. Dogonasheva, A.A. Skokova

Shumakov National Medical Research Center of Transplantology and Artificial Organs, Moscow, Russian Federation

In certain categories of patients with end-stage heart failure (HF), short-term mechanical circulatory support (MSC) is successfully used as a mechanical "bridge" to heart transplantation (HTx). In predominantly left-ventricular (LV) dysfunction, the use of isolated coronary artery bypass, especially amidst high pulmonary hypertension (PH), seems to be a more physiological method of short-term MSC. **Objective:** to present the results of a series of clinical cases of the use of percutaneous left ventricular assist device (pLVAD) before HTx in potential recipients with predominantly LV dysfunction and concomitant high PH. **Materials and methods.** Three potential heart recipients with predominantly left-sided HF and high pre-transplant PH (pulmonary vascular resistance, PVR, 4.7–6.6 Wood units) who required MSC due to progression of hemodynamic disorders were included in the study. A standard venous extracorporeal membrane oxygenation (ECMO) cannula (26 F) was used for percutaneous left atrial-femoral artery (LA–FA) bypass. The cannula was passed from the transfemoral route through the interatrial septum into the left atrial cavity. A paracorporeal centrifugal pump provided blood injection through a standard arterial ECMO cannula (15 F). **Results.** pLVAD unloaded the left ventricle effectively (PCWP reduced from 27–32 to 15–20 mmHg), reduced pre-transplant PH (mean pulmonary artery pressure (mPAP) reduced from 45–53 to 28–33 mmHg) and improved systemic hemodynamics (cardiac index (CI) increased from 1.8–1.9 to 2.1–2.6 l/min/m^2 and mean arterial pressure (mAP) from 56–59 to 70–75 mmHg). All these created the prerequisites for subsequent successful HTx. Against the background of pLVAD, transpulmonary pressure gradient (TPG) decreased from 15–25 to 13–15 mmHg, and PVR decreased from 4.7–6.6 to 2.7–3.4 Wood units. pLVAD flow rate was 2.9–3.8 L/min or 1.38–1.83 L/min/m^2 at 4700–7100 rpm. pLVAD duration ranged from 4 (n = 1) to 7 (n = 2) days. All patients underwent successful HTx. **Conclusion.** pLVAD is a highly effective method of short-term MSC in potential recipients with predominantly LV dysfunction and concomitant high PH, leading to rapid regression of the dysfunction against the background of left ventricular unloading. This short-term MSC technique can be successfully realized using standard ECMO cannulas and centrifugal pumps of any modification, without requiring additional special equipment.

Keywords: heart transplantation, mechanical circulatory support, pulmonary hypertension.

INTRODUCTION

Despite the progress in development of technology and clinical application of implantable left ventricular assist device (LVAD) systems, short-term mechanical circulatory support (MSC) by mono-, biventricular or total cardiac bypass remains one of the options for assisted circulation, which is successfully used in certain categories of patients as a mechanical "bridge" to heart transplantation (HTx) [1, 2].

The leading method of short-term MSC before transplantation is venoarterial extracorporeal membrane oxygenation (VA-ECMO), which, regardless of the character of central hemodynamic disorder (biventricular, LV-predominant or RV-predominant acute heart failure (AHF) or decompensated heart failure (HF), provides simultaneous support of systemic circulation and pulmonary gas exchange [3]. However, in AHF or acute decompensated HF, VA-ECMO is a non-physiological method of MSC, whose use may be accompanied by aggravated LV systolic dysfunction, leading to LV overload and pulmonary edema [4].

In LV-dominant dysfunction, the use of isolated coronary artery bypass in LV dysfunction seems to be a more physiological method of short-term MSC [5]. As one of

Corresponding author: Vitaly Poptsov. Address: 1, Shchukinskaya str., Moscow, 123182, Russian Federation. Phone: (963) 644-96-39. E-mail: poptsov_vit@mail.ru

the short-term MSC options for this type of cardiac pumping disorder, a percutaneous LV assist system called the TandemHeart percutaneous left ventricular assist device (CardiacAssist, Inc; Pittsburgh, USA), providing drainage of blood from the left atrium (LA) using a specially designed cannula, passed through the femoral vein and interatrial septum into the LA cavity, and subsequent injection with an external centrifugal pump through an arterial cannula into the femoral artery, was developed and introduced into clinical practice [6]. The effectiveness of TandemHeart in AHF/acute decompensated HF of various genesis has been demonstrated; it has been shown to be used as a method of pre-transplant MSC in HTx [7]. Besides, the use of percutaneous LVAD (pLVAD) seems to be more reasonable in potential recipients with high pre-transplant pulmonary hypertension (PH). This allows to estimate its degree of regression against volumetric unloading of the left heart and to make a choice between expediency of urgent HTx or long-term MSC using implantable LVAD [8].

We have developed an alternative approach to pLVAD implementation, using standard venous and arterial ECMO cannulas and a centrifugal pump as a short-term MSC method in potential cardiac recipients. This may increase the availability of this assisted circulation method.

The aim of the study was to present the results of our own series of clinical observations of the use of pLVAD as a method of pre-transplant MSC in potential heart recipients with LV-dominant dysfunction and accompanying high pulmonary hypertension (PH).

MATERIALS AND METHODS

The pLVAD program as a method of short-term pre-transplant MSC in potential cardiac recipients began in 2022, representing 2.9% of all cases of short-term pre-HTx MSC in a given year (3 of 103). Short-term MSC was used in 103 (48.6%) of the 212 HTx performed in 2022.

Clinical, hemodynamic, and echocardiographic manifestations of LV-dominant dysfunction associated with high pre-transplant PH were considered indications for this pre-transplant MSC method (Table 1).

The study included 3 patients (all men); the main parameters of their clinical, laboratory and instrumental examination before pLVAD implantation are presented in Table 2.

The pLVAD was implanted under intubation anesthesia in an operating room equipped with a fluoroscopic unit. Transesophageal echocardiography was also used to control atrial septal puncture (ASP) and positioning of the venous ECMO cannula tip in the left atrial lumen. LA cannulation was performed from percutaneous transfemoral venous access similarly to the previously described proprietary LA drainage technique for left atrial (LA) unloading (decompression) during peripheral VA-ECMO [9, 10]. The difference was in passing a larger diameter venous ECMO cannula into the LA cavity through the ASP (a 26 F venous ECMO cannula was used in all cases). The main pLVAD insertion stages were:

1. Anesthesia induction and tracheal intubation.
2. Pulmonary artery catheterization (Swan–Ganz thermodilution catheter).
3. Insertion of transesophageal echocardiography probe
4. Right or left femoral artery puncture and catheterization (creating a guaranteed vascular access) to facilitate subsequent insertion of peripheral arterial ECMO cannula.
5. Femoral artery puncture and catheterization (single-lumen catheter, diameter 14 G) on the side of subsequent cannulation with an arterial ECMO cannula to ensure guaranteed lower limb perfusion (mandatory condition).
6. Right femoral vein puncture and passing through its lumen in ascending direction with a long transseptal Endrys steel needle for LA puncture, including a curved external needle (diameter 17 G, length 75 cm) and an internal needle (diameter 19 G) with a curved elongated tip 22 G.
7. Image-guided LA transseptal puncture with fluoroscopic and echocardiographic imaging (Fig. 1).
8. Insertion of a transseptal catheter (8.5 F in diameter) into the LA cavity (see Fig. 1).
9. Insertion of super stiff guidewire (Amplatz Super Stiff J-tip guidewire 260 cm) into the LA cavity and further into one of the pulmonary veins through a transseptal catheter (see Fig. 2).

Table 1

Indications for pLVAD as a method of mechanical circulatory support before heart transplantation

SBP <90 mmHg
mAP <60 mmHg
rAP <14 mmHg
PCWP >25 mmHg
CI <2.0 L/min/m^2
VIS >5
rAP/PCWP <0.8
TAPSE >1.8 см
TPG >12 mmHg
PVR >3.5 Woods unit
No left atrial thrombus
No stenosing atherosclerosis (over 25%) of lower limb arteries

Note: SBP, systolic blood pressure; mAP, mean arterial pressure; RAP, right atrial pressure; PCWP, pulmonary capillary wedge pressure; CI, cardiac index; VIS, vasoactive inotropic score; TAPSE, tricuspid annular plane systolic excursion; TPG, transpulmonary pressure gradient; PVR, pulmonary vascular resistance.

10. Sequential dilatation of the puncture hole in the ASP using dilators from venous ECMO cannulas of increasing diameter (18, 20, 22, 24 and 26 F).
11. Insertion of venous ECMO cannula through the ASP into the LA cavity (Fig. 3).
12. Insertion of arterial ECMO cannula into the femoral artery (15 F diameter).
13. Connecting the venous and arterial ECMO cannula to the LVAD paracorporeal circuit lines (Fig. 4).
14. Initiation of percutaneous paracorporeal LVAD.

Table 2

Data of clinical, laboratory and instrumental examination of potential heart recipients before pLVAD implantation (n = 3)

Patient	Parameter									
	Sex	Age (years)	Height (cm)	Weight (kg)	Body surface (m^2)	HF (stages)	NYHA	AF	VIS	Waiting list (days)
1	M	41	176	60	1.75	2B	4	No	12	7
2	M	40	184	87	2.11	2B	4	Yes	6	4
3	M	57	182	86	2.10	2B	4	No	8	15
Patient	Parameter									
	LA (cm)	LA (mL)	RV (cm)	LVEDV (mL)	LVEF (%)	MV (regurgitation grade)	TV (regurgitation grade)	TAPSE (cm)	HR	mAP (mmHg)
1	4.7	85	2.6	179	18	3.0	1.5	2.3	105	59
2	6.4	165	3.4	374	16	3.0	2.0	1.9	94	56
3	5.3	112	3.2	228	19	3.0	2.0	2.2	110	57
Patient	Parameter									
	rAP (mmHg)	PASP (mmHg)	PCWP (mmHg)	PCWP (mmHg)	CI, L/min/m^2	TPG (mmHg)	PVR (Woods unit)	pHv	BEv (mmHg)	Lactate (mmol/l)
1	8	69	53	32	1.9	21	6.4	7.38	–2.8	2.1
2	10	74	54	29	1.8	25	6.6	7.37	–0.4	1.9
3	11	62	45	27	1.8	18	4.7	7.44	1.6	2.4
Patient	Parameter									
	PvO_2 (mmHg)	SvO_2, %	Na (mmol/L)	Urea (mmol/L)	Creatinine (μmol/L)	Total bilirubin (μmol/L)	ALT (units/L)	AST (units/L)	Total protein (g/L)	INR
1	35.7	66.6	128	3.6	40.3	25.5	6.6	12.9	67.2	1.31
2	39.0	72.0	131	9.7	39.8	52.1	17.3	28.7	58.7	1.33
3	27.0	54.3	142	11.2	84.1	144.6	38.6	117.7	57.6	1.31

Note: HF, heart failure class according to Strazhesko–Vasilenko; NYHA, New York Heart Association (NYHA) functional class; AF, atrial fibrillation; VIS, vasoactive inotropic score; LA, left atrium; RV, right ventricle; LVEDV, left ventricular end-diastolic volume; LVEF, left ventricular ejection fraction; MV, mitral valve; TV, tricuspid valve; TAPSE, tricuspid annular plane systolic excursion; HR, heart rate; mAP, mean arterial pressure; RAP, right atrial pressure; PASP, pulmonary artery systolic pressure; mPAP, mean pulmonary artery pressure; PCWP, pulmonary capillary wedge pressure; CI, cardiac index; TPG, transpulmonary pressure gradient; PVR, pulmonary vascular resistance; ALT, alanine transaminase; AST, aspartate transaminase, INR, international normalized ratio.

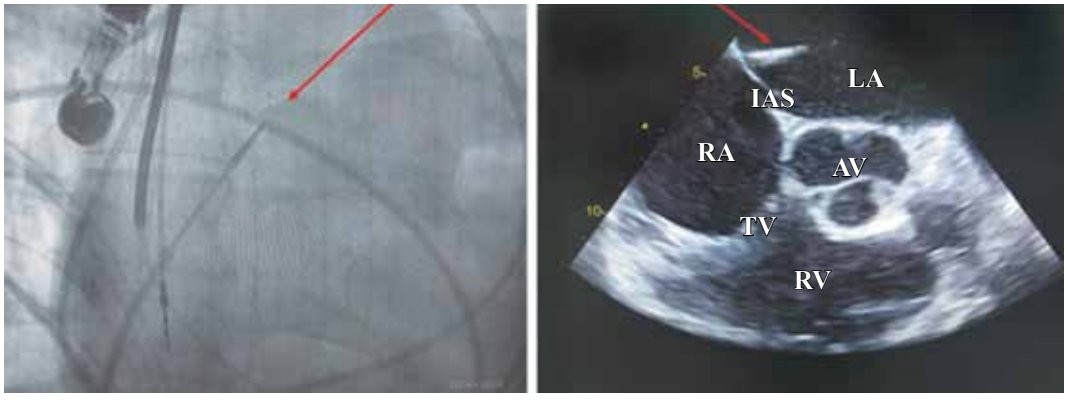

Fig. 1. Image-guided transseptal puncture for access to the left atrium and insertion of transseptal catheter (8.5 F diameter, indicated by red arrows) into its cavity using echocardiographic-fluoroscopic fusion imaging. AV, aortic valve; LA, left atrium; IAS, interatrial septum; RV, right ventricle; RA, right atrium, TV, tricuspid valve

Percutaneous LVAD was performed using Medos DeltaStream blood pump with a centrifugal pump (16 ml filling volume) (see Fig. 4).

Hypocoagulation was performed by continuous infusion of unfractionated heparin, maintaining the target level of activated clotting time at 140–160 sec.

Immediately before the start of cardiopulmonary bypass (CPB), during HTx surgery under transesophageal echocardiographic control, the venous ECMO cannula was brought down from the LA cavity to the level of the intrahepatic inferior vena cava, which corresponded to the 35–40 cm mark at the percutaneous entrance site. At this stage, blood was drained from left to right through the formed artificial defect in the ASP (Fig. 5). At all subsequent stages, including the CPB period and early postperfusion period, and taking into account the absence

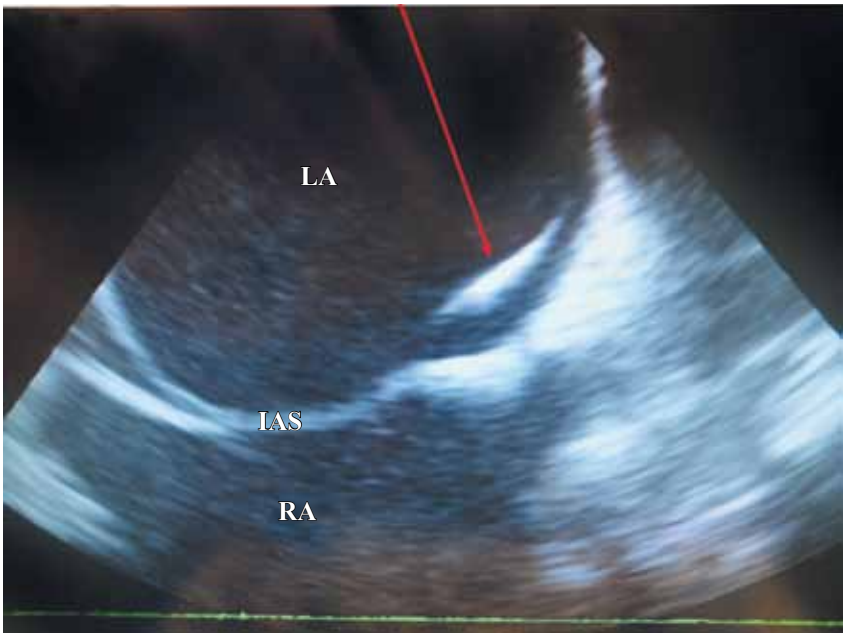

Fig. 2. Insertion of a super-stiff guidewire (Amplatz Super Stiff J-tip guidewire 260 cm, indicated by red arrow) into the left atrial cavity via transseptal catheter. LA, left atrium; IAS, interatrial septum; RA, right atrium

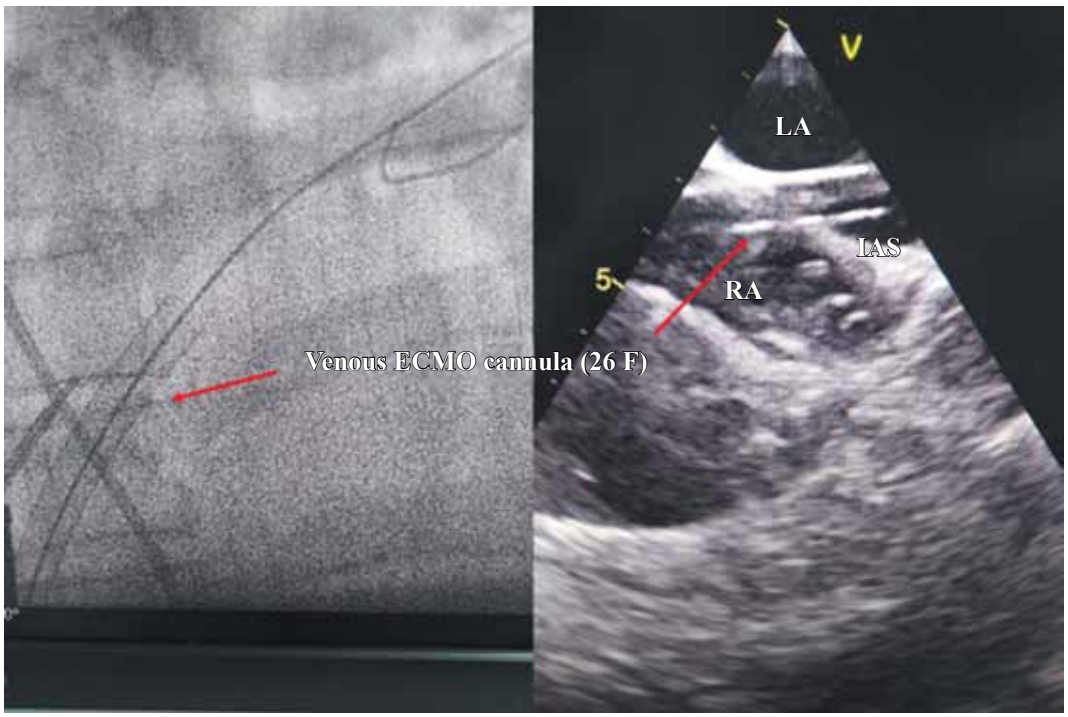

Fig. 3. Insertion of venous ECMO cannula (26 F) through the interatrial septum into the left atrial cavity. LA, left atrium; IAS, interatrial septum; RA, right atrium

of a membrane oxygenator in the circuit, extracorporeal blood flow was maintained at no more than 0.5 l/min to reduce admixture of venous blood pumped through the femoral arterial ECMO cannula into systemic circulation. In the case of severe heart graft dysfunction requiring post-transplant MSC, a membrane oxygenator was integrated into the extracorporeal circuit and thus switched to peripheral VA-ECMO. With a stable optimal cardiac graft function and no signs of delayed dysfunction of the transplanted heart, the venous and arterial ECMO cannulas were removed no earlier than 12 hours after the end of HTx surgery.

RESULTS

Uncomplicated LA puncture and cannulation was performed from percutaneous transfemoral venous access in all cases. Surgical intervention for percutaneous bypass lasted for 48 to 74 minutes. All patients were activated within 1 hour after the end of surgery and were on spontaneous breathing on oxygen therapy (4–6 l/min) until HTx. Percutaneous LVAD unloaded the left heart effectively (PCWP reduced from 27–32 to 15–20 mmHg), pre-transplant PH reduced (mPAP reduced from 45–53 to 28–33 mmHg) and systemic hemodynamics improved (CI increased from 1.8–1.9 to 2.1–2.6 l/min/m^2 and mAP from 56–59 to 70–75 mmHg), which set the stage for subsequent successful HTx (Table 3). Against the background of pLVAD, TPG decreased from 21 to 13 (patient 1), from 25 to 15 (patient 2), from 18 to 14 mmHg (patient 3), PVR from 6.4 to 2.9 (patient 1), 6.6 to 3.4 (patient 2), 4.7 to 2.7 Wood units (patient 3). The pLVAD flow rate was 2.9–3.8 L/min or 1.38–1.83 L/min/m^2 at 4700–7100 rpm. pLVAD lasted for 4 (n = 1) to 7 (n = 2) days.

The patients underwent HTx from male donors 54 (patient 1), 40 (patient 2), and 46 (patient 3) years of age with ischemia time of 167, 150, and 160 minutes, respectively. Two patients (patient 1 and 2) did not show early cardiac graft dysfunction. Hence, the extracorporeal pre-transplant LVAD circuit was removed 5 and 7 hours after the end of the surgical intervention, respectively. The highest dopamine and adrenaline doses in the early posttransplant period in both patients were 6 μg/kg/min and 40 ng/kg/min, respectively. Patient 3 had hemodynamic and echocardiographic signs of biventricular cardiac graft dysfunction, which required posttransplant

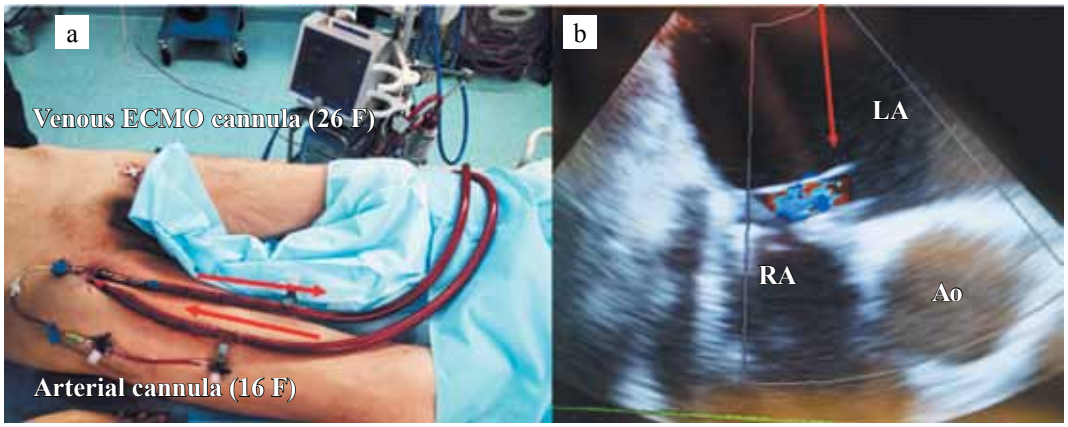

Fig. 4. Patient with pLVAD (a, red arrows indicate blood flow direction) and blood drainage from left atrium into venous ECMO cannula (26 F) (b, indicated by red arrow). Ao, aorta; LA, left atrium; RA, right atrium

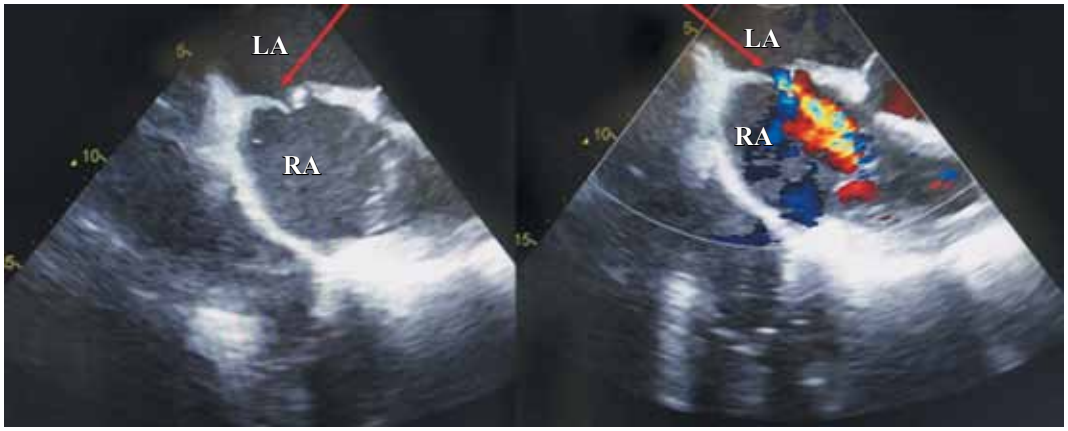

Fig. 5. Atrial septal defect (indicated by red arrows) formed after removal of drainage cannula from the left atrial cavity, with left-to-right blood shunt

MSC. A membrane oxygenator was integrated into the extracorporeal circuit of the pre-transplant LVAD, and it was transformed into a peripheral VA-ECMO, whose blood flow rate, centrifugal pump rpm and duration of application were 2.7 L/min, 6800 per min and 3 days, respectively. All patients survived and were discharged from the hospital. At the end of the follow-up period (December 31, 2022), all patients were alive. The follow-up period for the patients was 119 (patient 1), 90 (patient 2), and 35 (patient 3) days.

DISCUSSION

Despite the fact that according to ISHLT, over 50% of HTx are performed in patients with long-term pre-transplant MSC by implanted LVAD method, individual transplant centers, usually having a large annual volume of heart transplants, also adopt the practice of urgently performing them in patients with short-term MSC [11]. VA-ECMO remains the most commonly used short-term MSC before HTx with a predominant peripheral technique for its implementation [12]. VA-ECMO, simultaneously improving systemic blood flow and gas exchange, ensures survival to emergency HTx in most patients [13]. However, being a non-physiological method of MSC in patients with AHF or acute decompensated HF, which includes the majority of potential heart recipients, VA-ECMO can be accompanied by exacerbation of LV dysfunction, leading to left heart overload, pulmonary vascular congestion and pulmonary edema [14]. To resolve this pathological condition, various mechanical LV unloading methods have been proposed [15].

In potential cardiac recipients with LV-dominant failure (e.g., coronary heart disease), the use of isolated LVAD appears to be a more physiological and effective method of pre-transplant MSC. However, implementation of paracorporeal LVAD requires sternotomy with central cannulation of the left atrium or left ventricle and aorta. This increases the traumaticity not only of the LVAD, but also of subsequent HTx, which becomes a repeated surgical intervention with increased risk of peritransplant complications and death [17].

Table 3

Central hemodynamic parameters before and against the background of pLVAD (n = 3)

Parameter	Study phase	Patient 1	Patient 2	Patient 3
HR (mins)	Before LVAD	105	94	110
	Day 1 after LVAD	89	91	93
	Before HTx	84	90	88
mAP (mmHg)	Before LVAD	59	56	57
	Day 1 after LVAD	69	73	72
	Before HTx	70	71	75
rAP (mmHg)	Before LVAD	9	10	11
	Day 1 after LVAD	10	9	10
	Before HTx	8	8	9
PCWP (mmHg)	Before LVAD	53	54	45
	Day 1 after LVAD	40	38	32
	Before HTx	33	33	28
PCWP (mmHg)	Before LVAD	32	29	27
	Day 1 after LVAD	22	19	18
	Before HTx	20	18	15
CO (L/min)	Before LVAD	3.3	3.8	3.8
	Day 1 after LVAD	4.5	4.3	4.7
	Before HTx	4.5	4.4	4.9
CI, L/min/m^2	Before LVAD	1.9	1.8	1.8
	Day 1 after LVAD	2.6	2.0	2.2
	Before HTx	2.6	2.1	2.3
TPG (mmHg)	Before LVAD	21	25	18
	Day 1 after LVAD	18	19	14
	Before HTx	13	15	13
PVR (Woods unit)	Before LVAD	6.4	6.6	4.7
	Day 1 after LVAD	4.0	4.4	3.0
	Before HTx	2.9	3.4	2.7

Note: HR, heart rate; mAP, mean arterial pressure; RAP, right atrial pressure; mPAP, mean pulmonary artery pressure; PCWP, pulmonary capillary wedge pressure; CO, cardiac output; CI, cardiac index; TPG, transpulmonary pressure gradient; PVR, pulmonary vascular resistance.

The introduction into clinical practice of pLVAD technique implemented as TandemHeart pLVAD was aimed at increasing efficiency and reducing MSC traumaticity in patients with LV-dominant AHF or decompensated HF [17]. The method is based on LA transfemoral transvenous cannulation (21 F diameter) with a specially designed cannula with a beak-shaped, curved dilator to facilitate passage through the atrial septum. Arterial blood drained from the LA is pumped using a centrifugal pump through the femoral cannula (15 F diameter) into the systemic circulation [18]. LA cannulation is performed under fluoroscopic and echocardiographic control in an X-ray operating room. The pLVAD procedure lasts for 14 to 25 minutes [19].

The successful experience of using TandemHeart pLVAD as a highly effective short-term MSC before HTx as well as in severe cardiac transplant rejection has been demonstrated [7]. There is also accumulated experience of successful application of this short-term MSC technique in the treatment of patients with acute fulminant myocarditis of various etiology, myocardial infarction, as well as a method of preventive MSC during endovascular coronary interventions and transcatheter aortic valve replacement of high operational risk [20, 21]. TandemHeart pLVAD was used as a short-term MSC before implantation of long-term LVAD (bridge to bridge) systems [8].

Like any high-tech treatment method, short-term MSC realized using TandemHeart pLVAD has both advantages and disadvantages related to the risk of various complications. Transfemoral transvenous LA cannulation requires to be performed in the X-ray operating room conditions and by X-ray endovascular surgeons with extensive experience in transseptal LA puncture, considering the risk of aortic and atrial perforation. LA cannulation is associated with the risk of thrombosis at the LA cannula site, which increases the risk of cardioembolic complications [22]. If the drainage cannula depth into the LA cavity is insufficient, it can be dislocated into the right atrium, which will result in venous blood injection into systemic blood flow that will require either MSC termination or its transformation into VA-ECMO by integrating into the membrane oxygenator circuit [22]. In addition, there is a risk of lower limb ischemia due to cannulation of the return (arterial) cannula of the femoral artery. Possible complications include bleeding and purulent inflammation in the femoral cannulation site, arteriovenous fistula, femoral nerve damage, lymphocele, etc. [23]. The incidence of vascular complications with percutaneous LVAD ranges from 4.0 to 9.7 [24].

Introduction of transcatheter, minimally invasive LVAD techniques (e.g., Impella) has led to a reduction in the use of TandemHeart pLVAD [1]. However, the use of this MSC method seems still relevant in potential cardiac recipients with LV-dominant intracardiac hemodynamic disorders when implementing emergency HTx programs using short-term assisted circulation techniques.

Given the absence of a registered TandemHeart pLVAD in the Russian Federation, we assumed that this short-term MSC technique can be successfully implemented by using a standard venous ECMO cannula of the required size and design, which can be performed from transfemoral venous access through the right atrium and ASP into the LA cavity, provided there are radiological endovascular surgeons with experience in transseptal LA puncture. We have chosen the Medos venous ECMO cannula, which, unlike other counterparts, has no lateral drainage holes and will provide isolated drainage of arterial blood from the LA without admixture of venous blood from the right heart and inferior vena cava. In addition, one of the indications for pLVAD use was acute decompensated HF with LV-predominant intracardiac hemodynamics, requiring short-term MSC, and accompanied by high, borderline pre-transplant PH.

A series of presented clinical cases demonstrated the high hemodynamic efficiency and safety of this technique of pre-transplant short-term MSC by percutaneous paracorporeal LVAD. Application of this MSC method not only improved systemic hemodynamics, but also regressed PH to the level allowing to perform HTx by orthotopic technique effectively without development of severe right ventricular dysfunction of the heart transplant. In the absence of rapid PH regression, percutaneous LVAD can be used as an intermediate method of assisted circulation before implantation of a long-term LVAD (bridge-to-bridge) system [25]. If early dysfunction of the transplanted heart occurs, the pre-transplant LVAD circuit can be used for post-transplant VA-ECMO after integration of the membrane oxygenator. Our presented experience of short-term MSC by percutaneous LVAD can be used in the domestic medical practice not only as auxiliary circulation before HTx, but also in other clinical situations accompanied by critical LV dysfunction.

CONCLUSION

Percutaneous left ventricular assist device is a highly effective short-term MSC method in potential heart recipients with dominant LV dysfunction and concomitant high pulmonary hypertension, leading to rapid regression of the dysfunction against the background of LV unloading. Depending on the clinical situation, pLVAD can be considered a method of short-term MSC before urgent HTx or implantation of long-term MSC systems. This short-term MSC technique can be successfully implemented using standard ECMO cannulas for femoral transfemoral cannulation and centrifugal pump of any modification, without requiring additional special equipment.

The authors declare no conflict of interest.

REFERENCES

1. *Brown LJ, Estep JD*. Temporary percutaneous mechanical circulatory support in advanced heart failure. *Heart Failure Clin*. 2016; 12: 385–398.
2. *Reich H, Ramzy D, Moriguchi J et al*. Acceptable post-heart transplant outcomes support temporary MCS prioritization in the New OPTN/UNOS heart allocation policy. *Transplant Proc.* 2021; 53: 353–357.
3. *Gonzales MH, Acharya D, Lee S et al*. Improved survival after heart transplantation in patients bridged with extracorporeal membrane oxygenation in new allocation system. *J Heart Lung Transplant*. 2021; 40: 149–157.
4. *Xie A, Forrest P, Loforte A*. Left ventricular decompression in veno-arterial extracorporeal membrane oxygenation. *Ann Cardiothorac Surg*. 2019; 8: 9–18.
5. *Smith L, Peters A, Mazimba S et al*. Outcomes of patients with cardiogenic shock treated with TandemHeart percutaneous ventricular assist device: importance of support indication and definitive therapies as determinants of prognosis. *Catheter Cardiovasc Interv.* 2018; 92: 1173–1181.
6. *Kar B, Adkins LE, Civitello AB et al*. Clinical experience with the TandemHeart percutaneous ventricular assist device. *Tex Haert Inst J*. 2006; 33 (2): 111–115.
7. *Bruckner BA, Jacob LP, Gregoric ID et al*. Clinical experience with the TandemHeart percutaneous ventricular assist device as bridge to cardiac transplantation. *Tex Heart Inst J.* 2008; 35: 447–450.
8. *Gregoric ID, Jacob LP, La Francesca S et al*. The TandemHeart as a bridge to a long-term axial-flow left ventricular assist device. *Tex Heart Inst J*. 2008; 35: 125–129.
9. *Poptsov VN, Spirina EA, Slobodyannik VV.* Sposob gemodinamicheskoy razgruzki levogo zheludochka pri provedenii perifericheskoy veno-arterial'noy ekstrakorporal'noy membrannoy oksigenatsii (Patent na izobretenie № 2526880, zaregistrirovano 03.07.2014 g.).
10. *Poptsov VN, Spirina EA, Slobodyannik VV, Zakharevich VM, Eremeeva OA, Masyutin SA*. Chreskozhnoe transfemoral'noe drenirovanie levogo predserdiya kak metod ob''emnoy razgruzki levogo zheludochka pri provedenii perifericheskoy veno-arterial'noy membrannoy oksigenatsii u potentsial'nykh retsipientov serdtsa. *Vestnik transplantologii i iskusstvennykh organov*. 2013; 15 (4): 70–83.
11. *Viera JL, Ventura HO, Mehra MR*. Mechanical circulatory support in advanced heart failure: 2022 and beyond. *Progress in Cardiovasc Dis*. 2020; 63: 630–639.
12. *Hebert M, Noly PE, Lamarche Y et al*. Early and long-term outcomes after direct bridge-to-transplantation with extracorporeal membrane oxygenation. *Heart Surg Forum.* 2021; 24: E1033–E1042.
13. *Hess NR, Hickey GW, Sultan I, Kilic A*. Extracorporeal membrane oxygenation bridge to heart transplantation: trends following the allocation change. *J Card Surg*. 2020 Oct 14. doi: 10.1111/jocs. 15118.
14. *Guglin M, Zucker MJ, Neumann FJ*. Venoarterial ECMO for adults: JACC scientific expert panel. *J Am Coll Cardiol*. 2019; 73: 698–716.
15. *Tepper S, Masood MF, Baltazar Garsia M et al*. Left ventricular unloading by Impella device versus surgical vent during extracorporeal life support. *Ann Thorac Surg*. 2017; 104: 861–867.
16. *Ando M, Garan AR, Takayama H et al*. A continuous-flow external ventricular assist device for cardiogenic shock: evolution over 10 years. *J Thorac Cardiovasc Surg*. 2018; 156: 157–165.
17. *Thiele H, Sick P, Boudriot T, Diederich KW et al*. Randomized comparison of intra-aortic balloon support with a percutaneous left ventricular assist device in patients with revascularized acute myocardial infarction complicated by cardiogenic shock. *Eur Heart J.* 2005; 26: 1276–1283.
18. *Rajdev S, Krishnan P, Irani A et al*. Clinical application of prophylactic percutaneous left ventricular assist device (TandemHeart) in high-risk percutaneous coronary intervention using an arterial preclosure technique: single-center experience. *J Invasive Cardiol.* 2008; 20: 67–72.
19. *Sharma AB, Kovacic JC, Kini AS*. Percutaneous left ventricular assist device devices. *Intervent Cardiol Clin*. 2012; 1: 509–622.
20. *Alli OO, Singh IM, Holmes DR et al*. Percutaneous left ventricular assist device with TandemHeart for high-risk percutaneous coronary intervention: the Mayo clinic experience. *Catheterization Cardiovasc Interv*. 2012; 80: 726–734.
21. *Khalife W, Kar B*. The TandemHeart pLVAD in the treatment of acute fulminant myocarditis. *Tex Heart Inst J.* 2007; 34: 209–213.
22. *Gregoric ID, Bruckner BF, Jacob L et al*. Techniques and complication of TandemHeart ventricular assist device insertion during cardiac procedure. *ASAIO J*. 2009; 55: 251–254.
23. *Kreidieh B, Gray WA*. The road to support is paved with good interventions: vascular complications of percutaneous LVAD use. *Catheter Cardiovasc Interv*. 2020; 95: 317–318.
24. *Patel N, Sharma A, Dalia T et al*. Vascular complications associated with percutaneous left ventricular assist device placement: a 10-year US perspective. *Catheter Cardiovasc Interv.* 2020; 95: 309–316.
25. *Kurihara C, Kawabori M, Suguira T et al*. Bridging to a long-term ventricular assist device with short-term mechanical circulatory support. *Artificial Organs J.* 2018; 42: 589–596.

The article was submitted to the journal on 12.01.2023

DOI: 10.15825/1995-1191-2023-2-49-56

BIVENTRICULAR MECHANICAL CIRCULATORY SUPPORT. HISTORY AND CURRENT STATE OF THE PROBLEM

M.O. Zhulkov, D.A. Sirota, D.S. Khvan, A.G. Makaev, H.A. Agaeva, I.S. Zykov, A.V. Fomichev, O.V. Poveschenko, M.A. Surovtseva, A.M. Chernyavsky

Meshalkin National Medical Research Center, Novosibirsk, Russian Federation

Medical management of end-stage chronic heart failure (HF) has evolved significantly over the past few decades. With a better understanding of the pathophysiology of HF, new pharmacological agents have been synthesized. However, survival in this cohort of patients with medical treatment remains extremely low. This has stimulated the development of surgical methods of treatment. Recent technological advances in the development of mechanical circulatory assist devices have made possible a single-stage implantation of two centrifugal pumps as an alternative to a total artificial heart. Today ventricular assist devices can be implanted to provide both univentricular and biventricular support depending on the severity of hemodynamic disorders, target organ damage, likelihood of recovery and heart transplantation.

Keywords: heart transplantation, mechanical circulatory assist device, heart failure, circulatory support.

Despite all the efforts by doctors and scientists, nearly 300,000 patients worldwide die of HF as a primary or contributory cause each year [1]. Heart transplantation (HTx) remains the gold standard therapy for end-stage HF. However, this operation is severely limited by the number of available donor organs. That is why implantation of the left ventricular assist device (LVAD) has become the only and most effective alternative option to help this cohort of patients. Since the first LVAD was approved by the U.S. Food and Drugs Administration (FDA), the number of implanted devices has grown every year and now exceeds the number of heart transplants performed [2].

For many years, the development of surgical methods of treating HF was focused on restoring and maintaining the pumping function primarily of the left ventricle. As a result, much less attention has been paid to the study of pathogenesis and ways of maintaining right heart function. However, in the majority of cases, end-stage HF represents a biventricular heart dysfunction. In such cases, LVAD implantation is not only ineffective, but also associated with a high risk of right ventricular (RV) dysfunction. Thus, according to studies, right ventricular (RV) dysfunction is estimated to occur in 10% to 30% of patients post-LVAD implantation [3–5]. Data from the Interagency Registry for Mechanically Assisted Circulatory Support (INTERMACS) show that even with the current level of development of LVAD systems, 1-year survival for those with biventricular failure remains unchanged in different periods (2006–2012/2013–2016) at 56% versus 55%, respectively [6]. According to J.K. Kirklin et al., 368 biventricular assist devices (BiVADs) were implanted in 2011, with survival rates decreasing as the duration of biventricular mechanical support increased: 70% at 3 months, 62% at 6 months, 55% at 12 months, and 53% at 24 months of intervention [7].

Despite the discovery of a number of predictors of RV dysfunction (published literature identifies at least 25 different potential predictors of severe RV failure in LVAD recipients) post-LVAD implantation, most of them have low specificity and sensitivity and therefore are of low effectiveness in clinical practice [5, 8–12]. The absence of precise predictors of RV dysfunction has forced clinicians to use intraoperative decision-making tools based on the results of hemodynamic parameter studies after LVAD implantation or within hours/days after implantation. Lack of exact data and algorithms lead to longer decision-making in choosing a right heart mechanical support method, and also the optimum model of the device. Because of this, clinical results of this strategy were suboptimal, which explained the significant morbidity and mortality [13].

The bulkiness of the early LVAD models ruled out the possibility of concurrent implantation of two pumps in order to realize biventricular cardiac support [14–16]. For this reason, the only way to restore hemodynamics of pulmonary circulation was to use temporary extracorporeal mechanical circulatory support techniques [17]. Unfortunately, extracorporeal devices had a number of drawbacks – poor blood compatibility, high infection rate, high frequency of cerebrovascular complications and the need for a long hospital stay. This reduced the quality of life of patients significantly and triggered scientific interest in the development of implantable devices [18, 19].

Corresponding author: Alexander Makaev. Address: 15, Rechkunovskaya str., Novosibirsk, 630055, Russian Federation. Phone: (905) 198-33-31. E-mail: makaev_a@meshalkin.ru

Over the past decades, LVAD models have undergone significant technological improvement. However, the desire of surgeons to replicate the success of LVADs and implant the developed models of long-term mechanical circulatory support devices in the right side came with a number of challenges [6, 20]. The first models of devices implanted as BiVAD were pulsatile models. One of the most recognizable biventricular support devices was the Thoratec VAD system (Abbott Laboratories, Chicago, Illinois). Post-implant actuarial survival was 69.1 ± 5.0%, 48.7 ± 5.5%, 41.9 ± 5.5%, and 38.4 ± 5.6% at 1 month, 1 year, 3 years, and 5 years, respectively. Because of the ease of implantation, the device was widely used in patients with cardiogenic shock [21, 22].

Another pulsatile pump model currently used as a BiVAD is the EXCOR VAD (Berlin Heart AG, Berlin, Germany). This device has been widely used in the pediatric group. Despite the extracorporeal connection scheme and significant limitations in the postoperative period, EXCOR VAD is the only method of saving children with HF, it allows waiting for a donor organ. According to S.E. Bartfay et al., the overall 5-year survival rate after EXCOR Berlin Heart implantation was 90% for children and 75% for adults (P = 0.3), with a 1-year survival rate of almost 80% [23].

Subsequently, pulsatile models replaced axial and centrifugal pumps that generate continuous flow, such as the Jarvik-2000 VAD model (Jarvik Heart, NewYork, NY) [24–27]. According to the last report from INTERMACS, 618 continuous-flow BiVADs have been implanted [6]. The HeartMate II LVAD (Thoratec, Pleasanton, CA) has long been one of the best LVAD models because of the low risk of device thrombosis. However, limited experience of using this device for biventricular support has been published in the literature, since, due to significant dimensions of the device, single-stage implantation of two pumps required complete ventricular removal [28–30].

For this reason, miniaturization of engineered device models remains an important challenge for engineers. One widely known miniaturized device model is the Impella RP device (Abiomed Inc., Danvers, Massachusetts), approved in 2015 by the FDA as a percutaneous temporary support device. Later, a number of studies proved the high efficacy of this device as a right ventricular assist device (RVAD) in the short term. In the RECOVER RIGHT study, the survival rate was 78%, significantly higher than for open RVAD implantation options [31–33]. In 2019, a clinical case study of minimally invasive BiVAD was published; the Impella 5.0 and Impella RP (Abiomed, Inc, Danvers, Massachusetts) were first successfully used as devices. This was the first successful case of using a single-stage implantation of this device model as a bridge to transplantation in BiVAD configuration [34].

The small profile and possibility of intrapericardial concurrent insertion of two HeartWare HVAD devices (Medtronic Corp, Minneapolis, Minnesota) have generated great interest in application of this device as a BiVAD [35–40]. According to A. Loforte et al., the 1-year survival in a series of 13 implantations of HeartWare HVAD as BiVAD was 62% [36]. According to T. Krabatsch et al., HeartWare HVAD model was implanted as a BiVAD in 17 patients. The postload for the right device was artificially increased by local reduction of the outflow tract diameter, and the effective length of the inlet cannula was reduced by adding two 5-mm silicone rings. The 30-day survival rate was 82%, with 59% of patients being discharged home. In this patient series, postoperative bleeding was the most frequent complication (6 patients) [41]. A small series of S. Shehab et al. reported 100% survival in 3 patients and 54% survival in 13 patients [42]. In F.A. Arabía et al., 1-, 6- and 12-month survival rates post-BiVAD implantation (HeartWare HVAD model) were 89%, 68% and 62%, respectively. Moreover, there was no statistical difference in survival in comparison with the patients who received LVAD/temporary RVAD [43].

Recently, there have been a number of publications describing experience with the HeartMate III (Thoratec Inc., USA). J. Lavee et al. evaluated the safety and clinical efficacy of the HeartMate III in a BiVAD configuration in 14 patients at 6 medical centers worldwide. Nine of these patients (64%) were alive as of January 1, 2018. Eight of the 9 had continued on BiVAD support for 95 to 636 (mean 266) days: 7 at home, and 1 successfully transplanted after 98 days of BiVAD support. Five patients died after 10, 60, 83, 99, and 155 days of support, respectively. The causes of death were sepsis in three patients, as well as hemorrhagic stroke and right pump thrombosis [44]. According to D. McGiffin et al. in a series including 12 patients, actuarial survival at 18 months was 91.7%. At 18 months after the procedure, 5 patients (41.7%) had undergone cardiac transplantation, 5 patients (41.7%) were alive and on biventricular support, 1 patient had died (8.3%), and 1 patient had device explantation for myocardial recovery (8.3%) [45].

Despite the existing world experience in the use of BiVAD, the surgical technique for device implantation is still under discussion. Insertion of an LVAD inflow cannula through the left ventricular (LV) apex or diaphragmatic wall is considered convenient and safe in most cases. Placement of the RVAD inflow cannula into the RV cavity or right atrium remains less clear. However, RVAD thrombosis is one of the major problems of BiVAD with an event rate of 30% to 37% in early reports [42, 46–48]. The multicenter and recent single-center HeartMate III study as a BiVAD showed a lower rate of thrombosis (7–20%), but the inflow spigot and outflow tract locations remain an open question [44, 45].

The study in these series showed a trend towards a better result in the case of right atrial (RA) cannulation. However, it is unclear what factors contribute to more frequent right pump thrombosis. Potential advantages of RA cannulation may be the convenient positioning of the pump in the right pleural cavity compared with intrapericardial RVAD placement over the diaphragm, and the absence of RV and interventricular septum compression by the pump body. Whereas right ventricular cannulation can lead to 'swallowing' of the tricuspid valve leaflets or subclavian structures. This complication was often observed in the case of implantation of pulsatile RVAD models, where one of the solutions was tricuspid valve dissection. It should be kept in mind that although removal of tricuspid valve leaflets helps to solve the problem of 'swallowing' by the pump and partially thrombosis of the device, still in case of mechanical device failure, the patient will need immediate restoration of quasi-normal RV function. Another reason for higher frequency of RVAD thrombosis is the need to reduce rotor speed to the maximum allowable values in order to optimize pulmonary circulation hemodynamics. However, in the case of devices implementing hydrodynamic suspension of the rotor, such modes threaten to unbalance the rotor position in the pump cavity and to increase the risk of thrombosis. For this reason, the latest HeartMate III fully magnetic suspension centrifugal pump compares favorably with its predecessors. In a number of studies, the low rate of thrombosis reported when using the HeartMate III as an LVAD has also been noted in the RVAD configuration [33, 35].

The inflow cannula of mechanical circulatory support devices was designed based on LV geometry and is unsuitable for RA and RV cannulation. Therefore, in the case of RA cannulation, in order to reduce the intraluminal length of the RVAD inflow cannula, the pump profile was increased using felt plates glued together using Bioglue (CryoLife, Guildford, UK) (Fig.).

In reviewing the outcomes of inflow cannula placement for RVAD in a study by E.J. Maynes et al., pump thrombosis occurred at a similar rate between RA cannulation and RV cannulation groups: 3/10 (30.0%) versus 6/20 (30.0%), respectively. However, Kaplan–Meier analysis when censored for transplant showed higher survival with RA HVAD compared to RV HVAD (P = .036), with an estimated survival at 1 year of 91.7% (95% CI 77.3–100.0) in RA HVAD versus 66.2% (95% CI 48.9–89.6) for RV HVAD [51].

The series by S. Shehab et al. showed a higher incidence of pump thrombosis with inflow cannula implantation in the right ventricle compared with placement in the right atrium (50% versus 14%) [42]. The authors

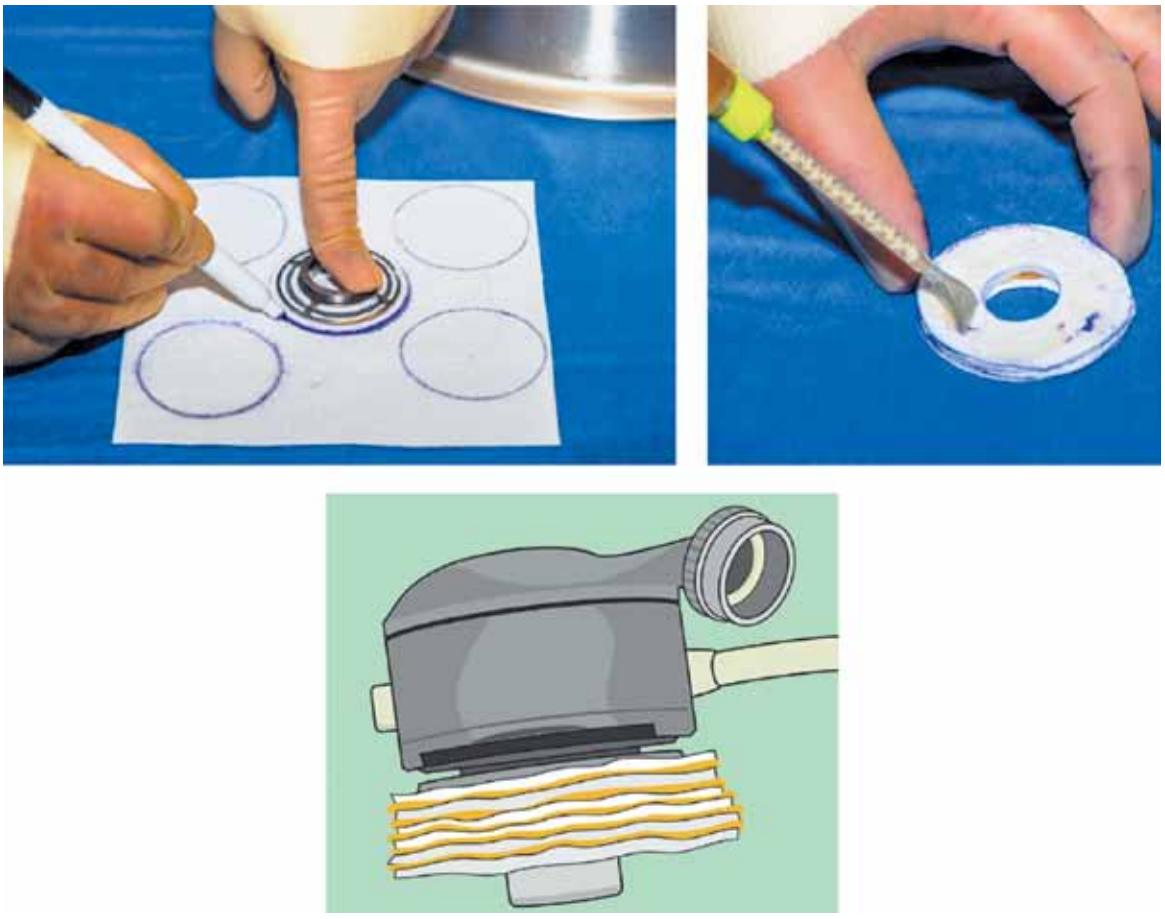

Fig. Preparation of the RVAD inlet cannula [49, 50]

concluded that this complication may have been associated with post-implant RV remodeling, which led to reduced chamber size [36, 39, 42].

Another object of controversy has been the RVAD outflow tract, since a number of surgeons have suggested the possible effectiveness of narrowing and lengthening the RVAD outflow line in order to optimally switch the two devices [48, 49]. On the contrary, in the BiVAD group by C. Lo et al., 9 out of 14 cases did not use RVAD outflow tract reduction [52]. A similar point of view is shared by E. Potapov et al., who point out that there is no need to narrow the outflow tract, and also recommend reducing the length of the prosthesis and anastomose the latter with the pulmonary trunk at an angle of 90° [48].

The timing of the decision to use BiVAD plays a key role in treatment outcomes. For example, according to T. Kuroda et al., 40% of BiVAD patients (HeartMate III model) received RVAD within 0–2 days post-LVAD implantation, and 23% of RVAD implantations were performed within 3–14 days [53]. Severe late RV failure among LVAD patients requiring mechanical support 3–12 months post-LVAD implantation is very rare [54]. Therefore, if BiVAD placement after LVAD implantation occurred earlier, the duration of BiVAD support is expected to be short (up to 17 days) [55–57].

J. Vierecke et al. investigated 37 long-term BiVADs, 342 LVAD + short-term RVAD implants and 34 total artificial heart (TAHs). Berlin Heart Excor (n = 5), HeartWare HVAD (n = 22), Thoratec pVAD (n = 10) were used as models for RVAD. The 1-year survival rate was 55% for patients with a continuous flow BiVAD; 52% for patients with an LVAD + short-term RVAD; 37% for patients with pulsatile BiVADs; and 36% for patients with a TAH. The adverse events profile remained high, with no significant difference among pump types. After 3 months of LVAD + short-term RVAD support, 46.7% still required ongoing support, and only 18.5% were weaned from RVAD support; 33.1% died. Device freedom from dysfunction and thrombosis was similar across all groups at 18 months (P = 0.63): 83% in patients with TAH, 82% in the pulsatile BiVAD model group, 95% in continuous-flow BiVAD patients, and 86% for patients with LVAD + short-term RVAD. Freedom from neurological deficit at 1 year was 84% for the TAH group, 73% for the pulsatile BiVAD flow, 76% for the continuous-flow BiVAD, and 94% for the LVAD + short-term RVAD group with no statistical difference between the investigated groups (P = 0.091). According to the authors, the LVAD + short-term RVAD group had the most favorable outcomes in terms of survival and freedom from complications. The possibility of easy weaning from extracorporeal RVAD models was an additional advantage [58].

The J.C. Cleveland Jr et al. study comparing LVAD and BiVAD implantation outcomes (Heartmate IP, VE, VXE, and Heartmate II LVAD models (Thoratec, Pleasanton, CA); the MicroMed Debakey Child left VAD (MicroMed, Houston, TX); Thoratec IVAD and PVAD pumps (Thoratec)) reported 6-month survival rates of 86% for LVADs and 56% for BiVADs (p < .0001). Adverse event rates, expressed as episodes / 100 patient-months for the BiVAD group compared with LVAD, were significantly higher for infection (33.2 *vs* 14.3), bleeding (71.6 *vs* 15.5), neurologic events (7.9 *vs* 2.6), and for device failure (4.9 *vs* 2.0) [59].

The question of choosing an optimal pump model for BiVAD is still open. For example, a group of authors led by A.C.W. Baldwin et al. report successful performance of BiVAD cardiac support with two different device models. In this case, after implanting a HeartMate II model as an LVAD and performing temporary RV support with CentriMag (Abbott Laboratories; Abbott Park, Ill) for long-term RVAD support, the patient was implanted with a HeartWare HVAD model [60]. A similar experience is also described in the works of J.J. Eulert-Grehn et al. and S. Saito et al. [47, 61].

In a recent study by D.M. Mancini et al., it was shown that 26% of patients after LVAD implantation, after several months of mechanical circulatory support, restored LV pumping function, so that the devices were ultimately explanted [62]. A similar strategy can be successfully implemented in the case of BiVAD support. According to E. Potapov et al., in a series of 10 patients treated with BiVAD, 3 cases showed a recovery of normal RV function to the extent that the RVAD device was stopped without explantation. Two patients were left with successfully functioning LVADs, one patient died of sepsis [63].

Thus, the strategy of concurrent implantation of two non-pulsatile mechanical circulatory support devices in a BiVAD configuration can be considered an effective alternative treatment option for patients with biventricular heart failure. Moreover, the latest HeartMate III centrifugal pump, fully magnetically levitated, can be used as a TAH in clinics that are unable to use the original TAH models. However, the issue of predictors of device-related complications requires further research.

The work was supported by the Russian Science Foundation, project 23-25-10013 (Agreement no. p-52 dated 03.04.23 with the Ministry of Science and Innovation Policy of the Novosibirsk Region).

The authors declare no conflict of interest.

REFERENCES

1. *Hunt SA, Abraham WT, Chin MH, Feldman AM, Francis GS, Ganiats TG et al.* American College of Cardiology; American Heart Association Task Force on Practice Guidelines; American College of Chest Physicians; International Society for Heart and Lung Transplantation; Heart Rhythm Society. ACC/AHA 2005 Guideline Update for the Diagnosis and Management of Chronic

Heart Failure in the Adult: a report of the American College of Cardiology/American Heart Association Task Force on Practice Guidelines (Writing Committee to Update the 2001 Guidelines for the Evaluation and Management of Heart Failure): developed in collaboration with the American College of Chest Physicians and the International Society for Heart and Lung Transplantation: endorsed by the Heart Rhythm Society. *Circulation*. 2005; 112 (12): e154–235. doi: 10.1161/CIRCULATIONAHA.105.167586.

2. *Kirklin JK, Naftel DC, Pagani FD, Kormos RL, Stevenson LW, Blume ED et al.* Seventh INTERMACS annual report: 15,000 patients and counting. *J Heart Lung Transplant*. 2015; 34 (12): 1495–1504. doi: 10.1016/j.healun.2015.10.003.
3. *Mehra MR, Park MH, Landzberg MJ, Lala A, Waxman AB.* Right heart failure: toward a common language. *Pulm Circ*. 2013; 3 (4): 963–967. doi: 10.1086/674750.
4. *Kormos RL.* The right heart failure dilemma in the era of left ventricular assist devices. *J Heart Lung Transplant*. 2014; 33 (2): 134–135. doi: 10.1016/j.healun.2013.12.019.
5. *Takeda K, Naka Y, Yang JA, Uriel N, Colombo PC, Jorde UP et al.* Outcome of unplanned right ventricular assist device support for severe right heart failure after implantable left ventricular assist device insertion. *J Heart Lung Transplant*. 2014; 33 (2): 141–148. doi: 10.1016/j.healun.2013.06.025.
6. *Kirklin JK, Pagani FD, Kormos RL, Stevenson LW, Blume ED, Myers SL et al.* Eighth annual INTERMACS report: Special focus on framing the impact of adverse events. *J Heart Lung Transplant*. 2017; 36 (10): 1080–1086. doi: 10.1016/j.healun.2017.07.005.
7. *Kirklin JK, Naftel DC, Kormos RL, Stevenson LW, Pagani FD, Miller MA et al.* The Fourth INTERMACS Annual Report: 4,000 implants and counting. *J Heart Lung Transplant*. 2012; 31 (2): 117–126. doi: 10.1016/j.healun.2011.12.001.
8. *Ochiai Y, McCarthy PM, Smedira NG, Banbury MK, Navia JL, Feng J et al.* Predictors of severe right ventricular failure after implantable left ventricular assist device insertion: analysis of 245 patients. *Circulation*. 2002 Sep 24; 106 (12 Suppl 1): I198–I202.
9. *Santambrogio L, Bianchi T, Fuardo M, Gazzoli F, Veronesi R, Braschi A et al.* Right ventricular failure after left ventricular assist device insertion: preoperative risk factors. *Interact Cardiovasc Thorac Surg*. 2006; 5 (4): 379–382. doi: 10.1510/icvts.2006.128322.
10. *Matthews JC, Koelling TM, Pagani FD, Aaronson KD.* The right ventricular failure risk score a pre-operative tool for assessing the risk of right ventricular failure in left ventricular assist device candidates. *J Am Coll Cardiol*. 2008; 51 (22): 2163–2172. doi: 10.1016/j.jacc.2008.03.009.
11. *Drakos SG, Janicki L, Horne BD, Kfoury AG, Reid BB, Clayson S et al.* Risk factors predictive of right ventricular failure after left ventricular assist device implantation. *Am J Cardiol*. 2010; 105 (7): 1030–1035. doi: 10.1016/j.amjcard.2009.11.026.
12. *Fitzpatrick JR 3rd, Frederick JR, Hiesinger W, Hsu VM, McCormick RC, Kozin ED et al.* Early planned institution of biventricular mechanical circulatory support results in improved outcomes compared with delayed conversion of a left ventricular assist device to a biventricular assist device. *J Thorac Cardiovasc Surg*. 2009; 137 (4): 971–977. doi: 10.1016/j.jtcvs.2008.09.021.
13. *Baran DA, Mehra MR.* Late-onset right heart failure after left ventricular assist device implant: quo vadis? *J Heart Lung Transplant*. 2017; 36 (1): 26–27. doi: 10.1016/j.healun.2016.12.001.
14. *Strueber M, Schmitto JD, Kutschka I, Haverich A.* Placement of 2 implantable centrifugal pumps to serve as a total artificial heart after cardiectomy. *J Thorac Cardiovasc Surg*. 2012; 143 (2): 507–509. doi: 10.1016/j.jtcvs.2011.07.034.
15. *Khvan DS, Chernyavsky AM, Efendiev VU, Sirota DA, Doronin DV, Fomichev AV et al.* A case of the "berlin heart excor" biventricular assist device implantation as a bridge to heart transplantation for a patient with dilated cardiomyopathy and terminal heart failure. *Russian Journal of Transplantology and Artificial Organs*. 2018; 20 (2): 69–73. [In Russ, English abstract]. https://doi.org/10.15825/1995-1191-2018-2-69-73.
16. *Zhulkov MO, Sirota DA, Fomichev AV, Grenaderov AS, Chernyavsky AM.* The problem of biocompatibility and thrombogenicity in mechanical circulatory assist devices. *Russian Journal of Transplantology and Artificial Organs*. 2020; 22 (4): 83–88. [In Russ, English abstract]. https://doi.org/10.15825/1995-1191-2020-4-83-88.
17. *Leidenfrost J, Prasad S, Itoh A, Lawrance CP, Bell JM, Silvestry SC.* Right ventricular assist device with membrane oxygenator support for right ventricular failure following implantable left ventricular assist device placement. *Eur J Cardiothorac Surg*. 2016; 49 (1): 73–77. doi: 10.1093/ejcts/ezv116.
18. *Saito S, Matsumiya G, Sakaguchi T, Miyagawa S, Yoshikawa Y, Yamauchi T et al.* Risk factor analysis of long-term support with left ventricular assist system. *Circ J*. 2010; 74 (4): 715–722. doi: 10.1253/circj.cj-09-0747.
19. *Saito S, Matsumiya G, Sakaguchi T, Fujita T, Kuratani T, Ichikawa H et al.* Fifteen-year experience with Toyobo paracorporeal left ventricular assist system. *J Artif Organs*. 2009; 12 (1): 27–34. doi: 10.1007/s10047-009-0448-5.
20. *Zhulkov MO, Fomichev AV, Alsov SA, Cleaver EN, Chernyavsky AM.* Current state of the problem and results of *ex vivo* perfusion of donor hearts. *Russian Journal of Transplantology and Artificial Organs*. 2019; 21 (4): 143–146. [In Russ, English abstract]. https://doi.org/10.15825/1995-1191-2019-4-143-146.
21. *Kirsch M, Vermes E, Damy T, Nakashima K, Sénéchal M, Boval B et al.* Single-centre experience with the Thoratec paracorporeal ventricular assist device for patients with primary cardiac failure. *Arch Cardiovasc Dis*. 2009 Jun-Jul; 102 (6–7): 509–518. doi: 10.1016/j.acvd.2009.03.010.
22. *Farrar DJ, Hill JD, Pennington DG, McBride LR, Holman WL, Kormos RL et al.* Preoperative and postoperative comparison of patients with univentricular and

biventricular support with the thoratec ventricular assist device as a bridge to cardiac transplantation. *J Thorac Cardiovasc Surg*. 1997; 113 (1): 202–209. doi: 10.1016/S0022-5223(97)70416-1.

23. *Bartfay SE, Dellgren G, Hallhagen S, Wåhlander H, Dahlberg P, Redfors B et al.* Durable circulatory support with a paracorporeal device as an option for pediatric and adult heart failure patients. *J Thorac Cardiovasc Surg*. 2021; 161 (4): 1453–1464.e4. doi: 10.1016/j.jtcvs.2020.04.163.
24. *Brenner P, Wirth TJ, Liebermann A, Mihalj M, Güthoff S, Hagl C et al.* First Biventricular Jarvik 2000 Implants (Retroauricular Version) Via a Median Sternotomy. *Exp Clin Transplant*. 2016; 14 (2): 215–223. doi: 10.6002/ect.2015.0053.
25. *Radovancevic B, Gregoric ID, Tamez D, Vrtovec B, Tuzun E, Chee HK et al.* Biventricular support with the Jarvik 2000 axial flow pump: a feasibility study. *ASAIO J*. 2003; 49 (5): 604–607. doi: 10.1097/01.mat.0000084109.47034.8a.
26. *Yoshioka D, Toda K, Yoshikawa Y, Sawa Y*. Over 1200-day support with dual Jarvik 2000 biventricular assist device. *Interact Cardiovasc Thorac Surg*. 2014; 19 (6): 1083–1084. doi: 10.1093/icvts/ivu312.
27. *Frazier OH, Myers TJ, Gregoric I.* Biventricular assistance with the Jarvik FlowMaker: a case report. *J Thorac Cardiovasc Surg*. 2004; 128 (4): 625–626. doi: 10.1016/j.jtcvs.2004.02.023.
28. *Loebe M, Bruckner B, Reardon MJ, van Doorn E, Estep J, Gregoric I et al.* Initial clinical experience of total cardiac replacement with dual HeartMate-II axial flow pumps for severe biventricular heart failure. *Methodist Debakey Cardiovasc J*. 2011; 7 (1): 40–44. doi: 10.14797/mdcj-7-1-40.
29. *Frazier OH, Cohn WE*. Continuous-flow total heart replacement device implanted in a 55-year-old man with end-stage heart failure and severe amyloidosis. *Tex Heart Inst J*. 2012; 39 (4): 542–546.
30. *Pirk J, Maly J, Szarszoi O, Urban M, Kotulak T, Riha H et al*. Total artificial heart support with two continuous-flow ventricular assist devices in a patient with an infiltrating cardiac sarcoma. *ASAIO J*. 2013; 59 (2): 178–180. doi: 10.1097/MAT.0b013e3182816cd9.
31. *Bhama JK, Bansal U, Winger DG, Teuteberg JJ, Bermudez C, Kormos RL et al.* Clinical experience with temporary right ventricular mechanical circulatory support. *J Thorac Cardiovasc Surg*. 2018; 156 (5): 1885–1891. doi: 10.1016/j.jtcvs.2018.04.094.
32. *Anderson MB, Goldstein J, Milano C, Morris LD, Kormos RL, Bhama J et al.* Benefits of a novel percutaneous ventricular assist device for right heart failure: The prospective RECOVER RIGHT study of the Impella RP device. *J Heart Lung Transplant*. 2015; 34 (12): 1549–1560. doi: 10.1016/j.healun.2015.08.018.
33. *Hall SA, Uriel N, Carey SA, Edens M, Gong G, Esposito M et al.* Use of a percutaneous temporary circulatory support device as a bridge to decision during acute decompensation of advanced heart failure. *J Heart Lung Trans*plant. 2018; 37 (1): 100–106. doi: 10.1016/j.healun.2017.09.020.
34. *Varian K, Xu WD, Lin W, Unai S, Tong MZ, Soltesz E et al.* Minimally invasive biventricular mechanical circulatory support with Impella pumps as a bridge to heart transplantation: a first-in-the-world case report. *ESC Heart Fail*. 2019; 6 (3): 552–554. doi: 10.1002/ehf2.12412.
35. *Shehab S, Newton PJ, Allida SM, Jansz PC, Hayward CS.* Biventricular mechanical support devices–clinical perspectives. *Expert Rev Med Devices*. 2016; 13 (4): 353–365. doi: 10.1586/17434440.2016.1154454.
36. *Loforte A, Montalto A, Della Monica PL, Contento C, Musumeci F.* Biventricular support with the HeartWare implantable continuous flow pump: an additional contribution. *J Heart Lung Transplant*. 2010; 29 (12): 1443–1444. doi: 10.1016/j.healun.2010.07.012.
37. *Hetzer R, Krabatsch T, Stepanenko A, Hennig E, Potapov EV*. Long-term biventricular support with the heartware implantable continuous flow pump. *J Heart Lung Transplant*. 2010; 29 (7): 822–824. doi: 10.1016/j.healun.2010.02.012.
38. *Strueber M, Meyer AL, Malehsa D, Haverich A*. Successful use of the HeartWare HVAD rotary blood pump for biventricular support. *J Thorac Cardiovasc Surg*. 2010; 140 (4): 936–937. doi: 10.1016/j.jtcvs.2010.04.007.
39. *Loforte A, Monica PL, Montalto A, Musumeci F*. HeartWare third-generation implantable continuous flow pump as biventricular support: mid-term follow-up. *Interact Cardiovasc Thorac Surg*. 2011; 12 (3): 458–460. doi: 10.1510/icvts.2010.250654.
40. *Chandola R, Buchholz H, Macarthur R.* Long-term use of low-molecular-weight heparin in a patient with Heartware BIVAD (HVAD) with underlying sustained ventricular fibrillation. *J Cardiol Cases*. 2016; 14 (6): 171–173. doi: 10.1016/j.jccase.2016.08.002.
41. *Krabatsch T, Potapov E, Stepanenko A, Schweiger M, Kukucka M, Huebler M et al.* Biventricular circulatory support with two miniaturized implantable assist devices. *Circulation*. 2011; 124 (11 Suppl): S179–S186. doi: 10.1161/CIRCULATIONAHA.110.011502.
42. *Shehab S, Macdonald PS, Keogh AM, Kotlyar E, Jabbour A, Robson D et al.* Long-term biventricular HeartWare ventricular assist device support – Case series of right atrial and right ventricular implantation outcomes. *J Heart Lung Transplant*. 2016; 35 (4): 466–473. doi: 10.1016/j.healun.2015.12.001.
43. *Arabia FA, Milano CA, Mahr C, McGee EC Jr, Mokadam NA, Rame JE et al*. Biventricular Support With Intracorporeal, Continuous Flow, Centrifugal Ventricular Assist Devices. *Ann Thorac Surg*. 2018; 105 (2): 548–555. doi: 10.1016/j.athoracsur.2017.08.019.
44. *Lavee J, Mulzer J, Krabatsch T, Marasco S, McGiffin D, Garbade J et al.* An international multicenter experience of biventricular support with HeartMate 3 ventricular assist systems. *J Heart Lung Transplant*. 2018; 37 (12): 1399–1402. doi: 10.1016/j.healun.2018.08.008.
45. *McGiffin D, Kure C, McLean J, Marasco S, Bergin P, Hare JL et al.* The results of a single-center experience with HeartMate 3 in a biventricular configuration. *J Heart Lung Transplant*. 2021; 40 (3): 193–200. doi: 10.1016/j.healun.2020.12.006.

46. *Shah P, Ha R, Singh R, Cotts W, Adler E, Kiernan M et al.* Multicenter experience with durable biventricular assist devices. *J Heart Lung Transplant*. 2018; 37 (9): 1093–1101. doi: 10.1016/j.healun.2018.05.001.
47. *Eulert-Grehn JJ, Lanmüller P, Schönrath F, Solowjowa N, Müller M, Mulzer J et al.* Two implantable continuous-flow ventricular assist devices in a biventricular configuration: technique and results. *Interact Cardiovasc Thorac Surg*. 2018; 27 (6): 938–942. doi: 10.1093/icvts/ivy228.
48. *Tran HA, Pollema TL, Silva Enciso J, Greenberg BH, Barnard DD, Adler ED et al.* Durable Biventricular Support Using Right Atrial Placement of the HeartWare HVAD. *ASAIO J*. 2018; 64 (3): 323–327. doi: 10.1097/MAT.0000000000000645.
49. *Bansal A, Akhtar F, Zwintscher NP, Ostrow S, Desai S, Fary D.* Use of the Heartmate 3 for biventricular support as a bridge to heart transplant-first US implant. *J Card Surg*. 2019; 34 (12): 1629–1631. doi: 10.1111/jocs.14290.
50. *Potapov E, Starck C, Falk V, Eulert-Grehn JJ*. Mechanical circulatory support: Technical tips for the implantation of a right ventricular assist device. *JTCVS Open*. 2021; 8: 37–40. doi: 10.1016/j.xjon.2021.09.046.
51. *Maynes EJ, O'Malley TJ, Patel P, Prochno KW, Wood CT, Choi JH et al*. Right atrial versus right ventricular HeartWare HVAD position in patients on biventricular HeartWare HVAD support: A systematic review. *Artif Organs*. 2020; 44 (9): 926–934. doi: 10.1111/aor.13675.
52. *Lo C, Gregory S, Stevens M, Murphy D, Marasco S.* Banding the Right Ventricular Assist Device Outflow Conduit: Is It Really Necessary With Current Devices? *Artif Organs*. 2015; 39 (12): 1055–1061. doi: 10.1111/aor.12497.
53. *Kuroda T, Miyagi C, Fukamachi K, Karimov JH.* Biventricular assist devices and total artificial heart: Strategies and outcomes. *Front Cardiovasc Med*. 2023; 9: 972132. doi: 10.3389/fcvm.2022.972132.
54. *Rame JE, Pagani FD, Kiernan MS, Oliveira GH, Birati EY, Atluri P et al.* Evolution of Late Right Heart Failure With Left Ventricular Assist Devices and Association With Outcomes. *J Am Coll Cardiol*. 2021; 78 (23): 2294–2308. doi: 10.1016/j.jacc.2021.09.1362.
55. *Shimada S, Nawata K, Kinoshita O, Ono M.* Mechanical circulatory support for the right ventricle in combination with a left ventricular assist device. *Expert Rev Med Devices*. 2019; 16 (8): 663–673. doi: 10.1080/17434440.2019.1635006.
56. *Yoshioka D, Takayama H, Garan RA, Topkara VK, Han J, Kurlansky P et al.* Contemporary outcome of unplanned right ventricular assist device for severe right heart failure after continuous-flow left ventricular assist device insertion. *Interact Cardiovasc Thorac Surg*. 2017 Jun 1; 24 (6): 828–834. doi: 10.1093/icvts/ivw409.
57. *Mangi AA*. Right ventricular dysfunction in patients undergoing left ventricular assist device implantation: predictors, management, and device utilization. *Surgical Treatment for Advanced Heart Failure*. 2013: 177–187. https://doi.org/10.1007/978-1-4614-6919-3_14.
58. *Vierecke J, Gahl B, de By TMMH, Antretter H, Beyersdorf F, Caliskan K et al.* Results of primary biventricular support: an analysis of data from the EUROMACS registry. *Eur J Cardiothorac Surg*. 2019; 56 (6): 1037–1045. doi: 10.1093/ejcts/ezz173.
59. *Cleveland JC Jr, Naftel DC, Reece TB, Murray M, Antaki J, Pagani FD et al.* Survival after biventricular assist device implantation: an analysis of the Interagency Registry for Mechanically Assisted Circulatory Support database. *J Heart Lung Transplant*. 2011; 30 (8): 862–869. doi: 10.1016/j.healun.2011.04.004.
60. *Baldwin ACW, Sandoval E, Cohn WE, Mallidi HR, Morgan JA, Frazier OH.* Nonidentical Continuous-Flow Devices For Biventricular Support. *Tex Heart Inst J*. 2017; 44 (2): 141–143. doi: 10.14503/THIJ-16-5878.
61. *Saito S, Sakaguchi T, Miyagawa S, Yoshikawa Y, Yamauchi T, Ueno T et al.* Biventricular support using implantable continuous-flow ventricular assist devices. *J Heart Lung Transplant*. 2011; 30 (4): 475–478. doi: 10.1016/j.healun.2010.11.013.
62. *Mancini DM, Beniaminovitz A, Levin H, Catanese K, Flannery M, DiTullio M et al.* Low incidence of myocardial recovery after left ventricular assist device implantation in patients with chronic heart failure. *Circulation*. 1998; 98 (22): 2383–2389. doi: 10.1161/01.cir.98.22.2383.
63. *Potapov E, Schweiger M, Vierecke J, Dandel M, Stepanenko A, Kukucka M et al.* Discontinuation of HeartWare RVAD support without device removal in chronic BIVAD patients. *ASAIO J*. 2012; 58 (1): 15–18. doi: 10.1097/MAT.0b013e3182376b7b.

The article was submitted to the journal on 06.03.2023

DOI: 10.15825/1995-1191-2023-2-57-62

PERICARDIAL WINDOW AS A SURGICAL METHOD FOR PREVENTING SIGNIFICANT POSTOPERATIVE PERICARDIAL EFFUSION

K.S. Kiryakov[1], A.R. Zakiryanov[1], T.A. Khalilulin[1, 2], N.Y. Zakharevich[1], O.A. Pozdnyakov[1], A.M. Goltz[1], D.S. Ivanov[1], A.A. Sukhachev[1], V.M. Zakharevich[1, 2]

[1] Shumakov National Medical Research Center of Transplantology and Artificial Organs, Moscow, Russian Federation

[2] Sechenov University, Moscow, Russian Federation

Postoperative pericardial effusion (PPE) represents a very common complication in cardiac surgery. Accumulation of a significant amount of free fluid in the pericardial cavity is a multifactorial process. Identifying the cause is not always possible. This complication occurs more frequently in patients after heart transplantation than in patients who underwent reconstructive cardiac surgery. Having hemodynamically significant effusion requires surgical evacuation of fluid from the pericardial cavity. This can affect the postoperative period and increase the length of stay at the hospital. For this reason, developing and ensuring widespread use of methods for prevention of this complication are urgent and relevant tasks.

Keywords: heart transplantation, pericardial window, pericardial effusion.

Objective: to provide data on practical application of the pericardial window procedure in heart transplant recipients for preventing significant pericardial effusion formation.

INTRODUCTION

Heart transplantation (HT) remains the gold-standard therapy in end-stage heart failure. The efficacy of HT today is not under dispute because of its significant advantage over drug therapy and alternative surgical interventions. Each year, about 300 HT surgeries are performed in the Russian Federation. This number is rising steadily. It is obvious that introduction of new methods of treatment and prevention of complications in this field is necessary to further develop and strengthen the position of transplantology in the Russian Federation. For many years now, the Shumakov National Medical Research Center of Transplantology and Artificial Organs (hereinafter referred to as Shumakov Center) in Moscow has remained the absolute leader in terms of the number of HTs performed. Since 2016, the center has performed about 200 HTs per year, which is the best indicator among all institutions in the world today [1]. The accumulated experience allows to reliably assess the current issues regarding the course of the postoperative period in HT recipients in the Russian Federation, including the incidence and significance of complications.

PPE is one of the most common findings after cardiac surgery [2–7]. This complication is also characteristic of cardiac recipients. The incidence of PPE in this group of patients is significantly higher due to different immunological and surgical components [2, 3]. Large pericardial effusions can cause compression of heart chambers, leading to decreased hemodynamic parameters. The only way to treat such conditions is additional surgical intervention, an undesirable event that affects the postoperative period. Today, one of the ways of radical prevention of this complication in reconstructive cardiac surgery is the pericardial window procedure or posterior pericardiotomy in one-stage with the main stage of surgery [8–11]. This method is widely used in clinical practice due to its simplicity, efficiency and safety.

At present, it is difficult to speak about the breadth of application of the procedure in cardiac transplantation practice. However, it is worth considering the effectiveness of its use in reconstructive cardiac surgery [12–15]. This surgical technique can reduce the incidence of pericardial effusions, the number of drainage operations performed and the length of stay in the hospital. Currently, this technique is used at Shumakov Center for HT recipients. Given the novelty and lack of clear indications for use, the effect on the postoperative period in cardiac transplant patients is being studied.

MATERIALS AND METHODS

In order to analyze the effectiveness of the method of surgical prevention of PPE in HT recipients, we performed the pleuropericardial window technique in 22 recipients at Shumakov Center during the main stage of surgery from December 2021 to December 2022. For

Corresponding author: Kirill Kiryakov. Address: 1, Shchukinskaya str., Moscow, 123182, Russian Federation. Phone: (499) 190-60-34. E-mail: Kiriakovmd@gmail.com

the purpose of objective analysis of the procedure, selection criteria were not used, and the pericardial window was performed randomly. The average time of stay and follow-up at the surgical hospital was 19 ± 10.3 days. Patient mean age was 45.9 ± 10.3 years, 86% men, 14% women. The prevalent pre-transplant diagnoses were: dilated cardiomyopathy (59%) and ischemic cardiomyopathy (36%). The vast majority of patients (95%) had no history of previous cardiac surgery. The mean time of the main stage of surgery was 51 ± 10.5 minutes. Cardiopulmonary bypass time was 103.7 ± 17.7 minutes. Heart graft ischemic time was 175.9 ± 62.8 minutes. The data of 190 patients who underwent HT in 2022 at Shumakov Center were used for comparison. The presence of severe pericardial effusion that required repeated surgical intervention due to signs of hemodynamically significant compression of the heart chambers and volume of free pericardial fluid ≥300 mL were assessed.

SURGICAL TECHNIQUE

The pericardial window procedure consists of excision of a 3–4 cm^2 area of the pericardium using electrocoagulation below the left diaphragmatic nerve, 4–5 cm down from the left inferior pulmonary vein (Fig. 1). After completion of the main stage of the operation, it is suggested to place a 27–30 F pleuropericardial drainage tube through the pericardial window into the left costophrenic angle in order to drain both the pleural cavity and the pericardial cavity (Fig. 2). The duration of pleuropericardial drainage should be no more than 72 hours from the time of surgery when the discharge rate reaches <100 mL per day. When the tube is removed, the skin defect should be sutured to prevent pneumothorax and pneumopericardium. After removal of the drainage tube, negative pressure in the pleural cavity creates active aspiration from the pericardial cavity, provided the latter is airtight. Thus, redistribution of fluid volume changes the character and significance of clinical manifestations of the effusion process. Besides, the pleural cavity is characterized by a greater resorption surface, which allows in some cases to be limited to conservative methods of treatment.

RESULTS

A standard protocol for assessing the presence of effusion in the pericardial cavity during echocardiography (EchoCG) was used, including daily examination during patient follow-up in the intensive care unit (ICU) and pericardial ultrasound twice a week after transfer to the surgical ward. The average amount of fluid content in the pericardial cavity was found to be 50–100 mL in 95% of patients, which is an acceptable norm and does not require active treatment. Only one patient, despite surgical prophylaxis, had massive pericardial and pleural effusion that required drainage of the pericardial cavity on day 27 after transplantation and two pleural cavity drainage procedures, which was due to hypoalbuminemia, deficiency of plasma coagulation factors, decreased diuresis and hypodynamic patient against edema syndrome. The patient also had fibrin clots in the pericardial cavity along the contour of the right ventricle and hemorrhagic discharge during drainage. This may indicate signs of delayed bleeding resulting from blood clotting disorders. Two more patients had significant left-sided pleural effusion, which required evacuation of fluid from the pleural cavity. Hydrothorax can be one of the predictable features of the method and develop due to fluid outflow through the pericardial window into the pleural cavity [10]. Of course, pleural effusion is also an undesirable postoperative event in this group of patients. But this complication does not affect hemodynamic characteristics of the graft, and surgical manipulation of evacuation of significant volume of fluid from the pleural

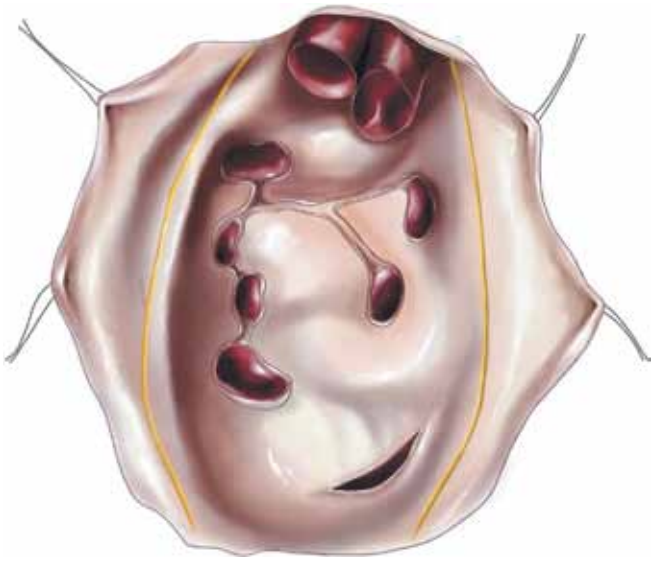

Fig. 1. Image of optimal localization of the pericardial window relative to the nearest anatomical structures

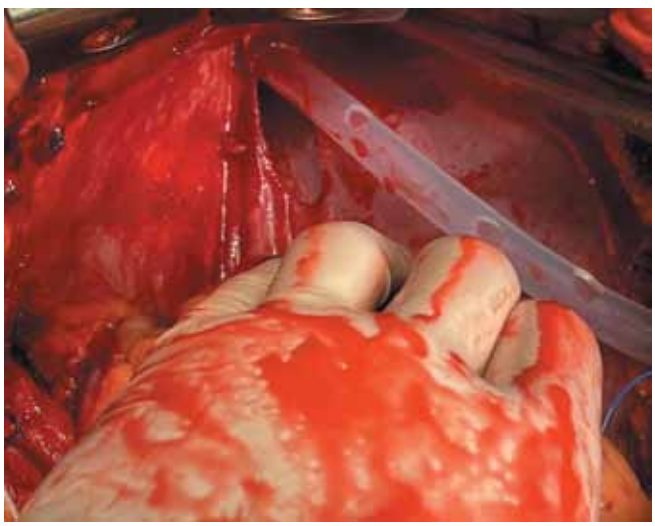

Fig. 2. An example of placement of a pericardial drainage tube after completion of the main stage of the operation

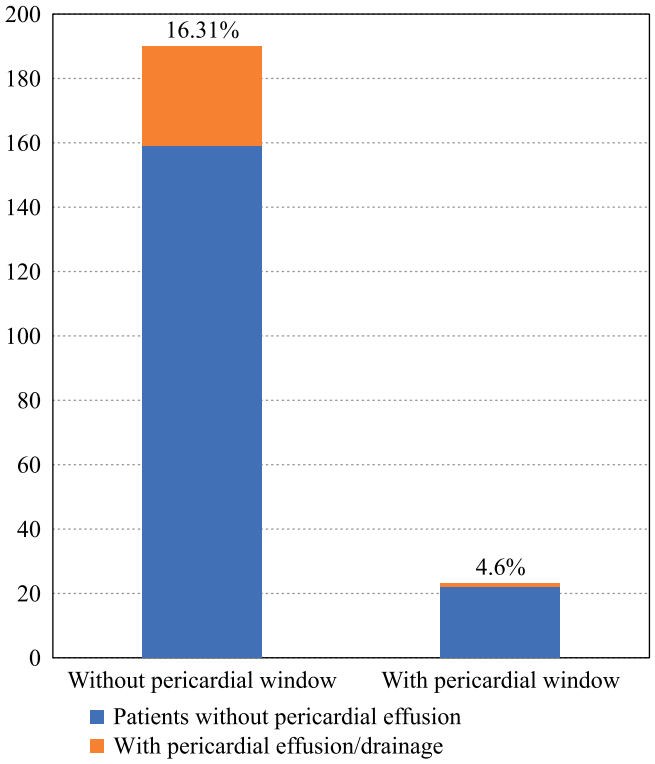

Fig. 3. Comparison chart

cavity compared to pericardial cavity drainage is a much gentler intervention, not requiring patient sedation.

In the group of patients who underwent HT without undergoing a pleuropericardial window, severe pericardial effusion requiring surgical evacuation of fluid was noted in 16.3% of cases. This shows the advantage of the presented procedure and the difference between the groups by more than 10% $p > 0.05$ (Fig. 3).

DISCUSSION

At first glance, such a complication as fluid accumulation in the pericardial cavity does not have obvious negative consequences for patients and sometimes is not considered by clinicians as a serious problem requiring special attention. However, as practice shows, the increase in free fluid volume in the pericardial cavity in the early postoperative period negatively affects the patient's hemodynamic parameters, can cause arrhythmia, lead to compression of the heart chambers and cardiac tamponade. According to global statistics, PPE occurs in approximately 6–35% of patients after cardiac surgery [16–22]. According to the 2019–2022 statistics from our institution, this complication leads to significant heart graft dysfunction and requires additional surgical intervention in 15–20% of cases. It has been noted that HT recipients account for an average of 83% of all patients who underwent cardiac surgery and required drainage of the pericardial cavity in the postoperative period in the operating room. This once again proves the predisposition of this category of patients to accumulation of pathological amounts of pericardial fluid.

From our point of view, the most optimal method of radical treatment of large pericardial effusion is drainage of the pericardial cavity through subxiphoid access. This intervention does not require additional incisions and is performed by opening the sternotomy suture in the lower third for 5–6 centimeters and evacuating fluid, followed by placement of a drainage tube. The main advantage of subxiphoid access is the possibility to perform complete evacuation of pericardial effusion, which is not always possible when performing pericardial puncture, especially when accumulation is encysted along the posterior surface of the heart [23–25]. Pericardial puncture is also an effective procedure that is used as the method of choice in many institutions, and the procedural success rate is 97%. However, a prerequisite is to perform the procedure under ultrasound guidance, optimal ultrasound window, or to perform the puncture in an X-ray operating room [26]. Although drainage procedures and pericardial punctures have long been used as a safe treatment strategy in patients with this complication, it is worth bearing in mind that these surgical manipulations cause additional emotional stress for the patient, may increase length of stay at the hospital due to the need for extended follow-up, and are among the undesirable postoperative events in terms of clinical and economic factors.

Techniques for surgical prevention of severe pericardial effusion are used worldwide and are becoming increasingly common in reconstructive cardiac surgery due to the revealed effectiveness with regard to postoperative atrial fibrillation – reduced amount of effusion and decreased inflammatory response [12–15]. Pleuroperitoneal shunting using pericardial window or posterior pericardiotomy can significantly reduce the risk of hydropericardium, which is especially relevant in patients after heart transplantation. The advantage of performing a pleuropericardial window during the main surgical phase is to prevent the buildup of significant pericardial effusion due to effusion redistribution and, as a consequence, reduce the incidence of complication.

Given the data obtained, it can be concluded that surgical prevention of pericardial effusion in patients after heart transplantation by shunting is effective due to absence of signs of pathological fluid accumulation in 95% of cases, which exceeds by 10% the indicator of patients who did not undergo pericardial window during the operation. This technique can improve the efficiency of medical care for patients with end-stage heart failure, preventing this complication in patients after heart transplantation.

The question about indications and contraindications for the use of the method in everyday practice in heart transplant recipients is open because of the need to identify the main predisposing risk factors and determine

the probability of complications such as formation of hydrothorax due to fluid distribution.

CONCLUSION

The use of pleuropericardial window as a surgical method for prevention of significant PPE after heart transplantation may reduce the risks of repeated surgical interventions aimed at evacuating severe hydropericardium, and improve the early postoperative period.

The authors declare no conflict of interest.

REFERENCES

1. *Gautier SV, Khomyakov SM.* Organ donation and transplantation in the Russian Federation in 2021. 14th Report from the Registry of the Russian Transplant Society. *Russian Journal of Transplantology and Artificial Organs*. 2022; 24 (3): 8–31. https://doi.org/10.15825/1995-1191-2022-3-8-31.
2. *Ashikhmina EA, Schaff HV, Sinak LJ, Li Z, Dearani JA, Suri RM et al.* Pericardial effusion after cardiac surgery: risk factors, patient profiles, and contemporary management. *Ann Thorac Surg.* 2010; 89: 112–118.
3. *Kiriakov KS, Zakharevich VM, Khalilulin TA, Zakharevich NY, Abramova NN, Pozdnyakov OA.* Postoperative pericardial effusion: peculiarities of the development and course. *Russian Journal of Transplantology and Artificial Organs*. 2021; 23 (1): 131–139. https://doi.org/10.15825/1995-1191-2021-1-131-139.
4. *Pepi M, Muratori M, Barbier P, Doria E, Arena V, Berti M et al.* Pericardial effusion after cardiac surgery: incidence, site, size, and haemodynamic consequences. *Br Heart J.* 1994; 72: 327–331.
5. *Khassawneh M, Alfawaeer ZA, Attallah DM.* Incidence of Pericardial Effusion Post Pericardiotomy Diagnosis, Intervention and Treatment. *Int J Med Invest*. 2018; 7 (2): 39–46.
6. *Weitzman LB, Tinker WP, Kronzon I, Cohen ML, Glassman E, Spencer FC.* The incidence and natural history of pericardial effusion after cardiac surgery – an echocardiographic study. *Circulation.* 1984; 69: 506–511.
7. *Khan NK, Järvelä KM, Loisa EL, Sutinen JA, Laurikka JO, Khan JA.* Incidence, presentation and risk factors of late postoperative pericardial effusions requiring invasive treatment after cardiac surgery. *Interact Cardiovasc Thorac Surg*. 2017; 24 (6): 835–840. doi: 10.1093/icvts/ivx011.
8. *Sen O, Aydin U, Iyigun T, Reyhancan A, Timur B, Kadirogullari E et al.* Right pericardial window opening: a method of preventing pericardial effusion. *Gen Thorac Cardiovasc Surg*. 2020 May; 68 (5): 485–491. doi: 10.1007/s11748-019-01213-4. Epub 2019 Sep 26. PMID: 31559587.
9. *Kaya M, Utkusavaş A, Erkanlı K, Güler S, Kyaruzi M, Birant A et al*. The Preventive Effects of Posterior Pericardiotomy with Intrapericardial Tube on the Development of Pericardial Effusion, Atrial Fibrillation, and Acute Kidney Injury after Coronary Artery Surgery: A Prospective, Randomized, Controlled Trial. *Thorac Cardiovasc Surg*. 2016 Apr; 64 (3): 217–224. doi: 10.1055/s-0035-1548737. Epub 2015 Apr 14. Erratum in: *Thorac Cardiovasc Surg*. 2016 Apr; 64 (3): e1–e2. PMID: 25875954.
10. *Ali-Hasan-Al-Saegh S, Mirhosseini SJ, Liakopoulos O, Sabashnikov A, Dehghan HR, Sedaghat-Hamedani F et al.* Posterior pericardiotomy in cardiac surgery: systematic review and meta-analysis. *Asian Cardiovasc Thorac Ann*. 2015 Mar; 23 (3): 354–362. doi: 10.1177/0218492314541132. Epub 2014 Jun 19. PMID: 24948784.
11. *Zhao J, Cheng Z, Quan X, Zhao Z.* Does posterior pericardial window technique prevent pericardial tamponade after cardiac surgery? *J Int Med Res.* 2014 Apr; 42 (2): 416–426. doi: 10.1177/0300060513515436. Epub 2014 Feb 19. PMID: 24553479.
12. *Gaudino M, Sanna T, Ballman KV, Robinson NB, Hameed I, Audisio K et al*. Posterior left pericardiotomy for the prevention of atrial fibrillation after cardiac surgery: an adaptive, single-centre, single-blind, randomised, controlled trial. *Lancet.* 2021 Dec 4; 398 (10316): 2075–2083. doi: 10.1016/S0140-6736(21)02490-9. Epub 2021 Nov 14. PMID: 34788640.
13. *Uzun K, Günaydın ZY, Tataroğlu C, Bektaş O.* The preventive role of the posterior pericardial window in the development of late cardiac tamponade following heart valve surgery. *Interact Cardiovasc Thorac Surg*. 2016 May; 22 (5): 641–646. doi: 10.1093/icvts/ivv390. Epub 2016 Jan 26. PMID: 26819273; PMCID: PMC4892135.
14. *Ebaid HH, Emara AS, Emara MS, Elnaggar AE*. The value of pericardial window in preventing pericardial effusion after cardiac surgery. *The Egyptian Cardiothoracic Surgeon*. 2021; 3 (1): 28–34. https://doi.org/10.35810/ects.v3i1.167.
15. *Ezelsoy M, Oral MK, Saraçoğlu KT, Saraçoğlu A, Akpınar B.* Posterior Pericardial Window Technique to Prevent Postoperative Pericardial Effusion in Cardiac Surgery. *Kocaeli Med J.* 2019; 8 (2): 78–83.
16. *Vandenberg BF, Mohanty PK, Craddock KJ et al.* Clinical significance of pericardial effusion after heart transplantation. *J Heart Transplant.* 1988; 7 (2): 128–134.
17. *Valantine HA, Hunt SA, Gibbons R, Billingham ME, Stinson EB, Popp RL.* Increasing pericardial effusion in cardiac transplant recipients. *Circulation.* 1989; 79 (3): 603–609. doi: 10.1161/01.cir.79.3.603.
18. *Quin JA, Tauriainen MP, Huber LM, McIntire DD, Kaiser PA, Ring WS, Jessen ME.* Predictors of pericardial effusion after orthotopic heart transplantation. *The Journal of Thoracic and Cardiovascular Surgery.* 2002 Nov; 124 (5): 979–983. doi: 10.1067/mtc.2002.124387.
19. *Hauptman PJ, Couper GS, Aranki SF, Kartashov A, Mudge GH Jr, Loh E.* Pericardial effusions after cardiac transplantation. *J Am Coll Cardiol.* 1994; 23 (7): 1625–1629. doi: 10.1016/0735-1097(94)90666-1.
20. *Ciliberto GR, Anjos MC, Gronda E, Bonacina E, Danzi G, Colombo P et al.* Significance of pericardial effusion after heart transplantation. *Am J Cardiol.* 1995; 76 (4): 297–300. doi: 10.1016/s0002-9149(99)80085-x.
21. *Yu Z, Kittleson M, Patel J, Liou F, Yabuno J, Piponniau L et al.* Moderate Pericardial Effusions After Heart

Transplant: Do They Require Proactive Intervention?: Abstract# C1590. *Transplantation*. 2014 Jul 15; 98 (Issue): 427.

22. *Al-Dadah AS, Guthrie TJ, Pasque MK, Moon MR, Ewald GA, Moazami N.* Clinical course and predictors of pericardial effusion following cardiac transplantation. *Transplant Proc.* 2007; 39 (5): 1589–1592. doi: 10.1016/j.transproceed.2006.11.014.
23. *Moores DW, Allen KB, Faber LP, Dziuban SW, Gillman DJ, Warren WH et al.* Subxiphoid pericardial drainage for pericardial tamponade. *J Thorac Cardiovasc Surg.* 1995 Mar; 109 (3): 546–551; discussion 551-2. doi: 10.1016/S0022-5223(95)70287-3. PMID: 7877317.
24. *Petcu CP, Droc I.* The efficiency of surgical subxiphoid pericardial drainage and percutaneous pericardial drainage in pericardial effusions associated with cardiac tamponade. *Chirurgia (Bucur)*. 2013 Mar-Apr; 108 (2): 226–233. PMID: 23618573.
25. *Altıntaş G, Yaşar E, Kadiroğulları E, Hanedan MO, Diken Aİ, Çiçek ÖF et al.* A comparison of two surgical techniques for symptomatic pericardial effusion after cardiac surgery: subxiphoid open pericardial drainage and lateral thoracotomy. *Türk Göğüs Kalp Damar Cerrahisi Dergisi.* 2014; 22: 29–34.
26. *Tsang TSM, Enriquez-Sarano M, Freeman WK, Barnes ME, Sinak LJ, Gersh BJ et al.* Consecutive 1127 therapeutic echocardiographically guided pericardiocenteses: clinical profile, practice patterns, and outcomes spanning 21 years. *Mayo Clin Proc*. 2002 May; 77 (5): 429–436. doi: 10.4065/77.5.429. PMID: 12004992.

The article was submitted to the journal on 24.01.2023

DOI: 10.15825/1995-1191-2023-2-63-81

PROSPECTS FOR FABRICATION OF ARTIFICIAL HUMAN TISSUES AND ORGANS BASED ON 3D BIOPRINTING

D.V. Bulgin[1], A.L. Kovtun[2], I.V. Reshetov[3], E.Yu. Radomskaya[1, 4]

[1] Kurchatov Institute, Sochi, Russian Federation
[2] Russian Foundation for Advanced Research Projects in the Defense Industry, Moscow, Russian Federation
[3] Sechenov University, Moscow, Russian Federation
[4] Sirius University, Krasnodar Krai, Russian Federation

Three-dimensional (3D) printing is a method of creating a material object layer-by-layer in space from a virtual, mathematical model. 3D printing is based on additive technologies – a step-by-step formation of a structure by adding material to the base. 3D bioprinting is the fabrication of functional biological structures that mimic human organs and tissues. Analysis of scientific publications showed that in the near future, viable and fully functional artificial copies of individual human organs and tissues can be obtained.

Keywords: 3D bioprinting, additive technologies, biofabrication, tissue-engineered constructs, artificial organs, transplantology.

INTRODUCTION

Organ and tissue transplantation is a widely used method of treating severe organ pathology, extensive, irreparable damage to internal organs and tissues [1, 2]. Unfortunately, this method has major drawbacks – graft rejection, graft dysfunction, internal bleeding, postoperative infection, risk of malignant tumors, and complications associated with the use of nonspecific immunosuppressants [3, 4].

Another unresolved problem in transplantology is the global shortage of donor material. A working group of the Russian Transplant Society and the Shumakov National Medical Research Center of Transplantology and Artificial Organs, Moscow, Russian Federation annually collect, process and analyze data on organ donation and transplantation in Russia. According to estimates by Russian experts, only one tenth of those in need of organ transplantation in Russia have their annual need met (the need for organ transplantation in Russia is at least 11,000 kidney transplants per year; 2,000 for liver; 1,100 for heart, including heart-lung; 800 for lungs; 300 for pancreas) [5–8].

The development of additive technologies, research in regenerative medicine, tissue engineering, immunology (search for solutions to the biocompatibility problem), cryobiology (technologies for long-term storage of organs and tissues), materials science (biomaterials, synthetic materials, composite/hybrid materials), are essential for the development of modern methods of compensating the functions of damaged or lost organs and tissues [9–19].

The promise of 3D bioprinting was first demonstrated in 1988. Using ordinary office equipment (an inkjet printer) and software (standard graphic editor), it was shown that cells and cell adhesion proteins can be accurately positioned in space according to predetermined coordinates [20]. Currently, functional biological systems for *in vitro* studies, anatomical bioequivalents of various human tissues and organs with a complex, multicomponent structure are created using 3D bioprinting [21]. In the technological process, highly specialized (organ-specific) cells, growth factors, and various biocompatible materials are used [22], which provides adequate conditions for long-term functioning of the created tissue-engineered construct [23, 24]. In the global 3D bioprinting industry, consumer trends have been formed, the main research groups of developers and manufacturers have been identified. Based on existing basic additive technologies and the 3D bioprinting technique, methods for obtaining artificial organs and tissues, biocompatible matrices are being actively developed. The global 3D bioprinting market is valued at $1.4 billion and is projected to reach $4.4 billion by 2028 [25].

The main leading companies in the field of 3D bioprinting are presented in Table 1 [26, 27].

Chinese company Sichuan Revotek and American company Organovo are the two leading companies by the number of received patents for inventions related to 3D bioprinting [28].

The leading country in this field is the USA, where a kind of "roadmap" – a scenario for the commercializa-

Corresponding author: Dmitry Bulgin. Address: 177, Mira str., Vesyoloye, Adlersky District, Sochi, Krasnodar Krai, 354376, Russian Federation.
Phone: (862) 243-24-07. E-mail: bulgin@primatologia.ru

tion of regenerative medicine technologies in the field of tissue engineering and organ regeneration from 2000 to 2060 – has been created (Fig. 1) [29].

This scenario consists of the following stages [10]:

2000–2015, using the results of research in the field of tissue engineering and regenerative medicine to form a new global market of technologies, equipment and consumables;

2015, creation of new kinds of biopolymers to completely replace synthetic biodegradable matrices;

2025, creation of industrial biotechnological complexes for cultivation of autologous cells and development of tissue engineering technologies based on these cells;

2050, development of technologies for converting allogeneic cell genotype into autologous cell genotype;

2060, opening of a network of commercial repositories (tissue banks) for obtaining and long-term storage of personalized artificial bioequivalents of organs for a particular recipient.

BASICS OF 3D BIOPRINTING

The main component of any 3D bioprinter is a three-axis (X-Y-Z) positioning manipulator (Fig. 2).

The software controls the trajectory of automated system movement along the X, Y, Z axes and dosed supply of cellular elements, growth factors and other biomaterials into the created 3D structure. Thus, this technology turns virtual computer models (prototypes) of various organs into real artificial organs [30].

Currently, manufacturing companies offer a wide range of bioprinters for printing with live cells, which have different design and technical solutions. However, these devices retain the same operating principle for all models – layer-by-layer application of cell populations placed in a biocompatible support base (soluble hydro-

Table 1

Major companies leading the global 3D bioprinting market

America	Europe	Asia
Countries: – USA; – Canada. Companies: – Aspect, Aether, SE3D, Organovo, Tevido, BIOLIFE 4D, Seraph Robotics, BioRobots, ASLS, nScrypt	Countries: – Germany; – France; – Switzerland; – Sweden. Companies: – Ourobotics, Poietis, 3Dynamic, EnvisionTEC, regenHU, REGEMAT 3D, GeSiM, CELLINK, and 3D Bio	Countries: – China; – Japan; – South Korea; – Singapore. Companies: – Sichuan Revotek, Regenovo Biotech, ROKIT, Cyfuse, Pensees and Bio3D Tech

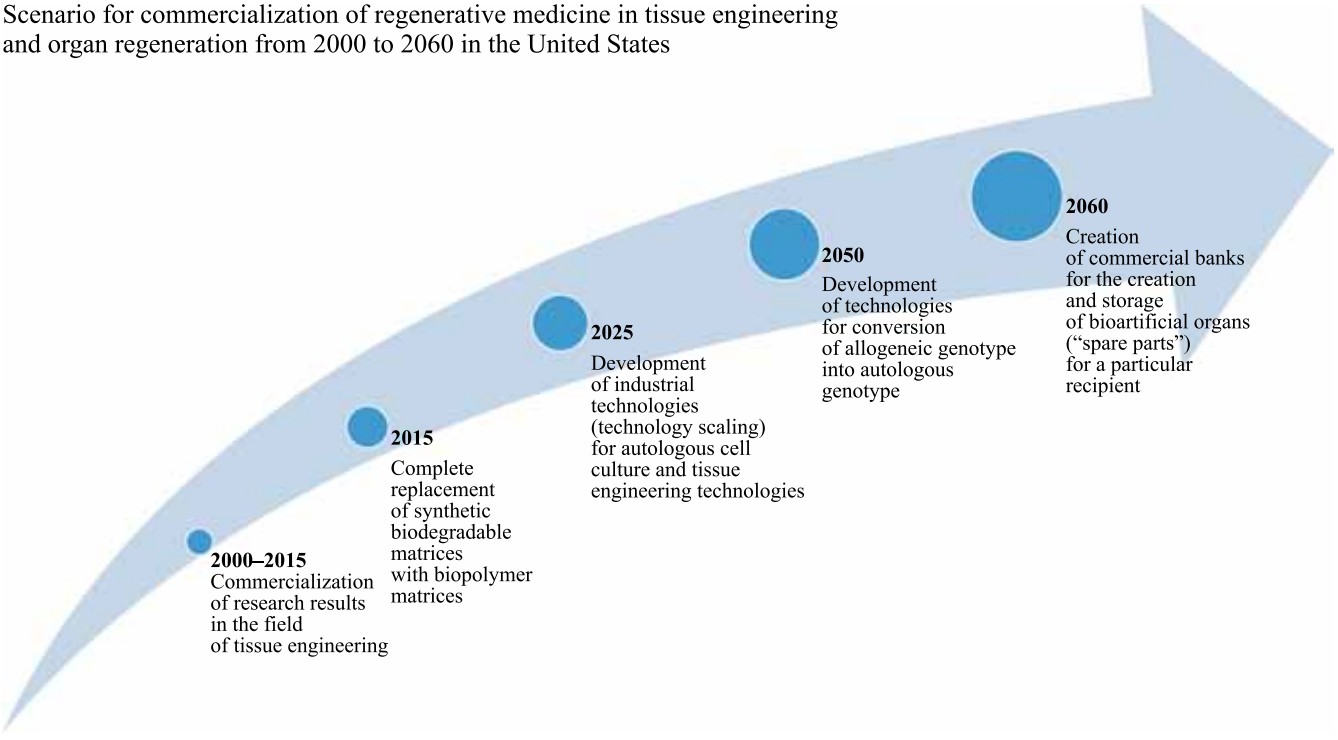

Fig. 1. Roadmap for the commercialization of regenerative medicine technologies in the United States [29]

gels) from the print head to the cell population building surface [31].

POSSIBLE OPTIONS FOR 3D BIOPRINTING

3D bioprinting is mainly based on three central approaches [32].

1. Continuous (extrusion) method: a constant stream comes from a syringe or special dispenser. Extrusion-based bioprinters use a mechanically or pneumatically driven system that places cells in the form of a filament.
2. Intermittent (droplet) method: inflow of microdroplets. Droplet-based bioprinters use heat-, piezo-, or acoustic-driven mechanisms to deposit droplets of cell suspension at high throughput.
3. Laser bioprinters use a non-contact method of applying a biomaterial, where high-frequency pulsed energy of the laser beam transfers a hydrogel drop containing cells to the receiving surface. This bioprinting method is referred to as "laser direct writing". This technology makes it possible to create structures with a density of 10^8 cells per 1 cm^3 and a resolution of 1 cell at high speed [33].

BIOMATERIALS FOR 3D BIOPRINTING

To obtain a functioning tissue-engineered construct, it is necessary to use carriers made of biomaterials with predetermined characteristics – natural, synthetic or composite materials. When choosing the most suitable materials and their production methods, it is necessary to simultaneously take into account many biological, physical and chemical parameters which determine internal architectonics, resorption time, biocompatibility (*immunological reactivity*), controlled release of bioactive substances (*specific extracellular matrix proteins, growth factors, cytokines*) in the matrix, which are responsible for proliferation and growth of cells regulating parenchymal-stromal and intercellular interactions [34–36]. Pore size and overall matrix porosity (Fig. 3 and 4) influence the rate of diffusion, drainage and delivery of oxygen, nutrients, various regulatory factors, removal of metabolic products due to formation of microvasculature, other homeostasis processes that are necessary to prevent ischemic injury and long-term preservation of full-fledged biological properties and physiological functions of the created tissue-engineered construct [36, 37].

It has been experimentally proven that with pore diameters exceeding 500 μm, cell migration is impossible because cells do not recognize the surface. Matrices with multiple, homogeneous and communicating pores (up to 70% porosity), having diameters from 50 μm to 500 μm, are ideal for the creation of tissue-engineered constructs [38, 39].

In recent years, biopolymers have been increasingly used as materials for creating biodegradable 3D matrices (Table 2). Unlike biodegradable synthetic polymers, biopolymers or their composites containing bioactive substances meet, to the greatest extent, the main requirements for matrices in tissue-engineered constructs, such as [40]:

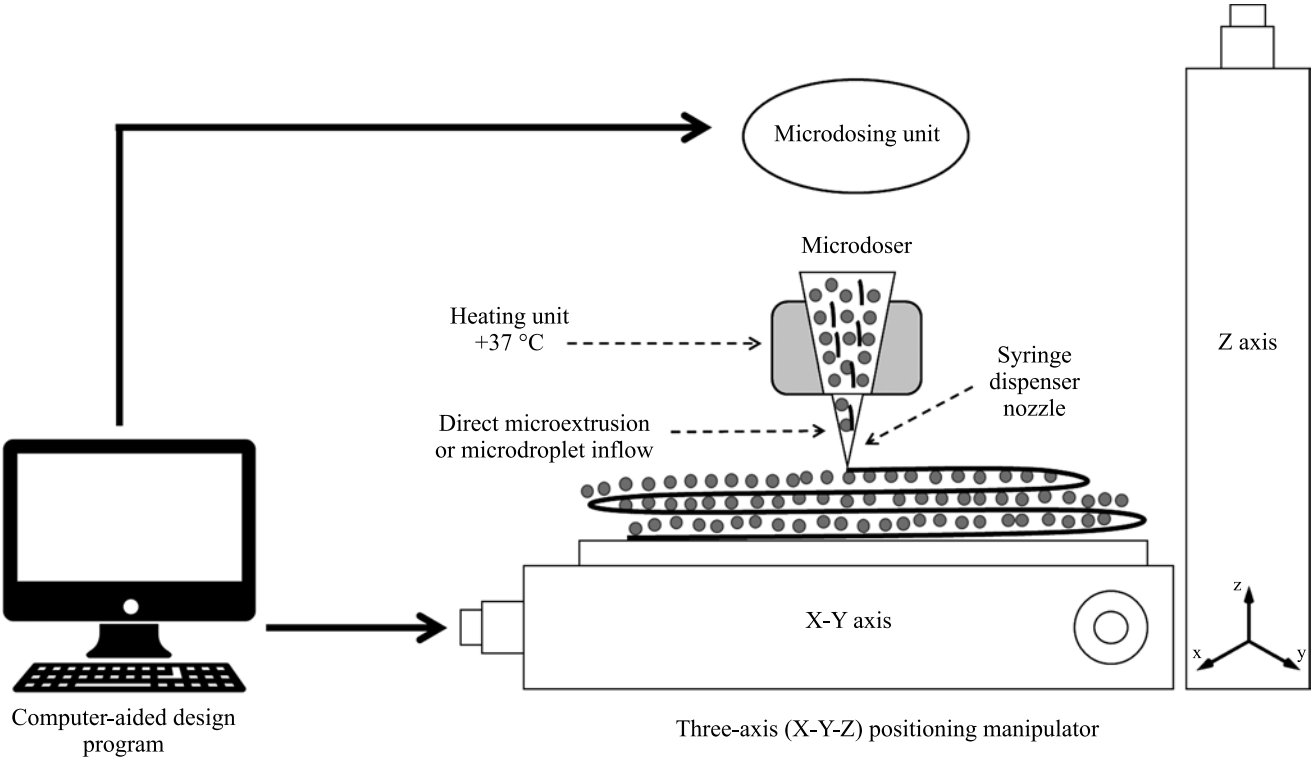

Fig. 2. Schematic representation of 3D bioprinting device

– biocompatibility of the product and its decomposition products;
– presence of biostimulating properties;
– ability to regulate biodegradation time;
– ability to neovascularize and neoinervate;
– withstand loads, provide strength and stability of tissue-engineered constructs, maintain viability of cellular elements;
– full connection to cell populations, stimulation and control of their growth;
– sterilization with preservation of biological and medical-technical characteristics of the obtained structure.

Encapsulation of cells within a semi-permeable biopolymer hydrogel is an attractive procedure that allows preserving the viability of cell populations during bioprinting [41]. Swedish researchers suggested using cellulose nanofibers in combination with cells. Chondrocytes bioprinted in nanocellulose exhibited a cell viability of 86% in the printed structure after 7 days of 3D culture [42]. Biodegradable matrices with up to 70% volumetric porosity were created based on aliphatic polyethers containing bioactive components such as hydroxyapatite, enzymes, growth factors and drugs [43]. It is important to consider the effect of various bioactive substances produced by the body in the course of responding to the implantation of a tissue-engineered construct – development of oxidative stress characterized by a high content of compounds that react by a free-radical mechanism [44]. Free radicals are capable of destroying cell membranes, damaging DNA molecules, and causing oxidative destruction of mitochondria. The method of creating tissue-engineered constructs based on microstructured biopolymer hydrogel matrices with antioxidant and antiradical activity seems promising [10, 45]. Advantages, disadvantages, as well as prospects of using some of the materials studied so far are presented in Table 3 [35, 46].

It should be noted that matrix elasticity has an influence on cell growth and differentiation. This should

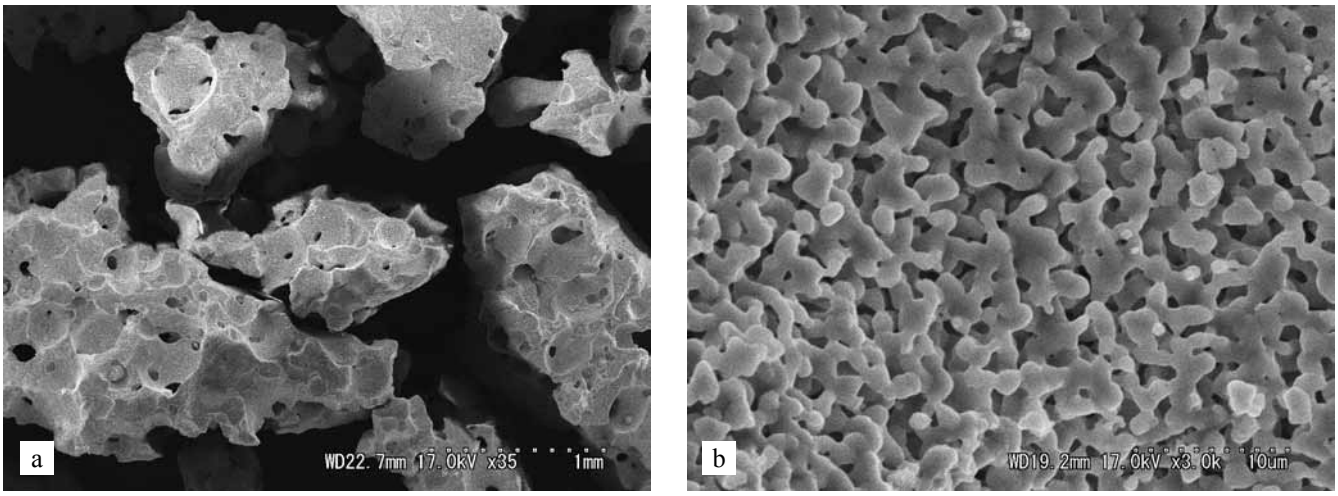

Fig. 3. Micrograph of a matrix based on beta-tricalcium phosphate (β-TCP) obtained by scanning electron microscopy. β-TCP granules contain multiple micropores ranging in size from 100 μm to 400 μm; total matrix porosity 75%. (a), macrostructure; (b), microstructure

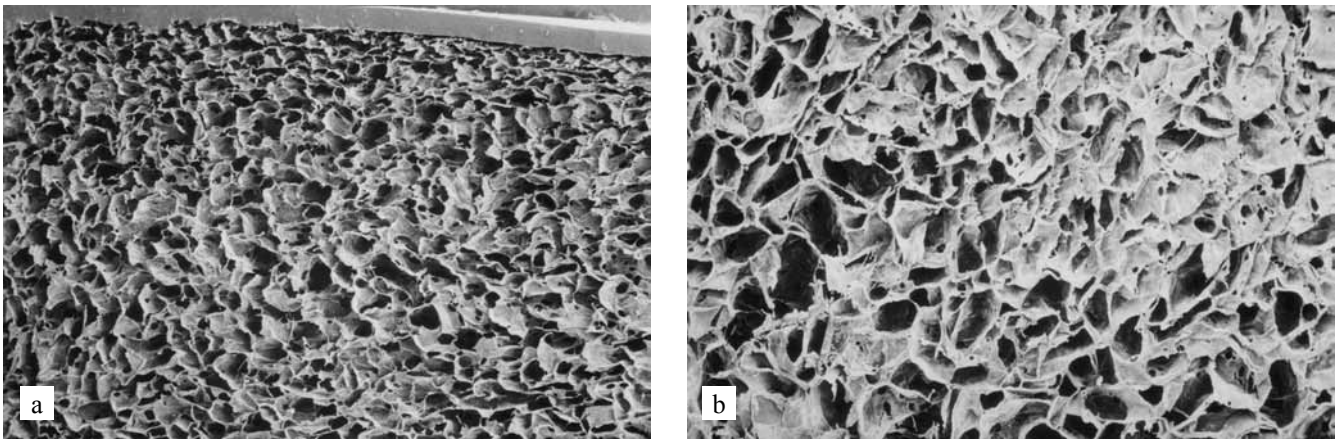

Fig. 4. Micrograph of collagen-based matrix obtained by scanning electron microscopy. (a), macrostructure; (b), microstructure, numerous micropores ranging in size from 50 μm to 500 μm

Table 2

Biopolymer materials most commonly used in tissue engineering and regenerative medicine [10]

Biopolymer	Source
Alginates	Polysaccharide from brown seaweed
Collagen, elastin	Extracellular matrix protein
Gelatin	Thermally denatured collagen
Chitosan	Chitin derivative (source: crayfish, crabs, shrimp)
Silk fibroin	Cocoon protein (silkworm)
Spidroin	Cobweb protein
Hyaluronic acid	Extracellular matrix component

be considered when choosing a carrier. However, soft polymers do not allow recreating an organ structure at micro- and nano-levels (Fig. 5).

THE CURRENT STATE OF RESEARCH IN THE FIELD OF 3D ORGAN BIOPRINTING

Numerous scientific publications confirm the promising use of 3D bioprinting both for research purposes and in clinical practice [47]. Constructs mimicking the myocardium [48], bone and cartilage tissue [49], blood vessels with multiple branches [50], skin [51], and peripheral nerves [52] were created. A liver model was presented to study pharmacokinetic processes (absorption, excretion, distribution and metabolism) *in vitro* [53]. For 3D bioprinting of spheroids, Japanese researchers used spherical cell aggregates consisting of chondrocytes, fibroblasts, bone marrow mesenchymal stem cells to create a miniature model of the trachea [54]. Scientists from Switzerland have created a functioning model of the alveolar-capillary membrane consisting of endothelial cells, basal membrane and alveolar epithelial cells [55]. Successful experiments were performed on models of laboratory primates to implant individual structural and functional components of the bronchopulmonary complex [56]. A technology has been developed for creating single-layer models of alveolar, bronchial and intestinal epithelium cells as a basis for complex structures of the airways and gastrointestinal tract, which can be used to assess the toxicity of pharmacological drugs [57]. A method for printing blood vessels using tissue spheroids with lumen, which form a complete vascular network when fused with each other, has been proposed [58]. It has been shown that vessels made only of cells, without any dense supporting scaffolds, can rapidly mature in a bioreactor and acquire properties comparable to those of natural blood vessels [59]. Multicellular spheroids composed of human umbilical vein endothelial cells (40% of all cell populations), human aortic smooth muscle cells (10%) and normal human dermal fibroblasts (50%) were used for 3D bioprinting of the blood vessel model. After culturing in a perfusion bioreactor, the resulting model in the form of a tubular structure (inner diameter of 1.5 mm) was successfully implanted into the abdominal aorta in a rat [60]. Researchers from Carnegie Mellon University (Pittsburgh, USA) developed a method for bioprinting heart and blood vessels using collagen, alginate, and fibrin as supporting materials. Since the structures made of the materials chosen by the researchers collapsed under their own weight during 3D printing, it was decided

Table 3

Main groups of materials for 3D bioprinting (advantages, disadvantages and prospects for use)

Material	Advantages	Disadvantages	Challenges	Prospects
Biomaterials	Natural origin, biocompatible, properties of natural tissues are preserved	Limitations in fabrication of materials with specified parameters	Risk of immune response, biodegradation, difficulties in fabricating multicomponent matrices with addition of synthetic materials	Development of bioactive matrices with predetermined characteristics, obtaining new composite materials
Synthetic materials	Polymeric materials with reproducible properties	Risk of developing an immune response, chemical instability, disruption of homeostasis in surrounding tissues	Fabrication of materials (biomimetics) based on the principles realized in living nature	Fabrication of composite biomaterials with predetermined characteristics, development of bioactive matrixes
Hybrid materials	Ideal combination of natural and synthetic polymer properties	None	Obtaining non-immunogenic matrixes with natural tissue properties and possibility of biodegradation	Development of bioactive matrixes with predetermined properties
Materials derived from decellularized tissues and organs	Natural origin, preservation of the tissue structural architectonics that existed before decellularization	Donor material is required	Risk of rejection reaction as a consequence of possible failures in the organ decellularization technology; obtaining a carrier while preserving all the characteristics of natural tissue	Obtaining organoids and functional models of bioengineered organs

to use a special gelatin scaffold to create organs. Then the temperature of the finished model was raised to a cell-friendly 37 °C, causing the gelatin support bath to melt in a nondestructive manner. This method was named FRESH (Freeform Reversible Embedding of Suspended Hydrogels) [61]. Using single cell-derived spheroids from human mesenchymal stem cells, a model of the urethra was created. The resulting structure was placed in a bioreactor for subsequent differentiation of stem cells into uroepithelial cells. After 10 days of maturation in the bioreactor, the tissue-engineered construct was successfully transplanted into a rat [62]. Recent preclinical studies indicate the possibility of transplanting 3D constructs from allogeneic human pancreatic beta cells in the treatment of type 1 diabetes [63]. Preclinical studies on animal models of acute liver failure are being conducted on the possibility of using allogeneic 3D constructs consisting of a combination of primary hepatocytes and human mesenchymal stem cells in the treatment of patients suffering from acquired or genetic liver diseases [64]. A technology of neural tissue creation using human-induced pluripotent stem cells (hiPSCs) derived from neural progenitor cells (NPCs) has been developed [65].

We obtained ring models of smooth muscle tissue of the human respiratory tract and intestine that responded to chemical stimulation in the form of contraction and relaxation of smooth muscle fibers. The fibers contracted when exposed to physiological histamine levels (0.01–100 μM) and relaxed when exposed to salbutamol, a drug used to relieve asthma attacks. Addition of transforming growth factor beta (TGF-β) to the airway muscle rings caused an increase in unstimulated muscle contraction and a decrease in response to salbutamol, a phenomenon also seen in chronic lung disease. The results show that 3D bioprinted smooth muscle is a physiologically relevant model *in vitro*, which can be used to study disease pathways and the effect of novel therapeutic agents on acute contraction and chronic tissue stenosis [66]. Researchers from Cornell University, USA, have developed a method of individual 3D bioprinting of intervertebral discs, which is ideal for a particular patient [67]. Note-

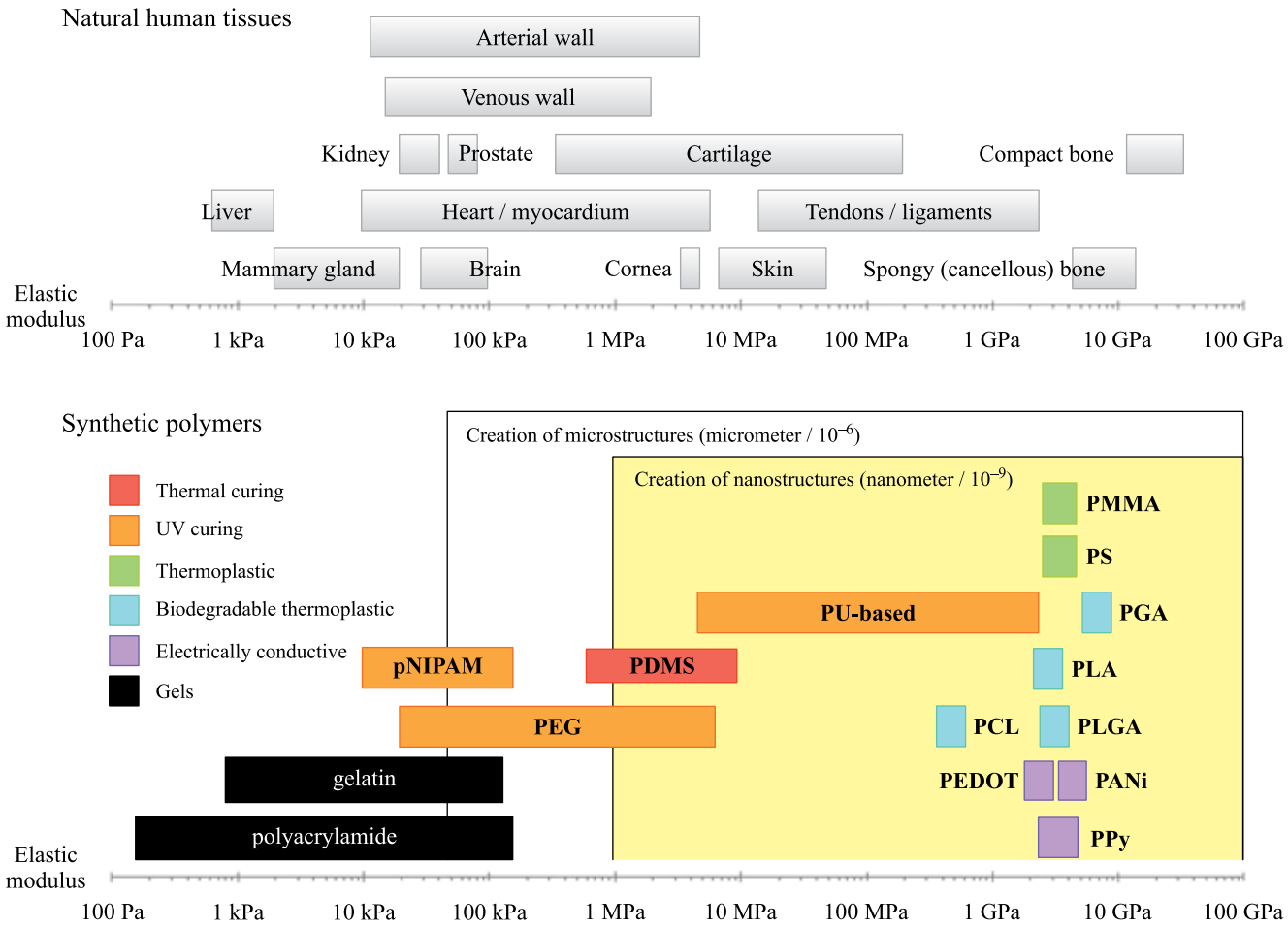

Fig. 5. Mechanical properties of natural human tissues and synthetic polymers. PDMS, polydimethylsiloxane; PU, polyurethane; PEG, polyethylene glycol; pNIPAM, poly-N-isopropylacrylamide; PMMA, polymethylmethacrylate; PS, polystyrene; PLGA, polylactic-co-glycolic acid; PGA, polyglycolic acid; PLA, polylactide; PCL, polycaprolactone; PANi, polyaniline; PPy, polypyrrole; PEDOT, poly-3,4-ehtylenedioxythiophene. Source: Annals of Biomedical Engineering, 2012; 40 (6), 1339–1355

worthy is the report on the creation of a bionic ear based on calf chondrocytes, hydrogel (alginate) and silver nanoparticles. The created construct repeats the anatomical shape of the human ear, has a built-in inductive antenna for capturing electromagnetic vibrations in the Hz and GHz ranges [68].

EXAMPLES OF SUCCESSFUL COMMERCIALIZATION OF 3D BIOPRINTING METHODS

Organovo (*San Diego, CA, USA*). Organovo was the first company to develop and market NovoGen Bioprinter® Platform, a 3D bioprinting equipment. The technological parameters of the platform make it possible to create functional models of bone tissue, tissue of the liver, kidney, intestine, skin, blood vessels, skeletal muscle, eye tissue, malignant tumors of the breast and pancreas [69, 70]. Multicellular tissue-engineered constructs with predetermined functions are created for pharmaceutical companies [71–73]. A significant success achieved by the company was the creation of an *in vitro* functioning 3D model of liver tissue (ExVive™ Human Liver Tissue). Primary human hepatocytes, Kupffer cells, stellate cells (Ito cells) and endotheliocytes were used in the creation of the model [74]. The resulting model functioned stably for 40 days [75, 76]. The company's specialists presented a three-layer model of the human vessel wall. All cell populations within the created construct were functionally active [77, 78]. The company is actively developing the technology to create a bioequivalent of the kidney [79].

TeVido Biodevices (*Austin, Texas, USA*). The company specializes in the production of a personalized artificial nipple-areola complex used in the final stage of breast reconstruction after radical mastectomy [80]. Another area of activity is the development of vascularized skin substitutes for the treatment of vitiligo, chronic wounds and burns. Autologous stem cells isolated from the patient's adipose tissue and dermis are used in the process of creating bioconstructs [81].

Nano 3D Biosciences (*Houston, Texas, USA*). The company develops a technology for creating tissue spheroids in a magnetic field (magnetic 3D bioprinting) for subsequent use in bioprinting. This technology makes it possible to obtain tissue models for *in vitro* studies in the shortest possible time [82–84].

Tissue Regeneration Systems (*Plymouth, Michigan, USA*). The company develops and manufactures polymeric implants for replacement of bone tissue defects. The company's products are certified by the U.S. Food and Drug Administration and are widely used in dentistry, maxillofacial surgery, traumatology and orthopedics, and neurosurgery [85].

nScrypt (*Orlando, Florida, USA*). Software development, production of biocompatible materials and equipment for 3D bioprinting – BFF (BioFabrication Facility) complex. In the process of printing, it is possible to simultaneously use up to 4 different types of biocompatible materials, including live cell populations. The capabilities of the complex allow creating defined structures up to 10 μm in diameter (the diameter of a human red blood cell is 7 to 10 μm), with a minimum working volume of material in the dispenser of 100 picoliters. In 2019, 3D bioprinting of human myocardial tissue was performed onboard the International Space Station, in zero gravity, together with the research biotechnology (space biotechnology) company Techshot (USA). Earth's gravity does not allow printing biological objects of large size – hydrogel bases do not hold their shape, spreading out under their own weight. The experiment proved the efficiency of a specially designed additive system under weightlessness [86].

The same companies (nScrypt and Techshot), with financial support from The Geneva Foundation (a nonprofit organization that funds research in military medicine), together with the United States Military Academy West Point, the Uniformed Services University, within the framework of research program 4D Bio3 (4-Dimensional Bioprinting, Biofabrication and Biomanufacturing – an interdisciplinary program of biomedical research and practical implementation of advanced biotechnologies for the US Army needs) [87], tested a shockproof version of the BFF – nRugged bioprinter. The equipment was deployed at the base of a U.S. Army medical unit in the desert terrain of North Africa, in the immediate vicinity of the active combat zone [88, 89].

During BFF field trials, a variety of tools and medical consumables were produced for both the military medical service and large multidisciplinary military hospitals, such as:

– disposable blade holder pens;
– hemostatic supplies;
– dressing material using antibacterial hydrogel;
– A functional meniscus model based on human mesenchymal stem cells and hydrogel as a matrix;
– acsurgical model of the 9th thoracic vertebra (Th 9) [90].

The choice of the meniscus as the object of the experiment was due to the high frequency of knee joint injuries among military personnel (meniscus injuries in military personnel occur 10 times more frequently than in civilians) [91]. The digital model used to print the meniscus was sent as an electronic file from the United States – this was the first demonstration of cyberfabrication, in which information about complex structures is transmitted via satellite communication to a remote location to produce a functional model [90].

Advanced Solutions Life Sciences, (*Louisville, Kentucky, USA*). The company develops 3D bioprinting software. These programs are used to create 3D computer models for subsequent fabrication of complex tissue-engineered constructs [92]. The in-house bioprinting

equipment BioAssemblyBot is a certified, fully robotic multifunctional device with a 6-axis EPSON robotic arm [93] for printing functional models of different tissues and organs, and implants with complex geometric forms [94]. The design features of the equipment allow printing vascularized tissue-engineered constructs for clinical application directly in the operating room – *in situ* bioprinting under aseptic conditions [95].

MicroFab Technologies Inc (*Plaino, Texas, USA*). The company is a pioneer in the field of liquid bioprinting (ink-jet dispensing). Currently, together with the US Armed Forces Institute of Regenerative Medicine and one of the leading medical research centers, Wake Forest Institute for Regenerative Medicine, the company is developing the technology of accelerated regeneration of skin burn wounds. The main goal of this project is to develop a method of bioprinting the skin directly onto the damaged area [96]. Another promising area of the company's activity is the creation of special sheath-conductors (bioabsorbable nerve guidance conduits) used for the growth of peripheral nerves. This construct is placed between the damaged sections of the nerve. The distal and proximal ends of the injured nerve are connected to the guidance conduit, and the nerve grows and regenerates within the conduit. Later the guidance conduit is completely resorbed [97].

ETEC (*Dearborn, Michigan, USA)*. The company produces 3D Bioplotter system using technologies developed at Freiburg Materials Research Center. They produce complex tissue-engineered constructs from various biocompatible materials [98–100]. 3D Bioplotter can simultaneously print using five different materials and their mixtures (living cell populations, polymer hydrogels, ceramics, metals) of different consistency (from paste-like to liquid), it is possible to use material of any origin, different concentration and with any additives (Table 4). Each user can use their own printing parameters [101].

The technology is based on extrusion from a syringe. The advantage of using a syringe-based material delivery system is the ability to 3D print at room temperature, which allows for inclusion of live cellular material in your printed designs. 3D Bioplotter comes with four types of print heads:

– Low temperature (2 °C to 70 °C);
– High temperature (30 °C to 250 °C);
– Ultra-high temperature (30 °C to 500 °C);
– UV-emitting (when used for printing photopolymer materials).

Cyfuse Biomedical (*Tokyo, Japan*). Tissue-engineered constructs are created on in-house equipment Regenova Bio 3D Printer using the scaffold-free biofabrication method. In the process of creation, spheroids are used – spherical cell aggregates formed from autologous or allogeneic cell populations of various origin. The method is based on the ability of living cells to form spherical aggregates when cultured on non-adhesive surfaces. Tissue spheroid is a group of 15 to 20 thousand cells interconnected to form a spatial three-dimensional structure in the shape of a sphere. Spheroids ranging in size from 400 to 600 μm can be single-cell, consisting of one type of cells, or multi-cellular, formed from different types of cells and biomaterials. During printing, fabric spheroids are "threaded" on a metal base formed from the thinnest needles (reminiscent of the kenzan, a base for attaching flowers when making Ikebana flower). Each needle is 1 cm long and 170 μm in diameter; the needles are arranged in a strictly defined sequence (9 × 9 or 26 × 26) at intervals of 400 μm from each other) [102]. The capabilities of Micro Needle Array Technology (MNAT) make it possible to make tissue constructs from different types of cell populations. Then, the resulting construct is incubated until the spheroids join together to form large cellular associates capable of independently synthesizing extracellular matrix components and forming a given structure. This technology opens up great opportunities for tissue and organ bioengineering [103]. In the future, it is possible to print pancreatic islets, myocardium, and skin [104, 105].

Regenovo Biotechnology (*Hangzhou, China*). The company designs and manufactures 3D bioprinting equipment – Regenovo 3D bioprinter, BIO-ARCHITECT X. A distinctive feature of the device is the high speed of model making. Special nozzles allow you to simultaneously create different types of fabrics with a high level of resolution. The presence of a high-precision infrared laser makes it possible to check the quality of the internal structure of the fabric during production. The 3D bioprinter uses an innovative microcomputed tomography system to print a wide range of tissues and organs (including skin, muscle, cartilage, bone, tendons, liver tissue). According to forecasts by the company, it

Table 4

Materials used when working with 3D Bioplotter

Bone tissue regeneration	Targeted drug transport (drug release)	Soft tissue biofabrication, organ bioprinting	Prototyping 3D models
Hydroxyapatite (HA)	Polycaprolactone (PCL)	Suspensions of living cell populations	Polyurethane (PU)
Tricalcium phosphate (TCP)	Poly-D,L-lactide-co-glycolide (PLGA)	Agar, chitosan, alginates, hyaluronic acid	Silicone
Titanium (paste)	Poly-L-lactide (PLLA)	Gelatin, fibrin, agarose, collagen	Acrylates

will be possible to carry out mass production of artificial tissues and organs for transplantation in 15–20 years. In addition to the equipment production, the company produces 3D printing biomaterials. Currently, the company offers more than 20 types of biomaterials from organic and inorganic polymers. Cell survival in Regenovo materials is 90%; they function for up to four months [106].

RegenHU (*Switzerland).* A software developer and manufacturer of equipment (bioprinters) and consumables based on collagen hydrogels. In the process of 3D bioprinting of functionally active bioequivalents of human skin, bone and cartilage tissues, up to 9 different components (cells, tissue spheroids, various biomaterials) are used simultaneously [107, 108]. A personalized 3D model of the human medial meniscus based on collagen hydrogel and autologous mesenchymal stem cells isolated from the patient's bone marrow was created. The obtained prototype was the starting point for subsequent development of technologies for manufacturing individual implants designed to replace damaged menisci [109]. The technology for creating a skin bioequivalent that is morphologically and functionally comparable with the native human skin has been developed [110]. A new concept of creating personalized myocardial tissue has been proposed. Cell populations and extracellular matrices were isolated from patients' adipose tissue (omentum). The cells were reprogrammed into pluripotent stem cells, and the extracellular matrix was transformed into a personalized collagen hydrogel. After mixing the cells with the hydrogel, the cells were differentiated into cardiomyocytes to create immunocompatible and vascularized patient-specific myocardial tissue [111].

Osteopore International, *Singapore.* Production of personalized implants for neurosurgery, traumatology, maxillofacial surgery and dentistry made of biodegradable polycaprolactone (PLC). PLC is a biodegradable polymer that can be completely disintegrated and reabsorbed *in vivo* through hydrolysis. The porous microstructure of the material, which mimics the structure of natural human cancellous bone, ensures colonization of bone marrow by cell populations, development of a network of vessels of the microvasculature. Complete replacement (bioresorption) of a PLC-based implant by the patient's own bone tissue occurs within 18–24 months [112–114].

OxSyBio, *United Kingdom*. 3D bioprinting technologies are based on the use of hydrogel microdroplets (polymersomes) covered with a lipid layer. Living cells are placed in the polymersomes, which protects the cellular material from damage during the printing process. Each droplet is the same size as a cell and can be positioned to within 1 μm. With this printing method, structures of various geometric shapes can be formed. The created constructs conduct electrical impulses, like nerve cells, in a certain direction. Significant advances have been made in the development of biomaterials for the treatment of wound surfaces. There are plans to create complex organs by combining synthetic materials with live cell cultures to create organs and tissues for transplantation [115, 116].

FUTURE PROSPECTS AND DUAL-USE TECHNOLOGIES

Analysis of domestic and foreign research publications on this topic has indicated that it is possible to come up with technologies for creating fully functioning artificial organs using 3D bioprinting by the end of the next decade [117]. However, at present, the use of bioprinted tissues and organs in preclinical studies and in clinical practice is very limited [118, 119]. A number of significant technological problems need to be solved for this purpose. The resulting 3D printed constructs are static, they are not capable of reproducing the natural dynamic nature of tissue – processes of natural regeneration and repair, which include conformational changes in the structure [120]. It is necessary to improve the characteristics of biomaterials capable of supporting cell proliferation and differentiation [121–123]. A promising direction is the creation of biocompatible matrices made from biomaterials and cellular elements that respond to stimuli, such as temperature, pH, humidity, electricity, magnetic field, light, sound waves or to a combination of these stimuli [124]. The development of models that change their morphology over time, according to the given stimuli from the environment, has already begun [125]. Creation of vascularized models is an extremely difficult task [126, 127]. For human tissues and organs of normal anatomic shape and size, it is necessary to develop technologies that allow integrating blood vessels into the created model. The existing 3D bioprinting methods do not allow for simultaneous formation of blood vessels and other elements forming the parenchyma and stroma of the organ [128]. Full-fledged vascularization ensures long-term, adequate functioning of the bioprinted construct [129]. More advanced bioprinters are needed to create the vascular component in the printed model; the resolution and speed of current equipment are insufficient [130, 131]. Below are the optimal technical characteristics of the equipment for 3D bioprinting of the future [132]:

- high degree of freedom and speed of movement in space, allowing to apply biomaterials to uneven surfaces of the damaged organ and to restore lost tissue ex tempore;
- high resolution and accuracy of printing, allowing to apply biomaterials an accuracy that corresponds to the structure of native tissue;
- possibility of simultaneous use of various types of biomaterials for making heterocellular tissues similar by structure and functions to those of native tissue;
- compactness for work in sterile conditions (laminar flow box);

– possibility to sterilize biomaterials in the process of bioprinting;
– full automation that facilitates bioprinting without user intervention;
– versatility, which allows users to modify and expand the technical capabilities of the equipment for multipurpose use;
– ease of use, allowing users with minimal skills and experience to operate the equipment.

It should be noted that any revolutionary technology always has dual-use potential [133, 134]. The possibilities of using the 3D bioprinting method in the creation of new classes of weapons, means of combat support, special and dual-use products are presented in Table 5 [135, 136].

CONCLUSION

Further improvement of 3D bioprinting technologies will solve the problem of donor material shortage and significantly expand the possibilities of practical transplantology [137–140]. Broad prospects are opening up for the development of new medical devices and pharmacological preparations, *in vitro* studies of the effects of various bacteriological, chemical and physical factors on the human body: bacteriology, immunology (*ex vivo* creation of an artificial immune system), toxicology, radiation biology, and radiation medicine [141–143]. The use of 3D printing for preoperative planning and production of phantom organs for educational purposes will improve the professional skills of surgeons and enable them to repeatedly refine the surgical technique, thus requiring less time to perform the operation. Organ models can completely replace experiments on laboratory animals, significantly reduce the cost of drug development and reduce the time required for laboratory trials [144–146].

We hope that the information presented in this review will be informative for creating fully functional anatomical bioequivalents of human organs using additive

Table 5

Potential for 3D bioprinting

Application	Description
Camouflage	The use of hybrid biomaterials with stealth characteristics to create clothing and coatings that are hardly visible in radar, infrared and other spectrums
Combat identification	Biomarkers for identifying one's own and allied soldiers (the biological analogue of the friend-or-foe identification system)
Computers, databases	DNA-based computers, biological models for computer algorithms. Associative memory, computing devices using biomaterials. Artificial intelligence – proteins as a means of working with information and energy
Foodstuff	Nutritional supplements to protect the digestive system from adverse environmental factors
Remote monitoring of soldier's health	Creation of implantable biosensors allowing real-time remote monitoring of body vital functions in combat conditions, environmental control for timely warning of enemy use of weapons of mass destruction
Lightweight armor	Protection of soldiers and combat systems, protective coatings with living tissue characteristics, creation of self-healing armor for body protection
Protection of combat electronic systems from ionizing radiation and electromagnetic radiation	Incorporation of hybrid biomolecules into components of electronic systems, biomolecular-based diodes and transistors
Combat robotics	Biological prototype constructs for creating self-propelled bionic platforms, creation of anthropomorphic robot
Reducing equipment size and weight	Molecular electronics, biochips, nanotechnology
Environmental monitoring systems in a battle zone	Creation of miniature diagnostic systems (mini lab on a chip) to detect and recognize chemical, biological and radioactive substances
Military field therapy, military field surgery	Acceleration of wound regeneration, creation of artificial tissues and organs
Artificial immune system (creation of 3D human immune system)	Vaccines with a shortened period of immunity, creation of protection (on the basis of gene and cell technologies) against weapons of mass destruction, new methods of treatment of wounded servicemen. Biological approach to maintaining combat capability in extreme conditions: The possibility of designing a fundamentally new complex protein (protein machine) that can neutralize a pathogenic organism within 24 hours; Studying the mechanisms of regulation and expression of new genes and substances created by the body as it enters and exits extreme conditions; DNA editing in a living organism; Biomolecules that can neutralize the effects of prolonged lack of sleep

technologies based on 3D bioprinting. The near future will confirm or refute our expectations and predictions.

The authors declare no conflict of interest.

REFERENCES

1. *Gautier SV.* Klinicheskaja transplantologija kak samostojatel'noe napravlenie mediciny. *Medicinskij al'manah.* 2008; 5: 14–19.
2. *Gautier SV*. Transplantology 2008–2018: a decade of advancement. *Russian Journal of Transplantology and Artificial Organs*. 2018; 20 (4): 6–7.
3. *Khubutia MSh, Zhao AV, Shadrin KB*. Postoperative complications in liver transplant recipients: modern cconsiderations of pathogenesis and main areas of prophylaxis and treatment. *Russian Journal of Transplantology and Artificial Organs.* 2009; 11 (2): 60–66. (In Russ.). doi: 10.15825/1995-1191-2009-2-60-66.
4. *Klimusheva NF*. Transplantacija solidnyh organov: puti optimizacii i povyshenija jeffektivnosti. [Dissertation]. M., 2016; 48.
5. *Bagnenko SF, Reznik ON*. Key problems of transplantation development and the objectives of higher medical education. *Transplantologiya. The Russian Journal of Transplantation.* 2017; 9 (3): 192–210. doi: 10.23873/2074-0506-2017-9-3-192-210.
6. *Gautier SV, Khomyakov SM.* Organ donation and transplantation in Russian Federation in 2017. 10th report of the national registry. *Russian Journal of Transplantology and Artificial Organs*. 2018; 20 (2): 6–28. (In Russ.). doi: 10.15825/1995-1191-2018-2-6-28.
7. *Gautier SV, Khomyakov SM*. Organ donation and transplantation in the Russian Federation in 2019. 12th report from the Registry of the Russian Transplant Society. *Russian Journal of Transplantology and Artificial Organs.* 2020; 22 (2): 8–34. doi: 10.15825/1995-1191-2020-2-8-34.
8. *Gautier SV, Khomyakov SM.* Organ donation and transplantation in the Russian Federation in 2020 13th Report from the Registry of the Russian Transplant Society. *Russian Journal of Transplantology and Artificial Organs.* 2021; 23 (3): 8–34. doi: 10.15825/1995-1191-2021-3-8-34.
9. *Ma PX.* Biomimetic materials for tissue engineering. *Adv Drug Deliv Rev.* 2008; 60 (2): 184–198. doi: 10.1016/j.addr.2007.08.041.
10. *Sevastianov VI.* Technologies of tissue engineering and regenerative medicine. *Russian Journal of Transplantology and Artificial Organs.* 2014; 16 (3): 93–108. (In Russ.). doi: 10.15825/1995-1191-2014-3-93-108.
11. *Kim JA, Kim HN, Im SK, Chung S, Kang JY, Choi N*. Collagen-based brain microvasculature model *in vitro* using three-dimensional printed template. *Biomicrofluidics*. 2015; 9 (2) : 024115. doi: 10.1063/1.4917508.
12. *Mori H, Gupta A, Torii S, Harari E, Jinnouchi H, Virmani R, Finn AV.* Clinical implications of blood-material interaction and drug eluting stent polymers in review. *Expert Rev Med Devices*. 2017; 14 (9): 707–716. doi: 10.1080/17434440.2017.1363646.
13. *Kuevda EV, Gubareva EA, Gumenuyk IS, Karal-ogly DD*. A Study of Biocompatibility of Acellular Matrices of Primate Lungs and the Potential for Their Application as Tissue-Engineering Constructions. *Sovremennye tehnologii v medicine.* 2017; 9 (4): 82–88. doi: 10.17691/stm2017.9.4.10.
14. *Repin VS, Saburina IN*. Ot transplantacii organov k reparativnym sferoidam i "ıkrotkanjam" v suspenzionnoj 3D-kul'ture. *Kletochnaja transplantologija i tkanevaja inzhenerija.* 2012; 7 (1): 106–108.
15. *Gautier SV, Shagidulin MYu, Onishchenko NA, Krasheninnikov ME, Il'inskii IM, Mozheiko NP et al.* Correction of cronic liver failure by transplantation of liver cells suspension and cell-engineering designs (experimental investigation). *Annals Of The Russian Academy Of Medical Sciences.* 2013; 68 (4): 44–51. doi: 10.15690/vramn.v68i4.610.
16. *Layek B, Lipp L, Singh J.* Cell Penetrating Peptide Conjugated Chitosan for Enhanced Delivery of Nucleic Acid. *Int J Mol Sci.* 2015; 16 (12): 28912–28930. doi: 10.3390/ijms161226142.
17. *Reznik ON, Kuzmin DO, Skvortsov AE, Reznik AO*. Biobanks are an essential tool for transplantation. history, current state, perspectives. *Russian Journal of Transplantology and Artificial Organs.* 2016; 18 (4): 123–132. doi: 10.15825/1995-1191-2016-4-123-132.
18. *Ugraitskaya SV, Shishova NV, Gagarinskiy EL, Shvirst NE, Kaurova SA, Goltyaev MV et al.* Effect of Helium on Cryopreservation of HeLa and L929 Cells. *Biophysics.* 2018; 63 (3): 510–517.
19. *Hasan M, Fayter AER, Gibson MI.* Ice Recrystallization Inhibiting Polymers Enable Glycerol-Free Cryopreservation of Microorganisms. *Biomacromolecules.* 2018; 19 (8): 3371–3376. doi: 10.1021/acs.biomac.8b00660.
20. *Klebe RJ*. Cytoscribing: a method for micropositioning cells and the construction of two- and three-dimensional synthetic tissues. *Exp Cell Res.* 1988; 179 (2): 362–373. doi: 10.1016/0014-4827(88)90275-3.
21. *Thayer P, Martinez H, Gatenholm E.* History and Trends of 3D Bioprinting. *Methods Mol Biol.* 2020; 2140: 3–18. doi: 10.1007/978-1-0716-0520-2_1.
22. *Mota FB, Braga LAM, Cabral BP, Conte Filho KG.* Future of Bioprinted Tissues and Organs: A Two-Wave Global Survey. *Foresight and STI Governance.* 2022; 16 (1): 6–20. doi: 10.17323/2500-2597.2022.1.6.20.
23. *Balyasin MV, Baranovsky DS, Demchenko AG, Fayzullin AL, Krasilnikova OA, Klabukov ID et al.* Experimental orthotopic implantation of tissue-engineered tracheal graft created based on devitalized scaffold seeded with mesenchymal and epithelial cells. *Russian Journal of Transplantology and Artificial Organs.* 2019; 21 (4): 96–107. doi: 10.15825/1995-1191-2019-4-96-107.
24. *Kokorev OV.* Sanogeneticheskoe obosnovanie primenenija tkaneinzhenernyh konstrukcij na osnove poristogo nikelida titana pri patologii razlichnogo geneza. [Dissertation]. Tomsk, 2019. 44.
25. Grand View Research (2021) 3D Bioprinting Market Size, Share and Trends Analysis Report by Technology (Magnetic Levitation, Inkjet-based), by Application (Medical, Dental, Biosensors, Bioinks), by Region, and

Segment Forecasts, 2021–2028, San Francisco, CA: Grand View Research. Available from: https://www.grandviewresearch.com/industry-analysis/3d-bioprinting-market.

26. *Choudhury D, Anand S, Naing MW.* The arrival of commercial bioprinters – Towards 3D bioprinting revolution! *Int J Bioprint.* 2018; 4 (2): 139. doi: 10.18063/IJB.v4i2.139.
27. *Mota C, Camarero-Espinosa S, Baker MB, Wieringa P, Moroni L.* Bioprinting: From Tissue and Organ Development to *in vitro* Models. *Chem Rev.* 2020; 120 (19): 10547–10607. doi: 10.1021/acs.chemrev.9b00789.
28. *Mota F, Braga L, Rocha L, Cabral B.* 3D and 4D bioprinted human model patenting and the future of drug development. *Nat Biotechnol.* 2020; 38 (6): 689–694. doi: 10.1038/s41587-020-0540-1.
29. Advances in replacement organs and tissue engineering. Technical Insights, Frost & Sullivan. 2008. Available from: https://store.frost.com/advances-in-tissue-engineering-and-organ-regeneration-technical-insights.html.
30. *Ozbolat IT, Bashirul Khoda AKM.* Design of a New Parametric Path Plan for Additive Manufacturing of Hollow Porous Structures With Functionally Graded Materials. *J Comput Inf Sci Eng.* 2014; 14 (4) doi: 10.1115/1.402841831.
31. *Korovin AE, Nagibovich OA, Peleshok SA, Kopylenkova TI, Shilin VP, Ol'hovik AYu* i dr. 3D-modelirovanie i bioprototipirovanie v voennoj medicine. *Klinicheskaja patofiziologija*. 2015; 3: 17–23.
32. *Ozbolat IT, Yu Y.* Bioprinting toward organ fabrication: challenges and future trends. *IEEE Trans Biomed Eng.* 2013; 60 (3): 691–699. doi: 10.1109/TBME.2013.2243912.
33. *Schiele NR, Corr DT, Huang Y, Raof NA, Xie Y, Chrisey DB.* Laser-based direct-write techniques for cell printing. *Biofabrication.* 2010; 2 (3): 032001. doi: 10.1088/1758-5082/2/3/032001.33.
34. *Bogorodskij SJe, Vasilec VN, Krotova LI, Minaeva SA, Mironov AV, Nemec EA i dr.* Formirovanie bioaktivnyh vysokoporistyh polimernyh matriksov dlja tkanevoj inzhenerii. *Perspektivnye materialy*. 2013; 5: 44–54.
35. *Gulay YuS, Krasheninnikov ME, Shagidulin MYu, Onishchenko NA*. Hepatic tissue engineering (modern state of this problem). *Russian Journal of Transplantology and Artificial Organs*. 2014; 16 (2): 103–113. doi: 10.15825/1995-1191-2014-2-103-113.
36. *Onishchenko NA, Gulay YuS, Shagidulin MYu, Nikolskaya AO, Bashkina LV*. Development of implantable cell-tissue-engineering designs of auxiliary liver for the treatment of liver failure. *Genes & Cells.* 2015; 10 (1): 6–17.
37. *Murua A, Portero A, Orive G, Hernández RM, de Castro M, Pedraz JL.* Cell microencapsulation technology: towards clinical application. *J Control Release.* 2008; 132 (2): 76–83. doi: 10.1016/j.jconrel.2008.08.010.
38. *Wu C, Pan J, Bao Z, Yu Y.* Fabrication and characterization of chitosan microcarrier for hepatocyte culture. *J Mater Sci Mater Med.* 2007; 18 (11): 2211–2214. doi: 10.1007/s10856-007-3071-0.
39. *Zhao S, Zhang J, Zhu M, Zhang Y, Liu Z, Tao C et al.* Three-dimensional printed strontium-containing mesoporous bioactive glass scaffolds for repairing rat critical-sized calvarial defects. *Acta Biomater.* 2015; 12: 270–280. doi: 10.1016/j.actbio.2014.10.015.
40. *Kirillova AD.* Tkanespecificheskie matriksy iz decelljuljarizovannyh fragmentov pecheni i sustavnogo hrjashha dlja tkanevoj inzhenerii. [Dissertation]. M., 2021. 27.
41. *Gasperini L, Mano JF, Reis RL.* Natural polymers for the microencapsulation of cells. *J R Soc Interface.* 2014; 11 (100): 20140817. doi: 10.1098/rsif.2014.0817.
42. *Markstedt K, Mantas A, Tournier I, Martínez Ávila H, Hägg D, Gatenholm P.* 3D Bioprinting Human Chondrocytes with Nanocellulose-Alginate Bioink for Cartilage Tissue Engineering Applications. *Biomacromolecules.* 2015; 16 (5): 1489–1496. doi: 10.1021/acs.biomac.5b00188.
43. *Moisenovich MM, Pustovalova OL, Arhipova AY, Vasiljeva TV, Sokolova OS, Bogush VG et al. In vitro* and *in vivo* biocompatibility studies of a recombinant analogue of spidroin 1 scaffolds. *J Biomed Mater Res A*. 2011; 96 (1): 125–131. doi: 10.1002/jbm.a.32968.
44. *Rhodes CJ.* Toxicology of the Human Environment – the critical role of free radicals. London: Taylor and Francis; 2000.
45. *Mahmood A, Patel D, Hickson B, DesRochers J, Hu X.* Recent Progress in Biopolymer-Based Hydrogel Materials for Biomedical Applications. *International Journal of Molecular Sciences.* 2022; 23 (3): 1415. doi: 10.3390/ijms23031415.
46. *Chistiakov DA.* Liver regenerative medicine: advances and challenges. *Cells Tissues Organs.* 2012; 196 (4): 291–312. doi: 10.1159/000335697.
47. *Murphy SV, Atala A.* 3D bioprinting of tissues and organs. *Nat Biotechnol.* 2014; 32 (8): 773–785. doi: 10.1038/nbt.2958.
48. *Gaetani R, Doevendans PA, Metz CH, Alblas J, Messina E, Giacomello A et al.* Cardiac tissue engineering using tissue printing technology and human cardiac progenitor cells. *Biomaterials.* 2012; 33 (6): 1782–1790. doi: 10.1016/j.biomaterials.2011.11.003.
49. *Fedorovich NE, Schuurman W, Wijnberg HM, Prins HJ, van Weeren PR, Malda J et al.* Biofabrication of osteochondral tissue equivalents by printing topologically defined, cell-laden hydrogel scaffolds. *Tissue Eng Part C Methods.* 2012; 18 (1): 33–44. doi: 10.1089/ten.TEC.2011.0060.
50. *Norotte C, Marga FS, Niklason LE, Forgacs G.* Scaffold-free vascular tissue engineering using bioprinting. *Biomaterials.* 2009t; 30 (30): 5910–5917. doi: 10.1016/j.biomaterials.2009.06.034.
51. *Lee W, Debasitis JC, Lee VK, Lee JH, Fischer K, Edminster K et al.* Multi-layered culture of human skin fibroblasts and keratinocytes through three-dimensional freeform fabrication. *Biomaterials.* 2009; 30 (8): 1587–1595. doi: 10.1016/j.biomaterials.2008.12.009.
52. *Owens CM, Marga F, Forgacs G, Heesch CM.* Biofabrication and testing of a fully cellular nerve graft. *Bio-*

fabrication. 2013; 5 (4): 045007. doi: 10.1088/1758-5082/5/4/045007.

53. *Chang R, Emami K, Wu H, Sun W.* Biofabrication of a three-dimensional liver micro-organ as an *in vitro* drug metabolism model. *Biofabrication*. 2010; 2 (4): 045004. doi: 10.1088/1758-5082/2/4/045004.
54. *Taniguchi D, Matsumoto K, Tsuchiya T, Machino R, Takeoka Y, Elgalad A et al.* Scaffold-free trachea regeneration by tissue engineering with bio-3D printing. *Interact Cardiovasc Thorac Surg*. 2018; 26 (5): 745–752. doi: 10.1093/icvts/ivx444.
55. *Horváth L, Umehara Y, Jud C, Blank F, Petri-Fink A, Rothen-Rutishauser B.* Engineering an *in vitro* air-blood barrier by 3D bioprinting. *Sci Rep*. 2015; 5: 7974. doi: 10.1038/srep07974.
56. *Gilevich IV, Sotnichenko AS, Karal-Ogly DD, Gubareva EA, Kuevda EV, Polyakov IS et al. In vivo* Experimental Study of Biological Compatibility of Tissue Engineered Tracheal Construct in Laboratory Primates. *Bull Exp Biol Med*. 2018; 164 (6): 770–774. doi: 10.1007/s10517-018-4077-y.
57. *Estermann M, Bisig C, Septiadi D, Petri-Fink A, Rothen-Rutishauser B.* Bioprinting for Human Respiratory and Gastrointestinal *in vitro* Models. *Methods Mol Biol*. 2020; 2140: 199–215. doi: 10.1007/978-1-0716-0520-2_13.
58. *Visconti RP, Kasyanov V, Gentile C, Zhang J, Markwald RR, Mironov V*. Towards organ printing: engineering an intra-organ branched vascular tree. *Expert Opin Biol Ther*. 2010; 10 (3): 409–420. doi: 10.1517/14712590903563352.
59. *Marga F, Jakab K, Khatiwala C, Shepherd B, Dorfman S, Hubbard B et al.* Toward engineering functional organ modules by additive manufacturing. *Biofabrication*. 2012; 4 (2): 022001. doi: 10.1088/1758-5082/4/2/022001.
60. *Itoh M, Nakayama K, Noguchi R, Kamohara K, Furukawa K, Uchihashi K et al.* Scaffold-Free Tubular Tissues Created by a Bio-3D Printer Undergo Remodeling and Endothelialization when Implanted in Rat Aortae. *PLoS One*. 2015; 10 (9): e0136681. doi: 10.1371/journal.pone.0136681.
61. *Hinton TJ, Jallerat Q, Palchesko RN, Park JH, Grodzicki MS, Shue HJ et al.* Three-dimensional printing of complex biological structures by freeform reversible embedding of suspended hydrogels. *Sci Adv*. 2015; 1 (9): e1500758. doi: 10.1126/sciadv.1500758.
62. *Yamamoto T, Funahashi Y, Mastukawa Y, Tsuji Y, Mizuno H, Nakayama K et al.* MP19-17 Human urethra-engineered with human mesenchymal stem cell with maturation by rearrangement of cells for self-organization – newly developed scaffold-free three-dimensional bio-printer. *The Journal of Urology*. 2015; 193 (4): e221–e222. doi: 10.1016/j.juro.2015.02.1009.
63. *Lemaire F, Moeun BN, Champion KS, Getsios S, Wadsworth S, Russo V et al.* P.170: Preliminary Results on the Development of a Perfusion Device to Study the Function of 3D Bioprinted Pancreatic Tissue *In Vitro*. *Transplantation*. 2021; 105 (12 Suppl 2): S72. doi: 10.1097/01.tp.0000804724.41562.ec.
64. *Dickman C, Campbell S, Tong H, Jalili R, Beyer S, Mohamed T et al.* 3D bioprinted hepatocyte and mesenchymal stem cell spheroids as a cell therapy for liver disease. *Journal of Hepatology*. 2022; 77 (S1): S764.
65. *Sharma R, Smits IPM, De La Vega L, Lee C, Willerth SM.* 3D Bioprinting Pluripotent Stem Cell Derived Neural Tissues Using a Novel Fibrin Bioink Containing Drug Releasing Microspheres. *Front Bioeng Biotechnol*. 2020; 8: 57. doi: 10.3389/fbioe.2020.00057.
66. *Dickman CTD, Russo V, Thain K, Pan S, Beyer ST, Walus K et al.* Functional characterization of 3D contractile smooth muscle tissues generated using a unique microfluidic 3D bioprinting technology. *FASEB J*. 2020; 34 (1): 1652–1664. doi: 10.1096/fj.201901063RR.
67. *Bowles RD, Gebhard HH, Härtl R, Bonassar LJ.* Tissue-engineered intervertebral discs produce new matrix, maintain disc height, and restore biomechanical function to the rodent spine. *Proc Natl Acad Sci U S A*. 2011; 108 (32): 13106–13111. doi: 10.1073/pnas.1107094108.
68. *Mannoor MS, Jiang Z, James T, Kong YL, Malatesta KA, Soboyejo WO et al.* 3D printed bionic ears. *Nano Lett*. 2013; 13 (6): 2634–2639. doi: 10.1021/nl4007744.
69. *Madden LR, Nguyen TV, Garcia-Mojica S, Shah V, Le AV, Peier A et al.* Bioprinted 3D Primary Human Intestinal Tissues Model Aspects of Native Physiology and ADME/Tox Functions. *iScience*. 2018; 2: 156–167. doi: 10.1016/j.isci.2018.03.015.
70. *Langer EM, Allen-Petersen BL, King SM, Kendsersky ND, Turnidge MA, Kuziel GM et al.* Modeling Tumor Phenotypes *In Vitro* with Three-Dimensional Bioprinting. *Cell Rep*. 2019; 26 (3): 608–623.e6. doi: 10.1016/j.celrep.2018.12.090.
71. *Nguyen DG, Pentoney SL Jr.* Bioprinted three dimensional human tissues for toxicology and disease modeling. *Drug Discov Today Technol*. 2017; 23: 37–44. doi: 10.1016/j.ddtec.2017.03.001.
72. *Hardwick RN, Viergever C, Chen AE, Nguyen DG.* 3D bioengineered tissues: From advancements in *in vitro* safety to new horizons in disease modeling. *Clin Pharmacol Ther*. 2017; 101 (4): 453–457. doi: 10.1002/cpt.569.
73. *Ma X, Liu J, Zhu W, Tang M, Lawrence N, Yu C et al.* 3D bioprinting of functional tissue models for personalized drug screening and *in vitro* disease modeling. *Adv Drug Deliv Rev*. 2018; 132: 235–251. doi: 10.1016/j.addr.2018.06.011.
74. *Norona LM, Nguyen DG, Gerber DA, Presnell SC, LeCluyse EL.* Editor's Highlight: Modeling Compound-Induced Fibrogenesis *In Vitro* Using Three-Dimensional Bioprinted Human Liver Tissues. *Toxicol Sci*. 2016; 154 (2): 354–367. doi: 10.1093/toxsci/kfw169.
75. Organovo Synthesizes Human Liver Tissue With 3D Bioprinting. Available from: https://www.bioprocessonline.com/doc/organovo-synthesizes-human-liver-tissue-with-d-bioprinting-0001/.
76. Architecture of ExVive™ 3D Bioprinted Human Liver Tissue with distinct hepatocellular (HC) and non-parenchymal cell (NPC) compartments. Available from: https://organovo.com/technology-platform/.

77. *Maina RM, Barahona MJ, Finotti M, Lysyy T, Geibel P, D'Amico F, Mulligan D et al.* Generating vascular conduits: from tissue engineering to three-dimensional bioprinting. *Innov Surg Sci.* 2018; 3 (3): 203–213. doi: 10.1515/iss-2018-0016.
78. *Fazal F, Raghav S, Callanan A, Koutsos V, Radacsi N.* Recent advancements in the bioprinting of vascular grafts. Biofabrication. 2021; 13 (3). doi: 10.1088/1758-5090/ac0963.
79. *Lawlor KT, Vanslambrouck JM, Higgins JW, Chambon A, Bishard K, Arndt D et al.* Cellular extrusion bioprinting improves kidney organoid reproducibility and conformation. *Nat Mater.* 2021; 20 (2): 260–271. doi: 10.1038/s41563-020-00853-9.
80. *Moroni S, Casettari L, Lamprou DA.* 3D and 4D Printing in the Fight against Breast Cancer. *Biosensors (Basel).* 2022; 12 (8): 568. doi: 10.3390/bios12080568.
81. TeVido BioDevices: Recuperating Lost Skin Pigmentation Through Advanced Cellular Therapy. Available from: http://tevidobiodevices.com.
82. Nano3D Biosciences Makes Major 3D Bioprinting Breakthrough in Breast Cancer Research. Available from: https://3dprint.com/22681/nano3d-rbcc-3d-print-cancer.
83. 3D Cell Culture Technologies Global Market Report 2021: COVID-19 Growth and Change to 2030 provides strategists, marketers and senior management with the critical information they need to assess the global 3d cell culture technologies market. Available from: https://www.researchandmarkets.com/reports/5446076/3d-cell-culture-technologies-global-market-report.
84. Rainbow Coral and Nano3D Biosciences Pursue New 3D Bioprinting Opportunities, Partnerships. Available from: http://www.rainbowbiosciences.com.
85. 3-D Printed Implants Hit The Market, Pave The Way For More Personalized Devices. Available from: http://tissuesys.com/trs_media/publications/The_Gray_Sheet_3D_Printer.pdf.
86. New NASA video shows how nScrypt's BFF bioprinter will be used in space. Available from: https://www.3dprintingmedia.network/spacex-launches-nscrypts-bff-bioprinter-space.
87. 4D Bio3 – The Geneva Foundation. Available from: https://genevausa.org/wp-content/uploads/2019/03/4d-bio3-with-dr.-ho.pdf.
88. Ruggedized 3D printers for medical use in harsh military environments. Available from: https://www.eetimes.com/ruggedized-3d-printers-for-medical-use-in-harsh-military-environments/.
89. Cadets research bioprinting to improve soldier care in the future. Available from: https://www.army.mil/article/232736/cadets_research_bioprinting_to_improve_soldier_care_in_the_future.
90. Bandages, Knee Cartilage, Surgical Tools Successfully 3D Printed in Desert Deployment Zone. Available from: https://www.odtmag.com/contents/view_breaking-news/2019-10-08/bandages-knee-cartilage-surgical-tools-successfully-3d-printed-in-desert-deployment-zone.
91. *Donohue MA, Zhou L, Haley CA.* Meniscus Injuries in the Military Athlete. *J Knee Surg.* 2019; 32 (2): 123–126. doi: 10.1055/s-0038-1676959.
92. *Strobel HA, Schultz A, Moss SM, Eli R, Hoying JB.* Quantifying Vascular Density in Tissue Engineered Constructs Using Machine Learning. *Front Physiol.* 2021; 12: 650714. doi: 10.3389/fphys.2021.650714.
93. Explore 6-Axis Robots by Series. Available from: https://epson.com/6-axis-robots-product-family.
94. A Robot That Prints Tissue. Available from: https://www.asme.org/topics-resources/content/a-robot-that-prints-tissue.
95. *Strobel HA, Gerton T, Hoying JB.* Vascularized adipocyte organoid model using isolated human microvessel fragments. *Biofabrication.* 2021; 13 (3). doi: 10.1088/1758-5090/abe187.
96. Bio-printed Constructs for Battlefield Burn Repairs. Available from: https://www.microfab.com/3-d-printing.
97. *Onode E, Uemura T, Takamatsu K, Yokoi T, Shintani K, Hama S et al.* Bioabsorbable nerve conduits three-dimensionally coated with human induced pluripotent stem cell-derived neural stem/progenitor cells promote peripheral nerve regeneration in rats. *Sci Rep.* 2021; 11 (1): 4204. doi: 10.1038/s41598-021-83385-9.
98. Digital fabricaton by multi-materials additive manufacturing 4D-Printing. Available from: https://www.fmf.uni-freiburg.de/de/projects/the-freiburg-3d-printing-alliance-f3d/the-freiburg-3d-printing-alliance-f3d.
99. *Ligon SC, Liska R, Stampfl J, Gurr M, Mülhaupt R.* Polymers for 3D Printing and Customized Additive Manufacturing. *Chem Rev.* 2017; 117 (15): 10212–10290. doi: 10.1021/acs.chemrev.7b00074.
100. *Ozbolat IT, Moncal KK, Gudapati H.* Evaluation of bioprinter technologies. *Additive Manufacturing.* 2017; 13: 179–200. doi: 10.1016/j.addma.2016.10.003.
101. EnvisionTEC: 3D-Bioplotter. Available from: https://3dsman.com/envisiontec-3d-bioplotter.
102. *Shudo Y, MacArthur JW, Kunitomi Y, Joubert L, Kawamura M, Ono J et al.* Three-Dimensional Multilayered Microstructure Using Needle Array Bioprinting System. *Tissue Eng Part A.* 2020; 26 (5–6): 350–357. doi: 10.1089/ten.TEA.2019.0313.
103. *Moldovan NI, Hibino N, Nakayama K.* Principles of the Kenzan Method for Robotic Cell Spheroid-Based Three-Dimensional Bioprinting. *Tissue Eng Part B Rev.* 2017; 23 (3): 237–244. doi: 10.1089/ten.TEB.2016.0322.
104. *Moldovan L, Barnard A, Gil CH, Lin Y, Grant MB, Yoder MC et al.* iPSC-Derived Vascular Cell Spheroids as Building Blocks for Scaffold-Free Biofabrication. *Biotechnol J.* 2017; 12 (12). doi: 10.1002/biot.201700444.
105. *Aguilar IN, Smith LJ, Olivos DJ 3rd, Chu TG, Kacena MA, Wagner DR.* Scaffold-free Bioprinting of Mesenchymal Stem Cells with the Regenova Printer: Optimization of Printing Parameters. *Bioprinting.* 2019; 15: e00048. doi: 10.1016/j.bprint.2019.e00048.
106. *Cui Y, Jin R, Zhang Y, Yu M, Zhou Y, Wang LQ.* Cellulose Nanocrystal-Enhanced Thermal-Sensitive Hydrogels of Block Copolymers for 3D Bioprinting. *Int J Bioprint.* 2021; 7 (4): 397. doi: 10.18063/ijb.v7i4.397.

107. *Daly AC, Pitacco P, Nulty J, Cunniffe GM, Kelly DJ.* 3D printed microchannel networks to direct vascularisation during endochondral bone repair. *Biomaterials.* 2018; 162: 34–46. doi: 10.1016/j.biomaterials.2018.01.057.
108. *Daly AC, Kelly DJ.* Biofabrication of spatially organised tissues by directing the growth of cellular spheroids within 3D printed polymeric microchambers. *Biomaterials*. 2019; 197: 194–206. doi: 10.1016/j.biomaterials.2018.12.028.
109. *Filardo G, Petretta M, Cavallo C, Roseti L, Durante S, Albisinni U et al.* Patient-specific meniscus prototype based on 3D bioprinting of human cell-laden scaffold. *Bone Joint Res.* 2019; 8: 101–106. doi: 10.1302/2046-3758.82.BJR-2018-0134.R1.
110. *Derr K, Zou J, Luo K, Song MJ, Sittampalam GS, Zhou C et al.* Fully Three-Dimensional Bioprinted Skin Equivalent Constructs with Validated Morphology and Barrier Function. *Tissue Eng Part C Methods.* 2019; 25 (6): 334–343. doi: 10.1089/ten.TEC.2018.0318.
111. *Noor N, Shapira A, Edri R, Gal I, Wertheim L, Dvir T.* 3D Printing of Personalized Thick and Perfusable Cardiac Patches and Hearts. *Adv Sci (Weinh)*. 2019; 6 (11): 1900344. doi: 10.1002/advs.201900344.
112. *Rai B, Oest ME, Dupont KM, Ho KH, Teoh SH, Guldberg RE.* Combination of platelet-rich plasma with polycaprolactone-tricalcium phosphate scaffolds for segmental bone defect repair. *J Biomed Mater Res A.* 2007; 81 (4): 888–899. doi: 10.1002/jbm.a.31142.
113. *Seen S, Young S, Lang SS, Lim TC, Amrith S, Sundar G.* Orbital Implants in Orbital Fracture Reconstruction: A Ten-Year Series. *Craniomaxillofac Trauma Reconstr.* 2021; 14 (1): 56–63. doi: 10.1177/1943387520939032.
114. *Laubach M, Suresh S, Herath B, Wille ML, Delbrück H, Alabdulrahman H et al.* Clinical translation of a patient-specific scaffold-guided bone regeneration concept in four cases with large long bone defects. *J Orthop Translat.* 2022; 34: 73–84. doi: 10.1016/j.jot.2022.04.004.
115. *Villar G, Graham AD, Bayley H.* A tissue-like printed material. *Science (New York, N.Y.)*. 2013; 340 (6128): 48–52. doi: 10.1126/science.1229495.
116. *Li J, Baxani DK, Jamieson WD, Xu W, Rocha VG, Barrow DA et al.* Formation of Polarized, Functional Artificial Cells from Compartmentalized Droplet Networks and Nanomaterials, Using One-Step, Dual-Material 3D-Printed Microfluidics. *Adv Sci (Weinh).* 2019; 7 (1): 1901719. doi: 10.1002/advs.201901719.
117. *Tibbetts JH.* The Future of Bioprinting: Multidisciplinary teams seek to create living human organs. *BioScience.* 2021; 71 (6): 564–570. doi: 10.1093/biosci/biab046.
118. *Vijayavenkataraman S, Yan WC, Lu WF, Wang CH, Fuh JYH.* 3D bioprinting of tissues and organs for regenerative medicine. *Adv Drug Deliv Rev.* 2018; 132: 296–332. doi: 10.1016/j.addr.2018.07.004.
119. *Murphy SV, De Coppi P, Atala A.* Opportunities and challenges of translational 3D bioprinting. *Nat Biomed Eng.* 2020; 4 (4): 370–380. doi: 10.1038/s41551-019-0471-7.
120. *Xiao Y, Ahadian S, Radisic M.* Biochemical and Biophysical Cues in Matrix Design for Chronic and Diabetic Wound Treatment. *Tissue Eng Part B Rev.* 2017; 23 (1): 9–26. doi: 10.1089/ten.TEB.2016.0200.
121. *Park SH, Jung CS, Min BH.* Advances in three-dimensional bioprinting for hard tissue engineering. *Tissue Eng Regen Med.* 2016; 13 (6): 622–635. doi: 10.1007/s13770-016-0145-4.
122. *Huang Y, Zhang XF, Gao G, Yonezawa T, Cui X.* 3D bioprinting and the current applications in tissue engineering. *Biotechnol J.* 2017; 12 (8): 1600734. doi: 10.1002/biot.201600734.
123. *Heinrich MA, Liu W, Jimenez A, Yang J, Akpek A, Liu X et al.* 3D Bioprinting: from Benches to Translational Applications. *Small*. 2019; 15 (23): e1805510. doi: 10.1002/smll.201805510.
124. *Ashammakhi N, Ahadian S, Zengjie F, Suthiwanich K, Lorestani F, Orive G et al.* Advances and Future Perspectives in 4D Bioprinting. *Biotechnol J.* 2018; 13 (12): e1800148. doi: 10.1002/biot.201800148.
125. *Mao S, Pang Y, Liu T, Shao Y, He J, Yang H et al.* Bioprinting of *in vitro* tumor models for personalized cancer treatment: a review. *Biofabrication.* 2020; 12 (4): 042001. doi: 10.1088/1758-5090/ab97c0.
126. *Gao G, Cui X.* Three-dimensional bioprinting in tissue engineering and regenerative medicine. *Biotechnol Lett.* 2016; 38 (2): 203–211. doi: 10.1007/s10529-015-1975-1.
127. *Zhu W, Yu C, Sun B, Chen S.* Bioprinting of Complex Vascularized Tissues. *Methods Mol Biol.* 2021; 2147: 163–173. doi: 10.1007/978-1-0716-0611-7_14.
128. *Yu J, Park SA, Kim WD, Ha T, Xin YZ, Lee J et al.* Current Advances in 3D Bioprinting Technology and Its Applications for Tissue Engineering. *Polymers (Basel).* 2020; 12 (12): 2958. doi: 10.3390/polym12122958.
129. *de Vries RB, Leenaars M, Tra J, Huijbregtse R, Bongers E, Jansen JA et al.* The potential of tissue engineering for developing alternatives to animal experiments: a systematic review. *J Tissue Eng Regen Med.* 2015; 9 (7): 771–778. doi: 10.1002/term.1703.
130. *Zhang J, Wehrle E, Rubert M, Müller R.* 3D Bioprinting of Human Tissues: Biofabrication, Bioinks, and Bioreactors. *Int J Mol Sci.* 2021; 22 (8): 3971. doi: 10.3390/ijms22083971.
131. *Dias JR, Ribeiro N, Baptista-Silva S, Costa-Pinto AR, Alves N, Oliveira AL. In situ* Enabling Approaches for Tissue Regeneration: Current Challenges and New Developments. *Front Bioeng Biotechnol.* 2020; 8: 85. doi: 10.3389/fbioe.2020.00085.
132. *Dababneh AB, Ozbolat IT.* Bioprinting Technology: A Current State-of-the-Art Review. *ASME J Manuf Sci Eng.* 2014; 136 (6): 061016. doi: 10.1115/1.4028512.
133. *Bobylov JuA.* Ob ugrozah novogo biologicheskogo oruzhija i biobezopasnosti Rossii. *Kachestvennaja klinicheskaja praktika*. 2008; (3): 94–99.
134. *Burenok VM, Ivlev AA, Korchak VJu.* Analiticheskij obzor dejatel'nosti Upravlenija perspektivnyh issledovatel'skih proektov MO SShA. *Razvitie voennyh tehnologij XXI veka: problemy, planirovanie, realizacija*. Tver': Kupol, 2009: 93; 624.
135. A Compendium of DARPA Programs. Available from: www.darpa.mil/body/strategic.html.

136. *Klabukov ID*. Issledovatel'skaja programma DARPA na 2015 god. M.: Issledovatel'skoe soobshhestvo, 2014; 96. doi: 10.2139/ssrn.2439081.
137. *Wang Z, Kapadia W, Li C, Lin F, Pereira RF, Granja PL et al.* Tissue-specific engineering: 3D bioprinting in regenerative medicine. *J Control Release.* 2021; 329: 237–256. doi: 10.1016/j.jconrel.2020.11.044.
138. *Jamee R, Araf Y, Naser IB, Promon SK.* The promising rise of bioprinting in revolutionalizing medical science: Advances and possibilities. *Regen Ther.* 2021; 18: 133–145. doi: 10.1016/j.reth.2021.05.006.
139. *Unagolla JM, Jayasuriya AC.* Hydrogel-based 3D bioprinting: A comprehensive review on cell-laden hydrogels, bioink formulations, and future perspectives. *Appl Mater Today.* 2020; 18: 100479. doi: 10.1016/j.apmt.2019.100479.
140. *Bea S.* Opt-out policy and the organ shortage problem: Critical insights and practical considerations. *Transplant Rev (Orlando).* 2021; 35 (1): 100589. doi: 10.1016/j.trre.2020.100589.
141. *Gardin C, Ferroni L, Latremouille C, Chachques JC, Mitrečić D, Zavan B.* Recent Applications of Three Dimensional Printing in Cardiovascular Medicine. *Cells.* 2020; 9 (3): 742. doi: 10.3390/cells9030742.
142. *Mota F, Braga LAM, Cabral BP, Conte Filho CG.* What is the future of lab-on-a-chip diagnostic devices? Assessing changes in experts' expectations over time. *Foresight*. 2021; 23 (6): 640–654. doi: 10.1108/FS-05-2021-0101.
143. *Li R, Ting YH, Youssef SH, Song Y, Garg S.* Three-Dimensional Printing for Cancer Applications: Research Landscape and Technologies. *Pharmaceuticals (Basel).* 2021; 14 (8): 787. doi: 10.3390/ph14080787.
144. *Giacomini KM, Krauss RM, Roden DM, Eichelbaum M, Hayden MR, Nakamura Y.* When good drugs go bad. *Nature.* 2007; 446 (7139): 975–977. doi: 10.1038/446975a.
145. *Niu SY, Xin MY, Luo J, Liu MY, Jiang ZR.* DSEP: A Tool Implementing Novel Method to Predict Side Effects of Drugs. *J Comput Biol.* 2015; 22 (12): 1108–1117. doi: 10.1089/cmb.2015.0129.
146. *Bandyopadhyay A, Dewangan VK, Vajanthri KY, Poddar S, Mahto SK.* Easy and affordable method for rapid prototyping of tissue models *in vitro* using three-dimensional bioprinting. *Biocybern Biomed Eng.* 2018; 38 (1): 158–169. doi: 10.1016/j. bbe.2017.12.001.

The article was submitted to the journal on 05.03.2023

DOI: 10.15825/1995-1191-2023-2-82-98

DECELLULARIZED UMBILICAL CORD STROMA IN TISSUE ENGINEERING AND REGENERATIVE MEDICINE: A SYSTEMATIC REVIEW

Yu.B. Basok[1], A.A. Kondratenko[2], L.I. Kalyuzhnaya[2], E.A. Volkova[1], K.A. Vorobyov[2], V.I. Sevastianov[1]

[1] Shumakov National Medical Research Center of Transplantology and Artificial Organs, Moscow, Russian Federation

[2] Kirov Military Medical Academy, St. Petersburg, Russian Federation

Despite great progress in the field of biomaterials for tissue engineering and regenerative medicine, the high requirements placed on artificial matrices (matrices, carriers, scaffolds) are the reason for the ongoing search for natural or synthetic extracellular matrix mimetics. Among such materials, decellularized umbilical cord (UC) stroma appears to be very attractive – it has a high content of hyaluronic acid, cytokines, and growth factors, and there are no ethical restrictions for its production. Decellularized UC stroma has been found to promote cartilage, liver tissue and nerve tissue repair, as well as wound healing. The review critically analyzes and summarizes published data on the ability of decellularized UC stroma to maintain the necessary conditions for adhesion, migration, differentiation and functional activity of adherent cells, thus stimulating the internal (physiological) regenerative potential of tissues. Literature was searched for in the following electronic databases: Medline/PubMed (www/ncbi.nlm.nih.gov/pubmed), Cochrane library (https://www.cochrane.org), and eLIBRARY/Russian Science Citation Index (https://www.elibrary.ru). Inclusion criteria were the presence of biomaterials obtained from decellularized human UC stroma. Exclusion criteria for papers included research objects as decellularized umbilical cord vessels (veins and arteries) and umbilical cord cell cultures. Twenty-five original articles in English and Russian were selected for analysis of the products obtained, their applications, decellularization methods and research results. The review also discusses the prospects for decellularized umbilical cord in medicine.

Keywords: umbilical cord stroma, decellularization, extracellular matrix, regenerative medicine, tissue engineering.

The concept of tissue engineering is to create functionally active cell-engineered constructs (CECs) to stimulate physiological regeneration of damaged tissues or tissue-engineered constructs (TECs)/tissue equivalents formed *in vitro* or *in vivo*, intended for temporary/permanent replacement of irreversibly damaged organs and tissues [1–3].

The main components of CECs/TECs are: cells and a cell carrier (synonyms: scaffold, framework, matrix or artificial matrix) whose function is to deliver and retain cells in the implantation site [4]. The most interesting are extracellular matrix (ECM) mimetics that mimic the natural ECM in composition and can maintain the viability and functional activity of cells for a long time, creating the necessary microenvironment for them [1, 5, 6].

When creating CECs/TECs *in vitro*, reproduction of not only biochemical but also biomechanical stimuli, which ensure the vital activity of cells in the body, is an important condition for achieving a high degree of resemblance to the natural tissue [7]. To simulate *in vitro* biomechanical forces, such as compression, tension, shear force, and hydrostatic pressure, special devices – bioreactors – are used, and for each organ the complex of such influences is individual [6–8].

An alternative way is the formation of CECs/TECs in the body by implanting a cell-free artificial matrix into the body. The task is to ensure migration of the recipient's own cells to it and stimulate their proliferation with subsequent replacement of the damage by a functionally active tissue [9]. Cell-free products created by decellularization from the biomaterial of animal or human organs and tissues have shown high bioactivity. In addition, such a product can be manufactured in advance and applied without prior preparation. This potentially accelerates its introduction into clinical practice and is of particular importance for military medicine [10–11].

Among them, decellularized umbilical cord stroma (Wharton's jelly, WJ) seems promising [12]. The WJ is a connective tissue that forms the bulk of the umbilical cord in humans and other mammals. The ECM obtained from WJ-derived mesenchymal stem cells (MSCs) contains structural components (collagens types I, II, III, IV, V, VI, XII, XIV, fibronectin, fibrillin and high-molecular-weight hyaluronic acid and sulfated glycosaminoglycans

Corresponding author: Yulia Basok. Address: 1, Shchukinskaya str., Moscow, 123182, Russian Federation. Phone: (499) 190-45-90. E-mail: bjb2005@mail.ru

(GAGs) such as chondroitin sulfates, heparan sulfate, dermatan sulfate) and numerous growth factors such as insulin-like growth factor (IGF-1) and IGF-binding proteins (IGFBPs) 1, 2, 3, 4 and 6, transforming growth factor alpha (TGF-α) and platelet-derived growth factor (PDGF), fibroblast growth factors (αFGF, βFGF), epidermal growth factors (EGFs), various isoforms of transforming growth factor beta (TGF-β1, 2, 3), vascular endothelial growth factor (VEGF), cytokines (with predominance of anti-inflammatory), matrix metalloproteinases (MMPs) and matrix metalloproteinase inhibitors (TIMPs). Expression of several immunomodulatory cytokines, such as RANTES (regulates activation, normal T-cell expression and secretion), interleukin receptor 6 (IL-6R), interleukin 16 (IL-16) and interferon gamma (IFN-γ), and proinflammatory cytokines, such as macrophage colony stimulating factor (MCSF), macrophage stimulating protein 1-alpha (MIP1a) were also found; tumor necrosis factor 1α and 1β receptor superfamily (TNF-RI and TNF-RII), interleukin 1 receptor antagonist (IL1RA), and wound healing-related cytokines including intercellular adhesion molecule 1 (ICAM-1), granulocyte stimulating factor (G-CSF) [13–17]. In addition, ECM derived from WJ-derived MSCs supposedly has immunomodulatory and some bacteriostatic effects [16, 17]. It has been described that decellularized WJ promotes cartilage repair [17], liver tissue [19], nerve tissue [20] and wound healing [21–23].

However, to the best of the authors' knowledge, no review has so far attempted to critically evaluate and summarize the evidence regarding the regenerative potential of decellularized UC stroma.

REVIEWED DATABASES AND SEARCH RESULTS

The literature search was conducted in electronic databases Medline/PubMed (www/ncbi.nlm.nih.gov/pubmed), Cochrane library (https://www.cochrane.org), and eLIBRARY, Russian Science Citation Index (https://www.elibrary.ru).

The following terms were used as a search query in Medline/PubMed: (umbil*[title] AND decell*[title]) OR (whart*[title] AND decell*[title]) OR (umbil*[title] AND acell*[title]) OR (whart*[title] AND acell*[title]) OR (umbil*[title] AND extracel*[title] AND matr*[title]) OR (whart*[title] AND extracel*[title] AND matr*[title]). Date of last search: March 19, 2023.

The following terms were used as a search query in Cochrane library: (extracell* AND umbil*) OR (decell* AND umbil*). Date of last search: March 25, 2023.

The following terms were used as a search query in eLIBRARY: decell* umbil* (search query 1), extracell* matrix* umbil* (search query 2), decellularization and umbilical cord (search query 3), "extracellular matrix" and umbilical cord (search query 4). Date of last search: March 25, 2023.

Inclusion criteria were: the presence of materials obtained from decellularized human UC stroma in the study. Full-text original articles in English and Russian were used in literature analysis. Exclusion criteria for articles were the use of decellularized vessels (veins and arteries) of the umbilical cord, as well as the study of umbilical cord cell cultures without using its ECM. In addition, conference proceedings, reviews, and preprints of articles were not included in the study.

The literature search process is shown in Fig. 1.

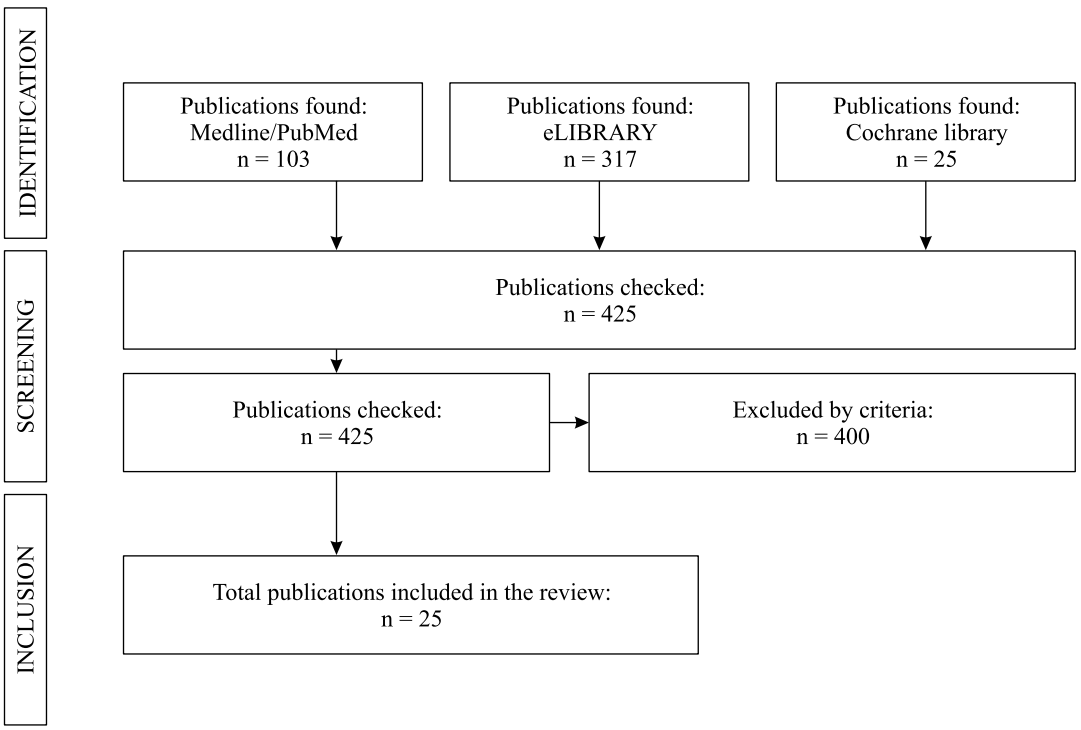

Fig. 1. Flow diagram of the literature search employed for this review

The initial search resulted in 425 publications. First of all, the results of the search for publications in each of the selected databases manually excluded articles on decellularization of umbilical cord vessels, the use of umbilical cord mesenchymal cells and their vesicles. Next, literature reviews and 2 clinical studies with no description of UC-derived products were excluded (decellularization was not confirmed). At the last stage, 4 repetitions were excluded: 3 publications were duplicated in the PubMed and eLIBRARY databases [17, 24, 25], one publication was reflected twice as a result of a PubMed search (publication [26] and its correction [27]). In 3 publications, the authors used only centrifugation as WJ processing. No quantitative control of genetic material content was presented. This was the reason for their exclusion from consideration in the review [10, 28, 29]. The results of another study were also decided not to be considered – the product obtained by the researchers was a fraction of the supernatant obtained after exposure of WJ to trypsin [30]. So, 25 articles were included in the study [11, 12, 16–21, 24–26, 31–44]. Eight described only *in vitro* studies [18, 19, 24, 25, 31–33, 37], four described only *in vivo* (animal) studies [34, 41, 43, 44], and 10 included both types of preclinical trials [11, 16, 17, 20, 21, 26, 35, 36, 38, 42]. No clinical studies meeting the inclusion criteria were found.

MAIN PARAMETERS AND RESEARCH RESULTS OF INCLUDED PUBLICATIONS

Results of the published works demonstrate that decellularized WJ (dWJ) refers to a biocompatible material capable of stimulating cell proliferation and positively influencing the regeneration processes of damaged organs and tissues (Table).

Gupta et al. when creating a matrix for vascular tissue engineering from silk fibroin, dWJ was functionalized to improve the remodeling properties and immunomodulation of the recipient response to introduction of the polymeric material. Powder of lyophilized dWJ was mixed with silk fibroin (5 mg dWJ per 1 ml of silk solution) before matrix molding. After lyophilization, the prosthetic porous vessel was coated with a nanofiber layer. The solution for obtaining the material by electrospinning consisted of silk fibroin and polycaprolactone in hexafluoro-2-propanol. After crosslinking using 1-ethyl-3-(3-dimethylaminopropyl) carbodiimide and N-hydroxysuccinimide in 80% ethanol for 12 hours, the scaffolds were washed in sterile water on a shaker for 12 hours and stored at 4 °C until further use [11]. Basiri et al. added dWJ, obtained using a similar technique, to a silk fibroin hydrogel before gelation. The biomaterial thus obtained, exhibited mechanical properties similar to those of cartilage [31].

Li et al. used dWJ as a cell carrier supporting the phenotypes and differentiation potential of hematopoietic progenitor cells [24]. Kehtari et al. demonstrated the ability of such a matrix to provide a microenvironment that promotes hepatocyte differentiation of pluripotent cells by activating transcription factors [19]. Azarbarz et al. presented the results of dWJ conjugated with gelatin for a 3D cell culture system. The differentiation of MSCs into insulin-producing cells was shown, confirmed by increased expression of insulin-specific genes and increased insulin release in response to glucose stimulation [32].

WJ is a reservoir of peptide growth factors involved in chondrogenesis. Xiao et al. showed that human dWJ can be a good alternative biomaterial for cartilage tissue engineering [33]. The biomechanical properties of dWJ and its homogeneous porous structure were sufficient to support rabbit chondrocytes cultured on them. Production of GAGs, collagen types I and II, and aggrecan by the cells was demonstrated [33]. At the same time, in a study by Foltz et al., during tracheal defect replacement, no chondrocyte recruitment into biocompatible dWJ and chondrocyte-induced collagen production were found. At the same time, the structure and physical characteristics of the biomaterial provided the necessary maintenance of tracheal patency [34]. Penolazzi et al. showed the therapeutic potential of dWJ and its effect on the functioning of degenerated intervertebral disc cells. The authors suggested that dWJ implantation may be sufficient for the functional repair of degenerated intervertebral discs [25].

A study by Jadalannagari et al. noted the migration of WJ-derived MSCs into the dWJ thickness on day 2. At the same time, the authors observed cell proliferation when cultured on dWJ, which, however, was lower than when cultured on the culture plate. Using a flat bone defect model, it was shown that human dWJ promoted adhesion and penetration of viable osteocytes into the biomaterial [26]. Yuan et al. used decellularized UC stroma for tendon healing. After cell removal, dWJ retained a significant amount of GAGs and collagen, preserved microstructure and tensile strength. The three-dimensional porous structure of dWJ promoted tenocyte migration, attachment, and proliferation. In an *in vivo* study, the decellularized product promoted tendon regeneration [35].

A study by Mann et al. established the stimulating effect of cryopreserved human dWJ on restoration of the integrity of a rat spine after intrauterine repair of spina bifida. The resulting biomimetic ECM improved organized cell growth and reduced acute inflammation [36]. In another study, a tissue-engineered coating consisting of rat adipose tissue MSCs and human dWJ accelerated healing of a rat tail wound. Reduced tail volume, improved angiogenesis and lymphangiogenesis were recorded [21].

Some researchers emphasize the applicability of human umbilical cord products to stimulate regeneration of different tissues. Dubus et al. showed by mass spectrometry in prepared lyophilized dWJ the presence of structural and adhesive proteins involved in wound healing

Table

General characteristics and results of studies included in this review

Study (last name, year)	Application	Product description	Decellularization methods	*In vitro* studies		*In vivo* studies		Results
				Object	Methods	Object	Methods	
1	2	3	4	5	6	7	8	9
Basiri, 2019 [31]	Cartilage repair and regeneration	dWJ/silk fibroin hydrogel	WJ was mixed with deionized water for 16 hours, centrifuged at 4 °C, the supernatant was stored at –80 °C	Human endometrial stem cells	Cell viability	–	–	The product improved the viability of cells studied
Gupta, 2021 [11]	Vascular tissue engineering	Two-layered silk fibroin tubular scaffold seeded with freeze-dried dWJ	WJ 1–2 cm in 4 °C deionized water for 16 hours, >70 μm fragments were removed, centrifuged at 5000 rpm for 10 minutes, 4 °C, freeze-dried	Human endotheliocytes, macrophages	Product cytotoxicity	Subcutaneous implantation in rabbits (n = 6), rabbit jugular vein implants (n = 3)	Histological studies, gene expression analysis, Doppler ultrasound	The biocompatible product induced cell recruitment after a month of subcutaneous implantation with expression of anti-inflammatory genes. Vascular implant was permeable after 3 months
Li, 2019 [24]	Bone marrow transplantation	3 mm thick fragments	Umbilical cord vessels were removed, umbilical cord stroma was decellularized with SAA solutions, cryopreserved	CD34+ cells	Flow cytometry, gene expression analysis	–	–	The product promotes megakaryocytic differentiation and supports primitive hematopoietic cell phenotypes
Kehtari, 2018 [19]	Liver tissue engineering	Porous matrix	Umbilical cord in Tris-EDTA buffer solution at 4 °C for 16 hours, decellularized with 0.03% SDS for 24 hours with shaking, washed, placed in a hypertonic saline at 37 °C for 3 hours, washed, cross-linked with acetic acid, freeze-dried	Human pluripotent stem cells	Viability, differentiation into hepatocytes	–	–	The cell-free product is able to support differentiation into hepatocytes

Continuation Table

1	2	3	4	5	6	7	8	9
Azarbarz, 2022 [32]	Differentiation of MSCs into IPCs	Gelatin-conjugated freeze-dried dWJ	The umbilical cord was incubated in NaCl (1 M) for 1 week, decellularized with 0.25% trypsin-EDTA solution for 24 hours, 1% Triton X-100 for 5 days. 24 hours, washed with PBS, freeze-dried. dWJ was gelatin-conjugated for 1 hour. 37 °C	WJ-MSCs	WJ-MSCs were differentiated into IPCs. IPCs were stained with dithizone. C-peptide secretion and expression of insulin-related genes were examined	–	–	Secretion of insulin by cells is higher than in the controls. The presence of the product is associated with an increase in dithizone-positive cells and increased expression of PDX-1, GLUT-2 and INS genes in IPCs
Xiao, 2017 [33]	Cartilage tissue engineering	Cylinders 8 mm in diameter, 2 mm thick	Homogenized WJ was frozen in water (4–5 times), centrifuged at 3000 rpm for 30 minutes, 5000 rpm for 30 minutes, 7000 rpm for 30 minutes, supernatant was withdrawn, centrifuged 10,000 rpm for 30 minutes, precipitate was freeze-dried	Rabbit chondrocytes	Cell viability, gene expression analysis, production of glycosaminoglycans and collagen	–	–	The biocompatible, bioactive cell-free product promoted chondrocyte activity *in vitro*
Foltz, 2022 [34]	Tracheal cartilage regeneration	dWJ	Amniotic membrane was removed, washed with PBS, decellularized with 0.01% SDS and sodium deoxycholate, centrifuged at 100 rpm, washed with 37 °C PBS for 24 hours, stored at 4 °C	–	–	Rabbit tracheal defect 10 × 20 mm, (n = 10)	Histological studies, determination of the relative content of collagen types 1 and 3, aggrecan	No product rejection reactions were detected. No induction of collagen production and chondrocyte recruitment was found. No significant differences in the content of collagen types 1 and 3 and aggrecan were observed at day 30

Continuation Table

1	2	3	4	5	6	7	8	9
Penolazzi, 2020 [25]	Intervertebral disc regeneration	dWJ	Umbilical cord was placed in 4 °C deionized water for 24 hours, decellularized with 4% sodium deoxycholate for 4 hours, treated with DNase for 3 hours (three times)	MSCs, human degenerated intervertebral disc cells	Cell viability and proliferation, gene expression analysis	–	–	Support of viability of the cells of the degenerated intervertebral disc and expression of critical homeostasis regulators
Jadalannagari, 2017 [26]	Tissue engineering	dWJ	Decellularized with 0.005% Triton X-100, SDS, sodium succinate, treated with DNase for 16 hours, SAAs removed	WJ-MSCs, HUVEC	Product cytotoxicity, PCR	Full-thickness parietal bone defect (5.0 mm in diameter) in mice (n = 4)	Histological studies, live-cell imaging	A biocompatible product that stimulates osteocyte migration after 24 hours and after 2 weeks *in vivo*
Yuan, 2022 [35]	Tendon regeneration	Freeze-dried dWJ, 20 × 10 × 2 mm	Decellularized with 1% SDS for 24 hours, 1% Triton X-100 for 24 hours, treated with nuclease for 12 hours, washed, freeze-dried	Rabbit tenocytes	Product cytotoxicity, proliferation, cell migration	Rabbit tendon defect (n = 54)	Histological studies, gene expression analysis	Biocompatibility with cells at day 7, stimulation of tendon maturation at week 12 after surgery
Mann, 2020 [36]	Regeneration after spina bifida repair	dWJ patch	–	Primary meningeal cells, human neonatal keratinocytes	Cell proliferation	Retinoid-induced spina bifida in fetal rats	Histological studies	The use of the patch reduced acute inflammation and cell apoptosis, and increased cell proliferation
Lu, 2023 [21]	Wound healing	dWJ, 3 × 5–8 cm fragment	Decellularized with 0.1% SDS, washed with PBS and medium 199 for 48 hours, 100 rpm, 37 °C	Rat adipose tissue MSCs	Cell viability and proliferation	Rats (n = 15)	Histological studies, tail volume measurements	The product stimulated cell proliferation at day 14 and accelerated the healing of rat tail wounds with reduced tail volume by week 5 of follow-up

Continuation Table

1	2	3	4	5	6	7	8	9
Dubus, 2022 [16, 17]	Regenerative medicine	Freeze-dried dWJ	Vessels and amniotic membrane were removed, decellularized with 1% Triton X-100 for 1 hour, treated with DNase for 24 hours, 37 °C with stirring, washed, freeze-dried	WJ-MSCs, human fibroblasts, osteocytes, neutrophils, and monocytes	Cytotoxicity, proliferation, flow cytometry, cytokine production	Subcutaneous implantation in rats (n = 4), calvarial bone regeneration (n = 2)	Histological studies	The biocompatible product did not activate neutrophil metabolic activity, it promoted anti-inflammatory macrophage polarization *in vitro*, and did not improve bone regeneration
Converse, 2017 [37]	Tissue engineering	dWJ fragments	Umbilical cord was placed in a hypertonic saline for 1 hour, decellularized with Triton X-100 for 1 hour, placed in hypertonic saline for 1 hour, deionized water for 1 hour, treated with enzyme for 12–16 hours, treated with N-lauroylsarcosine for 2 hours, with ethanol for 10 minutes, residual detergents were removed, cryopreserved	Bone marrow MSCs, umbilical cord hematopoietic and progenitor cells, human leukemia cell lines HL-60, Kasumi I, MV 411	Colonization of dWJ fragments by cells	–	–	Recellularized product
Koci, 2017 [20]	Nerve tissue repair and regeneration	dWJ-based hydrogel	Treated with 0.02% trypsin/0.05% EDTA solution, 0.1% peracetic acid, 4% ethanol, freeze-dried, solubilized with pepsin, and neutralized	Human bone marrow MSCs	Cell proliferation and migration	Focal cerebral ischemia in rats (n = 4)	Histological studies	*In vitro* cytocompatibility, active colonization of hydrogel by recipient cells was observed *in vivo* (anti-inflammatory macrophages were the predominant cell population)

End of Table

1	2	3	4	5	6	7	8	9
Ramzan, 2022 [18]	Cartilage tissue engineering	dWJ-based hydrogel	Umbilical cord was subjected to osmotic shock, treated with 0.05% trypsin for 2 hours at 37 °C, 1% Triton X-100 for 24 hours with stirring, washed, freeze-dried, crushed, solubilized with pepsin for 48 hours with stirring, neutralized, subjected to gelation	WJ-MSCs	Cell proliferation and viability, gene expression analysis	–	–	On day 7, the dWJ-based hydrogel provided scaffold support for cell proliferation and differentiation in the chondrogenic direction on day 28 of cultivation
Výborný, 2019 [38]	Nerve repair	Genipin-cross-linked dWJ-based hydrogel	Umbilical cord was treated with 0.02% trypsin/0.05% EDTA, 0.1% peracetic acid, 4% ethanol, freeze-dried, solubilized with pepsin, neutralized, cross-linked with genipin	WJ-MSCs, human fetal neural stem cells	Cell viability, proliferation and differentiation	Photochemical lesion of the cortex	Histological studies	Genipin-cross-linked dWJ-based hydrogel, retained *in situ* for up to 2 weeks without an adverse tissue response or inflammation
Kalyuzhnaya, 2019; Bolgarchuk 2020; Chebotarev 2020; Kondratenko 2021 [12, 39–44]	Regenerative medicine	dWJ and dWJ hydrogel lyophilisates, hydrogel wet form	Vessel was removed, homogenates were decellularized with SDS, washed, freeze-dried, solubilized with pepsin, and a liquid form was obtained. Liquid form was freeze-dried	Human, rat, mouse, porcine, and guinea pig fibroblasts	Viability	Full-thickness skin wounds in mice and pigs, cartilage defect in rabbits	Histological studies	Biocompatible products promote granulation tissue formation and epithelialization and hyaline cartilage healing

Note: SDS, sodium dodecyl sulfate; PBS, phosphate-buffered saline; HUVEC, human umbilical vein endothelial cells; WJ, Wharton's Jelly; dWJ, decellularized Wharton's jelly; IPCs, insulin-producing cells; MSCs, mesenchymal stem cells; SAAs, surface active agents; FBS, fetal bovine serum; EDTA, ethylenediaminetetraacetic acid.

process, such as collagen, fibronectin, tenascin, lumican, periostin, types I and II keratin, fibulin and fibrinogen beta chain [16, 17]. High levels of growth factors were detected in the culture medium after incubation in dWJ. A similar effect was not detected for native umbilical cord. At the same time, the release of bioactive molecules from the cell-free product did not lead to phagocyte activation and accumulation of reactive oxygen species. WJ-derived stromal cells and human fibroblasts that were cultured in dWJ maintained high viability. Subcutaneous implantation in rats showed no inflammatory reaction and formation of a connective tissue capsule or reaction to the foreign body with the presence of multinucleated giant cells. The implanted subcutaneous human UC product was completely remodeled within three weeks. Mouse macrophages produced significantly more anti-inflammatory mediators after 72 hours of contact with dWJ compared to the control. The action of native human UC on mouse macrophages under similar conditions resulted in dominant secretion of proinflammatory mediators by them [16, 17]. The same works established the antibacterial activity of dWJ, manifested by the presence of a microbial growth inhibition zone and reduction of bacterial adhesion. Converse et al. described in detail the procedures for making TECs from dWJ in the form of plates followed by recellularization [37].

The fabrication and properties of solubilized forms of dWJ are described in 4 publications. Koci et al. solubilized cell-free powdered WJ for hydrogel preparation with hydrochloric acid pepsin. The resulting product form contained higher amounts of sulfated GAGs compared with the product prepared from pig bladder, spinal cord, and brain using similar techniques. The dWJ products exhibited a short gel time, indicating rapid self-assembly of the structural molecules. They supported cell growth, proliferation and migration *in vitro*. And 24 hours after introducing the injected form of dWJ into the focal ischemic lesion in the motor area of the rat cerebral cortex, a compact gel structure populated by a dense layer of endogenous cells was formed within the lesion site. Macrophages were the predominant cell type present within the defect, with the M2 macrophage phenotype (CD206) accounting for 77.1 ± 6.5% of all macrophages contained in the gel [20].

Ramzan et al. obtained the hydrogel form by enzymatic digestion using pepsin in hydrochloric acid followed by gelation. The dWJ-derived gel thus obtained, functioned as a three-dimensional matrix that provided the necessary microenvironment for adhesion, migration, proliferation and differentiation of MSCs into the chondrogenic lineage *in vitro* [18].

Vyborny et al. used a solubilized form of chemically cross-linked dWJ hydrogel to repair rat cortical lesions. In *in vitro* experiments, the resulting product was shown to have no cytotoxic properties, and *in vivo* experiments showed *in situ* gelation without adverse inflammatory reactions [38].

A group of researchers from Kirov Military Medical Academy, headed by I.K. Kalyuzhnaya, patented dWJ products/products in lyophilized and solubilized hydrogel (which can be lyophilized) forms (Fig. 2). The decellularization procedure in this case can be performed using sodium dodecyl sulfate or 0.1 N sodium hydroxide [12, 39–44]. Biocompatible products have shown bioactivity regarding the healing of articular cartilage and skin defects [41–44].

Thus, the publications considered above show that dWJ-derived biocompatible and bioactive products can be used in various areas of regenerative medicine and cell technologies, such as a source of bioactive molecules in human cell culturing, in cellular immunotherapy, wound healing, hematopoietic cell transplantation, MSC differentiation in insulin-producing cells, repair of cartilage, intervertebral discs, tendons and nerve tissue, tissue engineering of vessels, liver and cartilage, and regeneration after spina bifida repair.

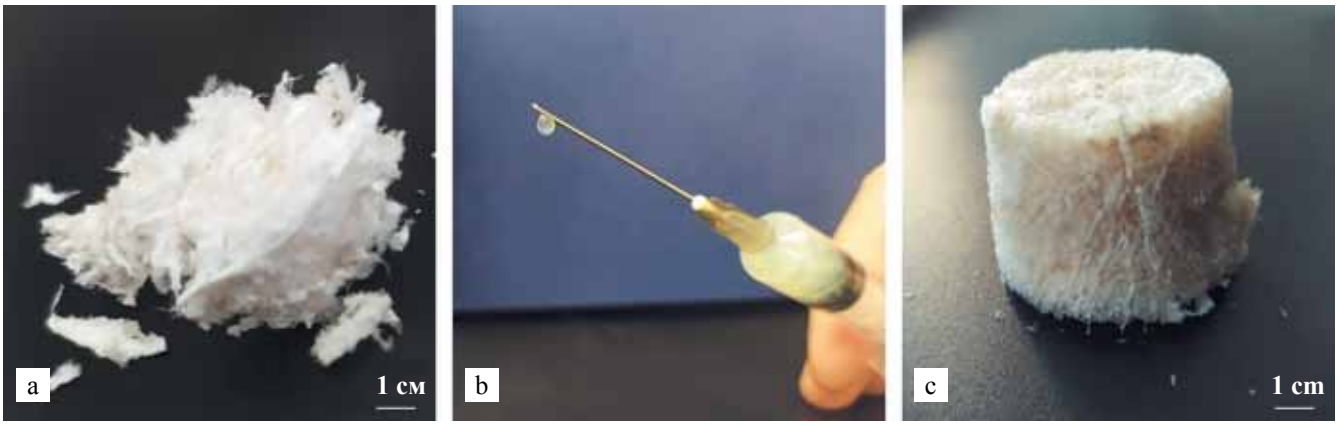

Fig. 2. View of various forms of decellularized human Wharton's jelly (dWJ). a, lyophilized dWJ [42]; b, solubilized form of dWJ; c, lyophilized solubilized form of dWJ [45]

PROSPECTS AND POSSIBLE APPLICATIONS OF DECELLULARIZED UMBILICAL CORD STROMA IN TISSUE ENGINEERING AND REGENERATIVE MEDICINE

The search for biomaterials for tissue engineering and regenerative medicine focuses mainly on the development of biomimetics that are capable of inducing specific cellular responses and formation of tissue equivalents. For optimal reproduction of the natural cell niche, an ideal biomimetic should be biocompatible, i.e., it should easily integrate into the surrounding tissue and form a single whole with it, while its degradation products should also have high biocompatibility. The biomimetic should support cell adhesion, proliferation, differentiation and secretion of its own ECM. The rate of matrix degradation should correspond to the regeneration rate of the recipient tissue. To integrate into the body, the biomaterial must have the ability to neovascularize and innervate [46]. In some cases, the biomaterial must withstand the mechanical stress characteristic of the area of its implantation, i.e., specific mechanical strength and plasticity are required [47]. In addition, sterilization and storage should not change the properties of the matrices, and use of the biomaterial should be as convenient as possible. Decellularized tissues have the most accurate reproduction of the cell niche, due to preservation of specific composition and morphology. Due to this, decellularization is considered to be one of the most promising methods of creating ECM mimetics [1].

The nonimmunogenicity of the decellularized product, as one of the main parameters of biocompatibility, is mainly due to the absence of genetic material of the original tissue [48]. The use of various decellularization methods and protocols provides reliable purification against the donor's genetic material, but, at the same time, can lead to loss of bioactive components and change the structure of ECM proteins. Effective removal of cells while preserving the microstructure and composition of ECM makes the finished cell-free product able to stimulate regeneration, as well as maintain cell activity [48]. Note that the publications studied do not compare the effectiveness of different UC stromal decellularization protocols. For example, optimization of the decellularization protocol improved the functional properties of cell-free blood vessels and articular cartilage and liver [49–51].

Allogeneic biomaterial for making cell-free products from it is often limitedly available and is not optimal for several reasons. The composition and structure of adult donor tissues are influenced by external and internal factors during the donor's life. Birth defects, diseases, age-related changes, the effects of stress, medications, and exposure to unhealthy work or environmental conditions significantly alter connective tissue components and architecture. Loss of ECM components along with increased cross-linking of collagen leads to deterioration of tissue biomechanical properties. Fibronectin levels change with age, impairing cell binding to ECM via integrin receptors [52]. Age-related changes in donor tissues inevitably worsen the properties of cell-free mimetics made from them and reduce their regenerative potential.

ECM properties inevitably deteriorate with age, which has prompted many researchers to neglect the risks of using xenogeneic biomaterials for tissue engineering. Worldwide, research is underway to create cell-free products from animal organs and tissues, provided that protocols are developed to ensure complete removal of cells, including genetic material [49–51, 53].

For the needs of tissue engineering and regenerative medicine, there are currently offers of commercial products based on decellularized ECM of allogeneic and xenogeneic origin [54, 55]. Nevertheless, human biomaterial for creating such products is preferable to available xenogeneic materials due to the potential danger of undesirable immune response when implanted into the recipient. Carbohydrate residue galactose α-1,3-galactose (α-Gal epitope), also called the major xenoantigen, is a component of membrane glycoproteins and glycolipids of cells of many mammals, except humans and some monkey species. Human blood contains a high titer of anti-α-Gal antibodies. There is an assumption that the wall of *Enterobacteriaceae* bacteria of the normal intestinal microflora contains galactose residues and stimulates the human immune system to produce these antibodies [56].

It is impossible to completely avoid the recipient's immune system response to the implantation of decellularized tissue. However, the type of the emerging immune response that occurs during implantation determines the possibility of a favorable healing outcome [57]. Sikari et al. and Huleichel et al. showed the connection between the products of biomaterials degradation and macrophage tissue phenotype, their expression of anti-inflammatory genes and protein production [58, 59].

Collagen cross-linking technologies promote product resistance to enzymatic degradation but reduce the moisture-absorbing properties of the material [60]. In addition, chemical cross-linking agents change the ultrastructure, composition and topology of the product surface [60]. However, the use of crosslinking agents seems to be necessary when there is a need for the artificial matrix to function in the body for the long-term. This points to the possibility of their use for decellularized UC stroma, given the rapid degradation (about 3 weeks) revealed in the study.

Interest in the use of extraembryonic tissues (including placenta, amniotic membrane and umbilical cord) as raw materials for use in regenerative medicine is due to their unique composition and properties [61]. The composition of embryonic and neonatal tissues is markedly different from that of adult tissues and has a greater

regenerative potential because it plays an important role in tissue morphogenesis [62]. In contrast to the adult, the mammalian foetus heals its wounds spontaneously by regeneration without associated scarring, provided that the injury has been inflicted at a sufficiently early stage of gestation, typically before the third trimester, after which there is a transition to the postnatal type of wound healing with a gentle elastic scar formation [63]. The unique feature of fetal phenotype tissues for wound healing without scarring may be associated with a higher content of antifibrotic isoform TGF-β3 in them, relative to TGF-β1 and TGF-β2 isoforms inherent in postnatal tissues [62].

While the clinical use of fetal membranes is well documented, the use of UC tissue is relatively new. The human UC is widely used for obtaining MSCs and endothelial cells, and can also serve as a source of hyaluronic acid. At the same time, WJ consists mainly of collagen (>500 mg/g tissue), proteoglycans and GAGs, such as hyaluronic acid and heparan sulfate, immobilized and embedded in the collagen network. The proportional ratio of collagens in WJ is: 47% (type I), 40% (type III), and 12% (type V). Hyaluronic acid constitutes up to 70% of GAG content in UC (approximately 4 mg/ml), which gives the tissue a special hydrophilicity [61, 64, 65]. Unique structural characteristics and the presence of growth factors make the UC an attractive source of biomaterial for the needs of regenerative medicine and tissue engineering.

It should be noted that among the publications found, to the surprise of the authors, no studies using xenogeneic UC were found. Given the property of low immunogenicity of provisory organs and the admissible difficulties in ensuring a constant supply of biomaterial when transferring the technology to production, the use of this type of biomaterial may be justified.

As shown by analysis of publications, decellularized human UC stroma can be successfully used to stimulate regenerative processes of different organs and tissues. Cell-free UC stroma can be used as an independent product; it can also be used to improve the biological properties of other materials. For ease of transport and storage, decellularized UC stroma is lyophilized. A variety of product forms can be made from WJ-derived ECM, including porous matrices, hydrogel compositions, tubular scaffolds, etc. It is possible to supplement compositions with amniotic material or with mineralized or demineralized bone ECM. Combinations of UC biomaterial with pharmaceutical carriers can be created. In some cases, injectable forms of WJ-derived ECM hydrogels with *in situ* polymerization abilities are considered more feasible because these materials can easily adjust to the surface topography and volume of the injured area, and osmotic forces contribute to the stretching of the hydrogel polymer network as it swells. For this purpose, the decellularized UC stroma is enzymatically solubilized.

In general, work in the field of obtaining biomaterial from decellularized UC began relatively recently: the first publication in the English-language literature appeared in 2016. In Russia, studies devoted to the described topic are carried out by only one group of scientists from Kirov Military Medical Academy in St. Petersburg [12, 39–44, 66]. This is probably the reason for the lack of clinical works that meet the review's inclusion criteria. At the same time, two clinical trials were initiated in Iran in 2022, devoted to the treatment of wrinkles using UC [67, 68]. However, there is no information on whether the UC used in these studies is decellularized.

CONCLUSION

Based on analysis of papers published in electronic databases, we can conclude that scientific research on the possibilities of dWJ application is a very promising area of regenerative medicine and tissue engineering. Researchers are using different methods to remove cells and create convenient forms for application of cell-free products from UC stroma. However, more conclusive evidence – additional studies, clinical and preclinical – is needed to finally determine the prognosis for the use of the technology in medicine.

The study was supported by the Russian Science Foundation under grant No. 211500251, https://rscf.ru/project/21-15-00251/.

The authors declare no conflict of interest.

REFERENCES

1. *Sevast'yanov VI.* Tekhnologii tkanevoy inzhenerii i regenerativnoy meditsiny. *Vestnik transplantologii i iskusstvennykh organov.* 2014; 16 (3): 93–108. doi: 10.15825/1995-1191-2014-3-93-108.
2. *Meleshina AV, Bystrova AS, Rogovaya OS, Vorotelyak YeA, Vasil'yev AV, Zagaynova YeV*. Tkaneinzhenernyye konstrukty kozhi i ispol'zovaniye stvolovykh kletok dlya sozdaniya kozhnykh ekvivalentov. *Sovremennyye tekhnologii v meditsine*. 2017; 9 (1): 198–220. doi: 10.17691/stm2017.9.1.24.
3. *Fominykh YeM, Mitrofanov NV, Zhivtsov OP, Struchkov AA, Zubritskiy VF, Lebedeva YuN i dr.* Transplantatsiya tkanevykh ekvivalentov v lechenii nekotorykh povrezhdeniy kozhi. *Vestnik transplantologii i iskusstvennykh organov*. 2020; 22 (1): 165–173. doi: 10.15825/1995-2020-1-165-173.
4. *Sevast'yanov VI, Grigor'yev AM, Basok YuB, Kirsanova LA, Vasilets NV, Malkova AP i dr.* Biosovmestimyye i matriksnyye svoystva polilaktidnykh gubok. *Vestnik transplantologii i iskusstvennykh organov.* 2018; 20 (2): 82–90. doi: 10.15825/1995-1191-2018-2-82-90.
5. *Liu H, Gong Y, Zhang K, Ke S, Wang Y, Wang J, Wang H.* Recent Advances in Decellularized Matrix-Derived Materials for Bioink and 3D Bioprinting. *Gels.* 2023*;* 9 (3): 195. doi: 10.3390/gels9030195.

6. *Basok YuB, Sevast'yanov VI.* Tekhnologii tkanevoy inzhenerii i regenerativnoy meditsiny v lechenii defektov khryashchevoy tkani sustavov. *Vestnik transplantologii i iskusstvennykh organov.* 2016; 18 (4): 102–122. doi: 10.15825/1995-1191-2016-4-102-122.
7. *Sevastianov VI, Basok YB, Grigor'ev AM, Kirsanova LA, Vasilets VN.* Formation of tissue-engineered construct of human cartilage tissue in a flow-through bioreactor. *Bulletin of Experimental Biology and Medicine*. 2017; 164: 269–273. doi: 10.1007/s10517-017-3971-z.
8. *Sevast'yanov VI, Basok YuB, Grigor'yev AM, Kirsanova LA, Vasilets NV.* Perfuzionnyy bioreaktor dlya sozdaniya tkaneinzhenernykh konstruktsiy. *Meditsinskaya tekhnika*. 2017; 303 (3): 9–11.
9. *Badylak SF*. Decellularized allogeneic and xenogeneic tissue as a bioscaffold for regenerative medicine: factors that influence the host response. *Annals of Biomedical Engineering*. 2014; 42 (7): 1517–1527. doi: 10.1007/s10439-013-0963-7. PMID: 24402648.
10. *Bakhtyar N, Jeschke MG, Mainville L, Herer E, Amini-Nik S.* Acellular gelatinous material of human umbilical cord enhances wound healing: a candidate remedy for deficient wound healing. *Frontiers in Physiology.* 2017; 8: 200. doi: 10.3389/fphys.2017.00200. PMID: 28421003.
11. *Gupta P, Chaudhuri GR, Janani G, Agarwala M, Ghosh D, Nandi SK, Mandal BB.* Functionalized silk vascular grafts with decellularized human Wharton's jelly improves remodeling via immunomodulation in rabbit jugular vein. *Advanced Healthcare Materials.* 2021; 10 (19): e2100750. doi: 10.1002/adhm.202100750. PMID: 34378360.
12. *Kalyuzhnaya LI, Chernov VE, Frumkina AS, Chebotarev SV, Zemlyanoy DA, Tovpeko DV, Kosulin AV.* Izgotovleniye tkaneinzhenernogo beskletochnogo matriksa pupoviny cheloveka. *Vestnik Rossiyskoy voyenno-meditsinskoy akademii.* 2020; 69 (1): 124–130. doi: 10.17816/brmma25980.
13. *Sobolewski K, Małkowski A, Bańkowski E, Jaworski S.* Wharton's jelly as a reservoir of peptide growth factors. *Placenta.* 2005; 26 (10): 747–752. doi: 10.1016/j.placenta.2004.10.008. PMID: 16226124.
14. *Gupta A, El-Amin SF, Levy HJ, Sze-Tu R, Ibim SE, Maffulli N.* Umbilical cord-derived Wharton's jelly for regenerative medicine applications. *Journal of Orthopaedic Surgery*. 2020; 15. doi: 10.1186/s13018-020-1553-7. PMID: 32054483.
15. *Fayon A, Helle D, Francius G*. Characterization of an innovative biomaterial derived from human Wharton's jelly as a new promising coating for tissue engineering applications. *Frontiers in Bioengineering and Biotechnology*. 2022; 10: 884069. doi: 10.3389/fbioe.2022.884069. PMID: 35769101.
16. *Dubus M, Scomazzon L, Chevrier J, Ledouble C, Baldit A, Braux J et al.* Antibacterial and immunomodulatory properties of acellular Wharton's jelly matrix. *Biomedicines*. 2022; 10 (2): 227. doi: 10.3390/biomedicines10020227. PMID: 35203437.
17. *Dubus M, Scomazzon L, Chevrier J, Montanede A, Baldit A, Terryn C et al.* Decellularization of Wharton's jelly increases its bioactivity and antibacterial properties. *Frontiers in Bioengineering and Biotechnology*. 2022; 10: 828424. doi: 10.3389/fbioe.2022.828424. PMID: 35360386.
18. *Ramzan F, Ekram S, Frazier T, Salim A, Mohiuddin OA, Khan I.* Decellularized human umbilical tissue derived hydrogels promote proliferation and chondrogenic differentiation of mesenchymal stem cells. *Bioengineering.* 2022; 9: 239. doi: 10.3390/bioengineering9060239.
19. *Kehtari M, Beiki B, Zeynali B.* Decellularized Wharton's jelly extracellular matrix as a promising scaffold for promoting hepatic differentiation of human induced pluripotent stem cells. *Journal of Cellular Biochemistry*. 2019; 120 (4): 6683–6697. doi: 10.1002/jcb.27965. PMID: 30417406.
20. *Kočí Z, Výborný K, Dubišová J.* Extracellular matrix hydrogel derived from human umbilical cord as a scaffold for neural tissue repair and its comparison with extracellular matrix from porcine tissues. *Tissue Engineering Part C Methods*. 2017; 23 (6): 333–345. doi: 10.1089/ten.TEC.2017.0089. PMID: 28471271.
21. *Lu J-H, Hsia K, Su CK, Pan YH, Ma H, Chiou SH, Lin CH.* A novel dressingcomposed of adipose stem cells and decellularized Wharton's jelly facilitatedwound healing and relieved lymphedema by enhancing angiogenesis and lymphangiogenesis in a rat model. *Journal of functional biomaterials.* 2023; 14 (2): 104. doi: 10.3390/jfb14020104. PMID: 36826903.
22. *Beiki B, Zeynali B, Seyedjafari E.* Fabrication of a three dimensional spongy scaffold using human Wharton's jelly derived extra cellular matrix for wound healing. *Materials Science and Engineering C-Materials for Biological Applications*. 2017; 78: 627–638. doi: 10.1016/j.msec.2017.04.074. PMID: 28576031.
23. *Bullard JD, Lei J, Lim JJ, Massee M, Fallon AM, Koob TJ.* Evaluation of dehydrated human umbilical cord biological properties for wound care and soft tissue healing. *Journal of Biomedical Materials Research Part B Applied Biomaterials*. 2019; 107 (4): 1035–1046. doi: 10.1002/jbm.b.34196. PMID: 30199609.
24. *Li D, Chiu G, Lipe B, Hopkins RA, Lillis J, Ashton JM et al.* Decellularized Wharton jelly matrix: a biomimetic scaffold for *ex vivo* hematopoietic stem cell culture. *Blood Advances.* 2019; 3 (7): 1011–1026. doi: 10.1182/bloodadvances.2018019315. PMID: 30940636.
25. *Penolazzi L, Pozzobon M, Bergamin LS, D'Agostino S, Francescato R, Bonaccorsi G et al.* Extracellular matrix from decellularized Wharton's jelly improves the behavior of cells from degenerated intervertebral disc. *Frontiers in Bioengineering and Biotechnology.* 2020; 8: 262. doi: 10.3389/fbioe.2020.00262. PMID: 32292779.
26. *Jadalannagari S, Converse G, McFall C, Buse E, Filla M, Villar MT et al.* Decellularized Wharton's jelly from human umbilical cord as a novel 3d scaffolding material for tissue engineering applications. *PLoS One*. 2017; 12 (2): e0172098. doi: 10.1371/journal.pone.0172098. PMID: 28222169.
27. *PLOS ONE Staff.* Correction: Decellularized Wharton's Jelly from human umbilical cord as a novel 3D scaffolding material for tissue engineering applications. *PLoS*

One. 2017 Mar 7; 12 (3): e0173827. doi: 10.1371/journal.pone.0173827. Erratum for: *PLoS One*. 2017 Feb 21; 12 (2): e0172098. PMID: 28267774.

28. *Jalili Z, Emamgolizadeh B, Abbaszadeh H, Jalili S, Derakhshani M, Yousefi M et al.* Effect of replacement of Wharton acellular jelly with fbs on the expression of megakaryocyte linear markers in hematopoietic stem cells CD34. *Asian Pacific Journal of Cancer Prevention.* 2022; 23 (10): 3281–3286. doi: 10.31557/APJCP.2022.23.10.3281. PMID: 36308350.
29. *Talebi M, Nozad Charoudeh H, Movassaghpour Akbari AA, Baradaran B, Kazemi T.* Acellular Wharton's jelly, potentials in t-cell subtypes differentiation, activation and proliferation. *Advanced Pharmaceutical Bulletin.* 2020; 10 (4): 617–622. doi: 10.34172/apb.2020.074. PMID: 33072540.
30. *Dan P, Velot É, Francius G, Menu P, Decot V.* Human-derived extracellular matrix from Wharton's jelly: An untapped substrate to build up a standardized and homogeneous coating for vascular engineering. *Acta Biomaterialia.* 2017; 48: 227–237. doi: 10.1016/j.actbio.2016.10.018. PMID: 27769940.
31. *Basiri A, Farokhi M, Azami M, Ebrahimi-Barough S, Mohamadnia A, Rashtbar M et al.* A silk fibroin/decellularized extract of Wharton's jelly hydrogel intended for cartilage tissue engineering. *Progress in Biomaterials.* 2019; 8 (1): 31–42. doi: 10.1007/s40204-019-0108-7. PMID: 30706299.
32. *Azarbarz N, Khorsandi L, Nejaddehbashi F, Neisi N, Nejad DB.* Decellularized Wharton's jelly scaffold enhances differentiation of mesenchymal stem cells to insulin-secreting cells. *Tissue Cell.* 2022; 79: 101938. doi: 10.1016/j.tice.2022.101938. PMID: 36152380.
33. *Xiao T, Guo W, Chen M, Hao C, Gao S, Huang J et al.* Fabrication and *In Vitro* study of tissue-engineered cartilage scaffold derived from Wharton's jelly extracellular matrix. *BioMed Research International*. 2017; 2017: 5839071. doi: 10.1155/2017/5839071. PMID: 29214173.
34. *Foltz KM, Neto AE, Francisco JC, Simeoni RB, Miggiolaro AFRDS, do Nascimento TG et al.* Decellularized Wharton jelly implants do not trigger collagen and cartilaginous tissue production in tracheal injury in rabbits. *Life (Basel)*. 2022; 12 (7): 942. doi: 10.3390/life12070942. PMID: 35888031.
35. *Yuan Z, Cao F, Gao C, Yang Z, Guo Q, Wang Y.* Decellularized human umbilical cord Wharton jelly scaffold improves tendon regeneration in a rabbit rotator cuff tendon defect model. *The American Journal of Sports Medicine.* 2022; 50 (2): 371–383. doi: 10.1177/03635465211055722. PMID: 34739346.
36. *Mann LK, Won JH, Trenton NJ, Garnett J, Snowise S, Fletcher SA et al.* Cryopreserved human umbilical cord versus acellular dermal matrix patches for in utero fetal spina bifida repair in a pregnant rat model. *Journal of neurosurgery. Spine*. 2019; 32 (2): 321–331. doi: 10.3171/2019.7.SPINE19468. PMID: 31675701.
37. *Converse GL, Li D, Buse EE, Hopkins RA, Aljitawi OS.* Wharton's jelly matrix decellularization for tissue engineering applications. *Methods in Molecular Biology*. 2018; 1577: 25–33. doi: 10.1007/7651_2017_61. PMID: 28786033.
38. *Výborný K, Vallová J, Kočí Z, Kekulová K, Jiráková K, Jendelová P et al.* Genipin and EDC crosslinking of extracellular matrix hydrogel derived from human umbilical cord for neural tissue repair. *Scientific Reports*. 2019; 9 (1): 10674. doi: 10.1038/s41598-019-47059-x. PMID: 31337821.
39. *Bolgarchuk OO, Kalyuzhnaya LI, Chernov VE, Chebotarev SV, Simanov AG, Chernutskiy AM.* Optimizatsiya protsedury detsellyulyarizatsii soyedinitel'noy tkani pupoviny cheloveka dlya sozdaniya tkaneinzhenernogo ranevogo pokrytiya. *Izvestiya Rossiyskoy voyenno-meditsinskoy akademii.* 2020; 39 (S3-1): 13–18.
40. *Kondratenko AA, Kalyuzhnaya LI, Sokolova MO, Chernov VE.* Sokhrannost' vazhneyshikh strukturnykh komponentov pupoviny cheloveka posle detsellyulyarizatsii kak etapa izgotovleniya vysokoregenerativnogo ranevogo pokrytiya. *Biotekhnologiya*. 2021; 37 (5): 61–65. doi: 10.21519/0234-2758-2021-37-5-61-65.
41. *Chebotarev SV, Kalyuzhnaya LI, Khominets VV, Chernov VE, Frumkina AS, Zemlyanoy DA i dr.* Regenerativnyye effekty gidrogelya iz biomateriala pupoviny cheloveka v vosstanovlenii povrezhdeniy sustavnogo khryashcha. *Klinicheskaya i eksperimental'naya khirurgiya. Zhurnal imeni akademika B.V. Petrovskogo.* 2020; 8 (4): 119–125. doi: 10.33029/2308-1198-2020-8-4-119-125.
42. *Kondratenko AA, Tovpeko DV, Kalyuzhnaya LI.* Biologicheskiye effekty beskletochnogo tkaneinzhenernogo produkta iz pupoviny cheloveka. *Patogenez.* 2022; 20 (4): 53–62. doi: 10.25557/2310-0435.2022.04.53-62.
43. *Kalyuzhnaya LI, Chebotarev SV.* Gidrogel' iz pupoviny cheloveka v lechenii defektov sustavnogo khryashcha v eksperimente. *Izvestiya Rossiyskoy voyenno-meditsinskoy akademii*. 2020; 39 (S3-1): 37–40.
44. *Kalyuzhnaya LI, Khominets VV, Chebotarov SV, Kharkevich ON, Kudyashev AL, Chernov VE i dr.* Primeneniye biomateriala iz pupoviny cheloveka dlya vosstanovleniya povrezhdeniy sustavnogo khryashcha. *Profilakticheskaya i klinicheskaya meditsina*. 2019; 4 (73): 45–52.
45. *Kondratenko AA, Kalyuzhnaya-Zemlyanaya LI, Tovpeko DV, Sheveleva VS, Glushakov RI.* Biologicheskiye i funktsional'nyye svoystva liofilizirovannykh form tkaneinzhenernykh matriksov iz pupoviny cheloveka. *Vestnik transplantologii i iskusstvennykh organov.* 2023; 25 (1): 113–122. doi: 10.15825/1995-1191-2023-1-113-122.
46. *Shin H, Jo S, Mikos AG.* Biomimetic materials for tissue engineering. *Biomaterials.* 2003; 24 (24): 4353–4364. doi: 10.1016/s0142-9612(03)00339-9. PMID: 12922148.
47. *Nemets YeA, Lazhko AE, Grigor'yev AM, Basok YuB, Kirillova AD, Sevast'yanov VI.* Biosovmestimyye i funktsional'nyye svoystva tkanespetsificheskoy melkodispersnoy 3D-matritsy iz detsellyulyarizovannogo khryashcha svin'i. *Vestnik transplantologii i iskusstvennykh organov*. 2022; 24 (4): 73–84. doi: 10.15825/1995-1191-2022-4-73-84.
48. *Crapo PM, Gilbert TW, Badylak SF.* An overview of tissue and whole organ decellularization processes. *Bioma-*

terials. 2011; 32 (12): 3233–3243. doi: 10.1016/j.biomaterials.2011.01.057. PMID: 21296410.
49. *Simsa R, Padma AM, Heher P, Hellström M, Teuschl A, Jenndahl L et al.* Systematic *in vitro* comparison of decellularization protocols for blood vessels. *PLoS One*. 2018; 13 (12): e0209269. doi: 10.1371/journal.pone.0209269. PMID: 30557395.
50. *Sevastianov VI, Basok YuB, Grigoriev AM, Nemets EA, Kirillova AD, Kirsanova LA et al.* Decellularization of cartilage microparticles: Effects of temperature, supercritical carbon dioxide and ultrasound on biochemical, mechanical, and biological properties. *Journal of Biomedical Materials Research A*. 2023; 111 (4): 543–555. doi: 10.1002/jbm.a.37474. PMID: 36478378.
51. *Kirillova AD, Basok YuB, Lazhko AE, Grigoryev AM, Kirsanova LA, Nemets EA, Sevastianov VI.* Creating a tissue-specific microdispersed matrix from a decellularized porcine liver. *Inorganic Materials*: *Applied Research*. 2021; 12 (3): 812–819. doi: 10.1134/S2075113321030199.
52. *Tseluyko SS, Malyuk YeA, Korneyeva LS, Krasavina NP.* Morfofunktsional'naya kharakteristika dermy kozhi i yeye izmeneniya pri starenii (obzor literatury). *Byulleten' fiziologii i patologii dykhaniya*. 2016; 60. doi: 10.12737/20130.
53. *Basok YuB, Kirillova AD, Grigoriev AM, Kirsanova LA, Nemets EA, Sevastianov VI.* Fabrication of microdispersed tissue-specific decellularized matrix from porcine articular cartilage. *Perspektivnye materialy*. 2020; 5: 51–60. doi: 10.30791/1028-978x-2020-5-51-60.
54. *Potekayev NN, Frigo NV, Petersen YeV.* Iskusstvennaya kozha: vidy, oblasti primeneniya. *Klinicheskaya dermatologiya i venerologiya*. 2017; 6: 7–15. doi: 10.17116/klinderma20171667-15.
55. *Cramer MC, Badylak SF.* Extracellular Matrix-Based Biomaterials and Their Influence Upon Cell Behavior. *Annals of Biomedical Engineering*. 2020; 48 (7): 2132–2153. doi: 10.1007/s10439-019-02408-9. PMID: 31741227.
56. *Galili U*. Acceleration of wound healing by α-gal nanoparticles interacting with the natural anti-Gal antibody. *Journal of Immunology Research*. 2015; 2015: 589648. doi: 10.1155/2015/589648. PMID: 25922849.
57. *Dziki JL, Huleihel L, Scarritt ME, Badylak SF.* Extracellular matrix bioscaffolds as immunomodulatory biomaterials. *Tissue Engineering Part A*. 2017; 23 (19–20): 1152–1159. doi: 10.1089/ten.TEA.2016.0538. PMID: 28457179.
58. *Sicari BM, Johnson SA, Siu BF, Crapo PM, Daly KA, Jiang H et al.* The effect of source animal age upon the *in vivo* remodeling characteristics of an extracellular matrix scaffold. *Biomaterials*. 2012; 33 (22): 5524–5533. doi: 10.1016/j.biomaterials.2012.04.017. PMID: 22575834.
59. *Huleihel L, Hussey GS, Naranjo JD, Zhang L, Dziki JL, Turner NJ et al.* Matrix-bound nanovesicles within ECM bioscaffolds. *Science Advances*. 2016; 2 (6): e1600502. doi: 10.1126/sciadv.1600502. PMID: 27386584.
60. *Delgado LM, Bayon Y, Pandit A, Zeugolis DI.* To cross-link or not to cross-link? Cross-linking associated foreign body response of collagen-based devices. *Tissue Engineering Part B Reviews*. 2015; 21 (3): 298–313. doi: 10.1089/ten.TEB.2014.0290. PMID: 25517923.
61. *Roy A, Mantay M, Brannan C, Griffiths S.* Placental Tissues as Biomaterials in Regenerative Medicine. *BioMed Research International*. 2022; 2022: 6751456. doi: 10.1155/2022/6751456. PMID: 35496035.
62. *Lo DD, Zimmermann AS, Nauta A, Longaker MT, Lorenz HP*. Scarless fetal skin wound healing update. *Birth Defects Research Part C Embryo Today Reviews*. 2012; 96 (3): 237–247. doi: 10.1002/bdrc.21018. PMID: 23109319.
63. *Yannas IV.* Similarities and differences between induced organ regeneration in adults and early foetal regeneration. *Journal of the Royal Society Interface*. 2005; 2 (5): 403–417. doi: 10.1098/rsif.2005.0062. PMID: 16849201.
64. *Nanaev AK, Kohnen G, Milovanov AP, Domogatsky SP, Kaufmann P.* Stromal differentiation and architecture of the human umbilical cord. *Placenta*. 1997; 18 (1): 53–64. doi: 10.1016/s0143-4004(97)90071-0. PMID: 9032810.
65. *Franc S, Rousseau JC, Garrone R, van der Rest M, Moradi-Améli M.* Microfibrillar composition of umbilical cord matrix: characterization of fibrillin, collagen VI and intact collagen V. *Placenta*. 1998; 19 (1): 95–104. doi: 10.1016/s0143-4004(98)90104-7. PMID: 9481791.
66. *Kalyuzhnaya LI, Sokolova MO, Chernov VE, Zemlyanoy DA, Chebotarev SV, Chalisova NI i dr.* Vliyaniye beskletochnogo matriksa pupoviny cheloveka na dinamiku rosta i zhiznesposobnost' kul'tiviruyemykh kletok cheloveka i zhivotnykh *ex vivo*. *Geny i kletki*. 2021; 3: 72–79. doi: 10.23868/202110010.
67. https://trialsearch.who.int/Trial2.aspx?TrialID=IRCT20210612051545N3 [Internet]. World Health Organization: International Clinical Trials Registry Platform (ICTRP). [updated 2022 November 21; cited 2023 April 03]. Available from: https://trialsearch.who.int/Trial2.aspx?TrialID=IRCT20210612051545N3.
68. https://trialsearch.who.int/Trial2.aspx?TrialID=IRCT20210612051545N2 [Internet]. World Health Organization: International Clinical Trials Registry Platform (ICTRP). [updated 2022 November 21; cited 2023 April 03]. Available from: https://trialsearch.who.int/Trial2.aspx?TrialID=IRCT20210612051545N2.

The article was submitted to the journal on 11.04.2023

DOI: 10.15825/1995-1191-2023-2-99-106

ARTIFICIAL NERVE CONDUIT FOR GUIDING PERIPHERAL NERVE GROWTH (CADAVERIC STUDY)

A.G. Fedyakov[1, 2], E.A. Nemets[3], O.N. Dreval[2], A.V. Gorozhanin[1, 2], L.A. Sidneva[2], Z.H. Plieva[2, 4], M.A. Razin[2], N.V. Perova[5], V.I. Sevastianov[3, 5]

[1] Botkin Hospital, Moscow, Russian Federation
[2] Russian Medical Academy of Continuous Professional Education, Moscow, Russian Federation
[3] Shumakov National Medical Research Center of Transplantology and Artificial Organs, Moscow, Russian Federation
[4] Orthospine Clinic, Moscow, Russian Federation
[5] Institute of Biomedical Research and Technology, Moscow, Russian Federation

At present, the search for effective ways of restoring peripheral nerves with anatomical damage continues. Autoplasty still remains the gold standard, which, however, is not without its drawbacks. The use of nerve implants for promoting directional axon growth is essential and promising. **Objective:** to study the biomechanical properties of laboratory samples of an artificial nerve conduit (NGC) made of hybrid biomaterials and to, on cadaveric material, assess the technical feasibility of using them in surgical practice to repair extended peripheral nerve defects. **Material and methods.** The objects of the study were three electrospun NGC samples: from synthetic material (polycaprolactone, PCL) and hybrid biomaterials (PCL + gelatin or PCL + collagen). The work compared the physical and mechanical properties of NGC: stiffness, plasticity, elasticity, brittleness, resistance to chemical attack, their ability to be impregnated with liquid media, permeability, possibility of making an anastomosis between the implant and the nerve during surgical procedure. Cadaveric material was the object of the study: we used a dissected superficial sensory branch of the human right radial nerve, 2 mm in diameter, isolated on the forearm, about 12 cm in length, because it most corresponded to the diameter of the NGC samples tested. After surgery, the echogenic features of the implants and their anastomoses with the nerve were assessed by ultrasound imaging. **Results.** It was found that hybrid NGC samples, based on their biomechanical properties, are fundamentally suitable for use in surgical practice, to ensure growth and replacement of a peripheral nerve defect. However, the best composition of a nerve guide can be established after comparative preclinical study of the biocompatible and functional properties of hybrid material samples. **Conclusion.** The physical and mechanical properties of the investigated NGC samples made of hybrid biomaterials meet the technical requirements for implantable nerve conduits for surgical application.

Keywords: peripheral nerve damage, artificial nerve guide, nerve conduit, polycaprolactone, collagen, gelatin, regeneration.

The frequency of peripheral nerve injuries from limb injuries ranges from 1.5% to 13% and ranks first in terms of degree of disability of the injured. Disability in all nerve injuries reaches 60% [1], and about 45% of cases of nerve injuries in the Russian Federation occur among able-bodied citizens aged 21 to 35 years [2].

Every year in Russia, 4,000 to 7,000 people require surgical treatment for this condition [3]. Among the patients who underwent surgical treatment, only half of them have complete functional recovery of the nerve, 3% of patients have reduced sensitivity, while the motor function of the nerve is restored in less than 25% of patients [4, 5]. Such a low percentage of rehabilitation of patients with peripheral nerve injury is mainly due to the incomplete regenerative potential of the injured axon, as well as to the lack of necessary conditions for directed axonal growth from the proximal end to the distal end [6]. The high frequency of peripheral nerve injuries, accompanied by loss of ability to work, up to disability, makes finding new effective surgical approaches for surgical repair of damaged nerves an urgent task.

To restore the anatomical integrity of the damaged peripheral nerve, neurorrhaphy (surgical restoration of nerve trunk integrity by mobilizing and suturing its ends) is traditionally used in clinical practice, and if it is impossible, autoplasty with the patient's own nerve is used. Nerve autotransplantation is currently the gold standard treatment for peripheral nerve injuries accompanied by diastasis >3 cm. However, the neurological deficit arising in the area of innervation of the nerve used for autoplasty,

Corresponding author: Larisa Sidneva. Address: 2/1, bldg. 1, Barrikadnaya str., Moscow, 123242, Russian Federation. Phone: (988) 991-08-26. E-mail: larisa.sidneva@inbox.ru

the mismatch between the diameters of the donor and recipient nerves, and the significant duration of surgical intervention limit the use of this technique. An alternative approach to restoring the anatomical integrity of damaged nerve is to create and use peripheral nerve implants made of synthetic and/or natural polymeric materials called nerve guidance conduits (NGC) (also referred to as an artificial nerve conduit or artificial nerve graft), which are designed to promote directed axonal growth and provide good conditions for regeneration of damaged nerve.

Various variants of nerve conduits were proposed back in the 19th century, but the feasibility of their use was questioned until the second half of the 20th century, since simpler surgical techniques for nerve fiber mobilization and tensioning were used in parallel. Later, these surgical methods were abandoned because it became clear that nerve tension significantly reduces their regenerative potential [7, 8]. Nerve conduits began to be registered as medical devices since the mid-1980s, and they are becoming commercially available in clinical practice [9].

Meanwhile, there is still no universal artificial nerve conduit with perfect biocompatibility. Literature asserts the importance of the following basic requirements for fabrication of peripheral NGCs [5, 10–14]:

a) Biocompatibility;
b) Biodegradation/bioresorption rate should not exceed the nerve regeneration time;
c) Permeability and wall thickness (the ideal scaffold should be semi-permeable; conduit permeability increases with pore size: nerve channels with larger pores better support axonal growth, the optimal pore size range is 10–20 μm, which facilitates nutrient inflow and at the same time prevents fibroblast penetration and growth);
d) Acceptable mechanical properties (strength, elasticity, tension, flexibility, resistance to destruction and stretching, stitching capability);
e) Ability to create optimal conditions for accelerated and directed axonal growth followed by full functional and structural restoration of denervated tissue;
f) Implant production technology should facilitate the production of a linear range of products of different diameters and lengths;
g) Affordable price.

By structure, NGCs can be divided into hollow (in the form of closed tubes or longitudinally dissected cylinder) and filled with various materials.

NGCs can be made from biodegradable/bioabsorbable synthetic (e.g., polyvinyl alcohol, polyglycolic acid, polycaprolactone) and natural polymers (usually collagen/gelatin, chitosan, polyoxybutyrate). Each of these groups has its own advantages and disadvantages [15, 16]. Highly biocompatible products made of natural polymers are rapidly resorbed, have poor mechanical properties, and are expensive to produce. The qualities of medical products made of synthetic polymers are more reproducible, have good mechanical properties, but are inferior to natural polymers in terms of biocompatibility and are not bioactive.

In our opinion, a promising approach to the creation of artificial nerve grafts is to use hybrid biomaterials comprising both synthetic and natural polymers. Synthetic polymers allow NGCs to provide the required mechanical characteristics, while natural polymers ensure high biocompatibility and provide bioactive properties in terms of stimulating the regenerative processes of the damaged nerve. In our work on creation of laboratory NGC samples from hybrid biomaterial, we chose a synthetic polymer, polycaprolactone (with a low degradation rate), and a natural biopolymer, collagen (or gelatin, its denatured form), the main extracellular matrix protein.

The aim of this work was to study the technical feasibility of surgical application of NGC samples made of hybrid biomaterials based on polycaprolactone and collagen/gelatin on a nerve isolated from cadaveric material.

MATERIAL AND METHODS

Tubular NGCs with an internal diameter of 2 mm (Fig. 1) were made by electrospinning method, previously developed to create tissue-engineered constructs of small-diameter blood vessels [17], from a 10% (w/w) polycaprolactone solution (PCL, MM 80000, Sigma-Aldrich, USA, sample #1), PCL with added gelatin (Sigma-Aldrich, USA (sample #2) and PCL with collagen (Collost, Russia, sample #3) in hexafluoroisopropanol (NPO PIM-INVEST, Russia) using electrospinning

Fig. 1. NGC samples

device NANON-01A (MECC CO, Japan) at 25 kV voltage between electrodes, solution feed rate 4 ml/h, distance to collector 100 mm, spindle speed 1000 rpm, using 18 G needle. After the end of the solution application process, the obtained samples were dried in a thermostat at 37 °C for 2 hours, followed by evacuation to remove traces of solvent at a residual pressure of 10–20 mm Hg and temperature 37 °C for 24 hours.

NGC samples were subjected to mechanical testing on a Shimadzu EZ Test EZ-SX test frame (Shimadzu Corporation, Japan) at a tensile speed of 5 mm/minute. The following mechanical characteristics of the specimens were recorded: elongation at break, tensile strength at break, and Young's modulus, which characterizes the degree of elasticity of the NGC. Young's modulus was calculated in Trapezium X software, version 1.2.6.

Experimental work was carried out in a room with a temperature of +18 °C. During the study, the following physical, mechanical and technical properties of the samples were evaluated: stiffness, plasticity, elasticity, brittleness, chemical resistance, ability to be impregnated with liquid media, porosity, and possibility to make anastomosis between the implant and nerve (stitching with surgical needle, conducting a ligature). We used lever scales with loads of different weights, a caliper, liquid media (centrifuged human blood plasma, 0.5% novocaine solution, native human blood, 3% H_2O_2 solution), edible indigo carmine for staining transparent liquids, suture surgical material with non-absorbable monofilament thread and atraumatic cutting needle (Prolene 6-0, 45 cm).

Cadaveric material was the object of the study: we used a dissected superficial sensory branch of the human right radial nerve, 2 mm in diameter, isolated on the forearm, about 12 cm in length, because it most corresponded to the diameter of the presented samples (Fig. 2).

We simulated restoration of the injured nerve integrity by tandem suturing of the NGC with distal and proximal fragments of the crossed nerve. The surgery was microsurgical: a 3.5× headband magnifier and microsurgical instruments were used.

After layer-by-layer suturing of the wound, the echogenic characteristics of the implants and their anastomoses with the nerve were assessed through ultrasound-guided percutaneous needle biopsy in the tissues with a 7.5 MHz linear ultrasound probe.

RESULTS

Three NGC variants with the following dimensions were investigated: length and diameter of samples #1 (PCL), #2 (PCL + gelatin) and #3 (PCL + collagen) were 97.9 mm and 2.3 mm, 60.4 mm and 2.5 mm, and 49.1 mm and 3.2 mm, respectively.

The stiffness (based on tactile sensation) of the dry samples decreased in the following order: #3 > #2 > ##1. When dissecting the samples with a scalpel, it was noted that they were electrified in the dry state, sticking to the tool, the first and third samples slightly disentangled.

The physical and mechanical characteristics of NGC samples are summarized in Table. As can be seen from Table, the presence of gelatin in the nerve conduit (sample #2) does not affect its elongation at break, accom-

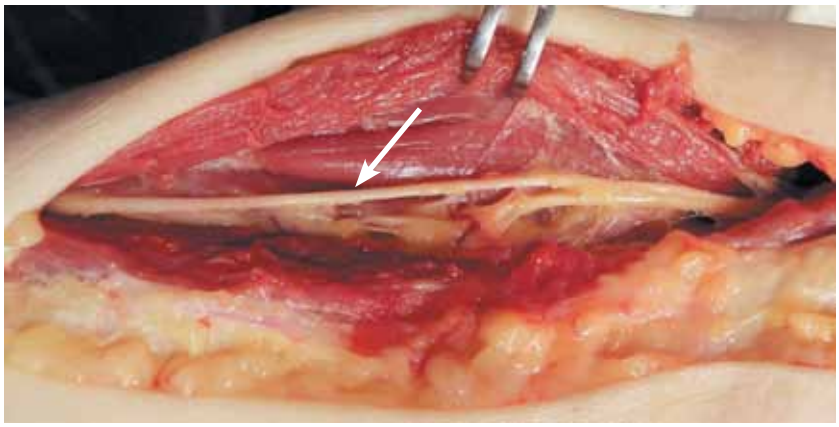

Fig. 2. Superficial sensory branch of the right radial nerve (indicated by arrow)

Table

Physical and mechanical characteristics of NGC

NGC	Young's modulus (MPa)	Tensile strength at break (N)	Elongation at break (%)
#1 (PCL)	5.5 ± 1.1	10.9 ± 1.6	477 ± 38
#2 (PCL + gelatin)	7.8 ± 2.6	24.3 ± 7.6	452 ± 32
#3 (PCL + collagen	10.5 ± 3.1	33.2 ± 6.9	357 ± 47

panied by a 30% increase in Young's modulus and a 2.5-fold increase in tensile strength at break compared to specimen #1 made of PCL. With collagen in the hybrid material (sample #3), the Young's modulus increases twice as much as that of NGC made of PCL, tensile strength at break increases 3-fold, and elongation at break decreases by 25%. Thus, introduction of gelatin and collagen increases the strength of NGC with a simultaneous slight decrease in its elasticity, especially noticeable when using a hybrid material with collagen (sample #3).

The obtained results were confirmed when assessing the resistance (rigidity) of the specimens to deformation changes. We evaluated the deformation of sample fragments, 5 mm long, in dry state under the influence of loads of different weights. Sample #1 began to deform under a load of 5 g or more. Deformation of the other two samples occurred under a 20 g weight (Fig. 3). The samples were not brittle under physical stress and did not crumble when cut with a scalpel.

To determine possible changes in the properties of the samples when interacting with various biological media and chemical compounds encountered during the operation, they were wetted: 1) in 0.5% novocaine solution; 2) 3% H_2O_2 solution; 3) in native human blood; 4) human blood plasma. Changes in the samples after 0.5, 1.0, 1.5, and 2.0 hours were assessed. All samples were gradually impregnated with solutions, becoming more elastic (based on tactile sensations). Sample #3, which is more hydrophilic in comparison with the others, was the best and fastest to be impregnated in the media. Sample #1 was the most hydrophobic. Dissolution, change of shape, significant loss of elasticity (deformation under own weight) was not noted in any of the examined samples.

Fig. 3. Assessment of stiffness and elasticity (deformation of sample #1 under a 5 g load)

We used 20-mm-long sample fragments to create anastomoses between the NGC and the nerve. Each specimen was tandemly sutured using an atraumatic needle (Prolene 6-0) to the pre-transected superficial sensory branch of the radial nerve (Fig. 4). Epineural sutures were placed on the nerve, and the NGC was sutured through its entire thickness. There were no difficulties with stitching in any of the specimens; however, sample #1 was the easiest to stitch. When creating an anastomosis, it is more convenient to inject from the epineurium side and then stitch the implant to its full thickness, with the knot better left on the outside of the nerve conduit to avoid formation of scar changes in the nerve tissue area. After wetting with novocaine solution, the specimens were easier to suture to the nerve because they became more elastic.

Permeability of the samples was assessed by filling their lumen from the neural side of the anastomosis with an aqueous solution of edible indigo carmine (Fig. 5). After dye injection, the sutures were noted to be tight, permeability of the NGC depended on the volume of the injected solution. All specimens passed the dye after some time, the most permeable being specimen #1 made of PCL.

Ultrasound imaging of the created anastomoses after layer-by-layer suturing of the wound was performed (Fig. 6). The following data were obtained during the study:– Anastomoses between the nerve and NGC spe-

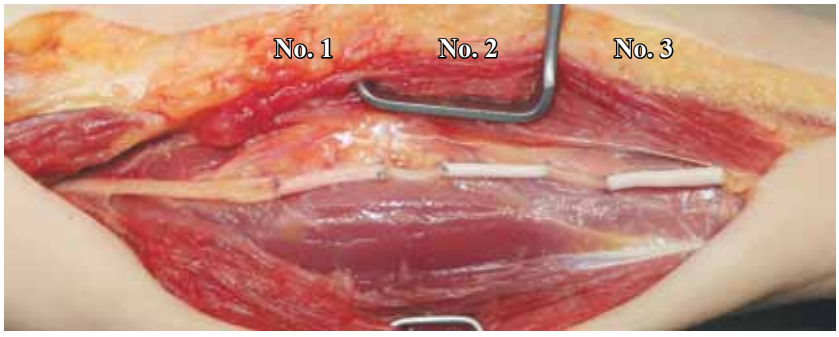

Fig. 4. Tandem anastomoses between the NGC and the superficial sensory branch of the radial nerve

cimens after soft tissue suturing was preserved in all cases;

– Echogenicity of all specimens relative to the nerve and surrounding soft tissues increased;
– Cross-sectional scanning of the implant revealed a hyperechogenic circumference, which differed from the nerve in ultrasound image;
– The NGC samples had different resistance to mechanical pressure on the surrounding tissues. Sample #1 had the lowest stiffness and elasticity – it shrank under the pressure of the ultrasound probe, flattened and did not fully recover its original rounded shape. Specimens #2 and #3 had high stiffness and elasticity, and did not change their configuration under pressure. Sample #3 was the most rigid.

DISCUSSION

NGC samples made of hybrid biomaterials (#2, PCL + gelatin; #3, PCL + collagen) are surgically suitable for creating artificial nerve conduits to repair extended peripheral nerve defects.

When hydrated, NGCs are lightweight, flexible, elastic, resilient, not brittle, porous tubes convenient for suturing to peripheral nerves. Hybrid nerve conduits are moderately hydrophilic, which *in vivo* is important to ensure cell adhesion as the initial stage of the regenerative process in the damaged nerve. Also, these samples have acceptable surgical porosity and are more preferable due to the ability to retain their shape, including when exposed to various liquid media and pressure of the surrounding tissues [16].

Surgical manipulations on the cadaveric material showed that all the presented NGC samples are convenient for surgical application (easily sutured, form tight anastomoses with the nerve, are not deformed and do not dissolve when exposed to various fluids used during surgery). The best nerve conduit composition will be selected during comparative preclinical studies of biocompatible and functional properties of hybrid material samples.

Ultrasound is the main method of monitoring the surgical restoration of the anatomical integrity of peripheral nerves: direct neurorrhaphy, autotransplantation, and

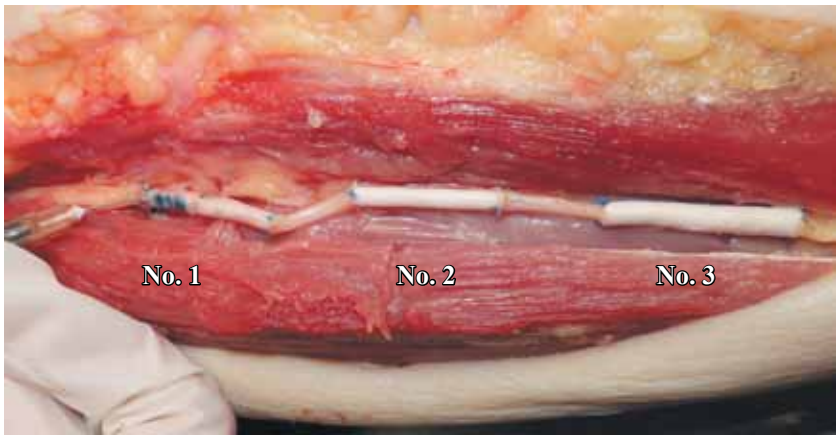

Fig. 5. Dye injection (aqueous solution of edible indigo carmine) into the NGC lumen

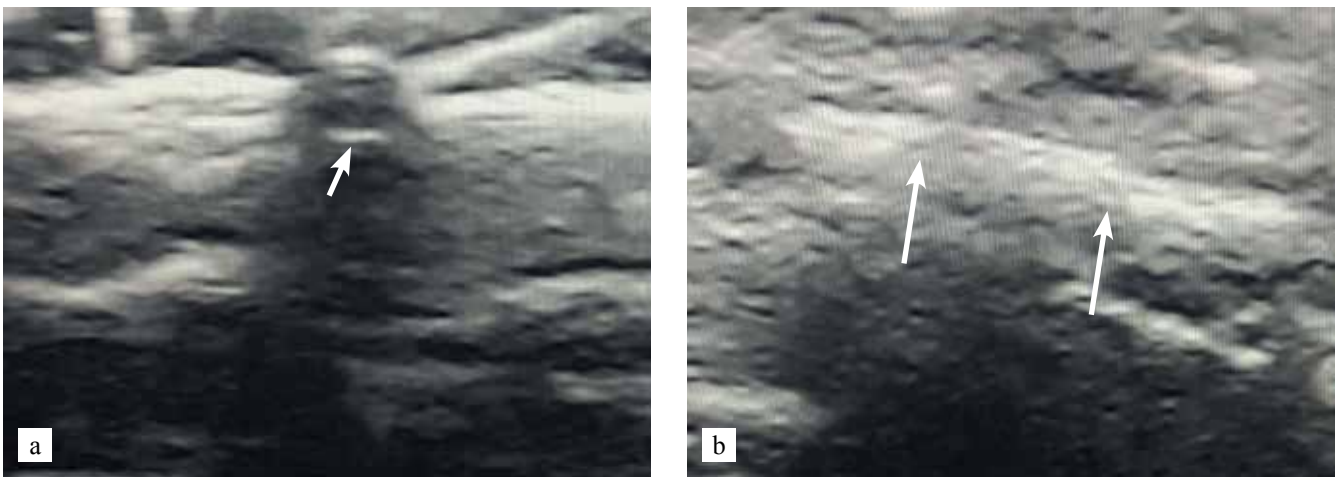

Fig. 6. Ultrasound picture of the NGC (indicated by arrows). a, cross section; b, longitudinal section

plasty using NGCs. This is due to the fact that morphological changes occurring in the postoperative period are ahead of the functional nerve, which can be assessed clinically or by electroneuromyography. To determine the adequacy of such interventions and their probable effectiveness, it is necessary to assess the formation of an end neuroma, regeneration of nerve fibers, severity of the cicatricial adhesive process in the surgical area, and anastomosis viability. In the case of NGCs, the carrying capacity of their membranes for ultrasound signal, which determines the possibility to visualize the regenerating nerve tissue in the graft lumen, is important. Creating an optimal material for NGC in terms of performing perfect ultrasound imaging is extremely difficult. By focusing only on this criterion, one will have to sacrifice more important (chemical, physical and biological) properties of NGC. Even the polyhydroxybutyrate-based membrane, which is several microns thick and used in neurosurgical practice for the prevention of cicatricial adhesions, reduces the capabilities of ultrasound imaging in the postoperative period [18].

During the reparative processes in the area of surgical intervention, the ultrasound image of prosthetic biotransformation will change over time. This is due to many factors: development of cicatricial adhesion process, neoangiogenesis, nerve fiber regeneration, and biotransformation of the NGC itself. The most important early (first 1–2 months after intervention) criterion of successful regeneration of nerve tissue, even in case of low ultrasound throughput of NGC, is the absence of terminal neuroma formation in the area of the proximal fragment of the nerve trunk involved in anastomosis. The indicated abortive regeneration sign (presence of terminal neuroma) does not depend on ultrasound characteristics of NGC materials and can be detected in all cases.

The following were limitations of NGC ultrasound assessment: not the highest degree of ultrasound imaging, and lack of possibility to assess the biotransformation of both the NGCs themselves and the surrounding tissues over time *in vivo*. Finding the optimal material for the NGC is a crucial step towards creating an effective peripheral nerve prosthesis, which can be a good alternative to the autograft. The advantage of using NGC in clinical practice is that the procedure of nerve extraction from the patient (in autografting) and the resulting complications at the donor site are eliminated, surgical time is reduced, and the intervention becomes simpler. Numerous studies show that the possibility of functional recovery when using NGC is equivalent to autotransplantation and direct nerve suturing in an experiment [19, 20].

CONCLUSION

The physical and mechanical properties of NGCs made of PCL and PCL-based hybrid biomaterials were investigated, and the technical feasibility of their surgical use to promote directional nerve growth and repair was studied. NGC samples consisting of hybrid materials showed fundamental biomechanical suitability for use in surgical practice to eliminate peripheral nerve defects.

The authors declare no conflict of interest.

REFERENCES

1. *Margasov AV.* Aktual'nye problemy travmy perifericheskih nervov. *RMZh*. 2018; 12 (1): 21–24.
2. *Goven'ko FS.* Hirurgija povrezhdenij perifericheskih nervov. SPb.: Feniks, 2010. 384.
3. *Sholomov II, Kireev SI, Levchenko KK*. Sostojanie nervno-myshechnogo apparata u bol'nyh s povrezhdenijami kljuchicy, kostej plechevogo pojasa i proksimal'nogo otdela plecha. *Prakticheskaja nevrologija i nejroreabilitacija*. 2008; 3: 16–18.
4. *Kuffler DP, Foy C.* Restoration of Neurological Function Following Peripheral Nerve Trauma. *International Journal of Molecular Sciences*. 2020; 21 (5): 1808.
5. *Houshyar S, Bhattacharyya A, Shanks R.* Peripheral Nerve Conduit: Materials and Structures. *ACS Chemical Neurosclence*. 2019; 16 (11): 52.
6. *English AW, Wilhelm JC, Ward PJ.* Exercise, neurotrophins, and axon regeneration in the PNS. *Physiology (Bethesda)*. 2014; 29: 437–445.
7. *Piao CD, Yang K, Li P, Luo M.* Autologous nerve graft repair of different degrees of sciatic nerve defect: stress and displacement at the anastomosis in a three-dimensional finite element simulation model. *Neural regeneration res*. 2015; 10 (5): 804–807.
8. *Millesi H, Meisl G, Berger A*. Further experience with interfascicular grafting of the median, ulnar, and radial nerves. *J Bone Joint Surg*. 1976; 58 (2): 209–218.
9. *Kehoe S, Zhang XF, Boyd D*. FDA approved guidance conduits and wraps for peripheral nerve injury: a review of materials and efficacy. *Injury*. 2012; 43 (5): 553–572.
10. *Chrząszcz P, Derbisz K, Suszyński K, Miodoński J, Trybulski R, Lewin-Kowalik J et al.* Application of peripheral nerve conduits in clinical practice: a literature review. Neurol. Neurochir. Pol. 2018; 52: 427–435.
11. *Miroshnikova PK, Lyundup AV, Bacalenko NP, Krasheninnikov ME, Zang Yu, Fel'dman NB, Beregovyh VV.* Perspektivnye nervnye konduity dlya stimulyacii regeneracii povrezhdennyh perifericheskih nervov. *Vestnik RAMN*. 2018; 73 (6): 388–400. doi: 10.15690/vramn1063.
12. *Velichanskaya AG, Abrosimov DA, Bugrova ML, Kazakov AV, Pogadaeva EV, Radaev AM et al*. Reconstruction of the rat sciatic nerve by using biodegradable and non-biodegradable conduits. *Sovremennye tehnologii v medicine*. 2020; 12 (5): 48–56. https://doi.org/10.17691/stm2020.12.5.05.

13. *Liu D, Mi D, Zhang T, Zhang Y, Yan J, Wang Y et al.* Tubulation repair mitigates misdirection of regenerating motor axons across a sciatic nerve gap in rats. *Sci Rep*. 2018; 8: 3443.
14. *Du J, Jia X.* Engineering nerve guidance conduits with three-dimenisonal bioprinting technology for long gap peripheral nerve regeneration. *Neural Regen Res*. 2019; 14: 2073.
15. *Goulart CO, Pereira Lopes FR, Monte ZO, Dantas SV, Souto A, Oliveira JT et al.* Evaluation of biodegradable polymer conduits – poly(l-lactic acid) – for guiding sciatic nerve regeneration in mice. *Methods*. 2016; 99: 28–36.
16. *Fornasari BE, Carta G, Gambarotta G, Raimondo S.* Natural-Based Biomaterials for Peripheral Nerve Injury Repair. *Front Bioeng Biotechnol*. 2020; 16 (8): 554257.
17. *Nemets EA, Surguchenko VA, Belov YuV, Xajrullina AI, Sevastianov VI.* Porous Tubular Scaffolds for Tissue Engineering Structures of Small Diameter Blood. *Inorganic Materials: Applied Research*. 2023; 14 (2): 400–407.
18. *Fedjakov AG, Dreval' ON, Kuznecov AV, Sevast'janov VI, Perova NV, Nemec EA et al.* Jeksperimental'noe obosnovanie primenenija gelevogo implantata "Sfero®Gel'" i plenochnogo implantata "JelastoPOB"® pri travme perifericheskoj nervnoj sistemy v jeksperimente. *Vestnik transplantologii i iskusstvennyh organov*. 2009; 11 (4): 75–80.
19. *Krarup C, Isben A, Boeckstyns M et al.* Effects of a Collagen Nerve Guide Tube in Patients With a Median or Ulnar Nerve Lesion. *American Association for Hand Surgery Annual Meeting*. 2011; 99.
20. *Archibald SJ, Shefner J, Krarup C et al.* Monkey Median Nerve Repaired by Nerve Graft or Collagen Nerve Guide Tube. *J Neurosci*. 1995; 15 (5): 4109–4123.

The article was submitted to the journal on 06.04.2023

DOI: 10.15825/1995-1191-2023-2-107-117

INTRAPERITONEAL INJECTION OF CELL-ENGINEERED PANCREAS IN RATS WITH EXPERIMENTAL TYPE I DIABETES (PRELIMINARY RESULTS)

A.S. Ponomareva, N.V. Baranova, A.O. Nikolskaya, L.A. Kirsanova, N.A. Onishchenko, Z.Z. Gonikova, G.N. Bubentsova, E.A. Volkova, Yu.B. Basok, V.I. Sevastianov

Shumakov National Medical Research Center of Transplantology and Artificial Organs, Moscow, Russian Federation

Creation of a bioartificial pancreas, including a cell-engineered construct (CEC) formed from pancreatic islets (islets of Langerhans) and a biocompatible matrix mimicking the native microenvironment of pancreatic tissue, is one of the approaches to the treatment of type 1 diabetes mellitus (T1D). **Objective:** to conduct preliminary *in vivo* studies of the functional efficacy of intraperitoneal injection of a cell-engineered pancreatic endocrine construct and a suspension of rat pancreatic islets in an experimental T1D model. **Materials and methods.** Tissue-specific scaffold was obtained by decellularization of human pancreatic fragments. The viability and functional activity of rat islets isolated with collagenase were determined. Experimental T1D was modeled by intraperitoneal injection of low-dose streptozotocin and incomplete Freund's adjuvant into rats. The rats were intraperitoneally injected twice with pancreatic CEC (n = 2) or islet suspension (n = 1). Glucose levels in the blood and urine of the rats were assessed. Histological examination of organs (pancreas and kidneys) of the experimental animals was carried out. **Results.** After the first injection, blood glucose levels gradually decreased in all animals by more than 47% of the initial values; by follow-up day 24, the glucose level rose to the initial hyperglycemic values. After repeated administration, a 63.4% decrease in glycemic level was observed in the rats with pancreatic CEC and a 47.5% decrease in the one with islet suspension. At week 5 of the experiment, blood glucose levels gradually increased in all animals. At the same time, the glycemic index of the rat with injected pancreatic CEC was 62% lower than the glycemic index of the rat with injected islets. **Conclusion.** Allogeneic pancreatic islets in pancreatic CEC increase the duration of stable glycemic level in T1D rats.

Keywords: pancreas, islets of Langerhans, cell-engineered construct, tissue-specific scaffold, diabetes model.

1. INTRODUCTION

T1D is an autoimmune disease characterized by critical loss of insulin-producing beta cells. Treatment of T1D with cell therapy seems promising. The current method of treatment of severe T1D islets is pancreatic islet transplantation according to the Edmonton Protocol [1–4], which requires a significant mass of islets from several donors [5]. After transplantation, the risk of diabetes complications is reduced, the number of hyperglycemic episodes is reduced, and in some cases complete insulin-independence is achieved [6, 7].

However, the problem of organ shortage and the limited functioning time of islets *in vivo* stimulates the search for tissue engineering and regenerative medicine technologies aimed at long-term preservation of their viability and functional activity. In the process of isolation, cultivation and transplantation, islets lose vascularization, innervation, and connection to extracellular matrix (ECM), which makes them even more susceptible to oxidative stress [8]. In addition, post-transplant islet damage is associated with immediate blood-mediated inflammatory responses, immune response, hypoxia and toxic effects of immunosuppressants [9–11].

At present, improvement of biotechnological methods gives hope for promising application of technologies based on creation of a tissue equivalent of the pancreatic endocrine, formed on the basis of insulin-producing cell components preserving long-term viability and functional activity and biocompatible matrix that provides them with the best conditions. The advantage of using islets in the creation of a tissue equivalent of pancreas over insulin-producing cells of other origin is that beta cells retain paracrine connections with all types of islet cells [12].

ECM components are important components of the pancreatic tissue equivalent, preventing cellular stress and contributing to preservation of islet viability and function. Biomatrices with ECM components are universal platforms for creating a tissue equivalent, as they provide structural and mechanical support to islets, serve

Corresponding author: Anna Ponomareva. Address: 1, Shchukinskaya str., Moscow, 123182, Russian Federation. Phone: (499) 196-26-61; (926) 585-23-73. E-mail: a.s.ponomareva@gmail.com

as a reservoir of growth factors, cytokines, antioxidants, and transmit signals to islet cells via integrins [13–15].

Previously, studies of biomatrices for pancreatic tissue equivalents have focused on artificial construction of scaffolds similar to the native pancreatic ECM, but none of them could accurately mimic the complexity of the actual ECM composition and structure [16–18].

Buitinga et al [19] reported that allogeneic islets transplanted on a porous scaffold platform to mice with experimental T1D were able to restore stable normoglycemia compared to islets transplanted without a scaffold. It was shown that when cultured on collagen-containing matrices for a long time after isolation, the islets remained viable and exhibited secretory activity [20, 21]. Transplantation of islets cultured on such matrices became more successful [22].

Recently, pancreatic decellularization technologies have been used as an alternative to obtaining a matrix with preserved features of pancreatic tissue structure and composition. When developing the protocols for obtaining tissue-specific decellularized scaffold, it is important to consider the preservation of native ECM components: structural proteins, glycoproteins and cell adhesion factors for its functional activity while removing DNA to minimize immune response during implantation of the pancreatic tissue equivalent [23–27].

It was found that islets cultured in the presence of tissue-specific scaffold from decellularized pancreas enhanced insulin secretion compared to isolated islets in monoculture [28, 29]. Wu et al [30] showed on an experimental T1D model that the pancreas tissue, recellularized by a population of insulin-producing cells, is able to control blood glucose levels in mice compared to the same cells cultured on Petri dishes.

We have previously described approaches to obtaining tissue-specific matrices from decellularized rat [31] and human [28] pancreas, showing preservation of structure, prolongation of viability and function of islets cultured with tissue-specific scaffold compared to islets cultured without biomatrix.

Thus, the *in vitro* functionality of the pancreatic tissue equivalent *in vitro* is directly related to preservation of the cellular component comprising it, which may ultimately be of crucial importance *in vivo* [32].

The **objective** of this work was to carry out preliminary *in vivo* studies of the functional efficacy of pancreatic CEC and isolated rat pancreatic islets when administered intraperitoneally to diabetic rats.

2. MATERIALS AND METHODS

2.1. Experimental animals

Experiments were carried out on male Wistar rats obtained from the laboratory animal nursery belonging to KrolInfo Ltd. A veterinary certificate confirming the absence of infectious diseases in the farm was presented. Acclimatization and maintenance of the laboratory animals were done in accordance with the interstate standard GOST ISO 10993-2-2009 "Medical products. Evaluation of biological effect of medical products." Part 2. "Requirements for the treatment of animals."

All manipulations with animals were performed in compliance with the bioethical principles approved by the European Convention for the Protection of Vertebrate Animals used for Experimental and other Scientific Purposes, 2005, and in accordance with the Rules of Laboratory Practice, approved by the Ministry of Health of Russia, No. 708 on August 23, 2010. A report on approval of experimental studies was received from the local ethics committee of Shumakov National Medical Research Center of Transplantology and Artificial Organs, dated January 28, 2021, Protocol No. 280121-1/1e.

2.2. Experimental type I diabetes model

T1D was modeled according to a known proprietary method on male Wistar rats for 16 days (Table 1) by intraperitoneal injection of low-dose streptozotocin every 7 days [33]. Streptozotocin was administered after 12 hours of fasting; the dose of the drug was determined at the rate of 25 mg/kg of animal body weight in the first injection, 20 mg/kg in the second injection, and 25 mg/kg in the third injection. To induce autoimmune inflammation, the animals were intraperitoneally injected 1 mL of incomplete Freund's adjuvant three times a day before each streptozotocin injection.

The animals were observed daily, their physical appearance was assessed, and the amount of water consumed by them was measured. Every week, we measured blood and urine glucose levels on an empty stomach, and monitored the dynamics of weight changes. Rats whose high glycemic level remained stable for two weeks were selected for further study.

2.3. Technology for obtaining tissue-specific scaffold from decellularized pancreatic tissue

To form a pancreatic tissue equivalent, a tissue-specific finely dispersed matrix was chosen as an ECM biomi-

Table 1

Scheme for TID modeling

Day	1	2	…	8	9	…	15	16
Injection of streptozotocin		25 mg/kg			20 mg/kg			25 mg/kg
Injection of incomplete Freund's adjuvant	1 mL			1 mL			1 mL	

metic, obtained by decellularization of human pancreas fragments (DHP scaffold) according to a protocol developed earlier [28]. The studies showed that DHP scaffold retains morphofunctional properties of the native ECM of pancreatic tissue, contains basic fibrillar proteins (type I collagen, elastin), has low immunogenicity (≤0.1% DNA), is not cytotoxic with respect to adhesion and proliferation of cell cultures [28].

The experimental studies were approved by the local ethics committee, Shumakov National Medical Research Center of Transplantology and Artificial Organs, dated March 16, 2018, Protocol No. 160318-1/1e. It was for the development of the technology for obtaining and studying tissue-specific matrices.

2.4. Isolation, identification and cultivation of rat pancreatic islets

Islets were isolated from the pancreas of male Wistar rats (Pr). They were subjected to inhalation euthanasia using Isoflurane (Kariozo Laboratories, Spain), and then the islets were excised under sterile conditions and immediately placed in a Petri dish with cold (+4 °C) Hanks' Balanced Salt Solution (HBSS) without Ca^{2+} and Mg^{2+} ions (Thermo Fisher Scientific, USA) containing amphotericin B. All further manipulations requiring sterility were performed in a laminar flow hood providing sterile air flow.

We injected 2 mL of collagenase NB 1 solution (activity 20 PZ U/g tissue) with neutral protease NP (activity 1.5 DMC U/g tissue) (Serva, Germany) intraparenchymatously into the pancreatic tissue by successive injections. Pr stretched tissue, without cutting, was carefully separated into 10–12 approximately equal parts with microtweezer, transferred into a vial, and incubated for 7–10 minutes in an orbital shaker incubator (Biosan, Latvia) at 37.0 °C with a rotation speed of 150 rpm. The action of collagenase was stopped by adding cold (+4 °C) HBSS. The formed small fragments were filtered through a 100 μm cell strainer (Corning-Costar, USA); the filtrate was collected into conical tubes, and centrifuged for 1 minute at 800 rpm. The supernatant was washed twice with fresh HBSS for 1–1.5 minutes at 1200–1300 rpm to obtain an islet suspension.

Islets were identified by dithizone staining (Sigma-Aldrich, USA) immediately after isolation. For this purpose, part of the suspension was mixed with dithizone solution (1 mg/mL) in a 2 : 1 volume ratio and incubated for 20–30 minutes at 37 °C.

Freshly isolated islets were resuspended in complete growth medium containing DMEM (glucose 1.0 g/L) (PanEco, Russia), 10% fetal calf serum (HyClone, USA), Hepes (Thermo Fisher Scientific, USA), 2 mM alanyl glutamine (PanEco, Russia), 1% antibiotic/antimycotic (Thermo Fisher Scientific, USA), were added to culture vials and cultured for 24 hours under standard conditions at 37 °C in a CO_2 incubator in a humidified atmosphere containing 5% CO_2.

2.5. Assessment of viability and functional activity of pancreatic islets

The viability of islets cultured for 24 hours was determined by fluorescent acridine orange/propidium iodide (AO/PI) staining (PanEco, Russia).

For staining, a portion of the islet suspension was placed in a Petri dish, mixed with the prepared working dye solution in a volume ratio of 2 : 1, and incubated in the dark for 15–30 minutes. Viable islets were counted using a Nikon Eclipse 50i fluorescent microscope (Nikon, Japan) at 10× magnification.

To determine the functional activity of islets after 24 hours of cultivation, insulin content was measured under the influence of a traditional hormone secretion stimulant. For this purpose, the growth medium was replaced with a fresh medium with a low glucose content of 1.0 g/L (2.8 mmol/L). After a 60-minute incubation under standard conditions, culture medium was sampled. The growth medium was then removed and replaced with fresh medium with a high glucose concentration of 4.5 g/L (25 mmol/L). After 60 minutes of incubation under standard conditions, the culture medium was also sampled (2 samples for each culture period) for enzyme-linked immunosorbent assay (ELISA) using Rat Insulin ELISA Kit (Thermo Fisher Scientific, USA).

2.6. Obtaining a cell-engineered pancreatic construct

A purified suspension of cultured islets was used as the cellular insulin-producing component of the pancreatic CEC. The islet suspension was obtained by centrifugation in a growth medium for 2 minutes at 1200 rpm, then purified in HBSS under the same regime.

For each pancreatic CEC sample, 2000 islets were selected, obtained from an average of 1.5 rat donor pancreas, resuspended in 1.0–1.2 mL of HBSS, and mixed with finely dispersed sterile DHP scaffold (10.0 ± 0.1 mg) from human pancreas.

The resulting pancreatic CEC sample was placed in a syringe with a 23 G needle size just before administration to recipient rats.

2.7. Intraperitoneal injection of cell-engineered pancreatic construct and islets of Langerhans

Three rats with severe and stable autoimmune T1D were selected for corrective therapy: a pancreatic CEC sample (2000 allogeneic islets of Langerhans with DHP scaffold) was injected intraperitoneally into the lower third of the abdomen of rats 1 and 3; rat 2 received 2000 allogeneic pancreatic islets in the form of a suspension.

All animals were observed for more than 12 weeks. The amount of water consumed by them was monitored daily. Body weight was monitored weekly, blood and urine glucose levels were determined. Capillary glycemic level was measured on an empty stomach weekly using Accu-Check Active glucose meter (Roche, Switzerland). All manipulations were performed in the morning hours (between 9 a.m. and 12 p.m.). The levels of glucose and ketone bodies in the urine were evaluated using Ketogluc-1 indicator strips (Biosensor AH, Russia).

2.8. Histological examination

The extracted pancreas and kidneys of all experimental animals were fixed in 10% neutral buffered formalin (NBF), dehydrated in alcohols of ascending concentration, then incubated in a chloroform/ethanol mixture, then transferred to chloroform and embedded in paraffin blocks.

Slices, 5 μm-tick, were obtained using an RM2245 microtome (Leica, Germany) and further stained with hematoxylin and eosin (H&E) and with Masson's trichrome for total collagen content. Immunohistochemical staining of main islet cell types was performed using antibodies to insulin and glucagon (Abcam, UK) and the Rabbit Specific HRP|DAB (ABC) Detection IHC kit imaging system (Abcam, UK).

2.9. Statistical analysis

Microsoft Excel software (2016) was used to perform statistical data processing. Student's t test was used to determine the statistical significance of differences in the mean between the samples when assessing the functional activity of the islets of Langerhans of healthy rats (insulin content in culture medium during glucose stimulation). The differences were considered statistically significant at $p < 0.05$.

3. RESULTS AND DISCUSSION

3.1. Experimental type I diabetes model

Four diabetic rats with fasting blood glucose – 15.8; 26.7; 28.1; 18.6 mmol/L – were selected for the experiment. Significant loss of body weight (from 350 g to 260 g), hypodynamia, non-healing wounds on the tail, yellowing of hair, thinning of hair, polyuria, and marked polydipsia were noted in the animals. Each animal consumed an average of 209 ± 6 mL of water per day – a healthy rat drinks 14 ± 3 mL of water/day.

Histological examination of rat pancreas samples with glycemic level of 18.6 mmol/L revealed changes in both exocrine parenchyma and pancreatic islets compared with the morphological picture of a healthy animal (Fig. 1, a–c). In the parenchyma, some lobules underwent dystrophic changes, and up to necrosis in some cases. Infiltration by inflammatory cells was observed in the islets: polymorphonuclear leukocytes and solitary macrophages were detected in the islet thickness and along its perimeter. Vacuolated and necrotized insulocytes were detected in the center of the islet, the shape of the islet also changed (Fig. 1, d). Immunohistochemical staining with antibodies to insulin was negative, which confirmed the death of beta cells (Fig. 1, e), while glucagon-positive cells in the islets were preserved (Fig. 1, f). The results

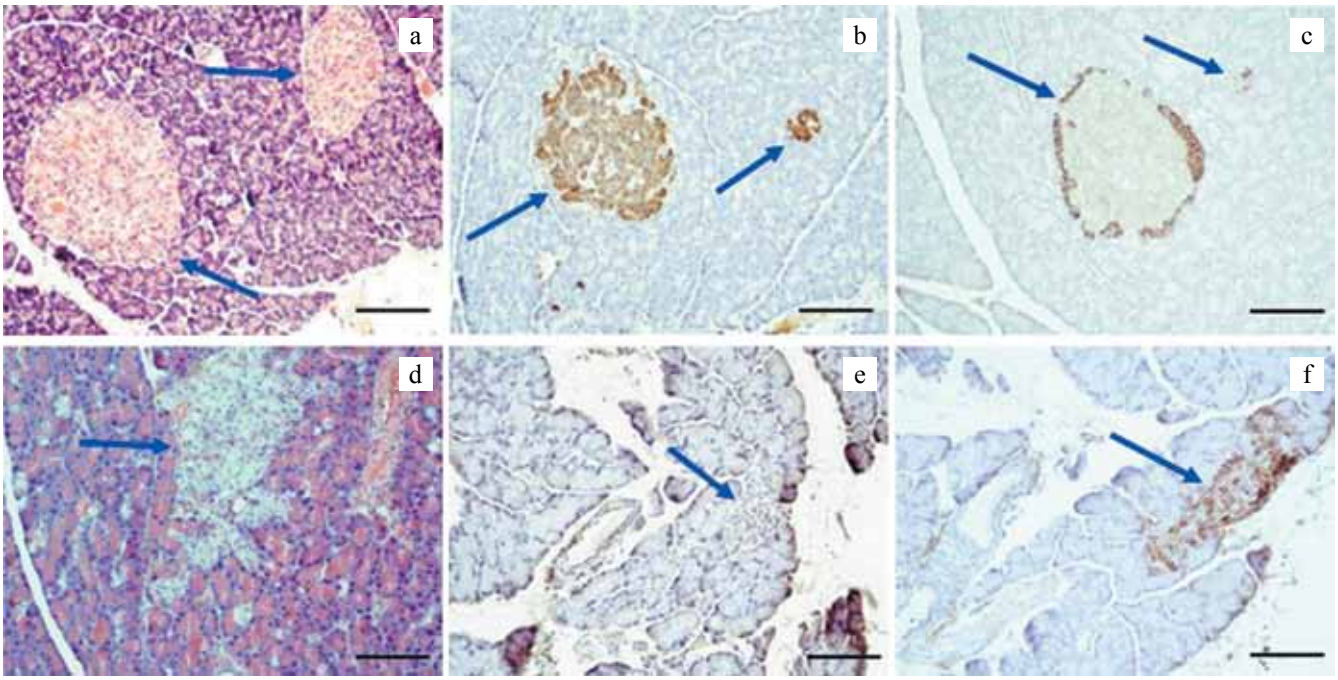

Fig. 1. Rat pancreas. a–c, healthy rat; d–f, rat with experimental T1D; a and d, H&E stain; b and e, insulin immunohistochemical staining; c and f, glucagon immunohistochemical staining. Arrows indicate pancreatic islets. Scale bar = 100 μm

obtained may indicate the effectiveness of the T1D induction model.

3.2. Viability and functional activity of isolated pancreatic islets

A large proportion of freshly isolated islets were round or oval in shape and mostly retained their integrity, indicating that the macrostructure of the islets was not damaged during isolation (Fig. 2, a). Dithizone selectively stained the pancreatic islets red-orange, while the acinar cells remained unstained (Fig. 2, b).

A day after isolation, the rat pancreatic islets were stained with vitamin dye to determine their viability. It was found that more than 95% of the islets remained viable (Fig. 2, c).

The functional activity (presence of hormonally active beta cells) of cultured islets was confirmed by the results of culture fluid samples taken at day 1 after incubation before and after stimulation with "hyperglycemic" glucose level of 4.5 g/L (25 mmol/L) (Fig. 3). The pre- and post-stimulation insulin levels in the samples were 185.4 ± 16.4 μIU/mL and 251.7 ± 16.6 μIU/mL, respectively, a 35.8% increase.

3.3. Results of intraperitoneal injection of pancreatic cell-engineered construct and islets of Langerhans

Animal follow-up continued for 87 days after the first injection of pancreatic CEC in rats 1 and 3 and islet suspension in rat 2 (Fig. 4, Table 2). Pancreatic CEC and islet suspension were reintroduced on day 24 of the experiment. Rat 1 was removed from the experiment on day 65 for histological analysis of the pancreas condition.

On day 5 after intraperitoneal injection of pancreatic CEC, glycemic level in rats 1 and 3 decreased by 28.5% and 23.5% from the initial values, respectively, while that in rat 2 (administration of islet suspension) decreased by 13.9%. On day 10, the glycemic level in rat 1 reached a minimum value of 9.2 mmol/L (65.5% decrease). In rat 3, the minimum glucose level was 14.7 mmol/L (47.7% decrease) by day 17 of follow-up. In rat 2, in the first 3 weeks after pancreatic CEC injection, glycemic levels reached its lowest level (a 48.1% decrease) on day 17.

On day 24, all the rats witnessed a sharp rise in glucose levels. So, it was decided to re-inject pancreatic CEC and islet suspension in the same animals. One week later, all rats had a sharp decrease in glycemic levels,

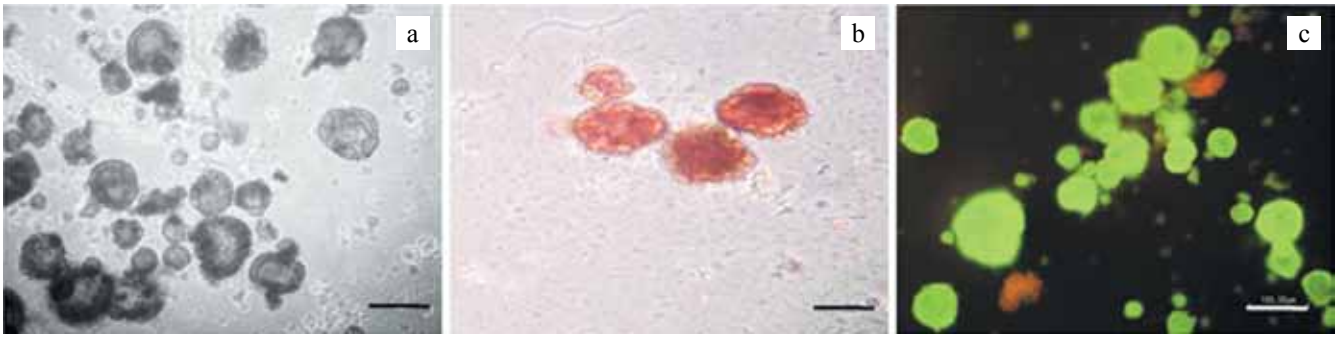

Fig. 2. Isolated rat pancreatic islets. a, light microscopy without staining; b, dithizone staining; c, islets cultured for 24 hours, acridine orange/propidium iodide (AO/PI) staining. Scale bar = 100 μm

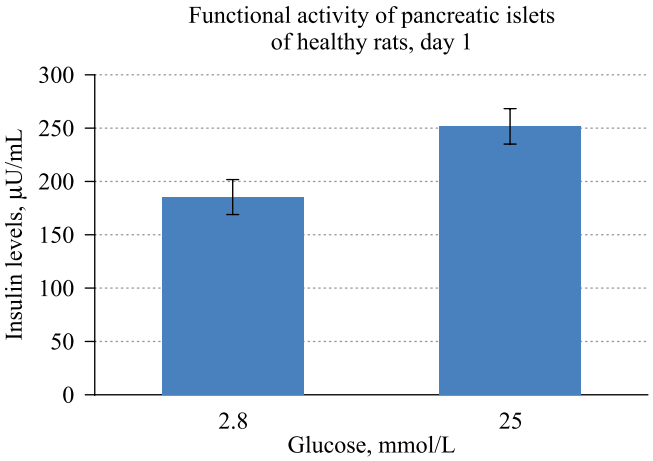

Fig. 3. Comparative analysis of insulin levels before and after glucose stimulation of cultured 1-day isolated rat pancreatic islets

decreasing by 47.5% in rat 2 and by 65.5% and 61.2% in rats 1 and 3, respectively.

Over the next 3 weeks, glycemic levels in rat 1 continued to fall, reaching 4.2 mmol/L by day 52, then gradually increasing. At the time rat 1 was withdrawn from the experiment (day 65), its blood sugar level was 11.7 mmol/L.

At these time periods up to day 87, rat 3 showed slight fluctuations in blood sugar levels with a tendency to increase (from 10.9 to 16.9 mmol/L).

In rat #2, we observed an unstable glycemic level up to day 73, then there was a return to the initial blood glucose concentrations (above 20 mmol/L), and an excess by 34.8% over the initial values. By day 87, the glucose level in rat 3 was 62% lower than that in rat 2.

After the first intraperitoneal injection, there was a decrease in urine glucose levels, which correlated with blood glucose levels in all animals. However, urine glucose concentration by day 24 increased sharply to the maximum (Table 3). On repeated administration, a significant decrease in urine glucose was observed in all rats up to day 65, with rat 1 having no glucose in its urine for 3 weeks, while blood normoglycemia was stable (4.2–6.7 mmol/L). After 65 days, rat 1 had a sharp jump in urine sugar levels with some increase in blood sugar (11.7 mmol/L). This was the reason for removing the animal from the experiment to evaluate the condition of the pancreas and kidneys. In rat 3, urine glucose levels fell to 2.8 mmol/L, and then it gradually increased. Rat 2 also had a short-term decrease in urine glucose levels, followed by an increase to 112 mmol/L by day 87, which in turn correlated with blood sugar levels.

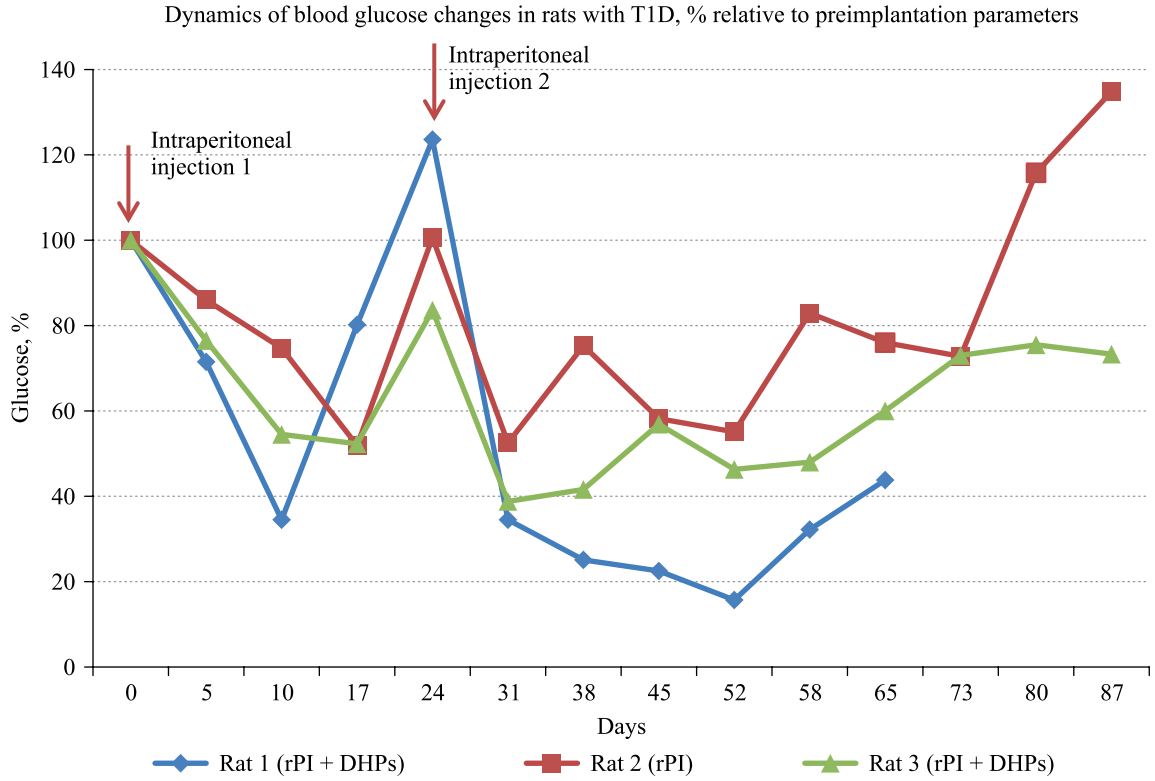

Fig. 4. Changes in blood glucose levels in rats with T1D model after intraperitoneal injection of cell-engineered pancreatic construct or islet suspension. rPI, rat pancreatic islets; DHPs, decellularized human pancreas scaffold

Table 2

Changes in blood glucose levels in the experimental animals

Day	Rat 2 (rPI), blood glucose, mmol/L	Rat 1 (rPI + DHPs), blood glucose, mmol/L	Rat 3 (rPI + DHPs), blood glucose, mmol/L
0 (injection 1)	15.8	26.7	28.1
5	13.6	19.1	21.5
10	11.8	9.2	15.3
17	8.2	21.4	14.7
24 (injection 2)	15.9	33.0	23.5
31	8.3	13.3	10.9
38	11.9	9.2	11.7
45	9.2	6.7	16.0
52	8.7	6.0	13.0
58	13.1	4.2	13.5
65	12.0	8.6	16.9
73	11.5	11.7	25
80	18.3	–	21.2
87	21.3	–	20.6

Evaluation of the content of ketone bodies in the urine of the animals revealed a decrease in ketone from 1.5 mmol/L to 0.5 mmol/L in all the three experimental rats.

After intraperitoneal injection of pancreatic CEC or islet suspension, all animals reduced their drinking water consumption from 209 ± 16 mL/day to 151 ± 11 mL/day. There was also a 30–40 g increase in body weight, healing of wounds on the tail, and restoration of hair structure and color.

Morphological analysis of pancreas and kidney samples revealed no differences in the organs of the three rats. No immunopositive beta cells were detected in the pancreas, both directly in the islets and in the pancreatic parenchyma as a whole (Fig. 5, a). This indicated the absence of regenerative processes and of the induction

Table 3

Changes in urine glucose levels in the experimental animals

Day	Rat 2 (rPI), urine glucose, mmol/L	Rat 1 (rPI + DHPs), urine glucose, mmol/L	Rat 3 (rPI + DHPs), urine glucose, mmol/L
0 (injection 1)	14–28	14–28	28–56
5	14	14	28
10	14–28	5.6	14
17	14–28	2.8–5.6	2.8
24 (injection 2)	56–112	112	56–112
31	2.8–5.6	5.6–14	2.8–5.6
38	2.8–5.6	5.6–14	2.8
45	14	0	14–28
52	5.6–14	0–2.8	14–28
58	14–28	0–2.8	14
65	14–28	112	5.6–14
73	28	–	14–28
80	14–56	–	28
87	56–112	–	28–56

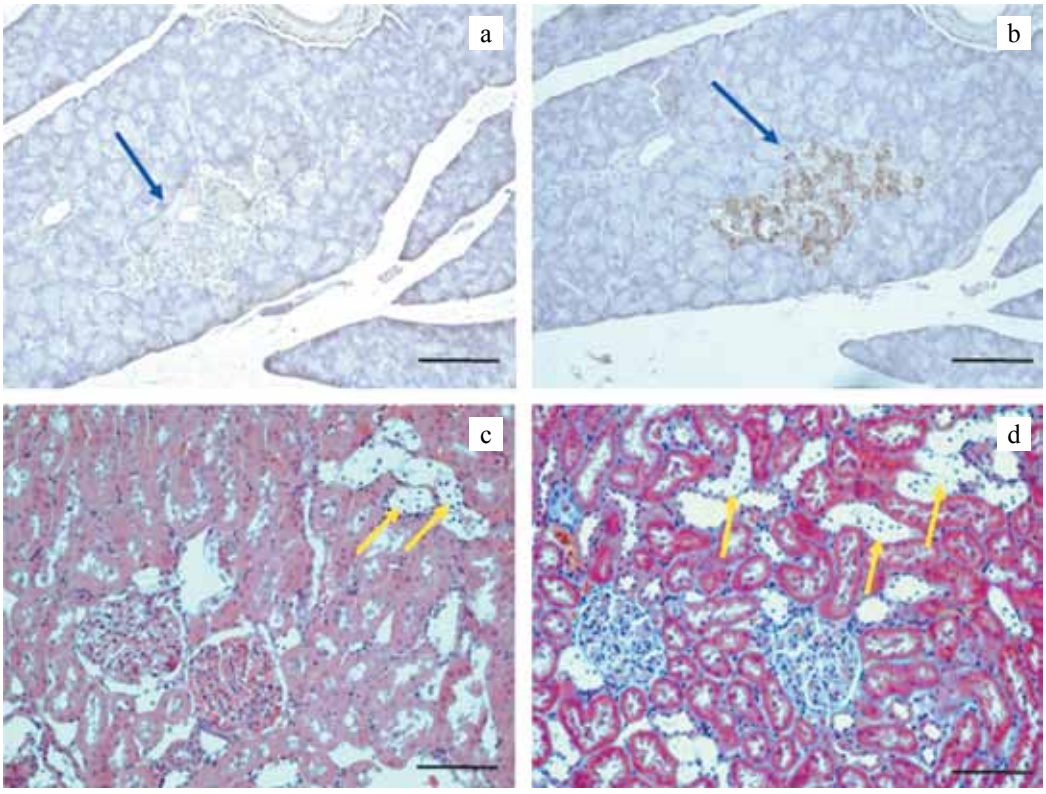

Fig. 5. Pancreas (a, b) and kidney (c, d) of experimental rats. a, no insulin positive beta cells in the islet; b, glucagon positive alpha cells in the islet; c, H&E stain; d, Masson's trichrome stain. Blue arrows indicate islets of Langerhans, yellow arrows indicate Armanni–Ebstein cells in tubular epithelium. Scale bar = 100 μm

effect of the transplanted islets on progenitor cells. At the same time, glucagon-positive alpha cells were clearly detected in the islets (Fig. 5, b). In histological preparations of the kidney, there were no marked degenerative changes in the vascular and tubular apparatus. At the same time, numerous vacuolated cells were detected in the tubule epithelium. We believe that these are the so-called Armanni–Ebstein cells, which are considered to be pathognomonic in diabetes mellitus (Fig. 5, c, d).

In tissue engineering and regenerative medicine, one can distinguish two mechanisms of CEC action *in vivo*, which underlie two approaches to the treatment of pathological organ conditions [34]:

– Stimulation of internal (physiological) regeneration of damaged tissue structures;
– Partial or complete temporary replacement of the functions of the damaged tissue structures.

This also applies to pancreatic CEC, in which tissue-specific scaffolds provide pancreatic islets with a longer survival time and efficient functioning *in vivo.*

Analysis of the results suggests that decreased glycemic level is not due to stimulation of the regeneration (restoration) of beta cells in the native islets, but due to the functional efficiency of allogeneic islets. At the same time, intraperitoneal injection of pancreatic CEC achieved a more pronounced antidiabetic effect in T1D rats compared to intraperitoneal injection of islet suspension.

CONCLUSION

From preliminary results obtained in the experimental T1D model, intraperitoneal injection of pancreatic CEC (xenogeneic tissue-specific scaffold in combination with allogenic islets of Langerhans) can be assumed to result in a significantly greater decrease in blood glucose concentration in rats compared to the islet suspension. Repeated intraperitoneal injection of pancreatic CEC and islet suspension increases the duration of stable glucose levels, but probably does not induce regenerative regeneration of pancreatic islet tissue.

It should be noted that, firstly, to confirm or refute the results obtained, experiments on a sufficient sample of animals are required in order to get statistically significant results. Secondly, the mechanism of hypoglycemic effect of allogeneic islets may depend on the localization site of pancreatic CEC and islet suspension. Apart from intraperitoneal administration, it is necessary to investigate in the T1D experimental model the functional effect of islets when they are transplanted as a suspension or implanted as part of CEC, for example, into the spleen, mesentery, omentum, or under the kidney capsule.

The authors declare no conflict of interest.

REFERENCES

1. *Fiorina P, Shapiro AM, Ricordi C, Secchi A.* The clinical impact of islet transplantation. *Am J Transplant*. 2008; 8: 1990–1997.
2. *Shapiro AM, Lakey RT, Ryan EA, Korbutt GS, Toth E, Warnock GL et al.* Islet transplantation in seven patients with type 1 diabetes mellitus using a glucocorticoid-free immunosuppressive regimen. *N Engl J Med*. 2000; 343 (4): 230–238. doi: 10.1056/NEJM200007273430401.
3. *Hering BJ, Clarke WR, Bridges ND, Eggerman TL, Alejandro R, Bellin MD et al.* Phase 3 trial of transplantation of human islets in type 1 diabetes complicated by severe hypoglycemia. *Diabetes Care*. 2016; 39 (7): 1230–1240. doi: 10.2337/dc15-1988.
4. *Barton FB, Rickels MR, Alejandro R, Hering BJ, Wease S, Naziruddin B et al.* Improvement in outcomes of clinical islet transplantation: 1999–2010. *Diabetes Care*. 2012; 35 (7): 1436–1445. https://doi.org/10.2337/dc12-0063.
5. *Ryan EA, Paty BW, Senior PA, Bigam D, Alfadhli E, Kneteman NM et al*. Five-year follow-up after clinical islet transplantation. *Diabetes*. 2005; 54: 2060–2069. https://doi.org/10.2337/diabetes.54.7.2060.
6. *Gerber PA, Lehmann R.* Islet transplantation in type I diabetes mellitus. *Diabetologe*. 2015; 11 (7): 545–552.
7. *Vantyghem MC, de Koning EJP, Pattou F, Rickels MR*. Advances in beta-cell replacement therapy for the treatment of type 1 diabetes. *Lancet*. 2019; 394 (10205): 1274–1285.
8. *Eguchi N, Damyar K, Alexander M, Dafoe D, Lakey JRT, Ichii H.* Anti-Oxidative Therapy in Islet Cell Transplantation. *Antioxidants*. 2022; 11: 1038. https://doi.org/10.3390/antiox11061038.
9. *Korsgren O, Nilsson B, Berne C, Felldin M, Foss A, Kallen R et al.* Current status of clinical islet transplantation. *Transplantation*. 2005; 79: 1289–1293. doi: 10.1097/01.tp.0000157273.60147.7c.
10. *Shapiro AM, Gallant HL, Hao EG, Lakey JR, McCready T, Rajotte RV et al.* The portal immunosuppressive storm: relevance to islet transplantation. *Ther Drug Monit*. 2005; 27 (1): 35–37. doi: 10.1097/00007691-200502000-00008.
11. *Bennet W, Sundberg B, Groth CG, Brendel MD, Brandhorst D, Brandhorst H et al.* Incompatibility between human blood and isolated islets of Langerhans: a finding with implications for clinical intraportal islet transplantation? *Diabetes*. 1999; 48 (10): 1907–1914. doi: 10.2337/diabetes.48.10.1907.
12. *Kumar N, Joisher H, Ganguly A.* Polymeric scaffolds for pancreatic tissue engineering: a review. *Rev Diabet Stud*. 2018; 14 (4): 334–353.
13. *Riopel M, Wang K.* Collagen matrix support of pancreatic islet survival and function. *Frontiers in Bioscience*. 2014; 19: 77–90. doi: 10.2741/4196.
14. *Lemos NE, de Almeida Brondani L, Dieter C, Rheinheimer J, Bouças AP, Bauermann Leitão C et al*. Use of additives, scaffolds and extracellular matrix components for improvement of human pancreatic islet outcomes *in*

vitro: A systematic review. *Islets*. 2017; 9 (5): 73–86. doi: 10.1080/19382014.2017.1335842.
15. *Salvatori M, Katari R, Patel T, Peloso A, Mugweru J, Owusu K, Orlando G.* Extracellular matrix scaffold technology for bioartificial pancreas engineering: state of the art and future challenges. *J Diab Sci Technol*. 2014; 8 (1): 159–169. doi: 10.1177/1932296813519558.
16. *Gazia C, Gaffley M, Asthana A.* Scaffolds for pancreatic tissue engineering. *Handbook of Tissue Engineering Scaffolds: Volume Two*. 2019; 765–786. doi: 10.1016/B978-0-08-102561-1.00032-4.
17. *Fisher SA, Tam RY, Shoichet MS.* Tissue mimetics: engineered hydrogel matrices provide biomimetic environments for cell growth. *Tissue Engineering*. 2014; 20 (5–6): 895–898. doi: 10.1089/ten.tea.2013.0765.
18. *Coronel M, Stabler C.* Engineering a local microenvironment for pancreatic islet replacement. *Curr Opin Biotechnol*. 2013; 24 (5): 900–908. doi: 10.1016/j.copbio.2013.05.004.
19. *Buitinga M, Assen F, Hanegraff M.* Micro-fabricated scaffolds lead to efficient remission of diabetes in mice. *Biomaterials*. 2017; 135: 10–22.
20. *Abualhassan N, Sapozhnikov L, Pawlick RL, Kahana M, Pepper AR, Bruni A et al.* Lung-derived microscaffolds facilitate diabetes reversal after mouse and human intraperitoneal islet transplantation. *PLoS One*. 2016; 11 (5): e0156053. doi: 10.1371/journal.pone.0156053.
21. *Szebeni GJ, Tancos Z, Feher LZ, Alfoldi R, Kobolak J, Dinnyes A, Puskas LG*. Real architecture for 3D Tissue (RAFT) culture system improves viability and maintains insulin and glucagon production of mouse pancreatic islet cells. *Cytotechnology*. 2017; 69 (2): 359–369. doi: 10.1007/s10616-017-0067-6.
22. *Amer LD, Mahoney MJ, Bryant SJ.* Tissue engineering approaches to cell-based type 1 diabetes therapy. *Tissue engineering*. 2014; 20 (5): 455–467.
23. *Damodaran G, Vermette P.* Decellularized pancreas as a native extracellular matrix scaffold for pancreatic islet seeding and culture. *J Tissue Eng Regen Med*. 2018; 12 (5): 1230–1237. doi: 10.1002/term.2655.
24. *Mendibil U, Ruiz-Hernandez R, Retegi-Carrion S, Garcia-Urquia N, Olalde-Graells B, Abarrategi A*. Tissue-specific decellularization methods: rationale and strategies to achieve regenerative compounds. *Int J Mol Sci.* 2020; 21: 5447. doi: 10.3390/ijms21155447.
25. *Rana D, Zreigat H, Benkirane-Jessel N, Ramakrishna S, Ramalingam M.* Development of decellularized scaffolds for stem cell-driven tissue engineering. *J Tissue Eng Regen Med*. 2017; 11 (4): 942–965. doi: 10.1002/term.2061.
26. *Shirakigawa N, Ijima H.* Decellularized tissue engineering. *Advances in Biomaterials for Biomedical Applications. Springer Nature Singapore Pte Ltd*. 2017; 66: 185–226. doi: 10.1007/978-981-10-3328-5_5.
27. *Sevastianov VI, Basok YuB, Grigoriev AM, Nemets EA, Kirillova AD, Kirsanova LA et al.* Decellularization of cartilage microparticles: Effects of temperature, supercritical carbon dioxide and ultrasound on biochemical, mechanical, and biological properties. *J Biomed Mater Res A*. 2023; 111 (4): 543–555. doi: 10.1002/jbm.a.37474.
28. *Sevastianov VI, Ponomareva AS, Baranova NV, Kirsanova LA, Basok YuB, Nemets EA et al*. Decellularization of Human Pancreatic Fragments with Pronounced Signs of Structural Changes. *Int J Mol Sci*. 2023; 24: 119. https://doi.org/10.3390/ijms24010119.
29. *Mirmalek-Sani SH, Orlando G, McQuilling JP, Pareta R, Mack DL, Salvatori M et al.* Porcine pancreas extracellular matrix as a platform endocrine pancreas bioengineering. *Biomaterials*. 2013; 34 (22): 5488–5495. doi: 10.1016/j.biomaterials.2013.03.054.
30. *Wu D, Wan J, Huang Y, Guo Y, Xu T, Zhu M et al.* 3D culture of MIN-6 cells on decellularized pancreatic scaffold: *in vitro* and *in vivo* study. *Biomed Res Int*. 2015; 2015: 432645. doi: 10.1155/2015/432645.
31. *Sevastianov VI, Baranova NV, Kirsanova LA Ponomareva AS, Basok YuB, Nemets EA, Gautier SV.* Comparative analysis of the influence of extracellular matrix biomimetics on the viability and insulin-producing function of isolated pancreatic islets. *J Gene Engg Bio Res*. 2021; 3 (2): 17–25. doi: 10.33140/igerb.03.02.02.
32. *Karaoz E, Genç ZS, Demircan PÇ, Aksoy A, Duruksu G.* Protection of rat pancreatic islet function and viability by coculture with rat bone marrow-derived mesenchymal stem cells. *Cell Death Dis*. 2010; 1: e36. doi: 10.1038/cddis.2010.14.
33. *Velikiy DA, Zakir'yanov AR, Klimenko ED, Onishchenko NA, Pozdnyakov OM.* Patent na izobretenie "Sposob modelirovaniya sakharnogo diabeta I tipa u krys" ot 27.09.2010.
34. *Sevastianov VI.* Technologies of tissue engineering and regenerative medicine. *Russian Journal of Transplantology and Artificial Organs*. 2014; 16 (3): 93–108. doi: 10.15825/1995-1191-2014-3-93-108.

The article was submitted to the journal on 10.04.2023

DOI: 10.15825/1995-1191-2023-2-118-128

INFLUENCE OF PROTEIN-PEPTIDE BIOREGULATOR ISOLATED FROM BOVINE SCLERA AND INCORPORATED INTO AN ALBUMIN-BASED CRYOGEL ON THE SCLERA IN A MODEL CULTIVATION OF A POSTERIOR EYE SEGMENT

O.V. Yamskova[1], M.S. Krasnov[1], E.V. Sidorsky[1, 2], V.I. Lozinsky[1]

[1] Nesmeyanov Institute of Organoelement Compounds, Moscow, Russian Federation
[2] Institute for Biomedical Problems, Moscow, Russian Federation

Delivering bioactive substances to certain spots in the human and animal body is a crucial task. To address this problem, we have developed a delayed-release bioactive substance carrier – an albumin-based cryogel obtained by cryostructuring. It was tested on an organotypic culture model of the posterior eye segment of a newt. **Objective:** to study the effectiveness of porous albumin-based cryogel obtained by cryostructuring and loaded with a bioregulator isolated from bovine sclera in different quantities in maintaining eye tissue integrity and preserving Iberian ribbed newt fibroblasts on an organotypic culture model. **Materials and methods.** Albumin sponges were obtained after being denatured at temperatures –15 °C, –17.5 °C, and –20 °C, with albumin levels 40 mg/mL, 50 mg/mL, and 60 mg/mL in a thermostatic cooler. Their modulus of elasticity was measured. Eye tissues were isolated from adult sexually mature Iberian ribbed newts of both sexes. The posterior segment of each eye was placed on a sponge sample of albumin cryogel in penicillin vials, sealed and placed in a thermostat. At the end of cultivation, the samples were fixed, washed, dehydrated, and embedded in paraffin. Paraffin sections were made, followed by staining. A Leica microscope (Germany) with an Olympus DP70 camera (Japan) was used to view histological sections. Fibroblast count in the histological sections was estimated using the ImageJ program. **Results.** Cryogel with initial albumin solution levels of 50 mg/mL obtained at –20 °C with 4.50 kPa elastic modulus, was chosen for the organ culture experiment. Histological studies showed that eye tissue integrity was maintained in the experiment when albumin-based scaffold was loaded with the bioregulator at doses of 2.46×10^{-5}, 2.46×10^{-7}, 2.46×10^{-9}, 2.46×10^{-13}, 2.46×10^{-15} μg. Moreover, the statistically significant difference for fibroblast count per unit area in the sclera partially correlates with the qualitative state of the posterior eye tissue itself. Groups where bioregulator isolated from the sclera had a dose of 2.46×10^{-7}, 2.46×10^{-9} and 2.46×10^{-15} μg, showed the best result as compared with the control group. **Conclusion.** Albumin-based scaffold as a carrier with a bioregulator adsorbed on it (doses of 2.46×10^{-5}, 2.46×10^{-7}, 2.46×10^{-9}, 2.46×10^{-13}, 2.46×10^{-15} μg) is effective in maintaining eye tissue integrity and preserving Iberian ribbed newt fibroblasts. Albumin cryogen is an effective carrier for delayed release of bioactive substances.

Keywords: targeted drug-delivery systems, albumin cryogel, elastic modulus, organ culturing, bioregulator, protective properties.

INTRODUCTION

Targeted delivery of bioactive compounds (BAC) to certain organs and tissues of the human or animal body is currently a crucial task [1–3]. Such delivery systems most often consist of two main components: the BAC itself and a carrier that provides transport and release of the active ingredient in the target area [4]. Such carriers are used in various forms, such as nanoparticles and nanocontainers, liposomes, polymeric micelles, gels, etc. [5]. In recent years, various biodegradable sponges, especially those based on naturally occurring polymers such as proteins and polysaccharides, have become increasingly popular among BAC carriers [6–12]. An important advantage of such carriers is their good biocompatibility, low immunogenicity, and nontoxicity both of the sponges themselves and of the products of their resorption or degradation during hydrolysis in the recipient's body. In particular, sponges based on denatured serum albumin proved to be effective carriers of both low-molecular-weight and high-molecular-weight BAC [13–15]. These biopolymer materials were obtained by the so-called cryostructurization method [16–18], which allows formation of macroporous and supermacroporous (spongy) polymer matrices upon shallow freezing of solutions of the corresponding precursors, when polycrystals of the frozen solvent act as pore formers [16, 19, 20]. The

Corresponding author: Mikhail Krasnov. Address: 28, Vavilova str., Moscow, 119991, Russian Federation.
Phone: (499) 135-64-92. E-mail: embrmsk@mail.ru

advantages of exactly such albumin sponges include the possibility, by simple techniques, to vary their size, shape, porosity and elasticity, as well as the BAC dose with which the carrier is loaded to achieve the required therapeutic treatment result.

For example, it has been demonstrated that one of the promising biomedical applications of these cryo-structured albumin sponges is their use as 3D carriers for tissue-specific protein-peptide bioregulators that activate repair processes [15, 21–23]. In the present work, we used a bioregulator isolated from bovine sclera, since the indicated peptide-protein complex added to the culture medium has, as previously shown, a protective effect on the state of posterior eye tissues [24]. The peptide-protein complex isolated from the sclera consists of peptides with molecular masses of 1054–5080 Da, as well as from bovine serum albumin with a molecular mass of 66385 Da. It is the complex of peptides and the indicated protein that has bioactivity since its individual components showed no pronounced effects on maintenance of posterior eye cells and tissues during cultivation [24]. At the same time, special attention has now been paid to the influence of the amount (dose) of such a bioregulator incorporated into the albumin sponge on the protective activity exhibited by this BAC delivery system, which was the aim of this study.

MATERIALS AND METHODS

Preparation of cryo-structured albumin carriers

Albumin sponges were synthesized according to a modified known technique [25]. Bovine serum albumin (99%) (DIA-M, Moscow, RF) was dissolved in a calculated volume of water, then urea (o.p.h.) (REACHIM, Moscow, RF) was added. The solution was placed in an ice bath and the necessary volume of aqueous L-cysteine solution (ultra grade) (Fluka, Switzerland) was added. The concentrations of the components in the reaction solutions prepared in this manner were as follows: albumin, 40 mg/mL or 50 mg/mL or 60 mg/mL; urea, 1.5 mol/L; and cysteine, 0.01 mol/L. These solutions were added in 1.5 mL portions to glass vials (internal diameter, 22 mm) or in 3 mL portions into the cells of a plastic 24-well plate. The solutions were frozen for 24 hours in a Proline 1840 programmable ultra cryostat chamber (Lauda, Germany): samples in vials at –20 °C, samples in a plate at either –15 °C, or –17.5 °C, or –20 °C, and then thawed at room temperature. The resulting spongy albumin cryogels were thoroughly washed with sterilized water to remove soluble substances and stored in a closed container at 4–6 °C until further use.

Determination of the elastic modulus of albumin sponges

The elastic moduli of water-swollen albumin sponges were measured on cylindrical specimens, 16 mm in diameter and 20 mm in height. Such measurements were performed according to the technique previously used for soft sponge cryogels [26]. The swollen albumin sponge was placed in a glass beaker filled with water to compensate for capillary forces during extrusion of liquid from communicating macropores during uniaxial compression of the cylindrical sample. To minimize the Archimedes' buoyant force, a 10-mm diameter, 2-mm thick disc punch connected to a TA-Plus automatic texture analyzer holder (Lloyd Instruments, UK) was used. Compression was performed at a rate of 0.3 mm/min to a 50% strain, and the compression modulus of elasticity (E) was determined using the instrument software. The sample for determining the modulus of elasticity included 6–8 samples per point. The obtained values were averaged in Excel 2010. Quantitative data were also analyzed using the SPSS 26.0 software package (IBM, USA). Elastic modulus values having a distribution other than normal were presented as median (Me) and 25% (Q1) and 75% (Q3) percentiles. Statistical significance of differences between the two independent groups was assessed using the Mann–Whitney U test. When comparing three or more independent groups, nonparametric Kruskal–Wallis one-way analysis of variance with Dunn's correction for posterior analysis was used. Differences were considered significant at significance level $p < 0.05$.

Incorporation of protein-peptide bioregulator into albumin sponge

The bioregulator was isolated from bovine sclera tissue according to the technique described earlier [27]. Working solutions with target concentrations from 3×10^{-4} mg/mL to 3×10^{-20} mg/mL were prepared using the obtained solution with a bioregulator concentration of 0.3 mg/mL by successive tenfold dilutions. To incorporate the bioregulator into the albumin carrier, a water-swollen sponge formed in a glass vial was placed on a glass filter and free liquid was removed for 3 minutes under the vacuum of a water-jet pump. After that, the material "squeezed out" in this way was placed into an aqueous solution with a known concentration of the bioregulator, where the sponge swelled rapidly. The sample was incubated for 4 hours at 4–6 °C, then frozen at –20 °C and freeze-dried using a FreeZone[1] freeze dryer system (Labconco, USA).

The mass (dose in micrograms) of the bioregulator included in the sponge carrier was calculated according to the concentration of the bioregulator and the volume of liquid absorbed by the sponge during swelling.

Comparison samples (2 groups) were sponges that were incubated in water without additives.

Investigation of the activity of the bioregulator-loaded sponge albumin carrier on an organotypic culture model of the posterior eye segment

The studies were performed on eye preparations of adult sexually mature Iberian ribbed newts, both sexes, taken from the aquarium belonging to the Koltzov Institute of Developmental Biology (Russia). At least 17 animals (34 eyes) were used in each experiment. The newts were anesthetized in a 2% solution of urethane (ethyl carbamate) in amphibian physiological solution (0.65% NaCl). After anesthesia, the heads of the animals were rinsed with 70% ethanol and the eyes were enucleated under standard laboratory light. The isolated eyes were placed in sterile 35-mm Petri dishes with amphibian nutrient medium (199–70% medium, 30% distilled water) [28]. The ocular tissue culture medium contained 350 mL of 199 medium, 150 mL of double distilled water, 0.15 mL of 1.0 M HEPES buffer, and 1 mL of 1% gentamicin. Before being added to vials, the medium was cold sterilized by passing it through cellulose acetate (CA) membrane filters (Nalgene, USA) with a pore size of 0.2 μm. Eye tissues were isolated under a binocular lens in the following sequence: the eyes were freed from the skin, then cut along the circumference, proximal to the limbus. The retinal growth area together with iris, cornea, and lens were discarded. The posterior part of each eye, which included the retina, pigment epithelium, vascular membrane, and sclera, was used for subsequent culturing.

When culturing the posterior part of the eye, the experimental specimens were divided into the following 11 groups:

1. Control, at the bottom of a glass vial in the absence of an albumin carrier.
2. Control, on a bioregulator-free albumin carrier.
3. On an albumin sponge, loaded with 2.46×10^{-1} μg of the bioregulator.
4. On an albumin sponge, loaded with 2.46×10^{-3} μg of the bioregulator.
5. On an albumin sponge, loaded with 2.46×10^{-5} μg of the bioregulator.
6. On an albumin sponge, loaded with 2.46×10^{-7} μg of the bioregulator.
7. On an albumin sponge, loaded with 2.46×10^{-9} μg of the bioregulator.
8. On an albumin sponge, loaded with 2.46×10^{-11} μg of the bioregulator.
9. On an albumin sponge, loaded with 2.46×10^{-13} μg of the bioregulator.
10. On an albumin sponge, loaded with 2.46×10^{-15} μg of the bioregulator.
11. On an albumin sponge, loaded with 2.46×10^{-17} μg of the bioregulator.

In the experimental groups (3–11), the posterior eye segment of the newt was placed on a bioregulator-loaded sponge sample in the appropriate concentration, located in a penicillin vial, washed with sterile culture medium, and then filled with serum-free medium (medium 199 without serum added). All vials were covered with sterile caps, then with ParafilmM film (USA), and placed in a thermostat. Cultivation was performed stationary in the dark at 20–22 °C for 72 hours without changing the culture medium.

The study of explant condition after cultivation was carried out on a series of paraffin sections. Eye tissues were fixed in Bouin's solution, washed three times with 70% ethanol after fixation for 12 hours, then dehydrated and embedded in paraffin. 7 μm-thick paraffin sections were made using an ERM 4000 microtome (Hestion, Australia), which were stained with hematoxylin and eosin after deparaffinization and hydration, and placed under a coverslip with adhesive fluid added. A Leica microscope (Germany) with an Olympus DP70 camera (Japan) was used to view histological sections. The number of fibroblasts on histological sections was estimated using the ImageJ program, estimating the number of sclera fibroblasts per 1 mm^2 of tissue. At least 50 sections were examined for each experimental point. The results were processed using Mann–Whitney U test and Student's t test.

RESULTS AND DISCUSSION

Obtaining spongy albumin carriers and their physical/mechanical properties

The physical and mechanical characteristics of BAC carriers are important in terms of the performance properties of delivery systems because they largely determine the operational capabilities of the respective drugs, especially under *in vivo* conditions. Since the cryo-structured albumin sponges obtained in this work were further tested as carriers of the peptide-protein bioregulator in model experiments on cultivation of the posterior eye segment, when the sponge was in a hydrated state, it was important to evaluate the mechanical characteristics of the carrier under the applied conditions, i.e., in aqueous medium. At the same time, we still varied albumin levels in the initial solutions used to obtain the sponge media, as well as the cryogenic treatment temperature of these solutions, which is known [16, 19, 20] to affect the porous morphology of polymeric cryogels.

The compression moduli of elasticity of the obtained sponge materials were measured using an automatic

texture analyzer (see the experimental part) using a disc punch (Fig. 1). The results of these measurements are summarized in Table.

The results obtained clearly indicate that increasing the protein levels in the initial solutions led to the formation, at least in the range of negative temperatures –15 °C to –20 °C, of cryo-structured albumin sponges with higher compression modulus of elasticity (with confidence $p < 0.001$ for samples synthesized at –15 °C; $p = 0.014$ for cryogels formed at –17.5 °C; and $p = 0.005$ for samples obtained at –20 °C). At the same time, the averaged *E* values [(A) in Table] and the corresponding moduli of elasticity found during statistical processing of the experimental data [(B) in Table] almost did not differ in absolute value. This emphasizes that the obtained information was reliable.

With the same protein concentration in the initial gel-forming system, more elastic spongy samples were obtained in the case of –15 °C cryogenic treatment temperature. However, considering also the literature data [25] on the efficiency of cryotropic gelation of albumin depending on the conditions of freezing of its initial solutions at the same negative temperatures of –15.0 °C, –17.5 °C and –20 °C, as well as the information obtained in preliminary experiments to evaluate the convenience of working with the obtained sponge carriers during organ cultivation of biological model, for further use in this study we chose albumin sponges synthesized by freezing at –20 °C of reaction solutions with a protein concentration of 50 mg/mL were chosen for further use in this study.

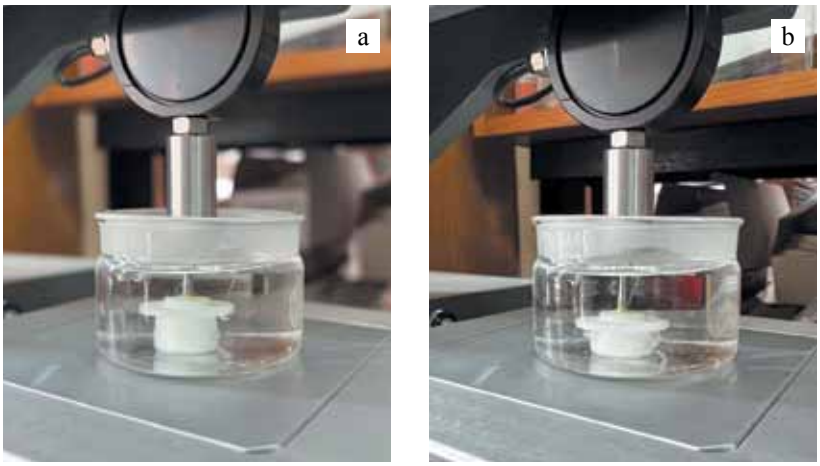

Fig. 1. Photographs of a sample of water-swollen cryo-structured albumin sponge before the onset of the effect of compression load (a) and during deformation under the applied load (b)

Table

Compression modulus of elasticity (*E*) of water-swollen albumin-based cryogels formed from initial solutions with different albumin content by freezing at three negative temperatures

Albumin levels in stock solution (mg/mL)	*E* (kPa) of albumin sponges formed by freezing at the following temperatures:					
	–15.0 °C		–17.5 °C		–20.0 °C	
(A) *E* values averaged using Excel 2010						
40	4.16 ± 0.46		4.07 ± 1.07		2.98 ± 0.45	
50	5.24 ± 0.22		5.03 ± 0.45		4.50 ± 0.76	
60	7.31 ± 0.82		5.71 ± 0.93		4.91 ± 1.08	
(B) *E* values found by statistical processing of the experimental values using the SPSS 26.0 software package						
	Me [Q1–Q3]	p	Me [Q1–Q3]	p	Me [Q1–Q3]	p
40	3.93 [3.74–4.77]	0.001* $p_{40–50} = 0.088$*	4.25 [3.43–4.89]	0.014* $p_{40–50} = 0.105$	2.97 [2.57–3.18]	0.005* $p_{40–50} = 0.006$*
50	5.20 [5.08–5.43]	0.001* $p_{40–60} = 0.001$*	4.96 [4.78–5.22]	0.014* $p_{40–60} = 0.004$*	4.94 [3.64–5.05]	0.005* $p_{40–60} = 0.004$*
60	7.42 [6.06–8.44]	0.001* $p_{50–60} = 0.031$*	5.58 [4.98–6.17]	0.014* $p_{50–60} = 0.194$	4.86 [3.49–5.78]	0.005* $p_{50–60} = 0.092$

* differences are statistically significant ($p < 0.05$).

Results of organ cultivation of the posterior part of a newt's eye using bioregulator-loaded sponge albumin carriers

When counting the number of cells (fibroblasts) in the sclera after culturing the posterior eye segment of Iberian ribbed newt on a bioregulator-free albumin sponge and albumin sponge loaded with bioregulator in different doses (see the experimental part), the results were obtained, shown in the form of diagrams in Fig. 2.

When the posterior part of the eye was cultured on albumin sponges in experimental groups 5, 6, 7, 9, and 10, when the dose of the bioregulator in the carrier was, respectively, 2.46×10^{-5}, 2.46×10^{-7}, 2.46×10^{-9}, 2.46×10^{-13} and 2.46×10^{-15} μg, fibroblast count in the sclera turned out to be significantly higher than in group 1, where the posterior part of the eye was cultured without the albumin sponge, and the posterior part of the eye of the newt was placed directly on the bottom of the cultivation glass vial. In addition, in experimental groups 6, 7, and 10, where the dose of bioregulator included in the sponge carrier was 2.46×10^{-7}, 2.46×10^{-9} and 2.46×10^{-15} μg, respectively, a significantly higher fibroblast count was detected compared to group 2 (cultivation of the posterior eye segment on a bioregulator-free albumin sponge). The graph shows that when sclera bioregulator was added at a dose of 2.46×10^{-11} μg, no significant differences in the fibroblast count per unit area of the sclera were observed relative to the control. It turns out that the dose dependence of the action of the bioregulator included in the cryogel is polymodal in nature.

Fibroblast count per unit area in the sclera partially correlated with the qualitative state of the tissues of the posterior part of the eye themselves. Specifically, their best condition compared to the control group 2 was also observed in groups 6, 7 and 10 (Fig. 3, a, b, g, j), where the dose of the bioregulator isolated from the sclera was, respectively, 2.46×10^{-7}, 2.46×10^{-9} and 2.46×10^{-15} μg.

Below is a description of the histological state of the posterior eye tissues in different experimental groups.

In the control ***group 1*** (Fig. 3, a), when culturing the posterior segment of a newt's eye on the bottom of a glass vial without an albumin carrier, retinal detachment (1) from the pigment epithelial layer (2), as well as detachment of the pigment epithelial layer from the choroid occurred. In the pigment epithelial layer itself, the pigment is shifted to the apical side, which indicates the instability of cells of this layer and their dedifferentiation. Signs of neuronal degradation and damage were observed in the retina. Scleral membrane showed signs of the beginning of tissue degradation, manifested by collagen fiber stratification with formation of cavities (3) between them and by small fibroblast (4) count per unit area (Fig. 2).

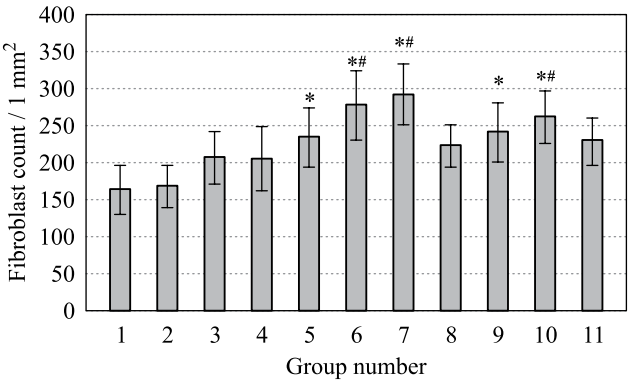

Fig. 2. Fibroblast count per unit sclera area in different experimental groups after cultivation of the posterior part of the eye. *, significant differences $p < 0.05$ from control group 1 (without albumin carrier); #, significant differences $p < 0.05$ from control group 2 (albumin sponge without bioregulator included)

In control ***group 2*** (Fig. 3, b), when culturing the posterior part of a newt's eye on an albumin sponge without adding any factors, a slightly better picture was observed than in control group 1. Retinal detachment (1) from the pigment epithelial layer (2) was partial, photoreceptor cell outgrowths and other retinal neurons were less damaged than in control group 1, but there was retinal neuronal death. The pigment in the pigment epithelial layer also tended to shift to the apical side, but this was not as pronounced as in control 1. The choroid remained dense. There were also elements of tissue degradation in the sclera, manifested by collagen fiber stratification and formation of small cavities (3) and by small fibroblast (4) count per unit area (Fig. 2).

In ***group 3*** (bioregulator in the carrier, 2.46×10^{-1} μg) retinal detachment (1) from the pigment epithelium (2) was also observed. The pigment in the pigment epithelial layer was shifted to the apical side, the choroid was dense without any signs of damage (Fig. 3, c). The sclera showed elements of tissue degradation expressed as cavities (3) between collagen fibers and insignificant difference from control groups in terms of fibroblast (4) count (Fig. 2).

In ***group 4*** (2.46×10^{-3} μg bioregulator in the carrier) (Fig. 3, d), retinal detachment (1) from the pigment epithelium (2) was also detected in places. The pigment in the pigment epithelium layer was shifted to the apical side, as in the previous group. The choroid was in good condition, dense, with no signs of degradation. There was death of retinal neurons. The sclera showed elements of tissue degradation expressed in the stratification of collagen fibers and formation of large cavities (3) and by small fibroblast (4) count per unit area, not significantly different from the control groups (Fig. 2).

In ***group 5*** (2.46×10^{-5} μg bioregulator in the carrier) (Fig. 3, b, e), there was pronounced death of retinal neu-

rons (1). The pigment in the pigment epithelial layer (2) was shifted to the apical side, as in the previous group. The choroid was in good condition, dense, and without signs of degradation. The sclera also showed elements of tissue degradation, manifested by collagen fiber stratification and formation of large cavities (3). In addition, fibroblast (4) count per unit area was not significantly different from the control group 2 (Fig. 2).

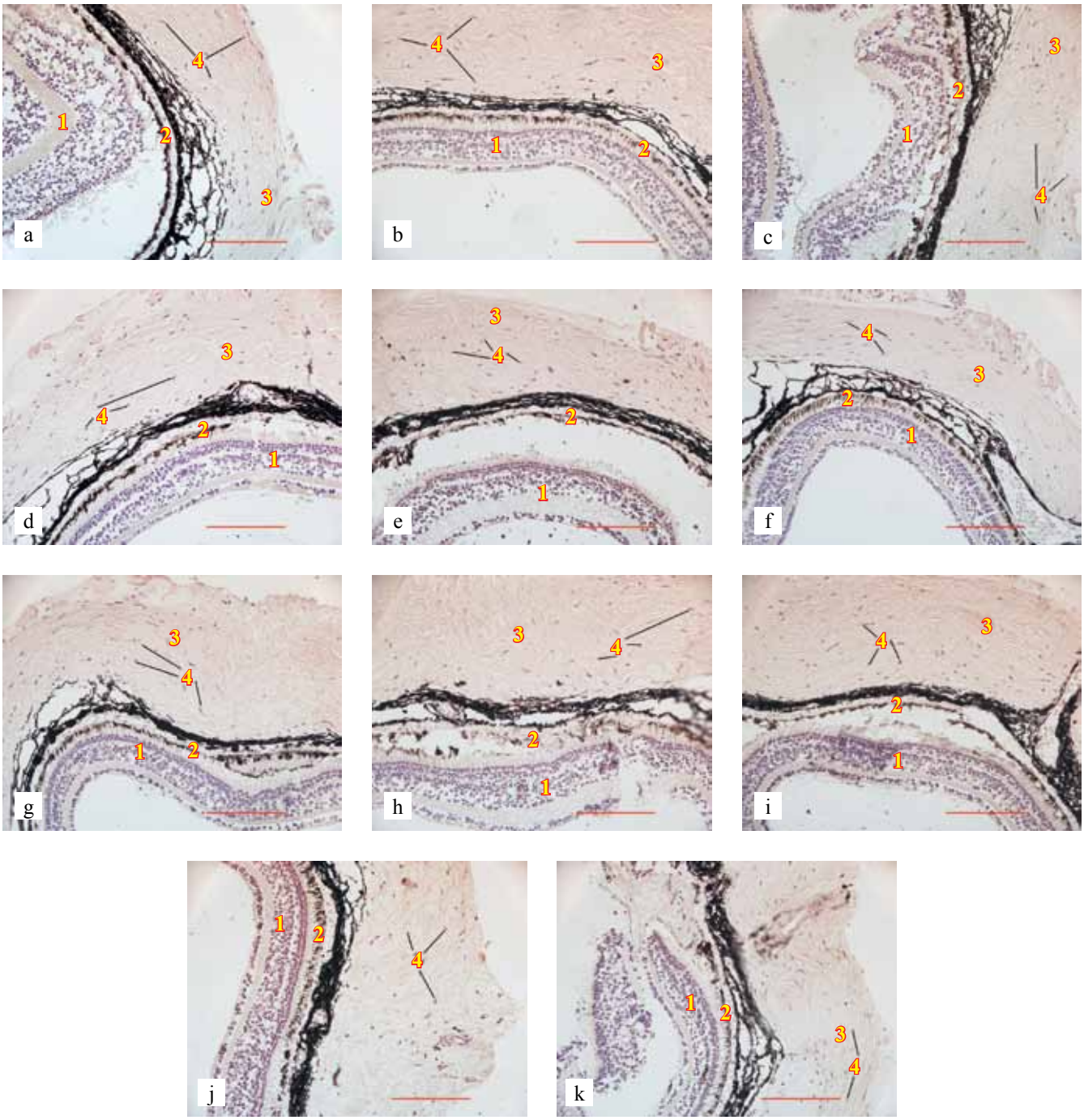

Fig. 3. Histological images of tissues of the posterior segment of the eye of an Iberian ribbed newt, after 3 days of cultivation: (a) without scaffold; (b) on a bioregulator-free albumin-based cryogel scaffold; (c) on an albumin-based cryogel scaffold with a sclera-derived bioregulator included in it at a dose of 2.46×10^{-1} μg; (d) on an albumin-based cryogel scaffold with a sclera-derived bioregulator included in it at a dose of 2.46×10^{-3} μg; (e) on an albumin-based cryogel scaffold with a sclera-derived bioregulator included in it at a dose of 2.46×10^{-5} μg; (f) on an albumin-based cryogel scaffold with a sclera-derived bioregulator included in it at a dose of 2.46×10^{-7} μg; (g) on an albumin-based cryogel scaffold with a sclera-derived bioregulator included in it at a dose of 2.46×10^{-9} μg; (h) on an albumin-based cryogel scaffold with a sclera-derived bioregulator included in it at a dose of 2.46×10^{-11} μg; (i) on an albumin-based cryogel scaffold with a sclera-derived bioregulator included in it at a dose of 2.46×10^{-13} μg; (j) on an albumin-based cryogel scaffold with a sclera-derived bioregulator included in it at a dose of 2.46×10^{-15} μg; (k) on an albumin-based cryogel scaffold with a sclera-derived bioregulator included in it at a dose of 2.46×10^{-17} μg. H&E stain. Metric scale = 200 μm (red line)

The histological sections of the preparations in ***group 6*** (2.46×10^{-7} μg bioregulator in the carrier) (Fig. 3, a, b, f) showed a markedly better picture than in the other groups. In particular, there was less retinal detachment (1) (partial detachment only from the edges), pigment was more evenly distributed in the pigment epithelial cells (2), indicating a stable differentiated state of these cells; there was almost no neuronal death. The sclera showed less signs of degradation, manifested by a smaller number and size of cavities (3) between collagen fibers, and a higher fibroblast (4) count per unit area of the sclera, significantly different from both control groups 1 and 2 about 1.6-fold (Fig. 2).

Sections in ***group 7*** samples (2.46×10^{-9} μg bioregulator in the carrier) (Fig. 3, a, b, g) showed partial retinal detachment (1) from the pigment epithelium (2) from the edges; the pigment was slightly shifted to the apical side; cavities (3) in the sclera were slightly larger than in group 6 preparations but smaller than in other groups; death of retinal neurons was insignificant. Fibroblast (4) count in the sclera differed significantly from both control groups by 1.7-fold (Fig. 2).

In ***group 8*** (2.46×10^{-11} μg bioregulator in the carrier) (Fig. 3, h), partial retinal detachment (1) from the edges was observed, while pigment displacement in the pigment epithelial cells (2) was practically not observed, but there were significant cavities (3) in the sclera. Fibroblast (4) count in the sclera did not differ significantly from both control groups (Fig. 2).

Histological sections of preparations in ***group 9*** (2.46×10^{-13} μg bioregulator in the carrier) (Fig. 3, b, i) showed retinal detachment (1) from the pigment epithelium (2), pigment shift to the apical side, and minor cavities (3) in the sclera. Fibroblast (4) count in the sclera differed significantly only from control group 1, and did not differ from control group (Fig. 2).

Sections of specimens from ***group 10*** (2.46×10^{-15} μg bioregulator in the carrier) (Fig. 3, a, b, j) had a better picture of the state of the posterior eye tissues compared with specimens from all other groups. The sclera was dense without tears, and there were practically no cavities. Pigment was slightly isolated from the pigment epithelial cells (2), and no displacement to the apical side was detected, indicating that these cells are in a stable differentiated state. Retinal detachment (1) from the pigment epithelium was observed only from the edges. Neuronal death was not severe, the choroid was compact. Fibroblast (4) count in the sclera differed significantly from both control groups about 1.5-fold (Fig. 2).

In ***group 11*** (2.46×10^{-17} μg bioregulator in the carrier) (Fig. 3, a, b, k), there was death of retinal neurons (1) and a slight detachment of the retina from the pigment epithelium (2) in the marginal areas. There was practically no pigment shift to the apical side. This indicates that these cells were in a stable differentiated state. Minor ruptures were found in the sclera (3). Fibroblast (4) count in the sclera did not differ significantly from both control groups (Fig. 2).

The detected differences in tissue state and fibroblast preservation during cultivation suggest that the sclera bioregulator only in certain amounts included in the albumin cryogel has a pronounced protective effect the state of the posterior eye tissues. The most prominent protective effect was observed when the posterior eye tissues of a newt was cultured on an albumin scaffold with the bioregulator included at doses 2.46×10^{-7} μg, 2.46×10^{-9} and 2.46×10^{-15} μg. It has been previously shown that there was a protective effect on the state of the posterior eye tissues when this bioregulator was included in a cryogel carrier at a dose of 2.46×10^{-7} μg [22]. The bioregulator, introduced into a cryo-structured albumin sponge, showed the most pronounced protective effect on the state of tissues and cells of the posterior part of the eye, also at doses 2.46×10^{-9} and 2.46×10^{-15} μg, and had a weak effect at other doses (Fig. 2). This fact revealed in this work also testified to the non-linear dose dependence of the action of the bioregulator. In this case, we did not observe the classical dependence – the higher the dose, the greater the effect. In other words, the activity of this bioregulator is characterized by a complex polymodal dose dependence. These results are consistent with the data obtained on the polymodal action of the sclera bioregulator in aqueous solution, which were obtained earlier [24].

This result also correlates with previously obtained information about a similar polymodal dependence for protein-peptide bioregulators isolated from other eye tissues, such as pigment epithelium [29], when the most pronounced biological effect on the posterior eye condition was observed at bioregulator concentrations of 10^{-9} and 10^{-17} mg/mL in culture medium. In terms of its content in albumin sponge, this corresponds to doses of 2.46×10^{-7} and 2.46×10^{-15} μg. Thus, the level of the protective activity of the bioregulator is determined by the concentration of this agent in the solution, which was used when the bioregulator was incorporated into the sponge albumin carrier.

CONCLUSION

A protein-peptide bioregulator isolated from bovine sclera was incorporated into a spongy cryo-structured carrier that was synthesized on the basis of serum albumin solutions with the addition of denaturant (urea) and thiol-reducing agent (cysteine) in doses ranging from 2.46×10^{-1} to 2.46×10^{-17} μg. The functionality of the BAC delivery systems obtained in this way was tested in experiments on organotypic culture model of the posterior eye segment of Iberian ribbed newts in order to find

out the effect of different doses of this bioregulator on the state of the sclera and on maintenance of the integrity of eye tissue (retina and pigment epithelium, choroid) and fibroblast preservation. According to histology data, it was shown that the most pronounced protective effect on the state of tissues of the posterior eye segment during cultivation occurred on the albumin scaffold with bioregulator doses of 2.46×10^{-7} μg, 2.46×10^{-9} and 2.46×10^{-15} μg. The results obtained indicate that cryostructured sponge albumin cryogel is an effective carrier for the release of bioactive compounds.

The work was carried out within the framework of the State assignment No. 075-03-2023-642 of the Ministry of Science and Higher Education of the Russian Federation. The authors express their sincere gratitude to Prof. Yulia Basok (Shumakov National Medical Research Center of Transplantology and Artificial Organs) for her help in the statistical processing of experimental data.

The authors declare no conflict of interest.

REFERENCES

1. *Langer R, Peppas NA*. Advances in biomaterials, drug delivery, and bionanotechnology. *AIChE Journal*. 2003; 49 (12): 2990–3006. doi: 10.1002/aic.690491202.
2. *Yun YH, Lee BK, Park K*. Controlled drug delivery: historical perspective for the next generation. *J Controlled Release*. 2015; 219 (1): 2–7. doi: 10.1016/j.jconrel.2015.10.005.
3. *Benoit DSW, Overby CT, Sims KR, Ackun-Farmmer MA*. Drug delivery systems. *Biomaterials Science* (4th Edn.). W.R. Wagner, S.E. Sakiyama-Elbert, G. Zhang, M.J. Yaszemski (Eds.). Academic Press, 2020: 1237–1266. ISBN: 978-0-12-816137-1.
4. *Tekade RK*. Drug Delivery Systems. Academic Press, 2019. 792 p. ISBN: 9780128144879.
5. *Svenson S*. Carrier-based drug delivery. *ACS Symp. Ser.* 2004; 879 (1): 2–23. doi: 10.1021/bk-2004-0879.ch001.
6. *Orekhova LYu, Kudryavtseva TV, Musaeva RS, Polkina SI, Chuprinina AV, Sadulaeva EA*. Review of extended-release drug delivery systems for non-surgical treatment of inflammatory periodontal diseases. *Parodontologiya*. 2022; 27 (4): 298–307. (In Russ.). doi: 10.33925/1683-3759-2022-27-4-298-307.
7. *Cao W, Zhou X, Tu C, Wang Z, Liu X, Kang Y et al*. A broad-spectrum antibacterial and tough hydrogel dressing accelerates healing of infected wound *in vivo*. *Biomaterials Advances*. 2023; 145 (1): article 213244. doi: 10.1016/j.bioadv.2022.213244.
8. *Platon IV, Ghiorghita CA, Lazar MM, Raschip EE, Dinu MV*. Chitosan sponges with instantaneous shape recovery and multistrain antibacterial activity for controlled release of plant-derived polyphenols. *Int J Molec Sci*. 2023$ 24 (5): article 4452. doi: 10.3390/ijms24054452.
9. *Jugur-Grodzinski J*. Polymers for tissue engineering, medical devices, and regenerative medicine: Concise general review of recent studies. *Polym Adv Technol*. 2006; 17 (3): 395–418. doi: 10.1002/pat.729.
10. *Bakhshpour M, Idil N, Percin I, Denizli A*. Biomedical applications of polymeric cryogels. *Appl Sci*. 2019; 9 (3): article 553. doi: 10.3390/9030553.
11. *Troy E*. Nature-based biomaterials and their application in biomedicine. *Polymers*. 2021; 13 (19): article 3321. doi: 10.3390/polym13193321.
12. *He Y, Wang C, Wang C, Xiao Y, Lin W.* An overview on collagen and gelatin-based cryogels: Fabrication, classification, properties and biomedical applications. *Polymers*. 2021; 13 (14): article 2299. doi: 10.3390/polym13142299.
13. *Lozinsky VI, Rodionov IA, Ciskaraschvili AV, Eskin NA*. Antibakterialnaya belkovaya gubka dlya chimioterapii inficirovannih ran i sposob yeye polucheniya. Pat. RF № 2637634 (2016); B.I. № 34 (2017).
14. *Lozinsky VI, Shchekoltsova AO, Sinitskaya ES, Vernaya OI, Nuzhdina AV, Bakeeva IV et al*. Influence of succinylation of a wide-pore albumin cryogels on their properties, structure, biodegradability, and release dynamics of dioxidine loaded in such spongy carriers. *Int J Biol Macromol*. 2020; 160 (1): 583–592. doi: 10.1016/j.ijbiomac.2020.05.251.
15. *Shaikhaliev AI, Krasnov MS, Sidorskii EV, Yamskova VP, Lozinsky VI*. Induction of osteogenesis in rabbit mandibular bone tissue using an albumin-based cryogenically structured porous 3D carrier loaded with a bioregulator. *Russian Journal of Transplantology and Artificial Organs*. 2022; 24 (1): 56–63. [In Russ, English abstract]. doi: 10.15825/1995-1191-2022-1-56-63.
16. *Lozinsky VI.* Principy i metody kriostrukturirovaniya polimernyh system dlya sozdaniya innovacionnyh materialov biomedicinskogo naznacheniya. *Gibridnye nanoformy bioaktivnyh i lekarstvennyh veshcestv*. Pod. red. M.Ya. Melnikova i L.I. Trachtenberga. M.: Technosfera, 2020. Glava 3: 69–101.
17. *Reichelt S*. Introduction to macroporous cryogels. *Meth Molec Biol*. 2015; 1286*:* 173–181. doi: 10.1007/978-1-4939-2447-9_14.
18. *Tripathi A, Melo JS*. Cryostructurization of polymeric systems for developing macroporous cryogel as a foundational framework in bioengineering applications. *J Chem Sci.* 2019; 131 (1): article 92. doi: 10.1007/s12039-019-1670-1.
19. *Kirsebom H, Mattiasson B*. Cryostructuration as a tool for preparing highly porous polymer materials. *Polym Chem*. 2011; 2 (5): 1059–1062. doi: 10.1039/c1py00014d.
20. *Lozinsky VI*. Cryostructuring of polymeric systems. 55. Retrospective view on the more than 40-years studies performed in the A.N. Nesmeyanov Institute of Organoelement Compounds with respect of the cryostructuring processes in polymeric systems. *Gels*. 2020; 6 (3): article 29. doi: 10.3390/gels6030029.

21. *Krasnov MS, Shaikhaliev AI, Korshakov EV, Efimenko MV, Soloshenkov PP, Davidova TR et al*. Induction of Osteogenesis in Rat Bone Tissue Using Cryogenically Structured Porous 3D Materials Containing a Bioregulator. *Bulletin of Experimental Biology and Medicine*, 2019; 168 (7): 113–117. [In Russ, English abstract]. doi: 10.1007/s10517-019-04657-z.
22. *Sidorskii EV, Krasnov MS, Yamskova VP, Lozinsky VI.* Cryostructuring of polymeric systems: 57 Spongy wide-porous cryogels based on the proteins of blood serum: preparation, properties and application as the carriers of peptide bioregulators. *Gels*. 2020; 6 (4): article 50. doi: 10.3390/gels6040050.
23. *Krasnov MS, Shaikhaliev AI, Korshakov EV, Gasbanov GA, Korgoloev RS, Sinitskaya ES et al*. The change in the condition of the bone tissue of the rat at the site of the defect *in vivo* under the action of a cryogenically structured albumin sponge containing a bioregulator. *Bulletin of Experimental Biology and Medicine*. 2020; 170 (12): 800–804. [In Russ, English abstract]. doi: 10.47056/0365-9615-2020-170-12-800-804.
24. *Sidorskii EV, Il'ina AP, Krasnov MS, Yamskova VP, Buryak AK, Yamskov IA*. Physicochimicheskie svoystva i biologicheskaya aktivnost peptidno-belkovogo kompleksa iz tkani sklery glaza byka. *Prikladnaya biochimiya i mikrobiologiya*. 2018; 54 (1): 82–88. [In Russ, English abstract]. doi: 10.7868/S0555109918010117.
25. *Rodionov IA, Grinberg NV, Burova TV, Grinberg VYa, Lozinsky VI.* Cryostructuring of polymeric systems. 40. Proteinaceous wide-pore cryogels generated by the action of denaturant/reductant mixtures on bovine serum albumin in moderately-frozen aqueous media. *Soft Matter*. 2015; 11 (24): 4921–4931. doi: 10.1039/c4sm02814g.
26. *Lozinsky VI, Kulakova VK, Grigoriev AM, Podorozhko EA, Kirsanova LA, Kirillova AD et al.* Cryostructuring of polymeric systems: 63. Synthesis of two chemically tanned gelatin-based cryostructurates and evaluation of their potential as scaffolds for culturing of mammalian cells. *Gels*. 2022; 8 (11): article 695. doi: 10.3390/gels8110695.
27. *Skripnikova VS, Krasnov MS, Beresin BB, Babushkina TA, Borisenko AV, Izmailov BA et al.* Low-molecular-weight Sclera Protein Biologically Active at Ultralow Doses. *Doklady Biochemistry and Biophysics*. 2007; 417 (5): 697–699. [In Russ, English abstract].
28. *Krasnov MS, Grigoryan EN, Yamskova VP*. An Organotypic Culture of the Newt Retina together with Other Tissues of the Posterior Eye Segment as a Model for Studying the Effects of Cell Adhesion Glycoproteins. *Biology Bulletin*. 2003; (1): 22–36. [In Russ, English abstract].
29. *Yamskova VP, Skripnikova VS, Molyavka AA, Il'ina AP, Krasnov MS, Margasyuk DV et al*. Structural-Functional Characteristics of a New Bioregulator Isolated from Bovine Pigmented Epithelium Tissue. *Biochemistry.* 2009; 74 (9): 1195–1203. [In Russ, English abstract].

The article was submitted to the journal on 12.04.2023

DOI: 10.15825/1995-1191-2023-2-129-139

GALECTIN-3 IN SOLID ORGAN RECIPIENTS: ROLE IN GRAFT PATHOLOGY AND PROSPECTS FOR USE

D.A. Velikiy[1], M.A. Osoblivaya[1], O.P. Shevchenko[1, 2]

[1] Shumakov National Medical Research Center of Transplantology and Artificial Organs, Moscow, Russian Federation

[2] Sechenov University, Moscow, Russian Federation

Galectin-3 (Gal-3) is an important regulator of cell adhesion, migration, proliferation, differentiation and apoptosis under pathophysiological conditions. It plays a crucial role in diseases associated with chronic inflammation and fibrosis. In recent years, there have been reports indicating changes in serum Gal-3 levels in solid organ transplant recipients in the verification of kidney, liver, heart and lung transplant pathologies. Studies on Gal-3 levels and dynamics in solid organ recipients may serve to assess graft conditions using new minimally invasive methods and to identify therapeutic targets for personalized therapy. The first clinical trial data on Gal-3 pharmacological inhibition are emerging. This review summarizes the current understanding of the role of Gal-3 in transplant pathology and the prospects for its use as a diagnostic marker and therapeutic target in solid organ recipients.

Keywords: galectin-3, solid organ transplantation, graft pathology.

INTRODUCTION

In recent years, as survival rate and quality of life of solid organ transplant recipients got better, noninvasive screening and diagnosis of graft pathology have gained special relevance. Early diagnosis and treatment of complications allows for long-term graft functioning. Currently, to determine and verify the pathology of a transplanted organ, invasive diagnostic methods are used, such as biopsy (endomyocardial, transbronchial, puncture), coronary angiography, bronchoscopy and others. Performing these actions involve recipient management protocols or is dictated by the appearance of graft dysfunction signs. Multiple use of invasive methods is associated with certain limitations and risk of complications.

Changes in the concentration of individual molecules in the plasma or serum of solid organ transplant recipients may be associated with clinical symptoms, prognosis and structural changes detected by biopsy and subsequent morphological examination of the graft. Given the accuracy of concentration measurements and proven diagnostic significance, such molecules are classified as biomarkers [1]. In transplantology, a separate direction has been developed for the study of biomarkers for the diagnosis and prognosis of post-transplant complications in solid organ transplant recipients in order to reduce the frequency of invasive diagnostic interventions or partially replace them; biomarkers may have a separate value as targets of therapy [2].

Gal-3 is one of the actively studied biomarkers. Multiple organs (i. e., kidneys, lungs, stomach, colon, uterus, etc.) and diverse cells (i.e., inflammatory, endothelial, muscle or tumor cells, and fibroblasts) express Gal-3, leading to different roles in various pathophysiological conditions. Gal-3 is of particular importance in the development of diseases associated with chronic inflammation and fibrosis [3].

The purpose of this review is to analyze recent data on the role of Gal-3 in graft complications and the prospects for its use as a diagnostic marker and therapeutic target in solid organ transplant recipients.

FEATURES OF THE STRUCTURE AND FUNCTION OF GAL-3

Molecularly, galectins belong to the family of β-galactoside-binding proteins that may interact with several intracellular proteins. This interaction occurs via a specific carbohydrate-recognition domain (CRD) [4], thus making galectins take part in various biological processes (activation of proinflammatory factors, adhesion induction, phagocytosis of neutrophils and macrophages, pre-mRNA splicing etc.) [5].

At present, there have been 15 galectins discovered in mammals. They are divided into three groups according to the organization of polypeptide domains: galectins with a single CRD, tandem-repeat galectins with two distinct CRDs, and galectins with a single N-terminal CRD (chimeric type) [6, 7].

Gal-3 has a unique organization of polypeptide domains, its chimeric and specific structure includes a CRD, a polypeptide fold domain that binds carbohydrates. Gal-3's CRD interacts with various carbohyd-

Corresponding author: Maria Osoblivaya. Address: 1, Shchukinskaya str., Moscow, 123182, Russian Federation. Phone: (499) 193-87-62. E-mail: osoblivaya-91@yandex.ru

rate-containing proteins, activating different signaling pathways. A collagen-like sequence links CRD to N-link domain and is composed of nine collagen-like sequences (proline/glycine-rich domain) cleavable by matrix metalloproteinase. The N-link domain is essential to Gal-3 bioactivity. This domain has two sites where serins are phosphorylated.

Human Gal-3 has a molecular weight of 35 kDa. It is encoded by a single gene, LGALS3, located on chromosome 14, locus q21–q22. Gal-3 has the unique ability to bind proteins in two ways: carbohydrate-dependent and carbohydrate-independent. Using the C-terminal CRD domain, Gal-3 can bind to glycoconjugates containing N-acetyllactosamine, while the N-terminal domain enables the multimerization process. The N-terminal domain of Gal-3 is able to bind with proteins inside a cell and is sensitive to proteolysis by matrix metalloproteinases. These Gal-3 features determine its biological properties [8].

Gal-3 expression has been found in various tissues: in epithelial and endothelial cells, in many types of immune cells as well as in sensory neurons [9, 10]. At the early stages of embryogenesis, Gal-3 expression in tissues is more pronounced and is mainly localized in kidneys, liver, epithelium and chondrocytes [11, 12].

The ratio of intra- and extracellular levels of Gal-3 determines its ability both to induce cell growth and differentiation and to inhibit these processes [13]. Gal-3 may also play an important role in protecting the body against pathogens. It has chemotactic properties towards macrophages and monocytes and enhances proinflammatory signals. It also participates in phagocytic clearance of apoptotic neutrophils by macrophages, induces neutrophil adhesion and activation of leukocyte proinflammatory factors [14].

Gal-3 is predominantly located in the cytoplasm and in small amounts in the cell nucleus. In addition, it is secreted onto the cell surface and into biological fluids. Depending on the location, Gal-3 has revealed opposite effects: intracellularly it protects cells from their death, while extracellularly it can cause their apoptosis.

Nuclear Gal-3 participates in regulation of gene transcription and matrix RNA splicing. Cytoplasmic Gal-3 is essential for maintaining cell viability because it interacts with several critical proteins, including K-Ras gene activated by guanosine-5'-triphosphate (GTP) and anti-apoptotic protein (Bcl-2). The anti-apoptotic effect of Gal-3 inside cells is realized by binding to specific protein synexin (phospholipid-binding and Ca^{2+}-dependent protein). The resulting complex penetrates into mitochondria, where Gal-3 binds to Bcl-2, which leads to stabilization of mitochondrial membranes and inhibits cytochrome C release [12].

Extracellular Gal-3 plays an important role in adhesive interaction between epithelial cells and the extracellular matrix. On the other hand, there is evidence that extracellular Gal-3 induces T-cell apoptosis [16]. All this suggests the involvement of Gal-3 in various pathophysiological processes, including cell growth and differentiation, apoptosis, inflammation and fibrosis [9, 15].

It has been shown that in some inflammatory diseases (rheumatoid arthritis, recurrent chronic vasculitis), as well as in the development of atherosclerosis, patients have increased plasma Gal-3 levels. This may be due to the proinflammatory effects of Gal-3, which include stimulation of immune cell migration in tissues, increased adhesion of leukocytes to the vascular wall and adhesion to laminin [17].

GAL-3 AS A SPLICING FACTOR

Pre-mRNA splicing is an important step in gene expression. During this process, immature pre-mRNA is transformed into mature mRNA from which cell proteins are read (translated). Splicing is a co-transcriptional process during which non-coding sites (introns) are excised from pre-mRNA molecules and coding sites (exons) are spliced together [18].

The criteria for splicing activity reduction and restoration were analyzed in a cell-free system to assess the role of Gal-3 in pre-mRNA processing. The results of the study suggested that Gal-3 is one of the proteins involved in nuclear pre-mRNA splicing. At the same time, disruption of the pre-mRNA splicing process can cause or modify various human diseases [19].

Another study to determine the intracellular localization of Gal-3 also showed that this marker is a splicing factor. Immunofluorescence microscopy revealed inclusions in nuclear structures containing both Gal-3 and known splicing factors (snRNPs and SC35). It was suggested that the domain structure of Gal-3, or more precisely the homologous CRD domain, is required for splicing activity. Experimental data confirmed that isolated Gal-3 CRD restored splicing activity in the galectin-depleted system, although the whole structure of Gal-3 was 10 times more effective at restoring splicing than either of the CRDs alone [20].

It was found that the addition of the proline- and glycine-rich N-terminal domain of Gal-3 to the splicing complex resulted in a dose-dependent inhibition of splicing activity and a concomitant blocking of active spliceosome formation. Whereas intact Gal-3 or its C-terminal domain had no effect on splicing activity or spliceosome formation. This determines the effect of the N-terminal domain on pre-mRNA splicing and suggests that Gal-3 forms oligomers or interacts with other splicing components [21].

BINDING OF GAL-3 AND MIRNAS

MiRNAs are a class of small (20–23 nucleotides long) endogenously encoded noncoding RNAs. They can regulate translation or directly degrade their target genes by binding to base binding regions. Because of their ability to regulate target genes, miRNAs play an important role in cellular processes such as cell differentiation, proliferation, and apoptosis. There is an increasing body of information on the role of miRNAs in cardiac function regulation and heart failure progression [22].

MiRNAs have been identified as an important regulator of ischemia-reperfusion-induced cardiac injury. Song Z et al. investigated the effects of miR-27-3p, Gal-3 and HIF1A (hypoxia-inducible factor 1-alpha) on cell viability and apoptosis in ischemic myocardial injury. The expression level of miR-27-3p was shown to be reduced in the myocardium during hypoxia. Overexpression of miR-27-3p, like HIF1A, reduced ischemia-reperfusion-induced myocardial injury. At the same time, overexpression of Gal-3 reduced the protective effect of miR-27-3p on cardiomyocyte injury, while downregulation of miR-27-3p promoted myocardial cell injury and was a stimulus for Gal-3 activation [23].

A study by Meiqi Zhang et al. in an *in vivo* and *in vitro* model of cardiac hypertrophy showed that expression of miR-27b was down-regulated in mice with cardiac hypertrophy. At the same time, the cardiac function of the mice with cardiac hypertrophy could be restored with the overexpression of miR-27b. Depletion of Gal-3 significantly attenuated cardiac hypertrophy in both *in vitro* and *in vivo* tests. It has been suggested that Gal-3 is a target gene of miR-27b; as a consequence, miR-27b can be used to exert a protective role against cardiac dysfunction and hypertrophy by decreasing the expression level of Gal-3 [24].

A study by Ali A Shati et al. investigated the effect of resveratrol (RES), an anti-apoptotic lectin that is highly overexpressed in ovarian cancer cells, on Gal-3 levels. In SKOV3 and OVCAR-3 OC cell lines, RES induced cell death and inhibited cell migration and invasion. RES enhances levels of miR-424-3p which is able to degrade Gal-3. The results of this study show that RES-induced apoptosis in cancerous cells is associated with increased levels of miR-424-3p and reduced levels of Gal-3 [25].

ROLE OF GAL-3 IN THE DEVELOPMENT OF FIBROTIC CHANGES AND INFLAMMATORY REACTIONS

The long-term post-transplant period can be characterized by graft fibrosis. Fibrotic changes in the transplanted organ result in graft dysfunction due to structural and functional remodeling. The main causes of fibrosis progression include acute or chronic graft rejection, as well as concomitant conditions such as diabetes mellitus, lipid metabolism disorders and others [3, 49].

It has been shown that during fibroblast division, Gal-3 moves from the cytoplasm to the cell nucleus, which, along with increased expression, may indicate the involvement of Gal-3 in proliferative processes. Activation and proliferation of resting fibroblasts occurs under the influence of Gal-3, which is secreted in the area of tissue damage [26]. Fibroblast activation stimulates the synthesis of cytoskeleton proteins COL1A1 (collagen, type I, alpha 1 chain) and aSMA (smooth muscle alpha-actin), which leads to fibrotic changes. There is evidence that Gal-3 can induce degradation of extracellular matrix components indirectly through its interaction with matrix metalloproteinases [27].

Gal-3 is a chemoattractant for monocytes and macrophages, which stimulates the processes of phagocytosis and secretion of cytokines, including interleukin-1. It has been established that Gal-3 can interact with tissue basophils inducing thereby the release of inflammatory mediators and development of hypersensitivity reactions. It has also been shown that Gal-3 participates in angiogenesis and development of atherosclerotic lesions in vessels [27].

Gal-3 expression is most expressed in lungs, spleen, stomach, adrenal glands, uterus and immune system cells, especially in cancer [28]. It is also expressed to a lesser extent in the heart, liver, kidneys, brain and pancreas [29]. At the same time, a change in plasma Gal-3 levels in patients with cardiovascular diseases [30], respiratory dysfunction [31] and liver dysfunction[32] has been shown, suggesting its possible diagnostic significance.

GAL-3 IN KIDNEY DISEASE AND TRANSPLANTATION

In the kidney, Gal-3 is expressed mainly in the collecting ducts of renal tubules, inside or on the apical membrane of α-intercalated cells. This suggests a role for Gal-3 in renal tubular development, possibly through intercellular adhesion or interaction with the extracellular matrix to promote tubulogenesis. In the adult kidney, Gal-3 expression is detected in basal and intercalated cells, in the proximal tubules and the major ascending branch [33].

Gal-3 binds to β-galactoside sugars in its carbohydrate recognition domain, exhibiting a variety of properties, including cell adhesion and proliferation via several glycosylated matrix proteins (laminin, fibronectin and integrins). Gal-3 also promotes pathological processes such as inflammation, angiogenesis and organ fibrogenesis in the presence of tissue damage. Gal-3 depletion has been found to reduce collagen matrix accumulation and severity of renal fibrosis [34, 35]. Other studies have shown that higher plasma or serum Gal-3 levels have

been associated with increased risk of chronic kidney disease (CKD) and rapid decline in renal function [33]. Tsai MT et al. found that higher plasma Gal-3 levels were associated with more severe renal fibrosis as verified by biopsy [36].

O'Seaghdha et al. presented evidence that level of Gal-3 circulating in the blood is inversely associated with renal function and development of CKD [37]. The findings are consistent with a study of the relationship between Gal-3 concentration and progression of congenital CKD [38]. Renal fibrogenesis, including after transplantation, has been found to depend on Gal-3 expression and secretion [33]. At the same time, experimental studies have shown that kidney damage and fibrosis can be prevented by pharmacological inhibition of Gal-3 [39, 40, 41].

Plasma Gal-3 has been found to be associated with organ fibrosis, but whether urinary Gal-3 is a potential biomarker of kidney disease progression has not been well explored. S.M. Ou et al. examined 280 patients that were divided into three groups based on their urinary Gal-3 levels (<354.6, 354.6−510.7, and ≥510.8 pg/mL). Criteria for evaluation of renal disease progression were defined as ≥40% decline in the estimated glomerular filtration rate (eGFR) or end-stage renal disease. Urinary Gal-3 levels were shown to correlate inversely with eGFR and positively with plasma Gal-3 levels, creatinine levels, and urine total protein to creatinine ratio (UPCR). Moreover, there was a gradual increase in urinary Gal-3 levels as CKD progressed, with the increase being greatest among patients with stage 5 CKD. Combined determination of urinary and plasma Gal-3 levels may provide greater diagnostic efficacy in monitoring renal disease [42].

In recent years, Gal-3 has been shown to modulate inflammation and immune cell infiltration in various pathophysiological conditions. Graft dysfunction is associated with activation of immune cells. In a study by Dang et al. on two groups of animals, Gal-3-null mice had less tubular damage, moderate fibrosis, and lower immune cell infiltration compared to the normal animal group that showed characteristic changes in the graft. in the form of renal tubular atrophy, as well as upregulation in Gal-3 expression in tissues and blood plasma [43]. This study suggests a potential role for Gal-3 in immune cell recruitment upon rejection, as evidenced by the improved outcome of kidney injury with pharmacological inhibition of Gal-3.

Thus, Gal-3 may play an important role in renal inflammation and fibrosis, which are involved in the development of kidney graft dysfunction. Further clinical studies are needed to investigate the potential association of Gal-3 with adverse outcomes in patients with CKD and in kidney transplant recipients.

GAL-3 IN PATIENTS WITH HEART FAILURE AND IN HEART TRANSPLANT RECIPIENTS

Several studies have shown the diagnostic potential of Gal-3 as a biomarker of development and progression of heart failure (HF). Changes in Gal-3 concentrations have been observed during the development of myocardial fibrotic disorders, as well as under the influence of drug therapy. The estimation of plasma Gal-3 levels in HF patients may allow to identify those patients who are at increased risk of rehospitalization [44, 45].

Yu.V. Shchukin et al. showed the pathogenetic role of Gal-3 in the development of HF. Blood Gal-3 level in patients was associated with the severity of chronic HF and correlated with markers of oxidative stress and inflammation [46].

In another study, it was also found that in patients with coronary heart disease, blood Gal-3 levels progressively increased according to HF severity. Moreover, Gal-3 levels in patients correlated with the level of inflammation markers: C-reactive protein and interleukin-6. It has been shown that Gal-3 is able to interact with the transmembrane glycoprotein CD98, thereby activating phosphatidylinositol-3-kinase thus triggering the alternative macrophage activation process. As a consequence, myocardial infiltration by activated macrophages increases [47].

It is known that the risk of subclinical chronic HF increases over time in heart recipients due to a combination of various pathological factors, which leads to the formation of graft myocardial fibrosis [48, 49]. The role of Gal-3 in heart recipients has been less studied, but it has been shown that patients with transplanted heart myocardial fibrosis have higher plasma Gal-3 concentrations than recipients without fibrotic changes [50].

In our previous study, it was established that over 75% of heart recipients at different periods after transplantation had fibrotic changes in graft myocardium verified by endomyocardial biopsy. In addition, it was shown that the proportion of patients with myocardial fibrosis in the late post-transplant period almost doubled among the cardiac recipients who had acute transplant rejection. At the same time, Gal-3 was diagnostically significant in transplant myocardial fibrosis: in heart recipients with plasma Gal-3 levels above a certain threshold value, the frequency of detecting fibrotic changes in the myocardium increased more than 1.5-fold [51].

The results of this work confirm the assumption that acute rejection crises influence the development of myocardial fibrosis in the transplanted heart. This occurs against the background of interstitial edema and infiltration by lymphocytes and macrophages, increased production of proinflammatory and profibrogenic mediators, typical for acute graft rejection. [52, 53].

GAL-3 IN LIVER DISEASE AND TRANSPLANTATION

Gal-3, involved in the development of fibrosis and inflammation, is actively expressed in patients with advanced liver disease. Gal-3 expression levels correlate with concentrations of markers of liver inflammation and hepatic decompensation and may be useful in identifying high-risk patients. Gal-3 has been shown to mediate hepatic stellate cell activation and plays an important role in the development of hepatic fibrotic changes. Gal-3 levels are higher in patients with cirrhosis than in the healthy cohort. Intrahepatic Gal-3 has also been detected in hepatocellular carcinoma and in liver biopsies of cirrhotic patients [32].

Gal-3 plays an important immunological role and has been found to contribute to the regulation of innate and adaptive immune responses. Gal-3 has been shown to decrease the number of monocytes by influencing differentiation from dendritic cells as well as T-cell antigen presentation. It also inhibits T cell activation by reducing T cell receptor levels and has been shown to induce IL-2 production and induce apoptosis of activated T cells and suppress their proliferation [54].

A study by H.W. Zimmermann et al. also showed that patients with advanced liver cirrhosis had significantly elevated serum Gal-3 levels. Moreover, Gal-3 levels correlated with such indicators as interleukin-6, granulocyte-macrophage colony-stimulating factor (GM-CSF), interleukin-8 and monocyte chemoattractant protein-1 (MCP-1) [55]. The established relationship between Gal-3 and activation of inflammatory and damaging factors in liver cirrhosis requires further study.

In liver transplantation, the level of circulating Gal-3 can be considered as a biomarker for identifying recipients with a higher risk of developing infectious complications, which are one of the important factors influencing recipient survival after transplantation. It has been shown that the serum Gal-3 levels in liver recipients with a higher incidence of infectious complications was significantly higher than that in other recipients [54].

GAL-3 IN LUNG TRANSPLANTATION

Lung transplantation (LT) is the only possible treatment for patients with end-stage lung diseases, such as emphysema, cystic fibrosis, pulmonary fibrosis and pulmonary arterial hypertension, which cannot be treated with medication [56, 57, 58]. Long-term recipient survival after LT is still lower than in other solid organ transplants, due to the development of chronic graft dysfunction [59]. Currently, there are several forms of chronic lung graft dysfunction – these are obliterative bronchiolitis syndrome and restrictive allograft syndrome.

Bronchiolitis obliterans syndrome (BOS) is characterized by bronchiolar thickening and obstruction due to damage and inflammation of epithelial cells and small subepithelial structures of the airways. Then a fibroproliferative stage develops with proliferation of fibroblasts and accumulation of collagen under bronchiolar epithelium, which leads to obliteration of airway lumen [60].

A study by Miriana d'Alessandro et al. assessed serum Gal-3 levels in recipients after LT with and without BOS, as well as in healthy control subjects to evaluate the potential diagnostic role of this biomarker [61]. It was found that in patients with verified BOS, Gal-3 levels were higher than in healthy subjects, but it did not differ significantly in comparison with lung recipients without signs of chronic graft dysfunction.

Respiratory complications associated with airway obstruction lead to postoperative graft dysfunction in lung recipients. Gal-3 is known to be actively expressed in inflammatory processes and fibrotic changes in various organs. Other potential biomarkers of respiratory diseases and post-transplant complications are small miRNA regulatory molecules.

In our previous work, miR-339 expression levels and Gal-3 concentrations were assessed in the plasma of lung recipients. Lung recipients with airway obstruction had significantly higher miR-339 expression levels and Gal-3 concentrations compared with recipients without any complications. Exceeding the calculated threshold values of miR-339 and Gal-3 in plasma in lung recipients was associated with a high risk of post-LT airway obstruction. Determination of miR-339 expression level in combination with Gal-3 may be promising for identification of lung recipients with high risk of respiratory complications and graft dysfunction [31].

GAL-3 INHIBITORS

Pharmacological inhibition of Gal-3 has been investigated to evaluate its involvement in target organ damage. This lectin binds to multiple cellular sites and has extracellular fixation and permeability abilities. This property is crucial for Gal-3 inhibitors, which are classified according to their carbohydrates' binding characteristics. The currently used Gal-3 inhibitors are listed in the Table [38].

The results of these multicenter studies will allow us to assess the prospects for the therapeutic use of Gal-3 inhibitors in fibrotic changes in various organs and in oncological diseases.

In a phase IIa, blinded, multicentre, randomized clinical trial, patients with stage 3b and 4 CKD received the Gal-3 inhibitor GCS100 [62]. In CKD patients who received the Gal-3 pharmacological inhibitor, the glomerular filtration rate significantly improved, the level of uric acid and urea nitrogen in the blood decreased compared with patients receiving placebo. The authors

of the study did not report any serious side effects when using GCS100 at a dosage of 1.5 mg/m^2 [63].

Lau et al. studied the use of modified citrus pectin (MCP) in hypertension-induced cardiovascular disorders in a randomized controlled trial. It was found that Gal-3 inhibition did not affect the expression of cardiac biomarkers of fibrosis but was associated with lower plasma creatinine levels and higher eGFR in patients treated with MCP [64].

In a study by Hirani et al., Gal-3 was evaluated as a therapeutic agent for the treatment of fibrosis in lung diseases. Inhaled Gal-3 inhibitor was found to be well tolerated in healthy individuals and reduces plasma biomarkers associated with pulmonary fibrosis in patients [65].

Additional preclinical studies are needed to confirm the feasibility of Gal-3 inhibition as a potential therapeutic target.

CONCLUSION

The biological effects of Gal-3 include involvement in the regulation of various pathophysiological processes, including cell growth and differentiation, apoptosis, inflammation, and fibrosis.

In solid organ recipients, a change in Gal-3 levels has been shown in graft pathology verification. In kidney transplantation, less severe tubular damage, a moderate degree of fibrosis and lower infiltration by immune cells in the graft were associated with lower Gal-3 levels. In liver transplantation, Gal-3 concentrations were significantly higher in recipients with advanced graft fibrosis and infectious complications. In heart and lung recipients, the diagnostic significance of Gal-3 with regard to the development of post-transplant complications has been shown both as an independent test and in combination with molecular genetic markers (miRNA). All this suggests that Gal-3 is a promising biomarker for detecting post-transplant organ damage.

Recent data from clinical studies on pharmacological inhibition of Gal-3 suggest the possibility of using this protein as a therapeutic target to slow down and prevent the development of graft pathology in solid organ recipients.

The authors declare no conflict of interest.

Table

Galectin-3 inhibitors [38]

Name	Structure	Pharmacokinetic	Clinical evidence
Modified citrus pectin (MCP)	Polypeptide formed with anhydro-galacturonic acid and galactose with shorter carbohydrate chains modified by pH and temperature	Gal-3 antagonist, soluble protein binding with Gal-3 carbohydrate recognition domain (CRD)	*Cancer:* Phase II, single-center, open label, trial evaluating the safety and efficacy of MCP on prostate-specific antigen kinetics in prostate cancer (NCT01681823) *Cardiac fibrosis:* Phase III, randomized study, single-center trial evaluating the efficacy of MCP treatment to reduce cardiac fibrosis in patients with hypertension. (NCT01960946)
GBC590 / GCS100 A combination of purified MCP (polymerized)	A combination of purified MCP (polymerized)	Gal-3 antagonist, soluble protein binding with CRD	*Renal disease:* – Phase I, open label study, evaluated the security of weekly doses of GCS-100 in patients with chronic kidney disease. (NCT01717248) – Phase IIa, placebo-controlled, randomized, single-blind study evaluated of weekly doses of GCS-100 in patients with chronic kidney disease and eGFR change. (NCT01843790) *Cancer:* – Phase II trials evaluated the reduction of metastasis and stabilized colorectal carcinomas during outcompeting Gal-3 in binding to its receptors. (NCT00110721)
Davanat and Belapectin	Galactomannan polysaccharide	Multivalent binding with Gal-3 CRD	*Liver fibrosis:* Phases I, II, and III study in a multi-center, study, to evaluate the safety and pharmacokinetic of modified Davanat in subjects with non-alcoholic steatohepatitis (NASH) with advanced hepatic fibrosis to improve portal hypertension and oesophagial varice (NCT02462967, NCT04365868)

REFERENCES

1. *Shevchenko AO.* Metody ocenki i sravnitel'nogo analiza klinicheskoj jeffektivnosti biomarkerov pri diagnostike ostrogo koronarnogo sindroma. *Biomarkery v laboratornoj diagnostike.* Pod red. V.V. Dolgova, O.P. Shevchenko, A.O. Shevchenko. M.: Triada, 2014. 288 s.
2. *Shevchenko OP, Aksyonova AV, Ulybysheva AA, Mozheiko NP, Nikitina EA, Orlov VI et al.* Comparative analysis of diagnostic significance of biomarkers' panels in cardiac recipients in the long term period after transplantation. *Russian Journal of Transplantology and Artificial Organs*. 2017; 19 (2): 27–33.
3. *Park S, Nguyen NB, Pezhouman A, Ardehali R.* Cardiac fibrosis: potential therapeutic targets. *Transl Res.* 2019 Jul; 209: 121–137. doi: 10.1016/j.trsl.2019.03.001.
4. *Lahtin M, Lahtin V, Aleshkin V, Afanas'ev S.* Lektiny poleznyh mikrobov: sistemnaja organizacija, funkcionirovanie i funkcional'noe supersemejstvo. *Pol'za. Mikroby*. 2011; 2: 155–165.
5. *Slack RJ, Mills R, Mackinnon AC.* The Therapeutic Potential of Galectin-3 Inhibition in Fibrotic Disease. *Int J Biochem Cell Biol*. 2021; 130: 105881.
6. *Argüeso P, Panjwani N.* Focus on molecules: Galectin-3. *Exp Eye Res*. 2011 Jan; 92: 2–3.
7. *Saccon F, Gatto M, Ghirardello A, Iaccarino L, Punzi L, Doria A.* Role of galectin-3 in autoimmune and non-autoimmune nephropathies. *Autoimmun Rev*. 2017; 16: 34–47.
8. *Menon RP, Hughes RC.* Determinants in the N-terminal domains of galectin-3 for secretion by a novel pathway circumventing the endoplasmic reticulum-Golgi complex. *Eur J Biochem*. 1999; 264: 569–576.
9. *Newlaczyl AU, Yu LG.* Galectin-3 – a jack-of-all-trades in cancer. *Cancer Lett*. 2011; 313: 123–128.
10. *De Oliveira FL, Gatto M, Bassi N, Luisetto R, Ghirardello A, Punzi L, Doria A.* Galectin-3 in autoimmunity and autoimmune diseases. *Exp Biol Med (Maywood)*. 2015; 240 (8): 1019–1028.
11. *Pugliese G, Iacobini C, Ricci C, Blasetti Fantauzzi C, Menini S.* Galectin-3 in diabetic patients. *Clin Chem Lab Med*. 2014; 52 (10): 1413–1423.
12. *Dumic J, Dabelic S, Flögel M.* Galectin-3: An open-ended story. *Biochim Biophys Acta*. 2006; 1760: 616–635.
13. *Ochieng J, Leite-Browning ML, Warfield P.* Regulation of cellular adhesion to extracellular matrix proteins by galectin-3. *Biochem Biophys Res Commun.* 1998 May 29; 246 (3): 788–791. doi: 10.1006/bbrc.1998.8708.
14. *Karlsson A, Christenson K, Matlak M, Björstad A, Brown KL, Telemo E et al.* Galectin-3 functions as an opsonin and enhances the macrophage clearance of apoptotic neutrophils. *Glycobiology.* 2009 Jan; 19 (1): 16–20. doi: 10.1093/glycob/cwn104.
15. *Chen SC, Kuo PL.* The role of Galectin-3 in the kidneys. *Int J Mol Sci*. 2016; 17 (4): 565.
16. *Novak R, Dabelic S, Dumic J.* Galectin-1 and galectin-3 expression profiles in classically and alternatively activated human macrophages. *Biochim Biophys Acta*. 2012 Sep; 1820 (9): 1383–1390.
17. *Gao Z, Liu Z, Wang R, Zheng Y, Li H, Yang L.* Galectin-3 Is a Potential Mediator for Atherosclerosis. *J Immunol Res*. 2020 Feb 14; 2020: 5284728.
18. *Montes M, Sanford BL, Comiskey DF, Chandler DS.* RNA Splicing and Disease: Animal Models to Therapies. *Trends Genet.* 2019 Jan; 35 (1): 68–87.
19. *Gajendra Singh, Divisha Rao, Alok Kumar*. Chapter 1 – Molecular Basis of Neurological Disorders. *The Molecular Immunology of Neurological Diseases*. Academic Press, 2021: 1–13.
20. *Rabinovich GA, Rubinstein N, Toscano MA.* Role of galectins in inflammatory and immunomodulatory processes. *Biochim Biophys Acta*. 2002; 1572 (2–3): 274–284.
21. *Yang RY, Hill PN, Hsu DK, Liu FT.* Role of the carboxyl-terminal lectin domain in self-association of galectin-3. *Biochemistry*. 1998 Mar 24; 37 (12): 4086–4092. doi: 10.1021/bi971409c.
22. *Chen WJ, Yin K, Zhao GJ, Fu YC, Tang CK.* The magic and mystery of microRNA-27 in atherosclerosis. *Atherosclerosis*. 2012 Jun; 222 (2): 314–323. doi: 10.1016/j.atherosclerosis.2012.01.020.
23. *Song Z, Zhong X, Ning Z, Song X.* The Protective Effect of miR-27-3p on Ischemia-Reperfusion-Induced Myocardial Injury Depends on HIF-1α and Galectin-3. *J Cardiovasc Transl Res*. 2022 Aug; 15 (4): 772–785.
24. *Zhang M, Cheng K, Chen H, Tu J, Shen Y, Pang L, Wu W.* MicroRNA-27 attenuates pressure overload-Induced cardiac hypertrophy and dysfunction by targeting galectin-3. *Arch Biochem Biophys*. 2020 Aug 15; 689: 108405. doi: 10.1016/j.abb.2020.108405.
25. *El-Kott AF, Shati AA, Ali Al-Kahtani M, Alharbi SA.* The apoptotic effect of resveratrol in ovarian cancer cells is associated with downregulation of galectin-3 and stimulating miR-424-3p transcription. *J Food Biochem*. 2019 Oct 11; 43 (12).
26. *Lin HM, Moon BK, Yu F, Kim HR.* Galectin-3 mediates genisteininduced G(2)/M arrest and inhibits apoptosis. *Carcinogenesis*. 2000 Nov; 21 (11): 1941–1945. doi: 10.1093/carcin/21.11.1941.
27. *Dickstein K, Cohen-Solal A, Filippatos G, McMurray JJ, Ponikowski P, Poole-Wilson PA et al.* ESC guidelines for the diagnosis and treatment of acute and chronic heart failure 2008: the Task Force for the diagnosis and treatment of acute and chronic heart failure 2008 of the European Society of Cardiology. Developed in collaboration with the Heart Failure Association of the ESC (HFA) and endorsed by the European Society of Intensive Care Medicine (ESICM). *Eur J Heart Fail*. 2008 Oct; 10 (10): 933–989. doi: 10.1016/j.ejheart.2008.08.005.
28. *Dong R, Zhang M, Hu Q, Zheng S, Soh A, Zheng Y, Yuan H.* Galectin-3 as a novel biomarker for disease diagnosis and a target for therapy. *Int J Mol Med*. 2018 Feb; 41 (2): 599–614.
29. *Drapkina O.M., Deeva T.A.* Galectin-3 – biomarker of fibrosis in patients with metabolic syndrome. *Russ J Cardiol.* 2015; 9 (125): 96–102.

30. *Blanda V, Bracale UM, Di Taranto MD, Fortunato G.* Galectin-3 in Cardiovascular Diseases. *Int J Mol Sci.* 2020 Dec 3; 21 (23): 9232.
31. *Shevchenko O, Tsirulnikova O, Sharapchenko S, Pashkov I, Bekov M, Shigaev E et al.* MiR-339 and galectin-3: diagnostic value in patients with airway obstruction after lung transplantation. *Transpl Int.* 2021 Sep; 34 (9): 1733–1739. doi: 10.1111/tri.13986.
32. *An Y, Xu S, Liu Y, Xu X, Philips CA, Chen J et al.* Role of Galectins in the Liver Diseases: A Systematic Review and Meta-Analysis. *Front Med (Lausanne).* 2021 Oct 27; 8: 744518.
33. *Sotomayor CG, Te Velde-Keyzer CA, Diepstra A, van Londen M, Pol RA, Post A et al.* Galectin-3 and Risk of Late Graft Failure in Kidney Transplant Recipients: A 10-year Prospective Cohort Study. *Transplantation.* 2021 May 1; 105 (5): 1106–1115.
34. *Mackinnon AC, Gibbons MA, Farnworth SL, Leffler H, Nilsson UJ, Delaine T et al.* Regulation of transforming growth factor-β1-driven lung fibrosis by galectin-3. *Am J Respir Crit Care Med.* 2012; 185: 537–546.
35. *Calvier L, Martinez-Martinez E, Miana M, Cachofeiro V, Rousseau E, Sádaba JR et al.* The impact of galectin-3 inhibition on aldosterone-induced cardiac and renal injuries. *JACC Heart Fail*. 2015; 3: 59–67.
36. *Tsai MT, Yang RB, Ou SM, Tseng WC, Lee KH, Yang CY et al.* Plasma Galectin-9 Is a Useful Biomarker for Predicting Renal Function in Patients Undergoing Native Kidney Biopsy. *Arch Pathol Lab Med.* 2023 Feb 1; 147 (2): 167–176.
37. *O'Seaghdha CM, Hwang SJ, Ho JE, Vasan RS, Levy D, Fox CS.* Elevated galectin-3 precedes the development of CKD. *J Am Soc Nephrol.* 2013; 24: 1470–1477.
38. *Boutin L, Dépret F, Gayat E, Legrand M, Chadjichristos CE.* Galectin-3 in Kidney Diseases: From an Old Protein to a New Therapeutic Target. *Int J Mol Sci*. 2022 Mar 14; 23 (6): 3124.
39. *Desmedt V, Desmedt S, Delanghe JR, Speeckaert R, Speeckaert MM.* Galectin-3 in Renal Pathology: More Than Just an Innocent Bystander. *Am J Nephrol*. 2016; 43 (5): 305–317.
40. *Prud'homme M, Coutrot M, Michel T, Boutin L, Genest M, Poirier F et al.* Acute kidney injury induces remote cardiac damage and dysfunction through the Galectin-3 pathway. *JACC Basic Transl Sci*. 2019; 4 (6): 717–732.
41. *Sun H, Jiang H, Eliaz A, Kellum JA, Peng Z, Eliaz I.* Galectin-3 in septic acute kidney injury: a translational study. *Crit Care.* 2021; 25 (1): 109.
42. *Ou SM, Tsai MT, Chen HY, Li FA, Lee KH, Tseng WC et al.* Urinary Galectin-3 as a Novel Biomarker for the Prediction of Renal Fibrosis and Kidney Disease Progression. *Biomedicines.* 2022 Mar 2; 10 (3): 585.
43. *Dang Z, MacKinnon A, Marson LP, Sethi T.* Tubular Atrophy and Interstitial Fibrosis after Renal Transplantation Is Dependent on Galectin-3. *Transplantation.* 2012; 93: 477–484.
44. *Karatolios K, Chatzis G, Holzendorf V, Störk S, Richter A, Binas D et al.* Galectin-3 as a Predictor of Left Ventricular Reverse Remodeling in Recent-Onset Dilated Cardiomyopathy. *Dis Markers*. 2018 Jun 19; 2018: 2958219.
45. *Binas D, Daniel H, Richter A, Ruppert V, Schlüter KD, Schieffer B, Pankuweit S.* The prognostic value of sST2 and galectin-3 considering different aetiologies in non-ischaemic heart failure. *Open Heart*. 2018 Feb 26; 5 (1): e000750. doi: 10.1136/openhrt-2017-000750.
46. *Shchukin YuB, Berezin II, Medvedeva EA, Seleznev EI, Dyachkov VA, Slatova LN.* Galectin-3 as a marker and mediator of endogenous inflammation and nitrosylation oxidative stress in patients with chronic heart failure. *Russ J Cardiol* 2013; 2 (100): 45–49.
47. *Belenkov YuN, Tatenkulova SN, Mareev VYu, Masenko VP, Balakhonova TV, Tripoten' MI i dr.* Vzaimosvjaz' urovnja provospalitel'nyh faktorov s vyrazhennost'ju serdechnoj nedostatochnosti pri ishemicheskoj bolezni serdca. *Serdechnaja nedostatochnost'*. 2009; 10 (3): 137–139.
48. *Shevchenko AO, Nikitina EA, Koloskova NN, Shevchenko OP, Gautier SV.* Controlled arterial hypertension and adverse event free survival rate in heart recipients. *Cardiovascular Therapy and Prevention*. 2018; 17 (4): 4–11.
49. *Hughes A, Okasha O, Farzaneh-Far A, Kazmirczak F, Nijjar PS, Velangi P et al.* Myocardial Fibrosis and Prognosis in Heart Transplant Recipients. *Circ Cardiovasc Imaging*. 2019 Oct; 12 (10): e009060. doi: 10.1161/CIRCIMAGING.119.009060.
50. *Shevchenko OP, Ulybysheva AA, Gichkun OE, Mozheiko NP, Stakhanova EA, Kvan VS, Shevchenko AO.* Galectin-3 in heart transplant rejection and fibrosis. *Russian Journal of Transplantology and Artificial Organs*. 2019; 21 (3): 62–68.
51. *Shevchenko OP, Ulybysheva AA, Mozheiko NP, Gichkun OE, Stakhanova EA, Vasilieva VP, Shevchenko AO.* Diagnostic value of galectin-3 in heart transplant recipients with myocardial complications. *Russian Journal of Transplantology and Artificial Organs*. 2020; 22 (1): 8–15.
52. *Gyöngyösi M, Winkler J, Ramos I, Do QT, Firat H, McDonald K et al.* Myocardial fibrosis: biomedical research from bench to bedside. *Eur J Heart Fail*. 2017 Feb; 19 (2): 177–191. doi: 10.1002/ejhf.696.
53. *Kyselovic J, Leddy JJ.* Cardiac Fibrosis: The Beneficial Effects of Exercise in Cardiac Fibrosis. *Exercise for Cardiovascular Disease Prevention and Treatment: From Molecular to Clinical*. Part 1. 2017: 257–268.
54. *Cervantes-Alvarez E, Limon-de la Rosa N, Vilatoba M, Pérez-Monter C, Hurtado-Gomez S, Martinez-Cabrera C et al.* Galectin-3 is overexpressed in advanced cirrhosis and predicts post-liver transplant infectious complications. *Liver Int.* 2022 Oct; 42 (10): 2260–2273.
55. *Zimmermann HW, Seidler S, Gassler N, Nattermann J, Luedde T, Trautwein C, Tacke F.* Interleukin-8 is activated in patients with chronic liver diseases and associated

with hepatic macrophage accumulation in human liver fibrosis. *PLoS One*. 2011; 6 (6): e21381.

56. *Bennett D, Fossi A, Bargagli E, Refini RM, Pieroni M, Luzzi L et al.* Mortality on the waiting list for lung transplantation in patients with idiopathic pulmonary fibrosis: a single-centre experience. *Lung*. 2015 Oct; 193 (5): 677–681.
57. *Bennett D, Lanzarone N, Fossi A, Perillo F, De Vita E, Luzzi L et al.* Pirfenidone in chronic lung allograft dysfunction: a single cohort study. *Panminerva Med.* 2020; 62 (3): 143–149.
58. *Cameli P, Bargagli E, Fossi A, Bennett D, Voltolini L, Refini RM et al.* Exhaled nitric oxide and carbon monoxide in lung transplanted patients. *Respir Med.* 2015; 109 (9): 1224–1229.
59. *Bergantini L, d'Alessandro M, De Vita E, Perillo F, Fossi A, Luzzi L et al.* Regulatory and effector cell disequilibrium in patients with acute cellular rejection and chronic lung allograft dysfunction after lung transplantation: comparison of peripheral and alveolar distribution. *Cells*. 2021; 10 (4): 780.
60. *DerHovanessian A, Wallace WD, Lynch JP 3rd, Belperio JA, Weigt SS.* Chronic lung allograft dysfunction: evolving concepts and therapies. *Semin Respir Crit Care Med*. 2018; 39 (2): 155–171.
61. *d'Alessandro M, Bergantini L, Fossi A, De Vita E, Perillo F, Luzzi L et al.* The Role of Galectins in Chronic Lung Allograft Dysfunction. *Lung*. 2021 Jun; 199 (3): 281–288. doi: 10.1007/s00408-021-00449-3.
62. A Phase 2a Study of Weekly Doses of GCS-100 in Patients with Chronic Kidney Disease, 9 January 2022.
63. Kidney Disease: Improving Global Outcomes (KDIGO) Diabetes Work Group. KDIGO 2022 Clinical Practice Guideline for Diabetes Management in Chronic Kidney Disease. *Kidney Int*. 2022 Nov; 102 (5S): S1–S127. doi: 10.1016.
64. *Lau ES, Liu E, Paniagua SM, Sarma AA, Zampierollo G, López B et al.* Galectin-3 Inhibition with Modified Citrus Pectin in Hypertension. *JACC Basic Transl Sci*. 2021 Jan 6; 6 (1): 12–21.
65. *Hirani N, MacKinnon AC, Nicol L, Ford P, Schambye H, Pedersen A et al.* Target-Inhibition of Galectin-3 by Inhaled TD139 in Patients with Idiopathic Pulmonary Fibrosis. *Eur Respir J*. 2021 May 27; 57 (5): 2002559. doi: 10.1183/13993003.02559-2020.

The article was submitted to the journal on 02.05.2023

DOI: 10.15825/1995-1191-2023-2-140-147

PROGNOSTIC SIGNIFICANCE OF GROWTH HORMONE IN PEDIATRIC LIVER TRANSPLANTATION

R.M. Kurabekova[1], O.V. Silina[1], O.M. Tsirulnikova[1, 2], I.E. Pashkova[1], O.E. Gichkun[1, 2], G.A. Olefirenko[1], S.Yu. Oleshkevich[1], A.R. Monakhov[1, 2], O.P. Shevchenko[1, 2]

[1] Shumakov National Medical Research Center of Transplantology and Artificial Organs, Moscow, Russian Federation

[2] Sechenov University, Moscow, Russian Federation

Growth hormone (GH) plays a leading role in the regulation of cell and tissue metabolism and growth. Its effects are mediated through the so-called somatomedins, among which the most important is the liver-produced insulin-like growth factor 1 (IGF-1). It has been reported that serum GH levels in liver recipients is related to the clinical transplant outcomes. **Objective:** to evaluate the prognostic significance of GH in pediatric liver transplantation (LT). **Materials and methods.** The study enrolled 148 children (61 boys) aged 2 to 60 months (median, 8) with end-stage liver disease resulting from biliary atresia (n = 86), biliary hypoplasia (n = 14), Byler disease (n = 15), Alagille syndrome (n = 12), Caroli syndrome (n = 5), and other liver diseases (n = 16, cryptogenic cirrhosis, fulminant and autoimmune hepatitis, Crigler–Najjar and Budd–Chiari syndromes, alpha-1 antitrypsin deficiency, glycogenosis and hepatoblastoma). All the patients were transplanted with the left lateral segment of the liver from a living related donor. GH concentrations were measured by enzyme immunoassay before, at one month and at one year after transplantation. **Results.** Median plasma GH levels in children with liver disease were 4.3 [1.6–7.2] ng/mL, significantly higher than in healthy children of the same age at 1.2 [0.3–2.4] ng/mL, p = 0.001, while mean height and body weight were lower than in healthy controls. GH levels decreased significantly after transplantation. At one month and one year later, the levels did not differ from those of healthy children (p = 0.74, p = 0.67, respectively). One month after transplantation, GH concentrations were lower in 1-year survivors than in non-survivors (p = 0.02); the diagnostically significant threshold GH level was 1.8 ng/mL. Prior to LT, plasma GH levels did not differ between 1-year survivors and non-survivors. Children with GH levels below 1.8 ng/mL post-LT were 9 times more likely to survive one year post-transplant than patients with levels above the threshold. **Conclusion.** GH concentrations in pediatric liver recipients is a positive prognostic indicator of pediatric LT outcomes.

Keywords: liver transplantation, growth hormone, pediatric transplantation, pediatric recipients.

INTRODUCTION

Pediatric liver transplantation (LT) for end-stage liver disease is currently the only radical method of treatment that can achieve not only high survival rates, but also full physical and social rehabilitation. According to international researchers, 1-year survival of living-donor pediatric liver recipients is 86–96% [1, 2]. The experience at the Shumakov National Medical Research Center of Transplantology and Artificial Organs shows that 1-year survival after transplantation exceeds 90% [3].

Currently, there are no accepted methods for predicting transplant outcomes in recipient children that are based on objective indicators. Validation of prediction methods is a promising approach to further improve LT outcomes in children [4, 5].

Important factors associated with longevity and quality of life are GH and IGF-1, which have received much attention in recent decades [6, 7].

GH and IGF-1 are significant links in humoral regulation of liver function: IGF-1 mediates anabolic and mitogenic effects of GH in peripheral tissues. Over 90% of IGF-1 circulating in systemic circulation is synthesized in the liver. IGF-1 production is regulated by GH, which stimulates its production by liver cells. In turn, IGF-1 regulates GH production in a negative feedback manner [8, 9].

The GH/IGF-1 axis controls cell and tissue growth, is closely connected with liver function and can affect survival of patients with liver diseases and transplant recipients [10, 11]. It is assumed that GH affects LT outcomes in children indirectly through regulation of growth and body weight, hepatocyte function and immune system activity [12–14]. In pediatric liver recipients, there is insufficient data on neurohumoral regulation of graft function.

Corresponding author: Rivada Kurabekova. Address: 1, Shchukinskaya str., Moscow, 123182, Russian Federation. Phone: (499) 190-53-41. E-mail: kourabr@yandex.ru

The aim of this work is to evaluate the prognostic significance of GH in liver transplantation in young children.

MATERIALS AND METHODS

The study included 148 children, 61 boys and 87 girls aged 2 to 60 months (median, 8) with end-stage liver disease. The study protocol was approved by the local ethics committee at Shumakov National Medical Research Center of Transplantology and Artificial Organs. To participate in the study, patients' legal representatives signed a written informed consent, which is kept in their medical records.

In the children enrolled for the study, the causes of liver failure were biliary atresia (n = 86), biliary hypoplasia (n = 14), Byler disease (n = 15), Alagille syndrome (n = 12), Caroli syndrome (n = 5), and other conditions (n = 16), such as cryptogenic cirrhosis, fulminant hepatitis, autoimmune hepatitis, Crigler–Najjar syndrome, Budd–Chiari syndrome, alpha-1 antitrypsin deficiency, glycogenosis, and hepatoblastoma. All patients underwent left lateral LT from a living related donor. After transplantation, patients received double- or triple-drug immunosuppressive therapy, which included tacrolimus, mycophenolates, and corticosteroids.

The comparison group consisted of 16 healthy children, 9 boys and 7 girls, examined after treatment for intestinal dysbacteriosis. The median age in the comparison group was 12 (6–25) months. To compare the recipients' anthropometric indicators, represented by mean values and mean quartile deviation, we used the WHO reference data for healthy children of the same age [15].

We measured growth hormone content in plasma obtained from venous blood collected on an empty stomach between 8 and 10 o'clock in the morning. Blood was collected in disposable plastic tubes (BD Vacutainer, Becton Dickinson, USA) containing anticoagulants (ethylenediaminetetraacetic acid or sodium citrate). Blood plasma obtained by centrifugation at 1500 g for 10 minutes was stored at –500 °C until analysis. Plasma GH levels were measured by enzyme immunoassay using a reagent kit (DBC, Canada) according to the manufacturer's instructions. The results of GH level measurements are represented by median and interquartile range values, 25th to 75th percentile.

Statistical analysis was carried out using parametric and nonparametric statistics methods. Fisher's exact test was used to compare parametric samples. The Mann–Whitney U test was used to compare independent nonparametric variables; paired Wilcoxon test was used to compare dependent samples; correlation analysis was performed according to Spearman's correlation. Differences were considered statistically significant at $p < 0.05$.

A receiver operating characteristic (ROC) analysis was performed to assess the information content of the test. The area under the ROC curve (AUC) reflects the probability with which the test is able to separate one group of patients from another. As a null hypothesis, it was assumed that the area under the ROC curve does not differ from 0.5. The threshold GH level, separating patients from healthy ones, was determined by plotting the dependences of sensitivity and specificity on plasma GH levels.

The diagnostic sensitivity and specificity of the test, as well as the optimal GH threshold level was determined at the point of maximum sum of sensitivity and specificity. Test sensitivity was defined as the proportion of patients with a positive test among all patients. Test specificity was defined as the proportion of healthy people with a negative result among all healthy people.

Relative risk (RR) was calculated using a four-field contingency table for the marker concentration threshold and estimated 95% confidence interval (CI). The RR value was considered statistically significant ($p < 0.05$) if the lower CI limit was above 1.

We also calculated test accuracy (Ac), positive predictive value (PPV) and negative predictive value (NPV). Method accuracy was defined as the proportion of correct results, the ratio of the number of true positive and true negative results to the total number of tests. The PPV, reflecting the probability of becoming ill with a positive test, was determined as the proportion of true positives in the total number of all positive results. The NPV, i.e., the probability of not getting sick with a negative test was determined as the proportion of true negatives in the total number of negative results.

Calculations were made using computer statistical programs MS Office Excel (MS, USA), SPSS Statistics 20 (IBM, USA), and Statistica 7.0 (StatSoft, Inc., USA).

RESULTS

The indication for LT in children aged 2–60 months (median, 8) was end-stage liver disease, which was, in 90% of cases, caused by congenital and hereditary hepatobiliary diseases and in 10% of cases by rare metabolic disorders. The main characteristics of liver recipients included in the study are presented in Table 1.

The comparison group included 16 virtually healthy children, 9 boys and 7 girls, who were examined after treatment for intestinal dysbacteriosis. The median age in the comparison group was 12 (6–25) months.

The age and sex composition of the recipient children included in the study and children in the comparison group did not differ ($p = 0.78$ and $p = 0.84$, respectively).

The mean height of the patients included in the study was 71.2 ± 8.2 cm and was significantly lower than the mean reference value for healthy children of the same age (75 ± 6 cm according to WHO data, $p = 0.00$). The body weight of the recipients was 7.9 ± 2.3 kg and was lower than in healthy children, 9.5 ± 2 kg, $p = 0.00$.

Table 1

Main characteristics of liver recipients

Characteristics	Indicators
Number (n)	148
Age (months), median (range)	8 (2–60)
Sex (n, %):	
Boys	61 (87)
Girls	41 (59)
Liver disease (n, %):	
Biliary atresia	86 (58.1)
Biliary hypoplasia	14 (9.5)
Alagille syndrome	12 (8.1)
Byler disease	15 (10.1)
Caroli syndrome	5 (3.4)
Others:	16 (10.8)
Cryptogenic cirrhosis	
Fulminant hepatitis	
Autoimmune hepatitis	
Crigler–Najjar syndrome	
Budd–Chiari syndrome	
Alpha-1 antitrypsin deficiency	
Glycogenosis	
Hepatoblastoma	

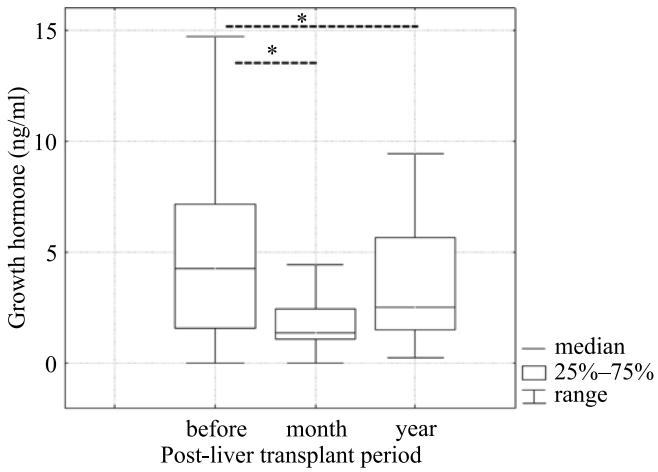

Fig. 1. GH levels in children before and at various times after LT. *, $p < 0.05$ compared to pre-transplant levels

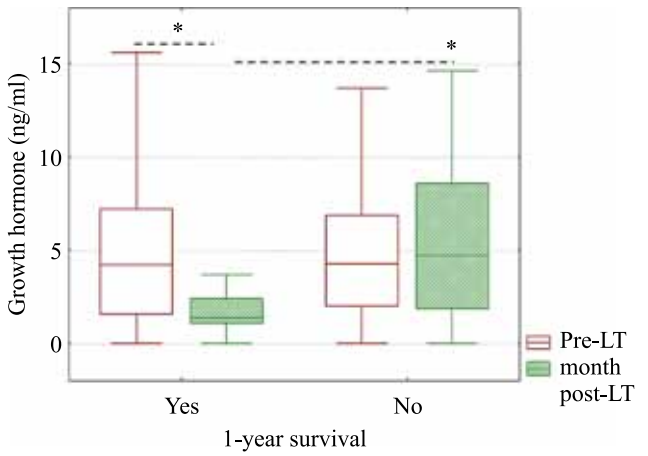

Fig. 2. GH levels before and one month after liver transplantation in 1-year survivors and non-survivors. *, $p < 0.05$

Recipients' height one year after transplantation averaged 82.1 ± 7.6 cm and remained significantly lower than the mean reference value for healthy patients of the same age (according to WHO data, 87 ± 7 cm, p = 0.00) [15]. Recipients' mean body weight of 11.5 ± 2.2 kg did not statistically differ from the reference values for healthy children of the same age, 12 ± 2 kg, p = 0.06.

Plasma GH level in children with liver disease was 4.3 [1.6–7.2] ng/mL and was significantly higher than those in healthy children of the same age, 1.2 [0.3–2.4] ng/mL, p = 0.001. Data on GH levels are presented as median and interquartile range.

Fig. 1 shows a comparative analysis of plasma GH levels in children before, one month, and one year after LT.

A month after LT, plasma GH level in the recipients was 1.4 [1.1–2.4] ng/mL, significantly lower than before the operation (p = 0.001). A year after transplantation, GH level in recipients was 2.5 [1.5–5.7] ng/mL, significantly lower than before surgery (p = 0.049). One month and one year post-LT, plasma GH level in the recipients did not differ from the levels in healthy children (p = 0.74; p = 0.67, respectively).

To study the association of GH with clinical outcomes of pediatric LT, a comparative analysis of blood GH content in children who survived and did not survive one year after transplantation was performed. The pre-transplant GH level was not associated with transplant outcomes one year later (r = 0.03, p = 0.32). Data on plasma GH levels before and one month after transplantation in recipients who survived and did not survive one year are shown in Fig. 2.

GH levels one month after transplantation in survivors were 1.4 [1.1 to 2.4] ng/mL, were significantly lower than those before surgery at 4.2 [1.5 to 7.2] ng/mL, p = 0.00. In recipients who did not survive this period, the GH content after one month was 5.6 [1.9–8.6] ng/mL, almost no different from that before surgery, 4.5 [2.0–6.9] ng/ml, p = 0.68. That is, with a favorable LT outcome, there was a significant decrease in GH levels, and with an unfavorable outcome, GH levels did not change. Pre-transplant GH concentrations did not differ between survivors and non-survivors (p = 0.78); one month post-transplantation, plasma GH levels in survivors were significantly lower than in non-survivors.

To determine whether data on blood GH levels in recipients one month later can be used to predict outcomes one year later, we analyzed the relationship between test sensitivity and specificity at different GH levels (Fig. 3).

Analysis showed that the AUC was 0.74 ± 0.10 [0.54–0.95], statistically significantly different from 0.5 (p = 0.025).

To determine a diagnostically significant GH threshold level, we performed an analysis based on plots of the dependence of test sensitivity and specificity on GH levels in child recipients one month after LT (Fig. 4).

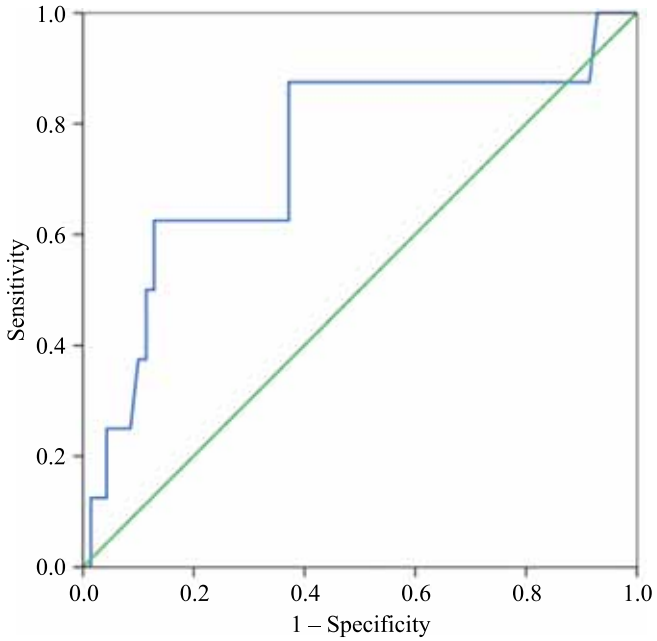

Fig. 3. ROC analysis of plasma GH levels in pediatric recipients one month after LT to assess 1-year survival, AUC = 0.74 ± 0.10; 95% CI 0.54–0.95, $p < 0.05$

Table 2

Characteristics of the test to assess 1-year recipient survival based on GH levels one month after LT

Characteristics	Values
AUROC, 95% CI	0.74 ± 0.10 [0.54–0.95]*
Sensitivity	0.875
Specificity	0.614
Growth hormone threshold	1.8 ng/mL
Relative risk, 95% CI	9.06 ± 1.04 [1.17–70.15]*
Test accuracy (Ac)	64%
Positive predictive value (PPV)	88%
Negative predictive value (NPV)	61%

*, $p < 0.05$.

The threshold GH level, which corresponds to the maximum specificity (0.614) and sensitivity (0.875) of the test, was 1.8 ng/mL. The result means that patients with post-transplant GH levels below the threshold have a 61.4% chance of surviving one year post-transplant, while those with GH levels above the threshold have an 87.5% chance of not surviving this period.

Calculation of RR showed that at GH levels above the threshold, the RR of not surviving one year was 9.06 ± 1.04 [CI 1.17 to 70.15], $p < 0.05$. Thus, recipients with a blood GH level >1.8 ng/mL one month after transplantation had a 9-fold higher risk of not surviving one year than recipients with lower levels of the hormone.

Table 2 presents the calculated informative characteristics of the test.

As can be seen from the table, test accuracy was 64%, which corresponds to the overall proportion of correct results. The PPV reflecting the probability of not surviving a year with a GH level above 1.8 ng/mL was 88%, and the NPV reflecting the probability of surviving a year with a hormone value below the threshold was 61%.

DISCUSSION

Prediction of pediatric LT outcomes is important because it provides an opportunity for a more personalized approach to patient management in the early stages after surgery. Current widely used methods for predicting survival in patients with liver failure based on complex indicators or the results of biochemical studies reflecting liver function, such as albumin levels, are not effective enough. This can be partly down to intensive replacement therapy in the early post-transplant period in liver recipients [16–18].

The height and body weight of children with end-stage liver disease are significantly lower than those of healthy children of the same age. The present study found that after LT, children recover their body weight to the level of healthy children of the same age and there is

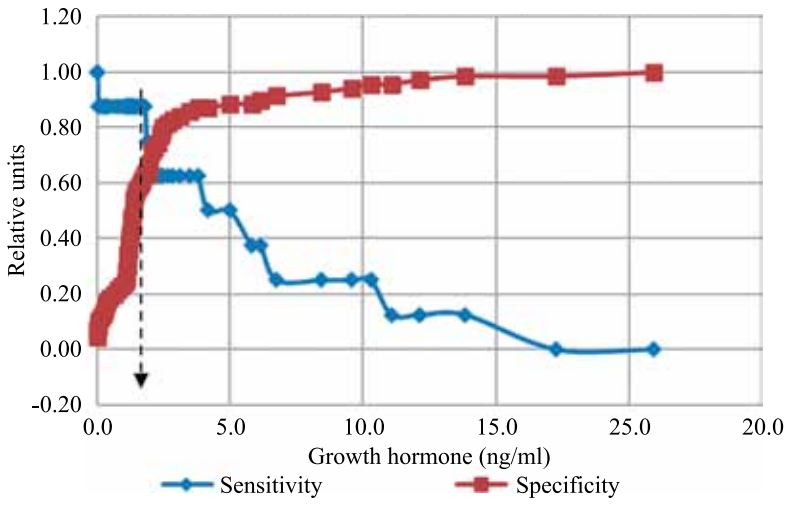

Fig. 4. Dependence of test sensitivity and specificity on GH concentrations in pediatric recipients one month post-LT

a tendency for increased average height of recipients. Earlier in our studies, it was shown that in children with hepatobiliary diseases, the GH level is elevated in combination with impaired IGF-1 synthesis in the liver and reduced IGF-1 levels in the blood; LT in children is accompanied by improved anthropometric parameters due to restoration of IGF-1 synthesis by donor liver cells and normalization of relations in the GH/IGF-1 axis [19, 20].

In this work, a reliable decrease in post-LT plasma GH levels was established. The decrease can be due to IGF-1 production by the graft; absence of significant GH dynamics is indirect evidence of insufficient IGF-1 production by a graft, i.e. graft functional failure. The findings confirm that liver graft plays a role in GH production.

The results of the present work showed that GH levels after one month negatively correlates with one-year transplant outcomes. This suggests that plasma GH tests can be used to predict LT outcomes in young children.

Based on the assessment of diagnostic efficiency of GH levels using common C-statistic methods: construction of ROC curve, determination of threshold values and calculation of informative characteristics of test, we show that plasma GH levels in liver recipient children one month after transplantation can be used to predict one-year survival with a 74 ± 10% probability. A test probability level of about 75% or more, is generally considered an indicator of a good test. A threshold GH level of 1.8 ng/mL separates high and low risk recipients from those at risk of not surviving 12 months after transplantation. Recipients with GH levels below the threshold (1.8 ng/mL) were 9 times more likely to survive the year than those with levels above the threshold. The overall accuracy of this test was 64%. The PPV and NPV were 88% and 61%, respectively. At GH levels below the threshold (negative test), the probability of one-year survival was 61%. At GH levels above the threshold (positive test), the probability of not surviving one year after transplantation was 88%. Thus, the test results have a high probability of predicting LT outcomes.

The data we obtained on the relationship between transplant outcomes and plasma GH levels in liver recipients are consistent with the data obtained by other authors, who showed the importance of body weight, which directly depends on GH levels, in survival. In adult liver recipients, a positive correlation of lower blood GH concentrations after transplantation with 3-month and 3-year survival was also established [10, 21].

The present work is an observational and retrospective hypothesis-driven study. To use GH as an objective laboratory criterion in predicting LT outcomes in children, a prospective clinical study of its diagnostic efficacy is needed.

CONCLUSION

Our work shows that GH levels in children one month after LT can serve as a positive prognostic indicator of transplant outcome; patients with GH levels below the threshold (1.8 ng/mL) may be 9 times more likely to survive one year after transplantation than those with hormone levels above the threshold. The results obtained may be useful for personalization of patient management, as well as for understanding the links between the neuroendocrine system and factors affecting liver graft function.

The authors declare no conflict of interest.

REFERENCES

1. *Moosburner S, Wiering L, Gül-Klein S, Ritschl P, Dziodzio T, Raschzok N et al*. Over 30 Years of Pediatric Liver Transplantation at the Charité-Universitätsmedizin Berlin. *J Clin Med.* 2022; 11 (4): 900. doi: 10.3390/jcm11040900.
2. *Yoon KC, Song S, Lee S, Kim OK, Hong SK, Yi NJ et al*. Outcomes of Split Liver Transplantation vs Living Donor Liver Transplantation in Pediatric Patients: A 5-Year Follow-Up Study in Korea. *Ann Transplant.* 2022; 3 (27): 935682. doi: 10.12659/AOT.
3. *Gautier SV, Khomyakov SM*. Organ donation and transplantation in the Russian Federation in 2021. 14th Report from the Registry of the Russian Transplant Society. *Russian Journal of Transplantology and Artificial Organs*. 2022; 24 (3): 8–31. https://doi.org/10.15825/1995-1191-2022-3-8-31.
4. *Hong SK, Yi NJ, Hong K, Han ES, Lee JM, Choi Y et al*. Risk Factors Affecting Outcomes in Pediatric Liver Transplantation: A Real-World Single-Center Experience. *Ann Transplant.* 2021; 28 (26): 929145. doi: 10.12659/AOT.
5. *Minich A, Arisar FAQ, Shaikh NS, Herman L, Azhie A, Orchanian-Cheff A et al*. Predictors of patient survival following liver transplant in non-alcoholic steatohepatitis: A systematic review and meta-analysis. *EClinicalMedicine.* 2022; 50: 101534. doi: 10.1016/j.eclinm.2022.101534.
6. *Berryman DE, Christiansen JS, Johannsson G, Thorner MO, Kopchick JJ*. Role of the GH/IGF-1 axis in lifespan and healthspan: lessons from animal models. *Growth Horm IGF Res.* 2008; 18 (6): 455–471. doi: 10.1016/j.ghir.2008.05.005.
7. *Junnila RK, List EO, Berryman DE, Murrey JW, Kopchick JJ*. The GH/IGF-1 axis in ageing and longevity. *Nat Rev Endocrinol.* 2013; 9 (6): 366–376. doi: 10.1038/nrendo.2013.67.
8. *Maes M, Sokal E, Otte JB*. Growth factors in children with end-stage liver disease before and after liver transplantation: a review. *Pediatr Transplant.* 1997; 1 (2): 171–175.
9. *Takahashi Y*. The Role of Growth Hormone and Insulin-Like Growth Factor-I in the Liver. *Int J Mol Sci.* 2017; 18 (7): 1447. doi: 10.3390/ijms18071447.

10. *Nicolini D, Mocchegiani F, Palmonella G, Coletta M, Brugia M, Montalti R et al*: Postoperative Insulin-Like Growth Factor 1 Levels Reflect the Graft's Function and Predict Survival after Liver Transplantation. *PLoS One.* 2015; 10 (7): e0133153. doi: 10.1371/journal.pone.0133153.
11. *Wu D, Zhang L, Ma S, Zhao Y, Chen R, Zhang F et al*. Low Growth Hormone Levels Predict Poor Outcome of Hepatitis B Virus-Related Acute-on-Chronic Liver Failure. *Front Med.* 2021; 8: 655863. doi: 10.3389/fmed.2021.655863.
12. *Dichtel LE, Cordoba-Chacon J, Kineman RD*. Growth hormone and insulin-like growth factor I regulation of nonalcoholic fatty liver disease. *J Clin Endocrinol Metab.* 2022; 107 (7): 1812–1824. doi: 1210/clinem/dgac088.
13. *Abdel-Wahab R, Hassan MM, George B, Carmagnani Pestana R, Xiao L, Lacin S et al*. Impact of Integrating Insulin-Like Growth Factor 1 Levels into Model for End-Stage Liver Disease Score for Survival Prediction in Hepatocellular Carcinoma Patients. *Oncology.* 2020; 98 (12): 836–846. doi: 10.1159/000502482.
14. *Liu Z, Cordoba-Chacon J, Kineman RD, Cronstein BN, Muzumdar R, Gong Z et al*. Growth Hormone Control of Hepatic Lipid Metabolism. *Diabetes.* 2016; 65 (12): 3598–3609. doi: 10.2337/db16-0649.
15. WHO Child Growth Standards based on length/height, weight and age. *Acta Paediatr Suppl.* 2006; 450: 76–85. doi: 10.1111/j.1651-2227.2006.tb02378.x.
16. *Wong CS, Lee WC, Jenq CC, Tian YC, Chang MY, Lin CY et al*. Scoring short-term mortality after liver transplantation. *Liver Transpl.* 2010; 16 (2): 138–146. doi: 10.1002/lt.21969.
17. *Hayashi PH, Forman L, Steinberg T, Bak T, Wachs M, Kugelmas M et al*. Model for End-Stage Liver Disease score does not predict patient or graft survival in living donor liver transplant recipients. *Liver Transpl.* 2003; 9 (7): 737–740. doi: 10.1053/jlts.2003.50122.
18. *Pan HC, Jenq CC, Lee WC, Tsai MH, Fan PC, Chang CH et al*. Scoring systems for predicting mortality after liver transplantation. *PLoS One.* 2014; 9 (9): e107138. doi: 10.1371/journal.pone.0107138.
19. *Shevchenko OP, Tsirulnikova OM, Tsirulnikova IE, Kurabekova RM, Olefirenko GA, Stepanova OI, Gautier SV*. Dynamics of insulin-like growth factor-1 (igf-1) in children after ab0-incompatible liver transplantation. *Russian Journal of Transplantology and Artificial Organs*. 2014; 16 (2): 46–51. (In Russ.) https://doi.org/10.15825/1995-1191-2014-2-46-51.
20. *Kurabekova RM, Tsiroulnikova OM, Pashkova IE, Makarova LV, Mozheiko NP, Monakhov AR, Shevchenko OP*. Association between Growth Hormone and Insulin-like Growth Factor-1 (IGF-1) Levels, Liver Function and Short-Term Survival of Paediatric Liver Recipients. *Russian Journal of Gastroenterology, Hepatology, Coloproctology*. 2020; 30 (4): 44–51. (In Russ.) https://doi.org/10.22416/1382-4376-2020-30-4-44-51.
21. *Salso A, Tisone G, Tariciotti L, Lenci I, Manzia TM, Baiocchi L*. Relationship between GH/IGF-1 axis, graft recovery, and early survival in patients undergoing liver transplantation. *Biomed Res Int.* 2014; 2014: 240873. doi: 10.1155/2014/240873.

The article was submitted to the journal on 14.04.2023

DOI: 10.15825/1995-1191-2023-2-148-157

DIAGNOSTIC AND THERAPEUTIC POTENTIAL OF TRANSFORMING GROWTH FACTOR BETA 1 IN SOLID ORGAN TRANSPLANTATION: RECENT RESEARCH FINDINGS

S.O. Sharapchenko[1], A.A. Mamedova[1], O.P. Shevchenko[1, 2]

[1] Shumakov National Medical Research Center of Transplantology and Artificial Organs, Moscow, Russian Federation

[2] Sechenov University, Moscow, Russian Federation

Clinical outcomes of solid organ transplantation depend on many factors. One of the main factors is the risk of post-transplant complications, which affect allograft and recipient survival. Multifactorial organ damage in post-transplant complications and the search for diagnostic and prognostic indicators of the condition have contributed to the study and selection of a wide range of proteomic and molecular genetic biomarkers, which have shown to be effective in solid organ transplantation. The use of biomarkers opens up additional possibilities for assessing the risk of complications and their early diagnosis. This potentially reduces the frequency of invasive diagnostic procedures. Transforming growth factor beta 1 (TGF-β1) regulates many biological processes, has anti-inflammatory and immunosuppressive effects, participates in immune response, and plays a key role in extracellular matrix (ECM) protein synthesis. ECM dysregulation leads to fibroblast hyperproliferation and increased collagen synthesis and, consequently, tissue fibrosis. The variability of the diagnostic and prognostic potential of TGF-β1 has been demonstrated in studies on recipients of various solid organs. The objective of this review is to analyze recent evidence on the role of TGF-β1 in the development of post-transplant complications and to assess its prospects as a marker of graft pathology or as a target for therapy.

Keywords: solid organ transplantation, complications diagnosis, transforming growth factor beta, TGF-β1, biomarkers, fibrosis, rejection, nephrotoxicity.

INTRODUCTION

Clinical outcomes of solid organ transplantation depend on many factors. One of the main ones is the risk of post-transplant complications, which affect allograft and recipient survival. Multifactorial organ damage in post-transplant complications and the search for diagnostic and prognostic indicators of the pathology have contributed to the study and selection of a wide range of proteomic and molecular genetic biomarkers, which have shown to be effective in heart, liver, kidney and lung transplantation.

The use of biomarkers opens up additional possibilities for assessing the risk of complications and their early diagnosis. This potentially reduces the frequency of invasive diagnostic procedures [1].

TGF-β1 is an important biomarker of post-transplant complications. It regulates many biological processes, has anti-inflammatory and immunosuppressive effects, participates in immune response, and plays a key role in ECM protein synthesis synthesis – ECM dysregulation leads to fibroblast hyperproliferation and increased collagen synthesis and, consequently, tissue fibrosis [2]. TGF-β1 is involved in the pathogenesis of many diseases and, what is particularly attractive, is that it has a high therapeutic potential [3].

The aim of this review was to analyze recent data on the role of TGF-β1 in post-transplant complications in solid organ recipients and to assess its prospects as a marker of graft pathology or as a target for therapy.

STRUCTURE AND BIOLOGICAL ROLE

TGF-β1 is one of the components of the TGF-β superfamily, whose members received their names according to the history of their molecular identification. They include activins (ACT), inhibins (INH), bone morphogenetic proteins (BMP), growth differentiation factors (GDF), and Müller inhibitory substance (MIS) [4]. TGF-β is a homodimer consisting of two polypeptide chains, each containing 112 amino acid residues, connected by a disulphide bond and forming a complex of a total molecular weight of 25 kDa. Currently, three TGF-β isoforms are known: TGF-β1 (the most common), TGF-β2, and TGF-β3 [5].

TGF-β was originally classified as an immunomodulatory cytokine that induces and maintains immune tolerance. TGF-β1 has anti-inflammatory and immunosuppressive effects due to cytokine production by T-lymphocytes; TGF-β2 is involved in the development of immune tolerance and is effective in suppressing macrophage inflammatory responses. However, despi-

Corresponding author: Sofya Sharapchenko. Address: 1, Shchukinskaya str., Moscow, 123182, Russian Federation. Phone: (499) 193-87-62. E-mail: transplant2009@mail.ru

te the structural similarities of the isoforms, more and more evidence point to differences in their biological properties: TGF-β1 and TGF-β2 have been shown to have predominantly profibrotic effects, while TGF-β3, in contrast, has been characterized as a fibromodulatory partner for the other two isoforms [6].

The biofunctions of TGF-β are realized through the TGFβRI, -II and -III receptors of the same name. When TGF-β binds to the receptors, activation of signaling pathways, including Smad-dependent ones, is triggered.

Activated TGF-β exerts its effects on cell proliferation, differentiation, and migration in part through its capacity to modulate the deposition of ECM components such as collagen, elastin, and fibronectin. Specifically, TGF-β isoforms have the ability to induce the expression of these proteins in mesenchymal cells and to stimulate the production of protease inhibitors that prevent enzymatic breakdown of the ECM. Dysregulation of these functions is associated with a change in the cellular structure, the cells acquire mesenchymal instead of epithelial properties [7].

Thus, the differences in the effects of TGF-β may be due to a variety of activation cascades in different cell types, peculiarities of the cellular environment, and the influence of other regulatory molecules.

TGF-β1 AND SMAD IN THE DEVELOPMENT OF PATHOLOGICAL PROCESSES

Smad is the main group of mediators of the biological action of TGF-β, which are activated in the development of a wide range of pathological processes in both humans and animals [8].

Three classes of Smads transcription factors have been identified: receptor-regulated Smads (R-Smads), common Smads (Co-Smads), and inhibitory Smads (I-Smads). R-Smads, including Smad1, Smad2, Smad3, Smad5, and Smad8, are directly activated through TGFβRI phosphorylation. Once Smad2 and Smad3 are activated, they bind to Smad4 to form a hetero-oligomeric complex Smad2–Smad3–Smad4, which translocates into the nucleus where it interacts with DNA directly or indirectly through other DNA-binding proteins, regulating transcription of target genes [9].

It is known that Smad3 has a profibrotic effect and is involved in the pathogenesis of kidney disease; Smad2 and Smad7 perform protective functions; Smad4 has a dual role, on one hand, it promotes Smad3-dependent renal fibrosis, on the other hand, it suppresses nuclear factor kappa B (NF-κB)--mediated inflammation via a Smad7-dependent mechanism [10].

Since the TGF-β/Smad3 complex is involved in transcription of a number of genes, this allows us to consider TGF-β as a promising marker of structural changes in organs, and Smad transcription factors as a target for correction of these processes [11].

ASSOCIATION OF TGF-β1 WITH BIOMARKERS OF POST-TRANSPLANT COMPLICATIONS: MIRNAS

MicroRNAs (miRNAs) are a group of small non-coding RNAs about 22 nucleotides long that circulate in biological fluids and regulate post-transcriptional gene expression [12]. Recent studies have shown promising applications of this class of signaling molecules for diagnosis of post-transplant complications, as well as potential targets for therapy [13].

A number of microRNAs involved in immune response reactions and development of structural changes of transplanted organs (primary dysfunction, fibrosis, acute cellular and humoral rejection) have been identified. An analysis of the mechanisms of action of some miRNAs revealed a link with TGF-β signaling pathways.

There is evidence of the involvement of miRNAs in renal inflammation and fibrogenesis and regulated by TGF-β1 via the Smad3 mechanism: miR-21, miR-93, miR-192, miR-216a, miR-377, miR-29, miR-200 [14].

A study by Zhang et al. showed that miR-27 upregulation increases cardiomyocyte activity and inhibits apoptosis, an effect mediated through TGFβRI receptors [15].

Suzuki et al. showed that miR-27 positively regulates mesenchymal gene induction with TGF-β participation [16]. Wang et al. described circulating miR-27 also as a regulator of myogenesis through TGF-β signaling pathway: miR-27 upregulation was associated with reduced myostatin level and muscle cell proliferation [17].

The effect of miR-27 on the development of bronchiolitis obliterans (BO), chronic rejection and fibrous obliteration of small airways after lung transplantation was investigated. In experiments on a model of orthotopic tracheal transplantation in mice, a protective effect of miR-27a-3p was shown by regulating TGF-β and Smad2/Smad4, as well as by maintaining dendritic cells in an immature state [18]. The authors point out the dual role of TGF-β, consisting, on one hand, in induction of tolerance and, on the other hand, in stimulation of myofibroblast transdifferentiation.

Participation of miR-27 in the mechanisms of myocardial fibrosis, BO, as well as the formation of immune response through influence on TGF-β reflects the prospects of the latter as a marker of structural changes in transplanted organs. This is supported by our earlier studies, which showed that plasma miR-27 and -339 upregulation in recipients was associated with the presence of histological signs of transplanted heart myocardial fibrosis [19]. At the same time, a significant decrease in miR-27 levels was observed in heart recipients with acute cellular rejection compared to recipients without rejection signs [20].

Recent studies by Cuiqiong et al. showed that the miR-101 family members play an important role in the pathogenesis of liver fibrosis. Through the TGF-β sig-

naling pathway, miR-101 regulates hepatic stellate cell activation and induces accumulation of extracellular matrix proteins in them [21].

The works of Li [22] and Pan [23] showed that miR-101 blocks TGF-β1/Smad2 signaling pathway by inhibiting RUNX1, which prevents development of postinfarction myocardial remodeling.

The overexpression of miR-142-3p in alveolar epithelial cells and lung fibroblasts is able to reduce the expression of transforming growth factor beta receptor 1 (TGFβ-R1) and profibrotic genes. Furthermore, exosomes isolated from macrophages present antifibrotic properties due in part to the repression of TGFβ-R1 by miR-142-3p transfer in target cells. Thus, macrophage-derived exosomes may fight against pulmonary fibrosis progression via the delivery of antifibrotic miR-142-3p to alveolar epithelial cells and lung fibroblasts [24].

TGF-β1 IN SOLID ORGAN RECIPIENTS

A wide range of immune and nonimmune cells, such as T-lymphocytes, monocytes, vascular endothelium and stromal cells, produce TGF-β under various conditions. According to numerous data, blood levels of TGF-β1 in healthy individuals vary widely (from 0.5 to 80 ng/mL) and are independent of gender [25, 26], but may vary with age. This fact was elucidated in more detail in the work of Okamoto et al.: the serum TGF-β1 level of healthy children under 14 years of age was significantly higher than that of healthy adults ($p < 0.01$), which obviously provides a reasonable basis for studying TGF-β1 in patients according to their belonging to the appropriate age group [27]. These results are also supported by our studies showing almost three-fold differences in the plasma TGF-β1 levels of healthy children and adults [28].

As a multifunctional cytokine, TGF-β1 is synthesized by a wide range of cells in various tissues and organs, stimulating the accumulation of ECM proteins.

TGF-β1 IN LIVER RECIPIENTS

The main source of TGF-β1 in liver tissues is stellate cells, whose profibrotic properties are activated under the influence of various factors [29].

In this aspect, TGF-β1 levels can be considered as a diagnostic or prognostic marker of liver pathology. Studies of a pediatric group of patients with end-stage liver failure, conducted at Shumakov National Medical Research Center of Transplantology and Artificial Organs, showed that TGF-β1 levels are associated with the presence of pathology and, moreover, the degree of organ damage [30].

Clinical studies of liver recipients have shown a tendency for increased TGF-β1 levels in the blood with preserved graft function (44.7 ± 7 ng/mL) compared to recipients with a history of rejection crises (32.7 ± 3 ng/mL) [31].

TGF-β1 IN KIDNEY RECIPIENTS

The source of TGF-β in the kidney is parenchymal cells, lymphocytes, or circulating TGF-β molecules in the blood. The extracellular concentration of TGF-β is primarily regulated by the conversion of inactive TGF-β to the active form, which is often overlooked by researchers because of the complex biological nature of TGF-β [32].

Plasma TGF-β1 level is a potential indicator of the progression of chronic kidney disease [33]. Experiments on animals have shown that TGF-β1 overexpression in the kidneys induced interstitial proliferation, tubular epithelial aerophagia and renal fibrosis with ECM accumulation in tubulointerstitium, capillaries and glomerulus, accompanied by decreased glomerular filtration rate [34]. Progressive renal fibrosis contributed to nephron dysfunction and albuminuria [35]. Genetically determined TGF-β1 deficiency in mice also led to inflammation of several organs, including the kidneys [36].

The effect of TGF-β on transplanted kidney has not been sufficiently studied. A study of TGF-β1 levels at 6 months after kidney transplantation showed higher TGF-β1 concentrations in the group of recipients with chronic rejection compared to the group without it; there was also a positive correlation between TGF-β1 levels and the total cellular infiltrate in kidney biopsies. Importantly, both groups had a history of biopsy-proven acute rejection, which characterizes TGF-β as a marker of chronic rejection [37].

However, Du et al. found that TGF-β1 levels in blood correlated directly with the duration of graft survival [38]. At the same time, TGF-β1 levels correlated positively with estimated glomerular filtration rate, and negatively with serum creatinine levels.

A recent observational cohort study of 1271 kidney transplant pairs showed that donor genotype frequencies of rs1800472 in TGF-β1 differed significantly between patients with and without graft loss ($p = 0.014$), and recipients carrying the T-allele of the TGF-β1 variant showed had a higher risk of graft loss in the long-term. Given that the T allele has a lower level of TGF-β1 expression, these results suggest a positive effect of TGF-β1 signal transduction on the long-term survival of transplanted kidney [39].

Due to both the profibrogenic and protective effects of TGF-β1, there are conflicting data in the literature on the effect of this growth factor on renal transplant survival.

TGF-β1 IN HEART RECIPIENTS

Infiltration by macrophages, suppression of lymphocyte function, fibroblast proliferation, and collagen synthesis are important processes regulated by TGF-β1 and leading to chronic heart failure (CHF). In the heart, TGF-β1 is synthesized by cardiomyocytes and fibroblasts and is released during myocardial infarction, pressure

overload, angiotensin II and noradrenaline administration, and inhibited by nitric oxide [40].

Numerous studies of patients with CHF show that type I and type III collagen gene expression is associated with TGF-β1 [41]. A study of patients with dilated cardiomyopathy at Shumakov National Medical Research Center of Transplantology and Artificial Organs showed the relevant results: plasma TGF-β1 levels of CHF patients was higher than that of healthy subjects (29.9 ± 19.7 ng/mL vs. 8.7 ± 7.5 ng/mL, p = 0.001) [42]. At the same time, after heart transplantation, the TGF-β1 level in the recipients' blood plasma significantly decreased, and in the long term reached the level characteristic of healthy individuals.

Obviously, the role of TGF-β1 in graft pathology in heart recipients is of particular practical interest. The detection of myocardial fibrosis associated with cyclosporine therapy has provided the basis for the assumption that this drug may contribute to diastolic dysfunction of the cardiac allograft [43]. Meanwhile, the effects of TGF-β1 on cardiac fibroblast proliferation vary. Some studies have reported that TGF-β1 stimulates cardiac fibroblast proliferation, while others have demonstrated its antiproliferative effects [44]. Such different results can be down to possible differences in differentiation of fibroblast populations, as well as to the influence of other growth factors.

A five-year follow-up by E. Aziz in 152 heart recipients allowed to assess the magnitude of TGF-β1 expression in cardiac transplants [45]. According to the results obtained, frequent episodes of cellular rejection during the first two years after transplantation were accompanied by higher TGF-β1 levels in tissues, and initiated a series of inflammatory and immune responses with subsequent diastolic dysfunction and myocardial fibrosis. In another study, the authors were able to show the association of TGF-β1 expression in biopsy specimens of transplanted hearts with the development of vasculopathy and low survival rates [46].

In heart recipients with the AA genotype of the rs1800470 polymorphism of the TGF-β1 gene, myocardial fibrosis verified by endomyocardial biopsy was detected more frequently than in G allele carriers, which may also indicate the association of the TGF-β1 gene polymorphism with transplant myocardial fibrosis [47].

TGF-β1 IN LUNG RECIPIENTS

According to the International Society for Heart and Lung Transplantation, the 5-year survival rate of lung recipients is about 53%. The main factor affecting long-term survival is chronic graft rejection, histologically characterized by BO, caused by inflammatory or fibrotic processes in the bronchioles [48]. Physiologically, BO is accompanied by airflow limitation due to significant structural changes in the graft (partial or complete occlusion of the airway lumen). Occlusion is often associated with destruction of the airway smooth muscle and elastin fibers. Among a variety of cytokines and growth factors, TGF-β plays the most significant role in this process [49].

In a number of studies, the authors studied the mechanisms of BO development, and established a positive correlation between the frequency of this complication and the level of TGF-β1 expression [50]. Moreover, as early as 1997, in an experiment on mice, TGF-β expression was found to have a direct influence on the development of severe interstitial fibrosis [51]. A study by Charpin et al. in 1998 showed that TGF-β expression increases in lung recipients even before manifestation of obvious clinical signs of BO [52]. Thus, in several patients, the maximum TGF-β1 levels in the tissue were recorded several months before BO was diagnosed, and these patients died within 2 years after diagnosis. These results suggest that increased TGF-β levels are an early prognostic marker of chronic rejection of transplanted lungs.

A number of studies also demonstrate the mechanism of TGFβ/Smad signaling cascade activation in fibrogenesis processes in a lung transplant, and the concept of TGF-β inhibition as a target for therapy underlies most ideas aimed at improving lung transplant outcomes [53, 54].

TGF-β1 AND IMMUNOSUPPRESSION

The use of calcineurin inhibitors has led to significant advances in transplantation with excellent short-term outcomes. For example, cyclosporine A (CsA) has revolutionized transplantology since the 1970s due to its immunosuppressive effect [55]. The powerful immunosuppressive properties of tacrolimus were discovered later in 1984 [56].

However, despite almost half a century of successful use of these drugs, a wide range of side effects that reduce recipient long-term survival, the main one being nephrotoxicity, remains the Achilles heel of most immunosuppressive regimens.

Fibrosis occurs through induction of epithelial-mesenchymal transition (EMT) processes by TGF-β1 produced by damaged parenchymal cells and macrophages. The triggering of PI3K/Akt/GSK-3β signaling cascade leads to increased expression of Ser-9-phosphorylated inactive form of GSK-3β and accumulation of β-catenin in cytoplasm followed by nuclear translocation [57]. The fact that TGF-β1 is involved in CsA-induced EMT allows us to evaluate possible ways of inhibiting this process.

A recent study by Nagavally et al. described the nephroprotective role of a natural flavonoid, chrysin, which inhibited TGF-β1 signal transduction and prevented cytoplasmic β-catenin accumulation. The authors cite promising results and point to the efficacy and safety of CsA in combination with chrysin, which will significantly

reduce the undesirable effects of immunosuppressive therapy [58].

Since tacrolimus directly or indirectly induces TGF-β1 expression, ways to combat chronic nephropathy are also being developed in relation to immunosuppressive therapy regimens [59].

Zhang et al. studied the effect of traditional Chinese phytotherapeutic agent, used in various inflammatory processes in the kidneys on the action of tacrolimus in rats. During the experiments, combined use of the drugs suppressed the expression of TGF-β1/Smad2/3/βig-h3 and proinflammatory cytokines, and weakened oxidative stress and apoptosis [60].

In addition, it should be noted that opportunistic infection (OI) remains a serious complication throughout the post-transplant period, jeopardizing the benefits of any long-term immunosuppressive therapy. From this point of view, evidence from Boix et al. suggesting TGF-β1 as a predictor of OI in the first year after liver and kidney transplantation are of great interest [61]. In their study, the authors showed that concentration of TGF-β >363.25 pg/mL in liver and TGF-β >808.51 pg/mL in kidney recipients were able to stratify patients at high risk of OI with a sensitivity and specificity above 70% in both types of solid organ transplantations.

Thus, TGF-β regulation acts as an important etiological factor in chronic nephrotoxicity and other immunosuppressant-induced complications, and the impact on this pathway can reduce the undesirable effects of therapy and potentially improve long-term transplant outcomes.

TGF-β1 AS A TARGET FOR THERAPY

One of the main tasks of transplantology is to achieve long-term graft and recipient survival, reducing possible post-transplant risks. Along with the development of new effective methods for diagnosing complications, there is an active search for therapeutic targets as a possible way to solve the problem.

Evidence of the role of TGF-β in fibrosis development became a breakthrough and led to increase in the number of studies aimed at searching for new drugs such as antisense oligonucleotides, neutralizing antibodies, cyclic pentapeptides, TGF-β ligand traps and small-molecule kinase inhibitor drugs, etc. [62].

To stop progressive fibrosis in experimental glomerulonephritis, Border et al. for the first time used *in vivo* injections of anti-TGF-β1 neutralizing antibodies. Injection of anti-TGF-β1 antibodies in acute mesenchymal proliferative glomerulonephritis suppressed ECM protein production and slowed fibrosis progression, which was histologically confirmed [63].

Another study aimed at developing an experimental therapy was the introduction of antibodies against TGF-β receptor type II (TGFβRII) inhibiting mesenchymal matrix growth, which was confirmed by decreased proteinuria compared to the control group of rats with glomerulonephritis [64].

Currently, drugs targeting members of the TGF-β superfamily or their receptors are under development, and dozens of antifibrotic agents with different targets are being tested; they are mostly chemically synthesized oligonucleotides. For example, injections of miR-326 into mice with induced pulmonary fibrosis were accompanied by antifibrotic effects through Smad7 regulation and a significant decrease in TGF-β1, Smad3, matrix metalloproteinase-9 (MMP-9) [65].

Preclinical trials have shown the effectiveness of therapy with antisense oligonucleotides that inhibit TGF-β gene expression and reduce tissue fibrosis in glomerulonephritis [66]. The possibility of highly selective antibodies SRK-181, whose key mechanism is to prevent the cleavage of TGF-β1 precursor and the release of mature TGF-β1, is also being studied [67].

Another highly effective selective inhibitor, AVID200, targets an altered TGFβRII receptor. It enhances the binding activity of TGFβRII to TGF-β1 and TGF-β3 and thus greatly reduces the binding activity to TGF-β2 [68].

Luangmonkong et al. found no visible side effects of lifelong blocking of TGF-β activity in mice, although in humans, its long-term systemic suppression was associated with a high risk of therapy toxicity and decreased regenerative tissue function, which is due to the functional pleiotropy of TGF-β [69].

The results published to date reveal the complexity of the process of developing therapeutic approaches using TGF-β1 in humans, which require a comprehensive study to minimize undesirable effects.

CONCLUSION

The validity of the concept of TGF-β1 as a diagnostic and prognostic marker of the risk of adverse events in solid organ transplantation has been confirmed by numerous studies in recent years. Both in experimental models and in the clinic, the key role of TGF-β1 in a wide range of biological processes, namely mechanisms of allograft tissue fibrosis, formation of immune tolerance, and in the cascade of inflammatory reactions against nephrotoxicity of immunosuppressive drugs used, has been shown. The role of TGF-β1 in very severe post-transplant complications – transplant rejection and fibrosis – is still the focus of research.

The variability of the diagnostic and prognostic potential of TGF-β1 has been demonstrated in studies of recipients of various solid organs. For example, post-lung transplant bronchiolitis obliterans and chronic rejection is associated with increased blood TGF-β1 levels, while in contrast, adverse events (progression of liver failure and fibrosis) in liver transplantation are associated with decreased TGF-β1 levels, and higher levels are typical for recipients with intact liver graft function. Studies in heart and kidney transplantation show conflicting evi-

dence on the profibrotic and antiproliferative effects of TGF-β1.

Equally important is the fact that TGF-β1 levels change with age, which necessitates a separate study of TGF-β1 in pediatric recipients.

Equally important is the fact that TGF-β1 levels change with age, which necessitates a separate study of TGF-β1 in pediatric recipients.

The authors declare no conflict of interest.

REFERENCES

1. *Choi J, Bano A, Azzi J.* Biomarkers in Solid Organ Transplantation. *Clin Lab Med.* 2019; 39 (1): 73–85.
2. *Tzavlaki K, Moustakas A*. TGF-β Signaling. *Biomolecules*. 2020; 10 (3): 487.
3. *Zhang H, Yang P, Zhou H, Meng Q, Huang X*. Involvement of Foxp3-expressing CD4+ CD25+ regulatory T cells in the development of tolerance induced by transforming growth factor-beta2-treated antigen-presenting cells. *Immunology.* 2008; 124: 304–314.
4. *Javelaud D, Mauviel A*. Mammalian transforming growth factor-βs: smad signaling and physio-pathological roles. *International Journal of Biochemistry and Cell Biology*. 2004; 36 (7): 1161–1165.
5. *Poniatowski LA, Wojdasiewicz P, Gasik R, Szukiewicz D.* Transforming growth factor beta family: insight into the role of growth factors in regulation of fracture healing biology and potential clinical applications. *Mediators Inflamm.* 2015; 2015: 137823.
6. *Wilson SE.* TGF beta-1, -2 and -3 in the modulation of fibrosis in the cornea and other organs. *Exp Eye Res.* 2021; 207: 108594.
7. *Verrecchia F, Mauviel A.* Transforming growth factor-β signaling through the smad pathway: role in extracellular matrix gene expression and regulation. *J Invest Dermatol.* 2002; 118 (2): 211–215.
8. *Wang W, Huang XR, Canlas E, Oka K, Truong LD, Deng C et al.* Essential role of Smad3 in angiotensin II-induced vascular fibrosis. *Circ Res.* 2006; 98 (8): 1032–1039.
9. *Vander Ark A, Cao J, Li X.* TGF-β receptors: in and beyond TGF-β signaling. *Cell Signal.* 2018; 52: 112–120.
10. *Chen L, Yang T, Lu DW, Zhao H, Feng YL, Chen H et al.* Central role of dysregulation of TGF-β/Smad in CKD progression and potential targets of its treatment. *Biomed Pharmacother.* 2018; 101: 670–681.
11. *Fujimoto M, Maezawa Y, Yokote K, Joh K, Kobayashi K, Kawamura H et al.* Mice lacking Smad3 are protected against streptozotocin-induced diabetic glomerulopathy. *Biochem Biophys Res Commun.* 2003; 305: 1002–1007.
12. *Shah R, Tanriverdi K, Levy D, Larson M, Gerstein M, Mick E et al.* Discordant expression of circulating microRNA from cellular and extracellular sources. *PLoS One.* 2016; 11 (4): e0153691.
13. *Novák J, Macháčková T, Krejčí J, Bienertová-Vašků J, Slabý O.* MicroRNAs as theranostic markers in cardiac allograft transplantation: from murine models to clinical practice. *Theranostics*. 2021; 11 (12): 6058–6073.
14. *Gu YY, Dou JY, Huang XR, Liu XS, Lan HY.* Transforming growth factor-β and long non-coding rna in renal inflammation and fibrosis. *Front Physiol.* 2021; 12: 684236.
15. *Zhang XL, An BF, Zhang GC.* MiR-27 alleviates myocardial cell damage induced by hypoxia/reoxygenation via targeting TGFBR1 and inhibiting NF-κB pathway. *Kaohsiung J Med Sci.* 2019; 35 (10): 607–614.
16. *Suzuki HI, Katsura A, Mihira H, Horie M, Saito A, Miyazono K.* Regulation of TGF-β-mediated endothelial-mesenchymal transition by microRNA-27. *J Biochem.* 2017; 161 (5): 417–420.
17. *Wang XH.* MicroRNA in myogenesis and muscle atrophy. *Curr Opin Clin Nutr Metab Care.* 2013; 16 (3): 258–266.
18. *Dong M, Wang X, L T, Wang J, Yang Y, Liu Y et al.* Mir-27a-3p attenuates bronchiolitis obliterans *in vivo* via the regulation of dendritic cells' maturation and the suppression of myofibroblasts' differentiation. *Clin Transl Med.* 2020; 10 (4): e140.
19. *Shevchenko OP, Velikiy DA, Sharapchenko SO, Gichkun OE, Marchenko AV, Ulybysheva AA et al.* Diagnostic value of microRNA-27 and -339 in heart transplant recipients with myocardial fibrosis. *Russian Journal of Transplantology and Artificial Organs.* 2021; 23 (3): 73–81.
20. *Velikiy DA, Gichkun OE, Sharapchenko SO, Mozheiko NP, Kurabekova RM, Shevchenko OP et al.* Diagnostic value of mirna-101 and mirna-27 in acute heart transplant rejection. *Russian Journal of Transplantology and Artificial Organs.* 2020; 22 (4): 20–26.
21. *Cuiqiong W, Chao X, Xinling F, Yinyan J.* Schisandrin B suppresses liver fibrosis in rats by targeting miR-101-5p through the TGF-β signaling pathway. *Artif Cells Nanomed Biotechnol.* 2020; 48 (1): 473–478.
22. *Li X, Zhang S, Wa M, Liu Z, Hu S.* MicroRNA-101 protects against cardiac remodeling following myocardial infarction via downregulation of runt-related transcription factor 1. *J Am Heart Assoc.* 2019; 8 (23): e013112.
23. *Pan Z, Sun X, Shan H, Wang N, Wang J, Ren J et al.* MicroRNA-101 inhibited postinfarct cardiac fibrosis and improved left ventricular compliance via the FBJ osteosarcoma oncogene/transforming growth factor-β1 pathway. *Circulation.* 2012; 126 (7): 840–850.
24. *Guiot J, Cambier M, Boeckx A, Henket M, Nivelles O, Gester F et al.* Macrophage-derived exosomes attenuate fibrosis in airway epithelial cells through delivery of antifibrotic miR-142-3p. *Thorax.* 2020; 75 (10): 870–881.
25. *Jung B, Staudacher JJ, Beauchamp D*. Transforming growth factor β super-family signaling in development of colorectal cancer. *Gastroenterology.* 2017; 152: 36–52.
26. *Meng XM, Nikolic-Paterson DJ, Lan HY.* TGF-β: the master regulator of fibrosis. *Nat Rev Nephrol.* 2016; 12 (6): 325–338.
27. *Okamoto Y, Gotoh Y, U emura O, Tanaka S, Ando T, Nishida M.* Age-dependent decrease in serum transforming growth factor TGF-beta 1 in healthy Japanese individuals; population study of serum TGF-beta 1 level in Japanese. *Dis Markers.* 2005; 21 (2): 71–74.
28. *Kurabekova RM, Shevchenko OP, Tsirulnikova OM, Mozheiko NP, Tsirulnikova IE, Olefirenko GA.* The re-

lationship of level of transforming growth factor beta 1 with liver fibrosis in children with congenital diseases of hepatobilliary system. *Klinicheskaya Laboratornaya Diagnostika (Russian Clinical Laboratory Diagnostics)*. 2017; 62 (4): 221–225 (in Russ.).
29. *Travis MA, Sheppard D.* TGF-b Activation and Function in Immunity. *Annu Rev Immunol.* 2014; 32 (1): 51–82.
30. *Kurabekova RM, Shevchenko OP, Tsiroulnikova OM, Mozheyko NP, Tsiroulnikova IE, Monakhov AR, Gautier SV.* Level of transforming growth factor beta-1 relates to congenital liver disease severity in children of early age. *Russian Journal of Transplantology and Artificial Organs*. 2016; 18 (3): 16–21 (In Russ.).
31. *Briem-Richter A, Leuschner A, Krieger T, Grabhorn E, Fischer L, Nashan B et al*. Peripheral blood biomarkers for the characterization of alloimmune reactivity after pediatric liver transplantation. *Pediatr Transplant*. 2013; 17 (8): 757–764.
32. *Israni AK, Li N, Cizman BB, Snyder J, Abrams J, Joffe M et al*. Association of donor inflammation- and apoptosis-related genotypes and delayed allograft function after kidney transplantation. *Am J Kidney Dis.* 2008; 52: 331–339.
33. *Lee SB, Kanasaki K, Kalluri R.* Circulating TGF-B1 as a reliable biomarker for chronic kidney disease progression in the African-American population. *Kidney Int*. 2009; 76: 10–12.
34. *Meng XM, Nikolic-Paterson DJ, Lan HY.* Inflammatory processes in renal fibrosis. *Nat Rev Nephrol*. 2014; 10: 493–503.
35. *Yuan Q, Tan RJ, Liu Y.* Myofibroblast in kidney fibrosis: origin, activation, and regulation. *Adv Exp Med Biol.* 2019; 1165: 253–283.
36. *Shull MM, Ormsby I, Kier AB, Pawlowski S, Diebold RJ, Yin M et al.* Targeted disruption of the mouse transforming growth factor-β1 gene results in multifocal inflammatory disease. *Nature.* 1992; 359: 693–699.
37. *Eikmans M, Sijpkens YW, Baelde HJ, de Heer E, Paul LC, Bruijn JA*. High transforming growth factor-β and extracellular matrix mRNA response in renal allografts during early acute rejection is associated with absence of chronic rejection. *Transplantation.* 2002; 73: 573–579.
38. *Du XX, Guo YL, Yang M, Yu Y, Chang S, Liu B et al.* Relationship of transforming growth factor-βl and arginase-1 levels with long-term survival after kidney transplantation. *Curr Med Sci.* 2018; 38: 455–460.
39. *Poppelaars F, Gaya da Costa M, Faria B, Eskandari SK, Damman J, Seelen MA*. A functional TGFB1 polymorphism in the donor associates with long-term graft survival after kidney transplantation. *Clin Kidney J*. 2021; 15 (2): 278–286.
40. *Sun Y, Weber KT.* Infarct scar: a dynamic tissue. *Cardiovasc Res.* 2000; 46 (2): 250–256.
41. *Moses HL.* TGF-beta regulations of epithelial cell proliferation. *Mol Prod Dev.* 1992; 32 (2): 179–183.
42. *Gichkun OE, Kurabekova RM, Olefirenko GA, Stahanova EA, Makarova LV, Shmerko NP et al.* Dinamika transformiruyushchego faktora rosta beta-1 u recipientov serdca. *Vestnik transplantologii i iskusstvennyh organov.* 2019; 21: 56.
43. *Karch DB, Billingham ME.* Cyclosporin-induced myocardial fibrosis: An unequally controlled case report. *Heart Transplant.* 1985; 4: 210–212.
44. *Frangogiannis NG.* Cardiac fibrosis. *Cardiovasc Res.* 2021; 117 (6): 1450–1488.
45. *Aziz T, Saad RA, Burgess M, Yonan N, Hasleton P, Hutchinson IV.* Transforming growth factor beta and myocardial dysfunction following heart transplantation. *European Journal of Cardio-Thoracic Surgery.* 2001; 20 (1): 177–186.
46. *Aziz T, Saad RA, Burgess M, Yonan N, Hasleton P, Hutchinson IV.* Transforming growth factor β in relation to cardiac allograft vasculopathy after heart transplantation. *J Thorac Cardiovasc Surg.* 2000; 119: 700–708.
47. *Gichkun OE, Shevchenko OP, Kurabekova RM, Mozheiko NP, Shevchenko AO.* The rs1800470 Polymorphism of the TGFB1 Gene Is Associated with Myocardial Fibrosis in Heart Transplant Recipients. *Acta Naturae.* 2021; 13 (4): 42–46.
48. *DerHovanessian A, Weigt SS, Palchevskiy V, Shino MY, Sayah DM, Gregson AL et al.* The role of TGF-β in the association between primary graft dysfunction and bronchiolitis obliterans syndrome. *Am J Transplant.* 2016; 16 (2): 640–649.
49. *Stewart S, Fishbein MC, Snell GI, Berry GJ, Boehler A, Burke MM et al.* Revision of the 1996 working formulation for the standardization of nomenclature in the diagnosis of lung rejection. *J Heart Lung Transplant.* 2007; 26: 1229–1242.
50. *Westall GP, Snel GI, Loskot M, Levvey B, O'Hehir RE, Hedger MP, de Kretser DM.* Activin biology after lung transplantation. *Transplant Direct.* 2017; 3 (6): e159.
51. *Sime PJ, Xing Z, Graham FL, Csaky KG, Gauldie J.* Adenovector-mediated gene transfer of active transforming growth factor-beta1 induces prolonged severe fibrosis in rat lung. *J Clin Invest.* 1997; 100: 768–776.
52. *Charpin JM, Valcke J, Kettaneh L, Epardeau B, Stern M, Israël-Biet D.* Peaks of transforming growth factor-β in alveolar cells of lung transplant recipients as an early marker of chronic rejection. *Transplantation.* 1998; 65 (5): 752–755.
53. *Yue YL, Zhang MY, Liu JY, Fang LJ, Qu YQ*. The role of autophagy in idiopathic pulmonary fibrosis: from mechanisms to therapies. *Ther Adv RespirDis*. 2022; 16: 17534666221140972.
54. *Ye Z, Hu Y.* TGF-β1: Gentlemanly orchestrator in idiopathic pulmonary fibrosis (Review). *Int J Mol Med.* 2021; 48 (1): 132.
55. *Cohen DJ, Loertcher R, Rubin MF, Tilney NL, Carpenter CB, Strom TB.* Cyclosporine: A New Immunosuppressive Agent for Organ Transplantation. *Ann Intern Med.* 1984; 101: 667–682.
56. *Bentata Y.* Tacrolimus: 20 years of use in adult kidney transplantation. What we should know about its nephrotoxicity. *Artif Organs.* 2020; 44 (2): 140–152.
57. *Liu Q, Ye J, Yu L, Dong X, Feng J, Xiong Y et al.* Mitigates Cyclosporine A (CsA)-Induced Epithelial-Mesenchymal Transition (EMT) and Renal Fibrosis in Rats. *Int Urol Nephrol.* 2017; 49: 345–352.

58. *Nagavally RR, Sunilkumar S, Akhtar M, Trombetta LD, Ford SM.* Chrysin Ameliorates Cyclosporine-A-Induced Renal Fibrosis by Inhibiting TGF-β1-Induced Epithelial-Mesenchymal Transition. *Int J Mol Sci.* 2021; 22 (19): 10252.
59. *Khanna A, Plummer M, Bromberek C, Bresnahan B, Hariharan S.* Expression of TGF-beta and fibrogenic genes in transplant recipients with tacrolimus and cyclosporine nephrotoxicity. *Kidney Int.* 2002; 62: 2257–2263.
60. *Zhang LY, Jin J, Luo K, Piao SG, Zheng HL, Jin JZ et al.* Shen-Kang protects against tacrolimus-induced renal injury. *Korean J Intern Med.* 2019; 34 (5): 1078–1090.
61. *Boix F, Alfaro R, Jiménez-Coll V, Mrowiec A, Martínez-Banaclocha H, Botella C, Muro M.* A high concentration of TGF-β correlates with opportunistic infection in liver and kidney transplantation. *Human Immunology.* 2021; 82 (6): 414–421.
62. *Neuzillet C, Tijeras-Raballand A, Cohen R, Cros J, Faivre S, Raymond E, de Gramont A.* Targeting the TGFβ pathway for cancer therapy. *Pharmacol Ther.* 2015; 147: 22–31.
63. *Border WA, Okuda S, Languino LR, Sporn MB, Ruoslahti E.* Suppression of experimental glomerulonephritis by antiserum against transforming growth factor beta 1. *Nature.* 1990; 346: 371–374.
64. *Kasuga H, Ito Y, Sakamoto S, Kawachi H, Shimizu F, Yuzawa Y, Matsuo S.* Effects of anti-TGF-β type II receptor antibody on experimental glomerulonephritis. *Kidney Int.* 2001; 60: 1745–1755.
65. *Das S, Kumar M, Negi V, Pattnaik B, Prakash YS, Agrawal A, Ghosh B.* MicroRNA-326 regulates profibrotic functions of transforming growth factor-β in pulmonary fibrosis. *Am J Respir Cell Mol Biol.* 2014; 50 (5): 882–892.
66. *Isaka Y.* Targeting TGF-β Signaling in Kidney Fibrosis. *Int J Mol Sci.* 2018; 19 (9): 2532.
67. *De Streel G, Bertrand C, Chalon N, Liénart S, Bricard O, Lecomte S et al.* Selective inhibition of TGF-β1 produced by GARP-expressing Tregs overcomes resistance to PD-1/PD-L1 blockade in cancer. *Nat Commun.* 2020; 11 (1): 4545.
68. *Nakano T, Lai CY, Goto S, Hsu LW, Kawamoto S, Ono K et al.* Immunological and regenerative aspects of hepatic mast cells in liver allograft rejection and tolerance. *PloS One.* 2012; 7 (5): 15.
69. *Luangmonkong T, Suriguga S, Bigaeva E, Boersema M, Oosterhuis D, de Jong KP et al.* Evaluating the antifibrotic potency of galunisertib in a human *ex vivo* model of liver fibrosis. *Br J Pharmacol.* 2017; 174: 3107–3117.

The article was submitted to the journal on 05.05.2023

DOI: 10.15825/1995-1191-2023-2-158-166

NORMOTHERMIC *EX VIVO* LUNG PERFUSION USING A DEVELOPED SOLUTION FOLLOWED BY ORTHOTOPIC LEFT LUNG TRANSPLANTATION (EXPERIMENTAL STUDY)

S.V. Gautier[1, 2], I.V. Pashkov[1], V.K. Bogdanov[1], D.O. Oleshkevich[1], D.M. Bondarenko[1], N.P. Mozheiko[1], N.S. Bunenkov[3–5], N.V. Grudinin[1]

[1] Shumakov National Medical Research Center of Transplantology and Artificial Organs, Moscow, Russian Federation
[2] Sechenov University, Moscow, Russian Federation
[3] Pavlov University, St. Petersburg, Russian Federation
[4] Almazov National Medical Research Centre, St. Petersburg, Russian Federation
[5] St. Luke's Clinical Hospital, St. Petersburg, Russian Federation

The continued unavailability of adequate organs for transplantation to meet the existing demand has resulted in a major challenge in transplantology. This is especially felt in lung transplantation (LTx). LTx is the only effective method of treatment for patients with end-stage lung diseases. Normothermic *ex vivo* lung perfusion (EVLP) has been proposed to increase the number of donor organs suitable for transplant – EVLP has proven itself in a number of clinical trials. The ability to restore suboptimal donor lungs, previously considered unsuitable for transplantation, can improve organ functionality, and thus increase the number of lung transplants. However, widespread implementation of *ex vivo* perfusion is associated with high financial costs for consumables and perfusate. **Objective:** to test the developed solution on an *ex vivo* lung perfusion model, followed by orthotopic LT under experimental conditions. **Materials and methods.** The experiment included lung explantation stages, static hypothermic storage, EVLP and orthotopic left LTx. Perfusion was performed in a closed perfusion system. We used our own made human albumin-based perfusion solution as perfusate. Perfusion lasted for 2 hours, and evaluation was carried out every 30 minutes. In all cases, static hypothermic storage after perfusion lasted for 4 hours. The orthotopic single-lung transplantation procedure was performed using assisted circulation, supplemented by membrane oxygenation. Postoperative follow-up was 2 hours, after which the experimental animal was euthanized. **Results.** Respiratory index before lung explantation was 310 ± 40 mmHg. The PaO_2/FiO_2 ratio had positive growth dynamics throughout the entire EVLP procedure. Oxygenation index was 437 ± 25 mm Hg after 120 minutes of perfusion. Throughout the entire EVLP procedure, there was a steady decrease in pulmonary vascular resistance (PVR). Initial PVR was 300 ± 100 dyn×s/cm^5; throughout the EVLP, PVR tended to fall, reaching 38,5 ± 12 dyn×s/cm^5 at the end of perfusion. **Conclusion.** A safe and effective EVLP using our perfusate is possible. The developed orthotopic left lung transplantation protocol under circulatory support conditions, supplemented by membrane oxygenation, showed it is efficient and reliable.

Keywords: lung transplantation, donation, perfusate, perfusion.

INTRODUCTION

Shortage of donor organs remains a major challenge in transplantology. The situation is especially critical in areas such as LTx. LTx is the only effective method of treatment for patients with end-stage lung diseases. In order to increase the number of donor organs that are suitable for transplant, EVLP is proposed. EVLP has shown to be effective in a number of clinical trials [1, 2].

The ability to restore suboptimal donor lungs, previously considered unsuitable for transplantation, allows for improving organ functionality. However, the spread of *ex vivo* perfusion technology in clinical practice is associated with high financial costs for consumables and perfusate [3]. Swedish company XVIVO leads the global market in terms of production of perfusate for donor lungs. The company accounts for about 70% of the market. Due to the small production capacity of this monopolistic company, countries that are just introducing *ex vivo* perfusion technology are experiencing a certain deficit [4].

Ex vivo perfusion is beginning to develop in Russia. Its active introduction in the country is being restrained by the high cost of the original perfusate (Steen Solution

Corresponding author: Nikita Grudinin. Address: 1, Shchukinskaya str., Moscow, 123182, Russian Federation. Phone: (903) 805-63-58. E-mail: Zbignev.religa@mail.ru

TM). In previous articles, we have presented a successful experience in using our Russian-made human albumin-based solution as perfusate. The only disadvantage of this solution is that it must be prepared before each EVLP procedure.

The purpose of the presented pilot study is to test our developed solution under experimental conditions on an *ex vivo* lung perfusion model followed by orthotopic LTx.

MATERIALS AND METHODS

Isolated lungs obtained from Romanov sheep weighing 25–30 kg were used in the experimental study. The experimental work program was approved by the Committee on Biological Safety and Bioethics, Shumakov National Medical Research Center of Transplantology and Artificial Organs. The work was performed in compliance with the rules of the European Convention for the Protection of Vertebrate Animals Used for Experimental and Other Scientific Purposes [5].

The experiment included lung explantation stages, static hypothermic storage, EVLP and orthotopic left LTx.

Donor and recipient were narcotized with zolazepam solution at 10 mg/kg, followed by a combination of isoflurane 2.5% to 3% vol. inhalation anesthetics. During explantation, central pressure monitoring and artificial ventilation were performed in the volume control mode at the rate of 8–10 ml/kg; peak inspiratory pressure did not exceed 25 cm a.c., positive end-expiratory pressure did not exceed 5 cm H_2O, respiratory rate was 25 bpm, and depth of anesthesia was adjusted using an isoflurane vaporizer. The explantation technique was described in detail in our previous article [6]. Celsior solution was used as a preserving agent.

Perfusion was performed in a closed circuit using Ex Stream perfusion system (Transbiotech, Russia); a balloon with deoxygenating mixture (N_2, 86%; CO_2, 8%; O_2, 6%) was connected to the oxygenator. A centrifugal CPB pump with a hydrophilic head was installed in the trunk system between the cardiotomy reservoir and oxygenator. The trunk after the oxygenator was connected to an 18 Fr cannula installed in the pulmonary artery. Outflow was performed actively through a funnel-shaped cannula sutured to the left atrial area. Pressure measurement in the trunk system was performed by installing three invasive sensors: the first was installed after the oxygenator to measure pressure in the proximal part of the perfusion system, the second was installed directly in the pulmonary artery cannula to measure perfusion pressure in the pulmonary artery. The third sensor measures pressure in a cannula inserted into the left atrium to monitor left atrial pressure. The lung graft at the moment of perfusion was placed in a chamber designed to allow *ex vivo* perfusion under sterile conditions [7]. We used our own Russian-made human albumin-based perfusion solution as perfusate. The perfusate was 1.5 liters in volume in all groups. Red cell mass was prepared by centrifugation of whole leukocyte-free blood for 15 minutes at 3,500 rpm. Meropenem 1000 mg, methylprednisolone 1000 mg, and short-acting insulin 10 units were added to the perfusate. The target hematocrit level was 15%. A general view of the perfusion system is shown in Fig. 1.

The perfusion time was 2 hours, evaluation was done every 30 minutes. PVR, dynamic compliance, respiratory index, glucose utilization rate and lactate gain were assessed. At the end of perfusion, the lungs were re-preserved with 2,000 mL of experimental solution antegrade. Static hypothermic storage after perfusion lasted for 4 hours in all observations. Postoperative follow-up was 2 hours, after which the experimental animal was euthanized.

The orthotopic left LTx procedure consisted of 3 stages:

Stage 1 (Anesthesia of experimental animal): Was performed in the same manner as in the donor procedure. All transplant surgeries were performed under cardiopulmonary bypass. Ex Stream device (Biosoft-M, Russia) with centrifugal pump Rotaflow (MAQUET, Germany) and oxygenator Affinity Fusion (Medtronic, USA) with a set of lines, were used as auxiliary circulation. Catheterization of the external jugular vein and common carotid artery for invasive monitoring was performed on the right side; arterial and venesection was performed on the left side, followed by cannulation after systemic heparinization. A 20 Fr venous cannula was inserted to the 20–25 cm mark, which corresponded to its position in the vena cava sinus. A 12 Fr arterial cannula was inserted into the common carotid artery to a 5–6 cm depth. After cannula positioning, artificial circulation was started at half of the calculated volume of 1,500 mL/min.

Fig. 1. General view of the closed perfusion system

Stage 2 (Left-sided thoracotomy, pneumonectomy): The skin incision was made at the level of the 5th intercostal space, wound edges were separated with a retractor. For better visualization of anatomical structures of the root, ventilation was stopped, and artificial circulation was switched on at the full estimated volume. When isolating the root, the pulmonary artery was first isolated and taken into a tourniquet, then pulmonary veins were isolated and taken into a holder. After all vascular structures were isolated, the pulmonary artery was sutured with a stapler, the pulmonary veins were ligated manually. The left main bronchus was sutured and crossed last with an 0.5 cm indent from the tracheal bifurcation. At the end of pneumonectomy, meticulous hemostasis was performed.

Stage 3 (Left lung transplantation): The lung graft was removed from a sterile bag containing a preservative and placed on a manipulation table, the left lung was separated. The pulmonary artery was severed from bifurcation, the left main bronchus was crossed with an indentation of one semicircle from the bifurcation. After the graft was placed in the wound, the bronchial anastomosis was placed first, using continuous locking PDS 4/0 sutures (Ethicon, USA). Next, atrial anastomosis was performed using Prolen 5/0 (Ethicon, USA) continuous winding suture on an atraumatic needle, and the pulmonary artery anastomosis was performed last, also using Prolen 7/0 (Ethicon, USA) continuous locking suture on an atraumatic needle.

Upon completion of the anastomoses, we resumed artificial ventilation, opened the clamp on the pulmonary artery and under visual control performed graft deaeration through the untied atrial anastomosis. Then the knot was tightened and tied at the atrial anastomosis, hemostasis control was performed. After hemodynamics stabilization, artificial circulation was stopped, and protamine was injected in the calculated dose. The observation period was 4 hours, the thoracotomy wound was not sutured. Blood samples were taken selectively from the left pulmonary veins every hour. Obtained data were plotted (pCO_2, pO_2 and respiratory index were assessed).

All experiments ended with taking graft biopsy specimens followed by morphological study. Microscopic analysis was performed using a light microscope, photos were taken using a digital camera. The obtained sections were evaluated for vascular thrombosis, hemorrhages, interstitial and alveolar edema development as well as cellular infiltration.

The experiment was terminated by euthanizing the animal with an injection of lethal dose of potassium chloride to trigger a cardiac arrest.

RESULTS

Respiratory index before donor lung explantation was 310 ± 40 mmHg. Throughout the entire *ex vivo* perfusion procedure, PaO_2/FiO_2 increase maintained positive dynamics. After 120 minutes of perfusion, the oxygenation index was 437 ± 25 mm Hg, which is a good indicator of restoration of respiratory lung function (Fig. 2).

From the beginning of perfusion, lactate level in the perfusate was 1.2 mmol/L, and a gradual increase in lactate level was noted throughout the *ex vivo* perfusion procedure. At the end of the EVLP procedure, lactate levels in the solution were 7.4 mmol/L, indicating adequate metabolism in the perfused lungs (Fig. 3).

Throughout the entire *ex vivo* perfusion procedure, PVR decreased steadily. Initial PVR was 300 ± 100 Dyn×s/cm^5, throughout the *ex vivo* perfusion, PVR tended to fall. At the end of perfusion, the PVR index was 38.5 ± 12 Dyn×s/cm^5, dynamics of PVR changes are shown in Fig. 4.

The PaO_2/FiO_2 ratio was 345 ± 25 mm Hg 60 minutes after orthotopic left LTx; the respiratory index was 360 ± 25 mm Hg after 120 minutes. Dynamics of the respiratory index are shown in Fig. 5).

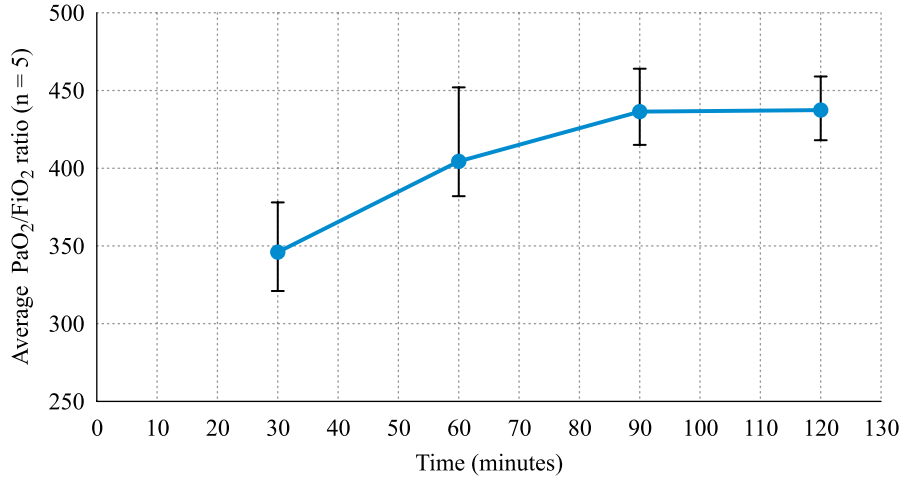

Fig. 2. Dynamics of the PaO_2/FiO_2 ratio at the *ex vivo* perfusion stage

Changes in lung compliance indices (dynamic compliance) during normothermic *ex vivo* machine perfusion procedure are shown in the graph (Fig. 6). The positive increase in values from the moment perfusion was initiated to the final measurement indirectly indicated a decrease in the amount of extravascular water in donor

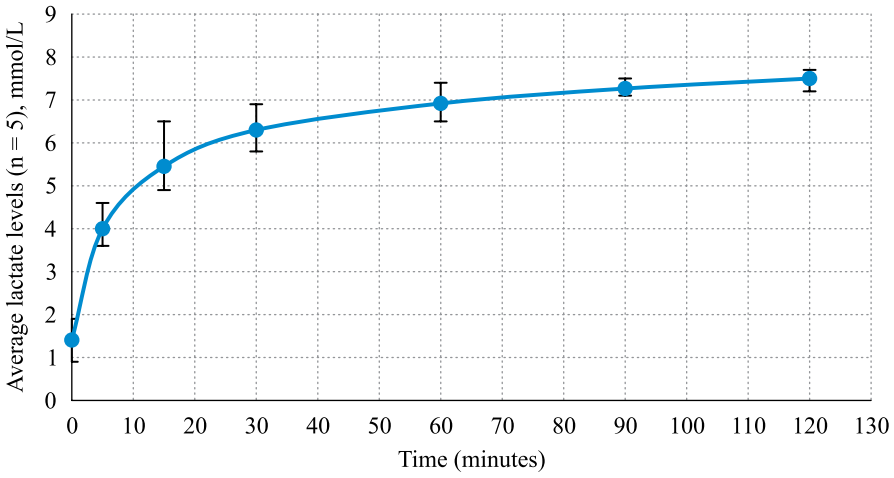

Fig. 3. Lactate levels during *ex vivo* perfusion

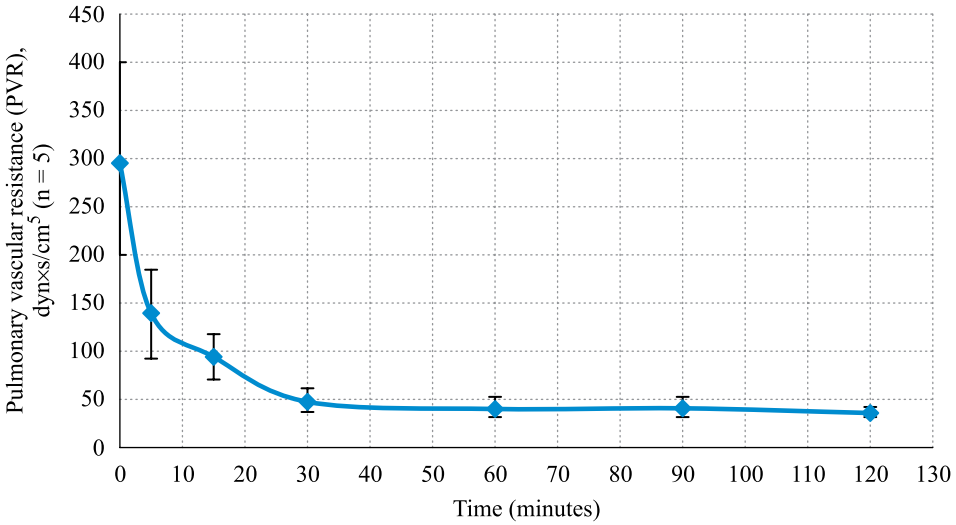

Fig. 4. Pulmonary vascular resistance dynamics

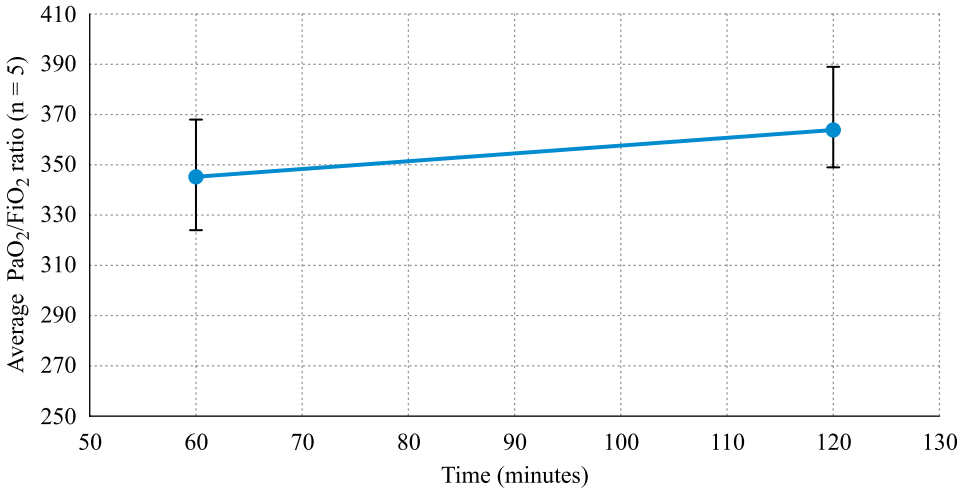

Fig. 5. Oxygenation index dynamics after transplantation

lungs, being a criterion for EVLP efficiency, and reflected positive dynamics of the functional status of the graft.

Throughout the entire *ex vivo* perfusion procedure, airway resistance decreased steadily. At the beginning of perfusion, resistance was 1.4 ± 0.5 cm H_2O/L/sec. At the end of perfusion, resistance was 0.7 ± 0.4 cm H_2O/L/sec. Dynamics of airway resistance during *ex vivo* perfusion are shown in Fig. 7.

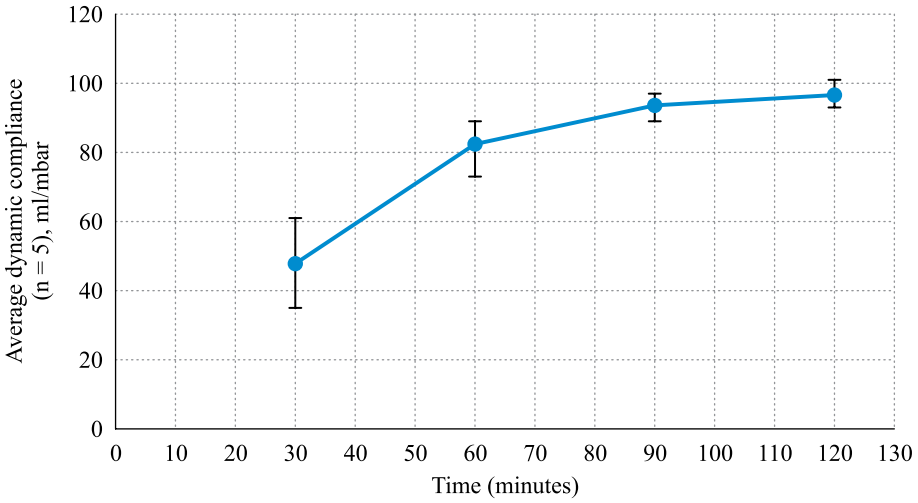

Fig. 6. Dynamic compliance dynamics

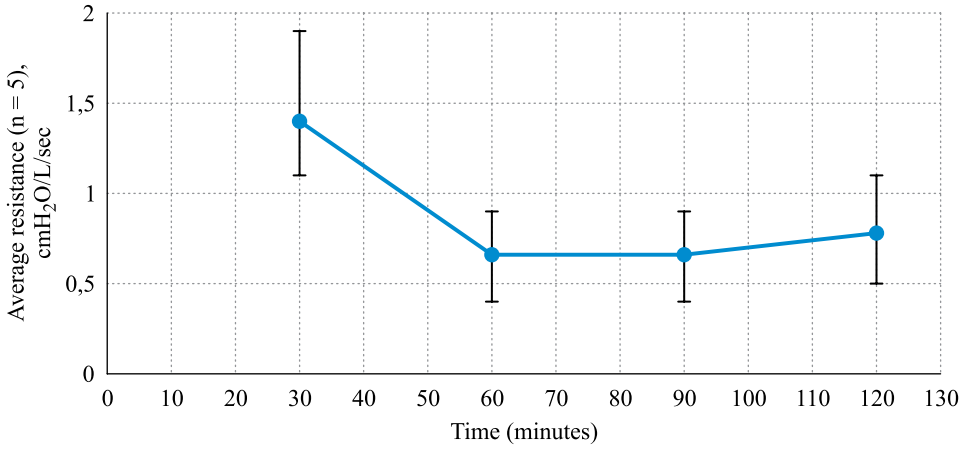

Fig. 7. Airway resistance dynamics during *ex vivo* perfusion

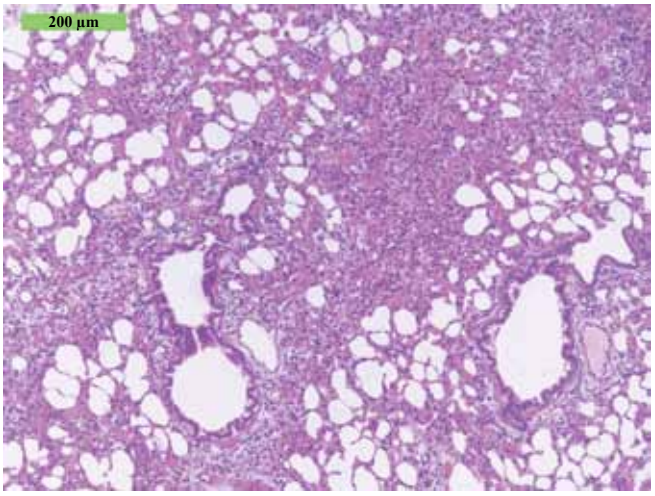

Fig. 8. Histological pattern, area of atelectasis taken before perfusion

Morphological data

Before *ex vivo* perfusion, histological material was taken from the atelectasis zones mainly in the posterior basal regions. Sections showed a classical picture of atelectatic pulmonary parenchyma in the form of recessed alveolar air spaces (Fig. 8).

Morphological examination of lung fragments from zones of expanded massive atelectasis, obtained after 120 minutes of perfusion, showed that the architectonics of the pulmonary parenchyma were preserved in all observations. Well swollen alveoli were noted in most sections. Microatelectatic zones were distributed heterogeneously and were found only in separate segments. Alveolar air spaces, as well as peribronchovascular interstitium were slightly thickened (Fig. 9).

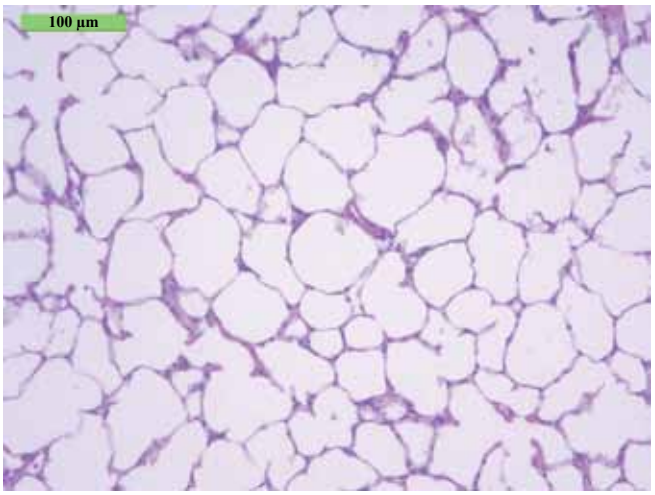

Fig. 9. Histological pattern, areas of expanded atelectasis, after *ex vivo* perfusion

DISCUSSION

The high demand for normothermic EVLP procedure creates prerequisites for coming up with alternative most technologically profitable solutions. More and more often in world literature, there are works featuring modifications of the original solution, and attempts are also being made to create a solution on the basis of official drugs commonly available in the clinic [10].

The developed original native solution for normothermic EVLP that is based on commonly available registered drugs is certainly the optimal solution for overcoming the existing challenges. In previous works, experimental testing of perfusion solutions prepared on the basis of drugs commonly available in the clinic achieved positive results. However, after *ex vivo* perfusion, LTx was not performed under experimental conditions [11, 12]. In this study, the main task was to create a model on a large animal, which is as close to clinical conditions as possible. The EVLP procedure was performed according to the previously described protocol using the original solution. After *ex vivo* perfusion, lung graft was preserved before the upcoming transplantation. The research work resulted in the development of a single-lung transplantation protocol on an experimental ram model.

Several animal models have been proposed in the world literature. However, in the present study, preference was given to rams due to the most surgically acceptable anatomy of the main vessels in the neck, which is necessary for adequate anesthetic support [13, 14]. In addition to setting up central access and invasive arterial pressure monitoring, central vessels can be cannulated on the contralateral side to implant a mechanical circulatory support system supplemented with membrane oxygenation, which was also implemented in this work. During transplantation, a circulatory assist device was implanted in order to prevent hydrostatic pulmonary edema and maintain adequate hemodynamics. Performing orthotopic LTx under assisted circulation significantly increases the duration of the experimental work, but at the same time avoids many complications and brings the experiment as close as possible to real clinical practice [15–17]. The experimental study achieved satisfactory oxygenation index values during *ex vivo* perfusion and two hours after orthotopic LTx. Dynamic compliance indicators during the early post-transplant period indirectly reflected the degree of ischemia-reperfusion injury in the donor lung; and values >50 mL/bar along with other indices suggest a low risk of early primary graft dysfunction. Limit airway resistance values during normothermic machine perfusion procedure and in the early post-transplant period remained within the limits of physiological norm; they were significantly lower than the generally accepted constants during artificial ventilation of the lungs. Low airway resistance is an indirect sign of satisfactory functional status of donor lungs, and also testify to the absence of parenchymal edema, accompanying primary graft dysfunction.

The dynamics of a decrease in PVR during perfusion indicates its adequacy and effectiveness. Experimental orthotopic single-lung transplantation under circulatory support with the use of peripheral cannulation of the central vessels showed easy implementation and high efficiency. The absence of pulmonary parenchymal edema and absence of pathological changes during perfusion and after orthotopic transplantation, according to histological study results, indicate that the technique is effective and safe [18, 19].

CONCLUSION

It is possible to conduct a safe and effective normothermic EVLP procedure using our own-made perfusion solution. The developed orthotopic left LTx protocol under assisted circulation, supplemented by membrane oxygenation, is efficient and reliable.

The authors declare no conflict of interest.

REFERENCES

1. *Chambers DC, Perch M, Zuckermann A, Cherikh WS, Harhay MO, Hayes DJ et al.* The International Thoracic Organ Transplant Registry of the International Society for Heart and Lung Transplantation: Thirty-sixth adult lung and heart–lung transplantation Report – 2019; Focus theme: Donor and recipient size match. *Journal of Heart and Lung Transplantation*. 2019; 38 (10): 1042–1055. doi: 10.1016/j.healun.2021.07.021.
2. *Ohsumi A, Kanou T, Ali A, Guan Z, Hwang DM, Thomas KW et al*. A method for translational rat *ex vivo* lung perfusion experimentation. *American Journal of Physiology-Lung Cellular and Molecular Physiology.* 2020; 319 (1): 61–70. doi: 10.1152/ajplung.00256.2019.
3. *Chakos A, Ferret P, Muston B, Yan TD, Tian DH. Ex vivo* lung perfusion versus standard protocol lung transplan-

tation-mid-term survival and meta-analysis. *Annals of Cardiothoracic Surgery*. 2020; 9 (1): 1–9.
4. *Nilsson T. Ex vivo* Lung Perfusion – Experimental and Clinical Studies. 2018: 88.
5. *Zoeller KA.* Pulsatile flow does not improve efficacy in *ex vivo* lung perfusion. *The University of Louisville s Institutional Repository. Electronic Theses and Dissertations*. 2013: 1651.
6. *Gautier SV, Tsirulnikova OM, Pashkov IV, Grudinin NV, Oleshkevich DO, Bondarenko DM et al.* Evaluation of the efficacy of a novel perfusion solution for normothermic *ex vivo* lung perfusion compared with Steen solution™ (animal experimental study). *Russian Journal of Transplantology and Artificial Organs*. 2021; 23 (3): 82–89. doi: 10.15825/1995-1191-2021-3-82-89.
7. *Gautier SV, Tsirulnikova OM, Pashkov IV, Filatov IA, Bogdanov VK, Grudinin NV et al.* Normothermic *ex vivo* perfusion of isolated lungs in an experiment using a Russian made perfusion system. *Russian Journal of Transplantology and Artificial Organs*. 2022; 24 (2): 94–101. doi: 10.15825/1995-1191-2022-2-94-101.
8. *Mohan S, Chiles MC, Patzer RE, Pastan SO, Husain SA, Carpenter DJ et al.* Factors leading to the discard of deceased donor kidneys in the United States. *Kidney.* 2018; 94 (1): 187–198. doi: 10.1016/j.kint.2018.02.016.
9. *Mattar A, Chatterjee S, Loor G.* Bridging to Lung Transplantation. *Critical Care Clinics*. 2019; 35 (1): 11–25. doi: 10.1016/j.ccc.2018.08.006.
10. *Buchko MT, Sayed H, Nader SA, Catherine JS, Sanaz H et al.* A low-cost Perfusate Alternative for *ex vivo* lung perfusion. *Transplant Proc*. 2020; 52 (10): 2941–2946. doi: 10.1016/j.transproceed.2020.05.007.
11. *Grudinin NV, Bogdanov VK, Sharapov MG, Bunenkov NS, Mozheiko NP, Goncharov RG et al.* Use of peroxiredoxin for preconditioning of heterotopic heart transplantation in a rat. *Russian Journal of Transplantology and Artificial Organs*. 2020; 22 (2): 158–164. doi: 10.15825/1995-1191-2020-2-158-164.
12. *Cypel M, Keshavjee S. Ex vivo* Lung Perfusion. *Operative Techniques in Thoracic and Cardiovascular Surgery*. 2014; 19 (4): 433–442. doi: 10.1053/j.optechstcvs.2015.03.001.
13. *Kotecha S, Jamie H, Jeremy F, Eldho P, Bronwyn JL, Helen W et al.* Continued Successful Evolution of Extended Criteria Donor Lungs for Transplantation. *Annals of Thoracic Surgery*. 2017; 104 (5): 1702–1709.
14. *Raghu G, Carbone RG.* Lung Transplantation: Evolving Knowledge and New Horizons. 2018. 370. doi. 10.1007/978-3-319-91184-7.
15. *Lee HJ, Hwang Y, Hwang HY, Park IK, Kang CH, Kim YW, Kim YT.* Use of Extracorporeal Membrane Oxygenation Prior to Lung Transplantation Does Not Jeopardize Short-term Survival. *Transplant Proc.* 2015; 47 (9): 2737–2742. doi: 10.1016/j.transproceed.2015.09.061. PMID: 26680084.
16. *Loor G Warnecke G, Villavicencio MA, Smith MA, Kukreja J, Ardehali A et al.* Portable normothermic ex-vivo lung perfusion, ventilation, and functional assessment with the Organ Care System on donor lung use for transplantation from extended-criteria donors (EXPAND): a single-arm, pivotal trial. *The Lancet Respiratory Medicine.* 2019; 7 (11): 975–984. doi: 10.1016/S2213-2600(19)30200-0.
17. *Tane S, Noda K, Shigemura N. Ex vivo* Lung Perfusion: A Key Tool for Translational Science in the Lungs. *Chest*. 2017; 151 (6): 1220–1228. doi: 10.1016/j.chest.2017.02.018.
18. *Ordies S, Frick AE, Claes S, Schols D, Verleden SE, Raemdonck DE et al.* Prone Positioning During *Ex vivo* Lung Perfusion Influences regional Edema Accumulation. *Journal of Surgical Research*. 2019; 239 (16): 300–308. doi: 10.1016/j.jss.2019.02.003.
19. *Yusen RD, Edwards LB, Kucheryavaya AY, Benden C, Dipchand AI, Goldfarb SB et al.* The Registry of the International Society for Heart and Lung Transplantation: Thirty-third Adult Heart Transplantation Report – 2016; Focus Theme: Primary Diagnostic Indications for Transplant. *Journal of Heart and Lung Transplantation*. 2016; 35 (10): 1158–1169. doi: 10.1016/j.healun.2015.08.014.

The article was submitted to the journal on 27.03.2023

DOI: 10.15825/1995-1191-2023-2-167-169

SUCCESSFUL LIVER TRANSPLANTATION FROM A DECEASED DONOR WHO WAS ON HEMODIALYSIS FOR 10 YEARS

D.A. Altman[1], O.M. Tsirulnikova[2, 3], A.E. Poltorak[1], V.V. Pchelnikov[2], B.Kh. Sarsenbayev[1], A.S. Ryzhykh[1], I.Ya. Bondarevsky[1], E.G. Muravyeva[1]

[1] Chelyabinsk Regional Clinical Hospital, Chelyabinsk, Russian Federation
[2] Shumakov National Medical Research Center of Transplantology and Artificial Organs, Moscow, Russian Federation
[3] Sechenov University, Moscow, Russian Federation

Objective: to analyze the possibility of using the liver of a donor undergoing hemodialysis as a transplant. **Materials and methods.** A case of successful liver transplantation (LT) from a 40-year-old deceased donor, who had been on hemodialysis for 10 years for chronic pyelonephritis and nephrosclerosis, is presented. Of the known hemodialysis complications of chronic kidney disease, the donor's medical records showed anemia and grade 3 arterial hypertension. **Results.** The recipient's post-LT period had no significant differences from the postoperative period of those that received liver from donors with standard criteria. **Conclusion.** Our first experience with the use of a liver transplant from a donor who was on hemodialysis, in the absence of other risk factors, suggests that the liver of this category of donors can be used for transplantation.

Keywords. Liver donor with end-stage renal disease, liver transplantation.

INTRODUCTION

In end-stage renal disease (ESRD), practically all organs and systems of the body are affected. Obviously, donors with ESRD belong to the group of expanded criteria donors. And the use of such patients as liver donors is in line with the global trend, i.e., expansion of liver donation criteria, and such cases have not been described by Russian researchers [2]. Such a factor as ESRD is likely to have a significant impact on the quality of LT. Organs of the digestive system are most frequently affected, which is due to the influence of uremia [3]. The liver has been shown to be involved in excretion of nitrogenous products. The majority of patients with chronic kidney disease show various pathological changes in the gastrointestinal tract organs, which can be detected by instrumental and laboratory tests [4]. But given the quality of renal replacement therapy at present, there are patients for which changes in their gastrointestinal tract organs are minimal against many years of long-term hemodialysis therapy.

MATERIALS AND METHODS

A case of successful LT from a 40-year-old deceased donor, who was on long-term hemodialysis for 10 years for chronic pyelonephritis and nephrosclerosis, is presented. Of the known hemodialysis complications of chronic kidney disease, the donor's medical records showed anemia and grade 3 arterial hypertension. Cause of death was parenchymal ventricular hemorrhage in the right hemisphere, cardiac tamponade in the III and IV ventricles, cerebral edema, and dislocation syndrome against the background of hypertension crisis. Donors with such causes of death are the most common [6]. After hemodialysis session and exclusion of uremic intoxication, cerebral death was pronounced. Given the high risk of viral hepatitis infection in patients receiving hemodialysis treatment, blood was tested by ELISA and PCR for viral hepatitis B and C, HIV infection, and syphilis. The tests detected no infections. Donor's anthropometric data were: height 178 cm and body weight 60 kg. Laboratory parameters (ALT, AST, total and direct bilirubin, blood sodium level) were within normal limits. The follow-up period in the intensive care unit was three days. Hemodynamics vasopressor support was performed with norepinephrine at a dose of 0.13 μg/kg/minute. According to ultrasound, anteroposterior dimension of the right lobe of the liver was 145 mm, that of the left lobe was 78 mm, liver parenchyma was of moderate echogenicity and normal sound conductivity, no signs of fatty hepatosis were detected. Macroscopic assessment of the liver: the liver margin was acute, no signs of fatty hepatosis were noted (Fig. 1, 2). There were also no signs of atherosclerosis of the aorta and large arteries. There were no reasons to refuse organ transplantation. The decision to procure an organ from this donor was made jointly with specialists from Shumakov National Medical Research Center of Transplantology and Artificial Organs.

Corresponding author: Aleksandr Poltorak. Address: 70, Vorovskogo str., Chelyabinsk, 454048, Russian Federation. Phone: (908) 062-49-26. E-mail: aleksandrpoltorak@yandex.ru

RESULTS AND DISCUSSION

It has been reported that in some cases, transplantation using an available organ from an expanded criteria donor is preferable than waiting for a standard criteria donor, which is due to the negative dynamics of the patient's condition while waiting for surgery [1]. And in our case, the postoperative period of a patient requiring LT from this expanded criteria donor as soon as possible did not differ significantly from the postoperative period of those that received liver from standard criteria donors. The recipient's length of intensive care and the dynamics of laboratory parameters are comparable with those of other recipients.

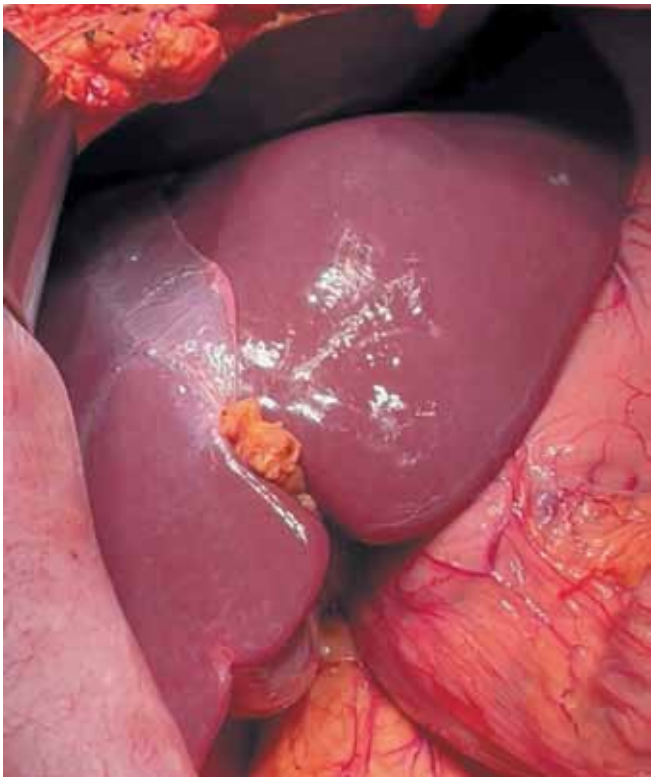

Fig. 1. Visual assessment of a liver from a donor who was on long-term hemodialysis

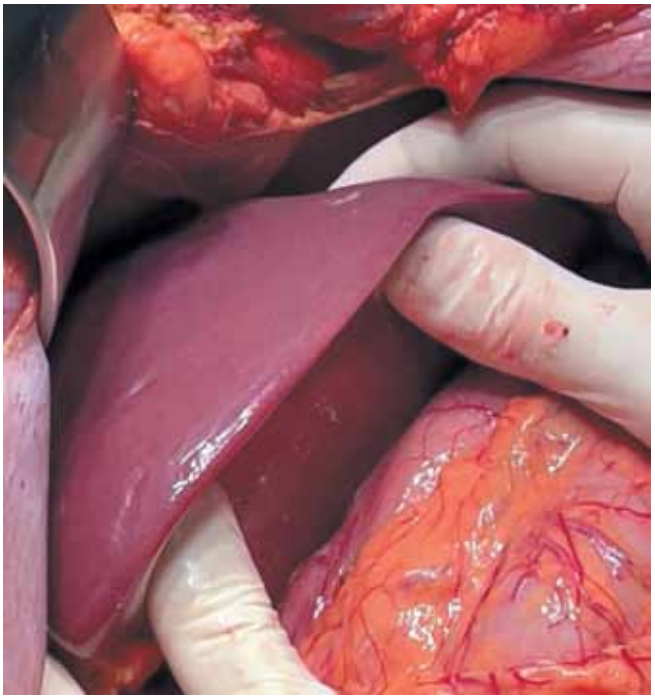

Fig. 2. Edge of the left lobe of the liver of a donor who was on long-term hemodialysis

A retrospective assessment of the morphological picture in the graft also confirmed the absence of signs of fatty hepatosis, it revealed single zonal necrosis, and the portal tracts were weakly fibrosed.

CONCLUSION

The first experience of using a liver transplant from a donor who was on long-term hemodialysis treatment, in the absence of such risk factors as age, transaminase levels, hemodynamic instability, duration of cold ischemia time, significant steatosis and hypernatremia [5], suggests that the liver of this category of donors can be used for transplantation. This reduces the LT waiting time for waitlisted candidates.

The authors declare no conflict of interest.

REFERENCES

1. *Flores A, Asrani SK.* The donor risk index: A decade of experience. *Liver Transpl*. 2017; 23 (9): 1216–1225. doi: 10.1002/lt.24799.
2. *Minina MG, Voronov DV, Tenchurina EA.* Evolution of liver donation in Moscow. Movement towards expanded donor selection criteria. *Russian Journal of Transplantology and Artificial Organs*. 2022; 24 (3): 102–110. [In Russ, English abstract]. doi: 10.15825/1995-1191-2022-3-102-110.
3. *Ryss ES, Ryabov SI, Lutoshkin MB, Panina IYu.* Pishchevaritel'naya sistema. *Lechenie khronicheskoy pochechnoy nedostatochnosti.* Pod red. S.I. Ryabova. SPb.: Foliant, 1997: 11–25. [In Russ].
4. *Levey AS, Coresh J, Balk E, Kausz AT, Levin A, Steffes MW et al.* National Kidney Foundation practice guidelines for chronic kidney disease: evaluation, classification, and stratification. *Ann Intern Med*. 2003; 139 (2): 137–147. doi: 10.7326/0003-4819-139-2-200307150-00013.
5. *Nemes B, Gámán G, Polak WG, Gelley F, Hara T, Ono S et al.* Extended criteria donors in liver transplantation Part I: reviewing the impact of determining factors. *Expert Rev Gastroenterol Hepatol*. 2016; 10 (7): 827–839. doi: 10.1586/17474124.2016.1149061.
6. *Gautier SV, Khomyakov SM.* Organ donation and transplantation in the Russian Federation in 2021 14th Report from the Registry of the Russian Transplant Society. *Russian Journal of Transplantology and Artificial Organs*. 2022; 24 (3): 8–31. [In Russ, English abstract]. doi: 10.15825/1995-1191-2022-3-8-31.

The article was submitted to the journal on 31.03.2023

DOI: 10.15825/1995-1191-2023-2-170-177

COMPARATIVE ANALYSIS OF THE PHARMACOKINETIC PARAMETERS OF TRANSDERMAL AND INJECTABLE FORMS OF NICOTINAMIDE

V.A. Ryzhikova[1], E.G. Kuznetsova[1], O.M. Kuryleva[1], L.A. Salomatina[1], S.V. Kursakov[2], A.O. Nikolskaya[1], V.I. Sevastianov[1, 2]

[1] Shumakov National Medical Research Center of Transplantology and Artificial Organs, Moscow, Russian Federation

[2] Institute of Biomedical Research and Technology, Moscow, Russian Federation

In recent years, oxidative stress, characterized by excess free radicals in the body, has been called the cause of many diseases. There is an active search for drugs with antioxidant properties that are suitable for long-term maintenance therapy. Nicotinamide (NAM), an antioxidant, is used to treat a variety of diseases, usually in oral or injectable form. Given the peculiarities of the drug regimen (dose, prolonged administration), a new dosage form of NAM, a microemulsion-based transdermal patch (TP), containing 20 mg/10 cm^2 of NAM, has been proposed. The objective of this work is to compare the pharmacokinetic parameters of intramuscular and transdermal NAM administration in animal experiments for 24 hours. **Materials and methods.** We used laboratory samples of nicotinamide TP based on a microemulsion-based transdermal delivery emulsion (TDS) with different content of sodium docusate transfer activator**.** The pharmacokinetics of transdermal and intramuscular injections were studied in male Chinchilla rabbits weighing 3.5–4.0 kg. Plasma NAM levels of the experimental animals were determined by high-performance liquid chromatography using a specially designed method on NUCLEODUR PFP columns (5 μm, 250 × 4.6 mm) using the mobile phase acetonitrile: deionized water. The samples were preliminarily purified by solid-phase extraction using Chromabond C18 Hydra cartridges. **Results.** When administered intramuscularly, the maximum blood NAM level was 13.3±1 μg/mL; when NAM transdermal forms were applied in the same dosage with different contents of the transfer activator, the levels did not differ significantly – 3.1 and 3.2 μg/mL. It was shown that in transdermal administration of NAM, concentration of the active substance remained at a constant level for ~6 hours. The bioavailability of NAM with transdermal administration was calculated relative to intramuscular administration: 1.43 for TP with 9.8% docusate sodium and 1.84 with 3.3% docusate sodium. **Conclusion.** NAM has a higher bioavailability when administered transdermally at 20 mg than when administered intramuscularly in the same dose. With transdermal administration, NAM concentration can be maintained at a constant level for a long time, without the jumps that are typical of intramuscular administration.

Keywords: transdermal therapeutic system, transdermal patch, antioxidant, nicotinamide, pharmacokinetics.

INTRODUCTION

In recent years, the possibility of using antioxidants as both the main and adjuvant agents in the treatment of a number of diseases caused by oxidative stress, has been actively studied [1, 2]. This condition leads both to damage at the cellular level and disruption of the functioning of entire organs and systems, resulting in diseases such as cancer, atherosclerosis, chronic renal failure, diabetes and its characteristic complications, autoimmune diseases, hemorrhagic shock, heart attacks, ischemic conditions, etc. It is known that oxidative stress also accompanies surgical procedures associated with reversible vascular ischemia [3]. It is worth noting that graft rejection, as well as graft dysfunction caused by ischemia/reperfusion injury, is often associated with oxidative stress [3–5]. In practice, various methods of donor pretreatment and antioxidant treatment of donor organs are actively used. At the same time, antioxidant therapy is also indicated for recipients to improve graft performance. However, instrumental methods that are mostly used are rather difficult to implement [4, 6]. A combination of antioxidant approaches seems to be a rational way out [4]. There is evidence of the benefits of using both antioxidant enzymes and some vitamin preparations with antioxidant properties among organ recipients. Natural antioxidants are also capable of reducing damage under oxidative stress, which has been shown in experiments on a model of liver ischemia/reperfusion injury, but their use is limited by the need for long-term continuous administration and large doses [6]. For example, the use of vitamins E and C after cardiac transplantation is

Corresponding author: Varvara Ryzhikova. Address: 1, Shchukinskaya str., Moscow, 123182, Russian Federation. Phone: (499) 196-26-61. E-mail: gavrjuchenkova@rambler.ru

recommended to protect blood vessels, but no large-scale studies in this area have been conducted [7].

In literature, pancreatic islet transplantation is mentioned as a promising alternative therapy for diabetes [8], which at all stages is accompanied by the use of antioxidants that promote islet cell engraftment, improve vascularization, and exhibit immunosuppressive properties [9]. Earlier studies in beta cell transplantation noted the positive effect of antioxidant drugs, including vitamins E and C [8].

We chose the water-soluble amide form of vitamin B_3, nicotinamide (NAM), a precursor of nicotinamide adenine dinucleotide (NAD), nicotinamide adenine dinucleotide phosphate (NAD^+) and their reduced forms as an antioxidant. NAD^+ derivatives play an enormous role in cellular homeostasis, generation, and inhibition of reactive oxygen species [10, 11].

The protective effect of NAM on insulin-producing β-cells has long been of particular interest; in addition, its stimulating effect on insulin secretion has been reported [12–17]. In addition to its protective effect in the treatment of diabetes, vitamin PP also plays a major role in islet cell repair [18]. The use of NAM in the therapy of diabetes can reduce the frequency or intensity of the most common complications of this disease, such as angiopathy, retinopathy, and neuropathy due to oxidative stress [11, 19–21]. The regenerative effect of NAM has been demonstrated in the restoration of liver tissue and its function in an experiment after partial hepatectomy [22]. The possibility of using NAM to reduce phosphate levels in hyperphosphatemic patients with renal failure who are on hemodialysis has been shown [23].

Constant, controlled rate of administration of appropriate drugs is an important condition for antioxidant therapy in transplantation [4]. A solution to this problem could be the use of reverse emulsions as part of transdermal therapeutic systems (transdermal patches, TP), which provide controlled continuous dosing of the active ingredient over a long period of time, delivering it to the target organs in unchanged form through the systemic circulation without first passing through the liver. The main advantages of TP include prolonged release of the active ingredient without jumps in its blood concentrations that can lead to adverse effects [24].

Given the physicochemical properties of nicotinamide (small molecular weight of 122.1 g/mol, hydrophilicity) [25] and the features of the regimen (long courses, oral or injected administration from 1 to 4 times a day, high doses, the need to divide the daily dose into several doses) [26], the authors developed a transdermal patch for nicotinamide (20 mg/10 cm^2) based on a microemulsion-based TDS [27]. The aim of this work is to carry out a comparative analysis of the pharmacokinetic parameters of nicotinamide in transdermal and intramuscular administration.

MATERIALS AND METHODS

Materials and equipment

Nicotinamide (molecular weight 122 g/mol Sigma, USA) in powder form was used as the active ingredient.

Laboratory samples of nicotinamide TP were made using materials and excipients approved for medical use and meeting the requirements of current regulatory documentation.

The microemulsion-based TDS for nicotinamide included the following components: deionized water, sodium dodecyl sulfate (AppliChem Panreac, Spain), apricot kernel oil (Desert Whale Jojoba Company Ltd, USA), α-tocopherol acetate (BASF SE, Germany), dioctyl sodium sulfosuccinate (docusate sodium) (Sigma, USA), and Decaglin PR (Decaglyn PR-20, Nikko Chemicals Co., Ltd., Japan).

To create the nicotinamide TP, the following auxiliary materials were chosen: elastic microbubble material Foam tape 9773 (3M, USA), sorbent base PALV-01 (Palma Group of Companies LLC, Russia), Skotchpak 9730 film (3M, USA).

Sodium citrate (NPO RENAM, Russia) was used to stabilize blood samples during *in vivo* studies.

All plasma samples, including calibration solutions, were purified from impurities using solid-phase extraction (SPE). Purification was performed using 3 mL Chromabond C18 Hydra cartridges (Macherey-Nagel, Germany) with a sorbent mass of 200 mg, which were prepared using solvents (acetonitrile (PanReac, Spain) and deionized water) used to create the mobile phase during chromatographic analysis.

Quantification of NAM in the samples by high-performance liquid chromatography (HPLC) was performed on a NUCLEODUR PFP column (5 μm, 250 × 4.6 mm Macherey-Nagel, Germany) with a NUCLEODUR PFP precolumn (4 × 3 mm, 5 μm Macherey-Nagel, Germany).

Equipment used in the work: DIAX 900 dispersant (Heidolph, Germany), UIS250V ultrasonic homogenizer (Heilscher, Germany), GH-200 analytical scales (AND, Japan), Rotina 38R centrifuge (Hettich, Germany), cleaning system Simplicity (Millipore, Germany), vacuum system with manifold and LiChrolut pump (Merck, Germany), Agilent 1260 Infinity chromatograph (Agilent Technologies, USA) equipped with diode matrix detector, column thermostat and Chem Station software (Agilent, USA).

Study design

The pharmacokinetics of NAM in transdermal and intramuscular injections was studied on male Chinchilla rabbits weighing 3.5–4.0 kg.

The rabbits were obtained from a nursery belonging to KrolInfo Ltd. The producer provided a veterinary certificate for the last animal health monitoring. All the experimental animals were specially bred and were not

previously involved in research. Quarantine was for 14 days. All manipulations didn't cause any pain to the animals and were conducted according to the rules adopted in the European Convention for the Protection of Vertebrate Animals Used for Experimental and other Scientific Purposes (ETS 123) Strasbourg, 1986) and in accordance with the Russian legislation: GOST 33215-2014 (Guidelines for accommodation and care of laboratory animals: Environment, housing and management) and GOST 33216-2014 (Guidelines for accommodation and care of laboratory animals: Species-specific provisions for laboratory rodents and rabbits).

Plasma NAM levels in transdermal and intramuscular administration was studied according to the developed design. The animals were divided into three groups at random. The first group of animals (n = 5) received NAM once intramuscularly at a dose of 20 mg. In the second (n = 7) and third groups (n = 5), we examined the pharmacokinetic parameters of the transdermal therapeutic system with the drug at the same dose but with different levels of the transdermal carrier of dioctyl sodium sulfosuccinate (3.3% and 9.8% respectively) in the microemulsion-based transdermal delivery system.

In groups 2 and 3, transdermal patch was applied to a pre-shaved dorsal skin area at the base of the neck. The drug was applied to healthy skin not earlier than one day after the hair removal procedure.

Blood sampling of the experimental animals was performed before administration of the drug, as well as at discrete time intervals from the marginal ear vein, into tubes with 3.8% sodium citrate solution. Blood sampling times for TP were 40, 50, 60 minutes, then every hour for 8 hours, 12, 15, 18, and 24 hours of application. For the injectable form: 5, 10 minutes, then for 1 hour every 10 minutes, then every hour for 8 hours after intramuscular injection of NAM.

Test tubes containing the blood samples from experimental animals were centrifuged for 5 minutes at 1500 rpm at room temperature, then the plasma was carefully collected.

HPLC for quantification of nicotinamide in the plasma of the experimental animals

Sample preparation

Eppendorf tubes were filled with 500 μL of blood plasma samples and diluted with distilled water in a 1 : 1 ratio. After stirring, the contents of the tubes were transferred to a previously activated SPE cartridge. The sample was passed at a rate of 1–1.5 mL/min, adjusting the rate using the manifold valve. A three-fold wash with water (1 mL each) was then performed, after which NAM was eluted with the mobile phase (acetonitrile:deionized water, 20:80, 1 mL). The eluate was then analyzed on a liquid chromatograph.

When preparing calibration solutions, 20 μL of a standard solution of NAM with a known concentration (6.25; 12.5; 25; 125; 250 μg/ml) was added to 480 μL of plasma, then 500 μL of deionized water was added, and SPE of calibration solutions was performed as described above.

Since NAM is present in all tissues of the animal body, to correctly estimate the amount of NAM in the studied samples, its background values were taken into account by performing plasma studies before applying the patch and subtracting the values obtained when processing the obtained data.

Quantification of nicotinamide

Quantification of NAM in blood plasma after SPE was performed by HPLC under the following conditions:

Mobile phase: acetonitrile:deionized water.
Elution mode: gradient (Table 1).
Mobile phase flow rate: 1 mL/min.
Column thermostat temperature: 40 °C.
Volume of injected sample: 20 μL.
Detection wavelength: 262 nm.
Chromatographic time: 30 min.
NAM retention time: ~11.8 minutes.

Calculation of pharmacokinetic parameters

Pharmacokinetic research method allows to give a number of quantitative characteristics of the processes of absorption, metabolism (biotransformation), distribution and removal of drugs from the body. For this purpose, the following parameters were calculated [28]:

– C_{max}, maximum concentration of the drug in blood plasma (μg/mL).
– T_{max}, time to reach maximum drug concentration (hour).
– AUC, the total area under the drug concentration curve from the time of its entry into the body until its complete removal from the body (h·mcg/mL).
– AUMC, the total area under the curve of the product of time and drug concentration in the body from the moment of its entry into the body until its complete removal from the body (h^2·mcg/mL);

Table 1

Composition of the mobile phase

Time (minutes)	Ratio of the components of the mobile phase (%)	
	Acetonitrile	Deionized water
0	0	100
5	0	100
6	5	95
11	5	95
16	30	70
21	30	70
24	0	100
30	0	100

– $T_{1/2}$, drug half-life – the period of time required for the concentration of the drug in the body to be reduced by one-half (hour);
– MRT, mean residence time – the average time that the drug spends in the body (hours);
– β, elimination rate constant (h^{-1});
– F, bioavailability.

Relative bioavailability was determined by comparing the total areas under the drug concentration curve from the time of entry into the body to complete removal from the body in transdermal and intramuscular injections. It was calculated by the formula:

$$F = \frac{AUC_{(TP)} \times D_{(injection)}}{AUC_{(injection)} \times D_{(TP)}},$$

where AUC is the area under the kinetic curve, D is the drug dose.

Pharmacokinetic parameters were calculated using a model-independent method.

Statistical processing of results

Normal distribution of experimental data was proved using the Shapiro–Wilk test on a small number of samples ($n \geq 5$). Significance of differences was determined using Student's t test (standard software package Microsoft Excel 2010). Differences were considered statistically significant at $p < 0.05$.

RESULTS AND DISCUSSION

A comparative analysis of the pharmacokinetic parameters of NAM in intramuscular and transdermal administration in rabbits was performed.

The averaged pharmacokinetic curves of NAM obtained by application of TP with different levels of transdermal carrier of docusate sodium (9.8% and 3.3%) and intramuscular injection (at the same dose of 20 mg) are presented in Fig.

As can be seen from Fig., for intramuscular administration of NAM, the maximum concentration (drug) in the blood was reached after 20 minutes, 13.3 ± 1.0 μg/mL. Then there was a sharp decrease to 5.3 ± 0.7 μg/mL by 2 hours after drug administration. By 8 hours of the experiment, the concentration was 0.30 ± 0.35 μg/mL.

When transdermal forms of NAM were applied with the same dosage with different carrier content, increase in blood concentrations was slower than with intramuscular injection, as shown in Fig. By the first hour, 2.2 ± 0.85 μg/mL and 1.4 ± 0.44 μg/mL drug were detected in the blood when the transdermal patch was applied with 3.3% and 9.8% carrier, respectively.

With this method of administration, the maximum NAM concentration in the blood for the patch with different transfer activator content did not differ significantly (~3.1 and 3.2 μg/mL), remaining constant within the statistical error for about 6 hours.

For TP with lower carrier content, the decrease in NAM concentration began after 7 hours of application, and after 15 hours NAM was no longer detectable in the blood. In the case of application of forms with more carrier, a gradual decrease in NAM levels was traced: the beginning of the decrease was noted after 8 hours of application, the drug concentration was 0.55 ± 0.35 μg/mL at 15 hours, and no NAM was detected in the blood plasma at 24 hours.

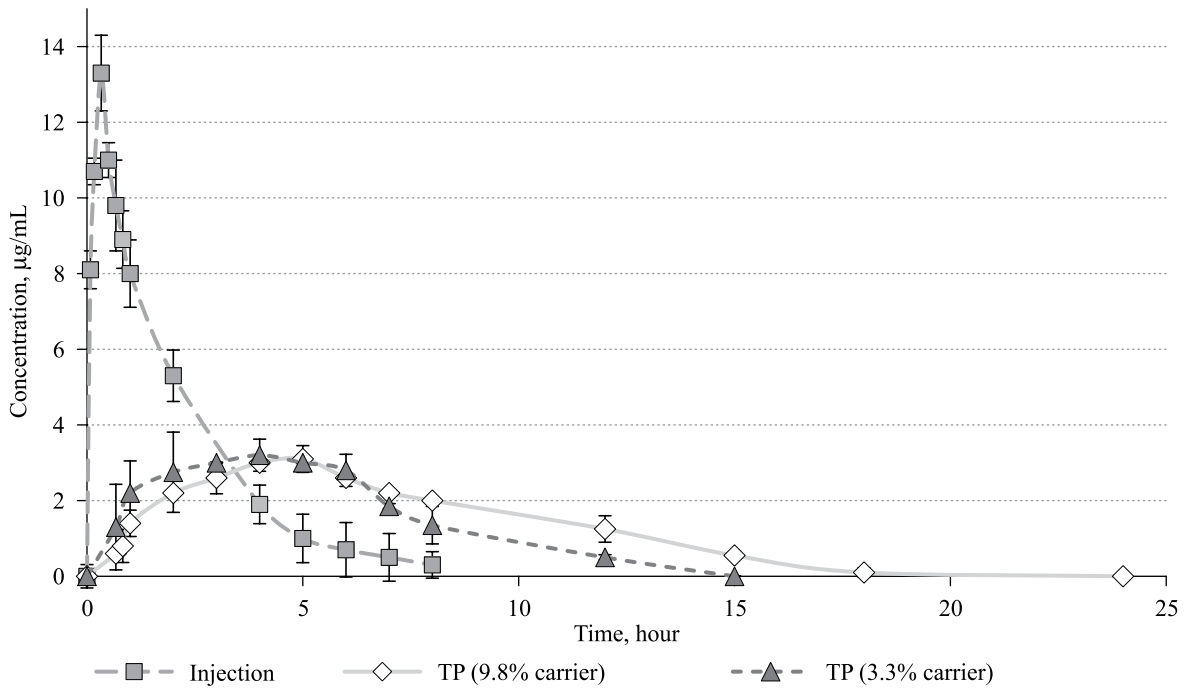

Fig. Averaged dynamics of plasma NAM levels in experimental animals with intramuscular and transdermal administration. Differences in the values of points (Δ) and (◊) are not statistically significant ($p > 0.05$)

Table 2

Pharmacokinetic parameters of nicotinamide with transdermal and intramuscular administration in rabbits

Parameters	Method of administration		
	Intramuscular, n = 5	Transdermal	
		Transdermal carrier content	
		3.3%, n = 7	9.8%, n = 5
C_{max}, μg/mL	13.3	3.2	3.1
T_{max}, h	0.33	4	5
β, 1/h	0.495	0.301	0.187
$T_{1/2}$, h	1.4	2.3	3.7
AUC, h·μg/mL	27.01	49.75	38.58
AUMC, h^2·μg/mL	50.12	320.89	245.5
MRT, h	1.9	6.5	6.4

Thus, with the transdermal method of nicotinamide delivery, there was a more uniform and prolonged drug entry into the blood, while the concentration remained at a constant level for ~6 hours.

The calculated pharmacokinetic parameters for single transdermal and intramuscular administration of NAM to experimental animals are presented in Table 2.

The average time that NAM spends in the body (MRT) in the transdermal patch groups in both cases was more than 6 hours. In the case of intramuscular injection, MRT was 1.9 hours. Thus, a transdermal nicotinamide therapeutic system can increase the mean residence time of the drug in the body by about 3 times compared to intramuscular injection.

The drug half-life $T^{1/2}$ was 3.7 and 2.3 hours for the drug forms with a higher and lower content of the transdermal transfer activator, respectively. This parameter was lower by almost 2.5 times – 1.4 hours – when NAM was administered intramuscularly.

Calculation showed that NAM had a higher bioavailability when administered transdermally than when injected intramuscularly (1.43 for TP with 9.8% carrier and 1.84 with 3.3% carrier).

Thus, the results of the *in vivo* studies and a comparative analysis of the pharmacokinetic parameters of NAM in transdermal and intramuscular administration showed the promise of the transdermal route of administration of the studied antioxidant.

CONCLUSION

In the course of this work, the pharmacokinetics of intramuscular and transdermal routes of NAM administration *in vivo* were studied using transdermal patches with different contents of the transdermal carrier activator of dioctyl sodium sulfosuccinate.

Application of the NAM 20 mg transdermal therapeutic system has been shown to provide higher bioavailability than intramuscular administration of this drug at the same dose. At the same time, the maximum drug concentration in the blood is 4 times lower and its residence time in the body is more than 3 times longer, which may promote prolonged drug effect. Changes in the drug concentrations in the blood for transdermal patch occur gradually over several hours in contrast to its sudden jump when NAM is administered intramuscularly. This is a definite advantage of the transdermal nicotinamide system in case of long-term use for prophylaxis and maintenance therapy.

The authors declare no conflict of interest.

REFERENCES

1. *Olefir YuV, Romanov BK, Kukes VG, Sychev DA, Prokofiev AB, Parfenova OK et al.* The role of oxidative stress in the pathogenesis of socially significant human diseases and ways of its drug correction. *Medical News of North Caucasus*. 2021; 16 (4): 450–455. [In Russ, English abstract]. https://doi.org/10.14300/mnnc.2021.16109.
2. *Vetsheva MS, Sviridova V, Podkorytova LO.* Antioxidant therapy in various deseases. Preventing opportunities (a literature review). *Kremlin medicine. Clinical Bulletin*. 2022; 1: 71–77. [In Russ, English abstract]. doi: 10.26269/y0z6-xs61.
3. *Ma A, Qi S, Chen H.* Antioxidant therapy for prevention of inflammation, ischemic reperfusion injuries and allograft rejection. *Cardiovasc Hematol Agents Med Chem*. 2008; 6 (1): 20–43. doi: 10.2174/187152508783329966. PMID: 18220719.
4. *Shi S, Xue F.* Current Antioxidant Treatments in Organ Transplantation. *Oxid Med Cell Longev.* 2016; 8678510. doi: 10.1155/2016/8678510; PMID: 27403232; PMCID: PMC4926011.
5. *Gori F, Fumagalli J, Lonati C, Caccialanza R, Zanella A, Grasselli G.* Ascorbic acid in solid organ transplantation: A literature review. *Clin Nutr.* 2022; 41 (6): 1244–1255. doi: 10.1016/j.clnu.2022.04.004; PMID: 35504167.
6. *Elias-Miró M, Jiménez-Castro MB, Rodés J, Peralta C.* Current knowledge on oxidative stress in hepatic ischemia/reperfusion. *Free Radic Res*. 2013; 47 (8): 555–568. doi: 10.3109/10715762.2013.811721; PMID: 23738581.
7. *Patel J.* Vitamin therapy after heart transplantation. *Expert Review of Cardiovascular Therapy*. 2015; 13 (10): 1071–1074. doi: 10.1586/14779072.2015.1086268.
8. *Mohseni Salehi Monfared SS, Larijani B, Abdollahi M.* Islet transplantation and antioxidant management: a comprehensive review. *World J Gastroenterol*. 2009; 15 (10): 1153–1161. doi: 10.3748/wjg.15.1153; PMID: 19291814; PMCID: PMC2658860.
9. *Eguchi N, Damyar K, Alexander M, Dafoe D, Lakey JRT, Ichii H.* Anti-Oxidative Therapy in Islet Cell Transplantation. *Antioxidants (Basel)*. 2022; 11 (6): 1038. doi: 10.3390/antiox11061038; PMID: 35739935; PMCID: PMC9219662.
10. *Makarov MV, Trammell SAJ, Migaud ME.* The chemistry of the vitamin B_3 metabolome. *Biochem Soc Trans*. 2019;

47 (1): 131–147. doi: 10.1042/BST20180420; PMID: 30559273; PMCID: PMC6411094.
11. *Maiese K.* Nicotinamide as a Foundation for Treating Neurodegenerative Disease and Metabolic Disorders. *Curr Neurovasc Res*. 2021; 18 (1): 134–149. doi: 10.2174/1567202617999210104220334; PMID: 33397266; PMCID: PMC8254823.
12. *Dedov II, Gorelysheva VA, Smirnova OM, Romanovskaya GA, Filippov IK.* Effects of antioxidants on lipid peroxidation and beta-cell function in patients with newly detected insulin-dependent diabetes mellitus. *Problems of Endocrinology*. 1995; 41 (5): 16–20. [In Russ]. https://doi.org/10.14341/probl199541516-20.
13. *Gorelysheva VA, Smirnova OM, Dedov II.* Nicotinamide in the treatment of insulin-dependent diabetes mellitus at the debut of the disease. *Problems of Endocrinology*. 1996; 42 (6): 26–30. [In Russ]. https://doi.org/10.14341/probl12057.
14. *Fadeeva NI, Balabolkin MI, Mamaeva GG, Kravchenko TV, Mishchenko BP, Knyazeva AP.* Primenenie nikotinamida i drugikh antioksidantnykh preparatov v kompleksnoy terapii sakharnogo diabeta 2-go tipa. *Diabetes mellitus*. 2001; 4 (1): 21–23. [In Russ]. https://doi.org/10.14341/2072-0351-6103.
15. *Bondar' IA, Klimentov VV.* Antioksidanty v lechenii i profilaktike sakharnogo diabeta. *Diabetes mellitus*. 2001; 4 (1): 47–52. [In Russ]. https://doi.org/10.14341/2072-0351-6108.
16. *Pandey A, Tripathi P, Pandey R, Srivatava R, Goswami SH.* Alternative therapies useful in the management of diabetes: A systematic review. *J Pharm Bioallied Sci.* 2011; 3 (4): 504–512. doi: 10.4103/0975-7406.90103.
17. *Alenzi FQ.* Effect of nicotinamide on experimental induced diabetes. *Iran J Allergy Asthma Immunol.* 2009; 8 (1): 11–18. PMID: 19279354.
18. *Banerje M, Kanitkar M, Bhonde RR.* Approaches towards endogenous pancreatic regeneration. *Rev Diabet Stud*. 2005; 2 (3): 165–176. doi: 10.1900/RDS.2005.2.165; PMCID: PMC1783561; PMID: 17491691.
19. *Ahmad AARAA, Sakovich VN.* The study of the clinical efficacy of nicotinamide-containing drugs in patients with initial forms of diabetic retinopathy. *Problems of environmental and medical genetics and Clinical Immunology*. 2013; 1 (115): 153–161. [In Russ, English abstract].
20. *Chandrasekaran K, Najimi N, Sagi AR, Yarlagadda S, Salimian M, Arvas MI et al.* NAD+ Precursors Repair Mitochondrial Function in Diabetes and Prevent Experimental Diabetic Neuropathy. *Int J Mol Sci*. 2022; 23 (9): 4887. doi: 10.3390/ijms23094887. PMID: 35563288; PMCID: PMC9102948.
21. *Jung KI, Han JS, Park CK.* Neuroprotective Effects of Nicotinamide (Vitamin B_3) on Neurodegeneration in Diabetic Rat Retinas. *Nutrients*. 2022; 14 (6): 1162. doi: 10.3390/nu14061162. PMID: 35334819; PMCID: PMC8950738.
22. *Wan HF, Li JX, Liao HT, Liao MH, Luo L, Xu L et al.* Nicotinamide induces liver regeneration and improves liver function by activating SIRT1. *Mol Med Rep*. 2019; 19 (1): 555–562. doi: 10.3892/mmr.2018.9688. Epub 2018 Nov 22. PMID: 30483782.
23. *Lenglet A, Liabeuf S, El Esper N, Brisset S, Mansour J, Lemaire-Hurtel AS et al.* Efficacy and safety of nicotinamide in haemodialysis patients: the NICOREN study. *Nephrol Dial Transplant.* 2017; 32 (5): 870–879. doi: 10.1093/ndt/gfw042. PMID: 27190329.
24. *Arefev AS, Zhukova IV.* Transdermal therapeutic systems, their types and advantages. *Innovative scientific research*. 2022; 1–3 (15): 13–20. doi: 10.5281/zenodo.6368638. – EDN CBFERX. [In Russ, English abstract].
25. Femb.ru [Internet]. Federal'naya elektronnaya meditsinskaya biblioteka. Gosudarstvennaya farmakopeya Rossiyskoy Federatsii, XIV izdanie, tom 3. Nikotinamid. FS.2.1.0143.18 [data obrashcheniya: 17.04.2023]. Dostupno na: https://docs.rucml.ru/feml/pharma/v14/vol3/1211.
26. Vidal.ru [Internet]. Spravochnik lekarstvennykh sredstv Vidal [data obrashcheniya: 17.04.2023]. Dostupno na: https://www.vidal.ru/drugs/molecule/735.
27. *Kuznetsova EG, Ryzhikova VA, Salomatina LA, Kuryleva OM, Sevastianov VI.* Percutaneous Delivery System for Nicotinamide Transdermal Therapeutic System. *Perspektivnye materialy*. 2023; 7: 12–24. [In Russ, English abstract].
28. *Belousov YuB.* Klinicheskaya farmakologiya i farmakoterapiya. M.: MIA, 2010. 872.

The article was submitted to the journal on 11.05.2023

INSTRUCTIONS TO AUTHORS

Articles should contain original information that has not been previously published and is not considered for publication in other editions. Fee for publication of manuscripts will not be charged.

The manuscript should be presented in Microsoft Word format A4, 1.5 spacing, and Times New Roman font size 12. Submit your article to the online submission system in accordance with the instructions on the journal's website https://journal.transpl.ru.

Structure of the article

The Title page should include:

- Initials (first name and patronymic) of the authors of the article should be specified before their respective last names.
- Full official name of the institution, city and country.
- If authors from different institutions participated in writing of the manuscript, it is necessary to correlate those with the names of the authors by adding a digital index uppercase after last name, and right before the name of the institution.

Information about the authors

For each author fully specify the last and the first name, patronymic and position in the relevant department/institution.

For correspondence

Fully specify the last and the first name, patronymic of the author, who will be holding correspondence, address (including postal code), telephone, fax number, e-mail.

Abstract

Each article must be accompanied by an abstract. The amount of text for the abstract of the original article should be of no more than 300 words, for a literature review, clinical observation – no more than 200 words. The abstract must fully comply with the content of the work. The abstract should not use abbreviations without prior expansion.

Abstract of ***the original article*** should contain the following sections: ***Objective***, ***Materials and methods***, ***Results***, ***Conclusion***. The abstract should present the most important results of the research.

Do not write: "*A comparative analysis of the sensitivity and specificity was conducted …*"

Should write: "*The sensitivity was ... % and ...%, p = , specificity, respectively ...% and ...%, p =* ".

Keywords

At the end of the abstract keywords must be given. To select the keywords a thesaurus of U.S. National Library of Medicine should be used – Medical Subject Headings (MeSH) at http://www.ncbi.nlm.nih.gov/mesh.

Conflict of interest

The author should inform the editor about the factual or potential conflict of interest have included the information about such conflict into the respective section of an article.

If there is no conflict of interest, the author should say so in the form like the following: "Author declares unawareness of the conflict of interest".

This information is supposed to be placed before the article text.

Text of article

Original article should include the following sections:

- Introduction
- Materials and methods
- Results
- Discussion
- Conclusion
- References

Review article should include an analysis of the literature with the presentation of modern sources (mainly in the last 5 years).

Clinical observation should be well illustrated (to reflect the essence of the problem) and include discussion with the use of literature data.

References in the text are indicated by number in square brackets: [1], [2, 5], [14–18] and ***in the references section are presented in order of their appearance in the text.*** All values given in the article should be expressed or duplicated in **SI** units.

References

The author is solely responsible for the accuracy of the data included in the references section of the article. References to unpublished papers or papers in print works are not allowed.

References are presented on a separate page.

The names of journals can be contracted in accordance with an embodiment of reduction adopted by the specific journal.

If the article quoted has DOI (a digital object identifier) or/and PMID (Pub Med identifier) they must be specified after the description of the article. To compile descriptions in References section NLM bibliographic reference citation standard is used – U.S. National Lib-

rary of Medicine (http://www.nlm.nih.gov/bsd/uniform_requirements.html). If the number of authors does not exceed 6, the bibliographic description includes all the authors. If the number of authors is more, only the first six authors should be indicated and then add et al.

Requirements for tables and figures

Tables should be placed into the text; they should have numbered heading and clearly labeled graphs, convenient and simple to read. Table's data must comply with the numbers in the text, but should not duplicate the information therein. Table references in the text are required.

Illustrations and drawings should be submitted in electronic format (JPEG or TIFF format with a resolution of at least 300 dpi and no smaller than 6 × 9 cm), in a volume of close to 1 MB. Drawings must include all copyright symbols – arrows, numbers, signs, etc. Figure captions should be submitted in a separate file with the extension *.doc. First, the name is given, then all arithmetic and alphabetical symbols (lettering) are explained.

Articles should be addressed to the Editor at:
Russian Journal of Transplantology and Artificial Organs
Shumakov National Medical Research Center of Transplantology and Artificial Organs
1, Shchukinskaya ul., Moscow 123182, Russian Federation
E-mail: **vestniktranspl@gmail.com**

Издание зарегистрировано в Госкомпечати РФ, № 018616 от 23.03.99 г.

Подписано к печати 5.07.23.

Тираж 1000 экз.

ООО «Издательство «Триада».
ИД № 06059 от 16.10.01 г.
170034, г. Тверь, пр. Чайковского, 9, оф. 514,
тел./факс: (4822) 42-90-22, 35-41-30
E-mail: triadatver@yandex.ru
http://www.triada.tver.ru

Заказ 27052